

TRIBOLOGICAL AND ANTIWEAR MECHANISMS OF FLUORINATED
ZINC DIALKYL DITHIOPHOSPHATE IN COMPARISON
TO ZINC DIALKYL DITHIOPHOSPHATE
IN ENGINE OILS

by

RAMOUN MOURHATCH

Presented to the Faculty of the Graduate School of
The University of Texas at Arlington in Partial Fulfillment
of the Requirements
for the Degree of

DOCTOR OF PHILOSOPHY

THE UNIVERSITY OF TEXAS AT ARLINGTON

May 2008

Copyright © by Ramoun Mourhatch 2008

All Rights Reserved

ACKNOWLEDGEMENTS

This research has been made possible by invaluable help, input and support from several people. First and foremost I wish to thank my advisor, Dr. Pranesh B. Aswath who has been my guide and mentor in the past 6 years. His support, help and guidance, combined with his patience and pleasant and inspiring personality as well as his exceptional knowledge in this field have been the key reason behind the progress in this work.

I would like to thank Dr. Ronal L. Elsenbaumer for his counsel and guidance throughout this research effort. I hereby acknowledge the time, supportive inputs and help of my graduate committee members, Dr. Efstathios Meletis, Dr. Choon-Un Kim, Dr. Wen Chan and Roger D. Goolsby and Dr. Harold Shaub.

I would like to thank the faculty members of the materials science and engineering department at Sharif University of Technology who laid the foundation of my knowledge in the field of materials science and metallurgical engineering. I also wish to thank all the faculty members of the department of materials science and engineering at the University of Texas at Arlington for their generous sharing of their knowledge and resources through out my graduate studies at this university. I would like to thankfully acknowledge the MSE staff, Mrs. Jennifer Standlee, who has always greeted me with a smile and has been more than helpful in many instances, and Mrs. Libia A. Cuauhtli and Mrs. Prudence Brett whose help has insured the timely progress of this research work. My special thanks to Dr. Jiechao C. Jiang and Michael Coviello who provided me with training on numerous equipments in the characterization lab as well as their significant help and contribution with the TEM work. Dr. Nasir Basit's help with the FIB work carried out at the NanoFAB facility a UTA and Dr. Nancy Michael's help with the AES work as well as her help and advice with several of the techniques used, is also greatly appreciated. Hysitron corporation's sharing of expertise and resources with regards to

nanomechanical testing is also deeply acknowledged. I am also grateful to Dr. Yongfeng Hu and Narayan Appathurai of the Canadian Light Source for their technical support and help with the XANES studies.

My deepest gratitude goes to my former and current colleagues, Dr. Xin Chen, Dr. Gabi Nehme, Mr. Krupal Patel, Sunit Munot, Hiroshi Ito, Kajal Parekh, Anuradha Somayaji, Bo-Hoon Kim, Mihir Patel, Eray Erkan, Hande Demirkiran, Hansika Parekh, Arunya Suresh and Beibei Wang in the tribology research group and the MSE department who not only have been great team members, and helpful with everything, but have also become among some of my best friends. Special thanks to the Platinum Research Organization team, Mr. David Owen, Matt Hawkins and Cork Jaeger for their practical guidance and sponsorship of this research effort.

At the end, I wish to thank my parents, Frances and Eddie Mourhatch, my brothers Ryan and Ramses and my fiancé, Sara Kiani for their being a constant source of love and encouragement and to my good friends, Fredrick Mirza, Behrang H. Hamadani, Arash Aslani, Solmaz Torabi, Soheil Samouhi, Caroline Zarnaghian and Ali Ghahremaninejad who have supported and encouraged me through out my graduate studies.

April 22, 2008

ABSTRACT

TRIBOLOGICAL AND ANTIWEAR MECHANISMS OF FLUORINATED ZINC DIALKYL DITHIOPHOSPHATE IN COMPARISON TO ZINC DIALKYL DITHIOPHOSPHATE IN ENGINE OILS

Ramoun Mourhatch, PhD.

The University of Texas at Arlington, 2008

Supervising Professor: Pranesh B. Aswath

Tribofilms generated in wear tests using lubricants containing fluorinated ZDDP and ZDDP were studied. Fluorinated ZDDP demonstrated superior wear performance compared to ZDDP under tribological conditions even at lower phosphorus levels. Chemical properties and the molecular structure of the fluorinated ZDDP were examined and presented in a previous companion study by Parekh and Aswath [1] using techniques such as NMR and DSC while this study examines the tribological behavior of this compound and the characteristics of the tribofilms formed by it.

Ball on cylinder tribological tests were conducted with lubricants containing this new fluorinated thiophosphate compound and compared to lubricants containing ZDDP. The antiwear performance of the two chemistries as well as tribofilms were then analyzed by a variety of techniques such as Scanning electron microscopy of the film as well as measuring the thickness of the film by using focused ion beam (FIB). The tribofilms were also chemically

analyzed using auger electron spectroscopy (AES) and X-ray absorption near edge structure (XANES) spectroscopy. A nano-indenter was used to study the mechanical properties of the tribofilms by obtaining modulus as a function of the thickness of the tribofilm. In addition the mechanical strength of the tribofilm was evaluated by conducting nano-scale scanning wear and nano-scratch tests. These different techniques have been used to develop a phenomenological model of the tribofilms generated by fluorinated zinc dialkyl dithiophosphate compounds and ZDDP under the testing conditions of this study.

TABLE OF CONTENTS

ACKNOWLEDGEMENTS	iii
ABSTRACT	v
LIST OF ILLUSTRATIONS.....	x
LIST OF TABLES.....	xvii
Chapter	
1. INTRODUCTION	1
1.1 Drive for this research	3
1.2 Objectives of research.....	5
1.3 Structure of this research.....	6
2. BACKGROUND	8
2.1 Tribology of engines: An overview	8
2.2 Wear in engines.....	9
2.2.1 Definition and mechanisms	9
2.2.2 Stages of wear in tribosystems.....	12
2.3 Lubrication in internal combustion engines	14
2.3.1 Lubrication regimes.....	15
2.3.2 Antiwear additives and boundary lubrication.....	19
2.4 Zinc dialkyl dithiophosphates.....	21
2.4.1 Chemical structure and properties of ZDDP	21
2.4.2 Neutral and basic ZDDP	22
2.4.3 Antiwear mechanisms of ZDDP	24
2.4.4 ZDDP-additive interactions.....	28
2.5 Fluorinated Zinc dialkyl dithiophosphate.....	30

2.5.1 Iron (III) fluoride and ZDDP interactions	30
2.5.2 Fluorinated the ZDDP	31
2.5.3 Fluorinated phosphorus compounds: Chemical structure	32
2.6 Tribological testing	33
3. APPROCH AND EPERIMENTAL	36
3.1 Methods and techniques: An overview	36
3.2 Tribological wear tests	36
3.2.1 UTA-built BOCLE	36
3.2.2 Plint [®] BOCLE	39
3.2.3 Fluid film thickness calculations and lubrication regime	40
3.3 Sample preparation and testing protocols	44
3.4 Tribofilm characterization	45
3.4.1 SEM / EDS	45
3.4.2 Focused ion beam (FIB)	45
3.4.3 Auger electron spectroscopy (AES)	46
3.4.4 Transmission electron microscopy	49
3.4.5 X-ray absorption near edge structure (XANES) spectroscopy	51
3.5 Nano-mechanical testing	53
3.5.1 Nano-indentation tests	54
3.5.2 Scanning wear test	58
3.5.3 Nano-scratch tests	58
4. LUBRICATION WITH ZDDP UNDER BOUNDARY LUBRICATION CONDITIONS	60
4.1 Materials and procedures	60
4.2 Results, observations and discussion	61

4.2.1 Friction, temperature and wear behavior	61
4.2.2 The effect of additives	65
4.2.3 Phosphorus concentration	66
4.2.4 TEM analysis of wear debris	68
4.2.5 SEM and FIB analysis of tribofilm	69
4.2.6 Nano-indentation and modulus mapping	71
5. COMPARISON OF TRIBOLOGICAL BEHAVIOR OF FLUORINATED ZDDP AND ZDDP	76
5.1 Materials and procedures.	76
5.2 Results, observations and discussion	77
5.2.1 Friction, temperature and wear data	77
5.2.2 SEM / EDS and FIB analysis of tribofilms	82
5.2.3 Nano-mechanical test	89
5.2.4 Transmission electron microscopy	97
5.2.5 Auger electron spectroscopy	102
6. LOAD AND DURATION EFFECTS ON TRIBOFILMS GENERATED BY FLUORINATED ZDDP AND ZDDP	106
6.1 Materials and procedures.	106
6.2 Results, observations and discussion	106
6.2.1 XANES spectroscopy	106
6.2.2 Nano-indentation	117
7. FLUORINATED ZDDP AND ZDDP TRIBOFILMS: A PHENOMENOLOGICAL MODEL	132
8. CONCLUSIONS	140
REFERENCES	144
BIOGRAPHICAL INFORMATION	161

LIST OF ILLUSTRATIONS

Figure		Page
2.1	Typical fuel energy and mechanical loss distributions in an internal combustion	9
2.2	Schematic images of four representative wear modes	10
2.3	Typical wear stages appearing over longer service times in sliding contacts	13
2.4	Schematic comparison of different lubrication regimes	17
2.5	Stribeck curve	18
2.6	Structural formula of (neutral) ZDDP	22
2.7	Monomer – dimer equilibrium of neutral ZDDP	23
2.8	The structure of basic ZDDP	24
2.9	Schematic diagram of tribofilm chemical structure	27
2.10	A possible chemical structure of a fluorinated phosphorus compound; X = R, OR, SR, R (may be same or different); X ≥ 1, n ≈ 1 or 2.....	33
2.11	Classification of tribology testing methods based on degree of realism.....	35
3.1	(a) Loading setup in the BOCLE: The load is applied pneumatically from the top of the setup. The vertical load cell directly measures the applied vertical load. The load is applied on the surface of the ring through a scuffing ball (steel or tungsten carbide) that is in contact with the steel ring. The friction load is measured by the friction load cell. (b) Friction force measurement: This load cell measures the horizontal force resisting the rotation of the ring, which is applied in the horizontal direction on the scuffing ball.....	38
3.2	(a) The thermocouple is connected to the ball close to the contact point. The temperature measured at this spot can be correlated with the actual contact temperature at the contact point. (b) Temperature vs. cycles and coefficient of friction vs. cycles graphs for a typical test. The arrows indicate points of major frictional	

	events which can be closely correlated with changes that occurred in the temperature.....	39
3.3	Schematics tribofilm thickness measurement using focused ion beam	46
3.4	Schematic layout of AES experimental setup.....	48
3.5	(a) Load function of trapezoidal single indentation test with; I: loading, II: holding and III: unloading segments, (b) Schematic of load-displacement curve.....	56
3.6	Load function of cyclic trapezoidal indentations	57
4.1	Friction, temperature and temperature gradient vs. number of cycles, data for a test run under 24 Kg applied load using a ¼” diameter ball (3.56 GPa Hertzian load, on base oil + ZDDP with 0.10 wt% P) and the resulted wear profiles of the wear track generated on the surface of the ring at different stages; (a) At the start of the test, (b) the onset of the plateau region, (c) in the middle of the plateau region, (d) at the end of the plateau region and the start of the breakdown of the tribofilm, (e) at the end of the 25000 cycles.....	62
4.2	Temperature vs. number of cycles of three tests run using base oil + ZDDP (0.10 wt% P) using a ¼” diameter ball, with the applied loads of 3.35 GPa (a), 3.46 GPa (b) and 3.56 GPa (c), Lines I and II indicate the onset and the end of the plateau region associated with the formation and breakdown of the tribofilm respectively. The onset temperature for each load is also shown in each graph and indicates an increase of between 5-10 degrees Celsius with increasing applied load	64
4.3	Wear volume data for tests run on three different formulations, containing ZDDP alone and with anti oxidant and detergent are shown. The tests were run using a ½ inch-diameter scuffing ball, for 25000 cycles.....	65
4.4	Wear volume vs. Hertzian contact load for the two different formulations: Base Oil + ZDDP with 0.10 and 0.05 wt% P. The tests were run using ¼ inch diameter tungsten carbide balls for 25000 cycles.....	67
4.5	Bright field transmission electron micrograph (20K x magnification) of the wear debris harvested from wear tests run using oil containing base oil with 0.1 wt.% P at a Hertzian contact load of 3.56 GPa for (a) 5000, (b) 15000 and (c) 25000 cycles	67
4.6	Energy dispersive X-ray (EDS) spectrum obtained from wear debris harvested from base oil sample containing ZDDP (0.10 wt% P) after 15000 cycles at the Hertzian contact load of 3.56 GPa	68

4.7	Secondary electron image of the wear track. The wear track shows a well-developed tribofilm over most of the surface, however, at certain locations the film has been ripped off from the surface.....	70
4.8	Energy dispersive X-ray (EDS) spectrum obtained from the tribofilm covering the wear track shown in figure 4.7	70
4.9	(a) A trench cut into the surface of a ring that was tested under boundary lubrication conditions. The smooth surface is a the tribofilm formed on the surface. The milling of the surface was conducted with gallium ion beam. (b) The image shows that the thickness of the tribofilm is approximately 100 nm thick and forms a very smooth surface conforming well to the substrate. The substrate is a 4140 steel with a fine pearlitic / bainitic microstructure. When ion milled, the softer Fe phase is preferentially removed revealing the underlying carbide structure.....	71
4.10	Force vs. displacement (penetration) graph for peak indentation loads ranging from 25 to 100 μ N for the wear test run using oil containing base oil with 0.1 wt.% P at a Hertzian contact load of 3.56 GPa for 15000 cycles.....	72
4.11	Plots of (a) reduced modulus and (b) hardness versus contact depth obtained from indents with peak loads ranging from 25 to 100 μ N for the same sample as in figure 4.10	74
5.1	Tribological data for wear test run for 15000 cycles under 3.56 GPa Hertzian contact load on oils containing 0.10 wt% P: (a) temperature and (b) friction vs. number of cycles (c) wear volume data.....	78
5.2	Tribological data for wear test run for 15000 cycles under 3.05 GPa Hertzian contact load on oils containing 0.01 wt% P: (a) temperature and (b) friction vs. number of cycles (c) wear volume data.....	79
5.3	Tribological data for wear test run for 50000 cycles under 3.05 GPa Hertzian contact load on oils containing 0.01 wt% P: (a) temperature and (b) friction vs. number of cycles (c) wear volume data.....	80
5.4	Wear data show for wear tests run on samples containing ZDDP and fluorinated ZDDP in base oil (0.10 wt% P) run under 3.56 GPa Hertzian contact load for 25K cycles.....	81
5.5	Wear data show for wear tests run on samples containing ZDDP and fluorinated ZDDP in fully formulated oil (0.01 wt% P) using the Plint® BOCLE	82

5.6	(a) Scanning electron micrograph of wear track from wear test run under 3.56 GPa Hertzian contact load for 15000 cycles on oil sample containing base oil and ZDDP (0.10 wt% P) and (b) EDS spectrum from the tribofilm Schematic layout of AES experimental setup.....	83
5.7	(a) Scanning electron micrograph of wear track from wear test run under 3.56 GPa Hertzian contact load for 15000 cycles on oil sample containing base oil and fluorinated ZDDP (0.10 wt% P) and (b) EDS spectrum from the tribofilm Schematic layout of AES experimental setup	83
5.8	Scanning electron micrographs of post test wear scar on the scuffing ball at (a) 100x and (b) 500x magnification for the wear test run under 3.56 GPa Hertzian contact load for 15000 cycles on oil sample containing base oil and ZDDP (0.10 wt% P). Several patches of tribofilm are observed as dark spots inside the wear scar, and (c) the EDS spectrum obtained from a patch of tribofilm.....	85
5.9	Scanning electron micrographs of post test wear scar on the scuffing ball at (a) 100x and (b) 500x magnification for the wear test run under 3.56 GPa Hertzian contact load for 15000 cycles on oil sample containing base oil and fluorinated ZDDP (0.10 wt% P). Several patches of tribofilm are observed as dark spots inside the wear scar, and (c) the EDS spectrum obtained from a patch of tribofilm.....	86
5.10	SEM micrographs of cross section of tribofilm and substrate on the edge of a trench ion milled by FIB for oils containing base oil and (a) ZDDP and (b) fluorinated ZDDP (both with 0.10 wt% P)	88
5.11	Load vs. vertical displacement graphs for peak indentation loads from 25 TO 100 μ N for tribofilms generated from (a) base oil + ZDDP and (b) base oil + fluorinated ZDDP	90
5.12	Plots of (a) hardness and (b) reduced elastic modulus vs. contact depth (vertical displacement of the tip) obtained from indents with peak loads ranging from 25 μ N to 1500 μ N for both tribofilm samples.....	92
5.13	Data from a 5000 μ N ramped force scratch test on the two tribofilm samples: (a) normal load (controlled) vs. vertical displacement and (b) lateral measured force and (c) coefficient of friction vs. lateral displacement (controlled).....	94
5.14	Three dimensional graphical SPM images of the tribofilm surfaces after scanning wear tests for (a) ZDDP and (b) fluorinated ZDDP tribofilms and (c) the cross sectional profile of worn surfaces.....	96

5.15	Transmission electron micrographs of wear debris flakes from ZDDP observed at (a) 20Kx and (b) 200Kx magnification, (c) diffraction pattern generated by the embedded particles and (d) the EDS spectrum obtained from the wear debris flakes	98
5.16	Transmission electron micrographs of wear debris flakes from fluorinated ZDDP observed at (a) 20Kx and (b) 200Kx magnification, (c) diffraction pattern generated by the embedded particles and (d) the EDS spectrum obtained from the wear debris flakes	99
5.17	(a) Bright field transmission electron micrograph (200Kx magnification) of the wear debris harvested from wear tests run using oil containing base oil with 0.1 wt.% P at a Hertzian contact load of 3.56 GPa for 15000 cycles and (b) the corresponding electron diffraction ring patterns and calculated d_{hkl} values	101
5.18	Auger phosphorus peaks for tribofilms generated using base oil and (a) ZDDP and (b) fluorinated ZDDP	103
5.19	Auger sulfur peaks for tribofilms formed by (a) ZDDP and (b) fluorinated ZDDP	104
5.20	A graph of concentration (arbit. units) vs. sputtering time (min) of phosphorus, sulfur and iron for (a) ZDDP (0.1 wt. % P) and (b) fluorinated ZDDP (0.1 wt. % P) in mineral oil	105
6.1	Phosphorus K-edge XANES spectra collected in TEY mode for tribofilms generated by samples containing base oil and ZDDP or fluorinated ZDDP under 16, 20 and 24 Kg applied scuffing loads and the same spectra recorded for model compounds, $Zn_3(PO_4)_2$ and $FePO_4$	108
6.2	Phosphorus K-edge XANES spectra collected in FLY mode for tribofilms generated by samples containing base oil and ZDDP or fluorinated ZDDP under 16, 20 and 24 Kg applied scuffing loads and the same spectra recorded for model compounds, $Zn_3(PO_4)_2$ and $FePO_4$	109
6.3	Phosphorus K-edge spectra (FLY mode) of untreated ZDDP powder and $Zn_4P_6O_{19}$ collected by Li and Kasrai <i>et al.</i>	110
6.4	Phosphorus L-edge XANES spectra collected in FLY mode for tribofilms generated by samples containing base oil and ZDDP or fluorinated ZDDP under 24 Kg applied scuffing load and the same spectra recorded for model compounds $FePO_4$, $Fe_4(P_2O_7)_3$ and $Zn_3(PO_4)_2$	111
6.5	Phosphorus L-edge spectra obtained by Kasrai <i>et al.</i> for different zinc polyphosphates	113

6.6	Sulfur K-edge XANES spectra collected in TEY mode for tribofilms generated by samples containing base oil and ZDDP or fluorinated ZDDP under 16, 20 and 24 Kg applied scuffing loads and the same spectra recorded for model compounds, ZnSO ₄ and ZnS.....	114
6.7	Sulfur K-edge XANES spectra collected in FLY mode for tribofilms generated by samples containing base oil and ZDDP or fluorinated ZDDP under 16, 20 and 24 Kg applied scuffing loads and the same spectra recorded for model compounds, ZnSO ₄ and ZnS.....	115
6.8	Sulfur L-edge XANES spectra collected in FLY mode for tribofilms generated by samples containing base oil and ZDDP or fluorinated ZDDP under 24 Kg applied scuffing load and the same spectra recorded for model compounds FeS and ZnS	116
6.9	Representative load, modulus and hardness vs. penetration graphs for tribofilms generated by fluorinated ZDDP and ZDDP (800 ppm P in base oil) by tests run under 16 Kg scuffing load for 15K cycles	119
6.10	Representative load, modulus and hardness vs. penetration graphs for tribofilms generated by fluorinated ZDDP and ZDDP (800 ppm P in base oil) by tests run under 20 Kg scuffing load for 15K cycles	120
6.11	Representative load, modulus and hardness vs. penetration graphs for tribofilms generated by fluorinated ZDDP and ZDDP (800 ppm P in base oil) by tests run under 24 Kg scuffing load for 15K cycles	121
6.12	Representative load, modulus and hardness vs. penetration graphs for tribofilms generated by fluorinated ZDDP and ZDDP (800 ppm P in base oil) by tests run under 24 Kg scuffing load for 5K cycles.....	122
6.13	Representative load, modulus and hardness vs. penetration graphs for tribofilms generated by fluorinated ZDDP and ZDDP (800 ppm P in base oil) by tests run under 24 Kg scuffing load for 25K cycles	123
6.14	Representative load, modulus and hardness vs. penetration graphs from cyclic nano-indentation tests performed on tribofilms generated by fluorinated ZDDP and ZDDP (800 ppm P in base oil) by tests run under 16 Kg scuffing load for 15K cycles	127

6.15	Representative load, modulus and hardness vs. penetration graphs from cyclic nano-indentation tests performed on tribofilms generated by fluorinated ZDDP and ZDDP (800 ppm P in base oil) by tests run under 20 Kg scuffing load for 15K cycles	128
6.16	Representative load, modulus and hardness vs. penetration graphs from cyclic nano-indentation tests performed on tribofilms generated by fluorinated ZDDP and ZDDP (800 ppm P in base oil) by tests run under 24 Kg scuffing load for 15K cycles	129
6.17	Representative load, modulus and hardness vs. penetration graphs from cyclic nano-indentation tests performed on tribofilms generated by fluorinated ZDDP and ZDDP (800 ppm P in base oil) by tests run under 24 Kg scuffing load for 5K cycles	130
6.18	Representative load, modulus and hardness vs. penetration graphs from cyclic nano-indentation tests performed on tribofilms generated by fluorinated ZDDP and ZDDP (800 ppm P in base oil) by tests run under 24 Kg scuffing load for 25K cycles	131
7.1	Tribofilm model constructed based on SEM and EDS data of tribofilms formed on the wear track of steel rings from ball on cylinder lubricity evaluation tests	133
7.2	Tribofilm model further constructed based on film thickness measurements (using FIB) and EDS data of wear debris (TEM) and transfer films formed on the scuffing balls from BOCLE tests.....	133
7.3	Tribofilm model further constructed based on Auger electron spectroscopy data	134
7.4	Tribofilm model further constructed based on nano-mechanical and nano-indentation testing data and observations.....	135
7.5	Tribofilm model further constructed based on XANES spectroscopy data.....	137

LIST OF TABLES

Table	Page
1.1 Common engine oil additives	2
1.2 Timeline of phosphorus (P) and sulfur (S) limits in engine oil specifications	4
2.1 DSC measurements of decomposition temperature of ZDDP in the presence of some of the additives used in commercial engine oils.....	30
3.1 Summarized specifications of the two BOCLE units used	40
3.2 Lubricant and surface parameters and calculated effective film thicknesses for the UTA BOCLE unit operating under 24 Kg (235.2 N) applied load.....	42
3.3 Lubricant and surface parameters and calculated effective film thicknesses for the Plint® BOCLE unit operating under 30 Kg (279 N) applied load.....	43
3.4 Specifications of the beamlines used in this study	53
4.1 Test matrix of wear tests performed	66
5.1 The calculated dhkl spacing for the ring patterns observed in figure 5.17 compared to observed values for iron and two types of iron oxide.....	102
6.1 Wear test matrix run for XANES and nano-indentation studies	107

CHAPTER 1

INTRODUCTION

Internal combustion engines provide the workhorse for most means of land transportation in today's world. Driven by ever-increasing fuel prices and energy costs coupled with environmental concerns, internal combustion engines have evolved into becoming more efficient than before. The technological advances that have led to higher efficiency, better fuel economy, lower emission and increased performance of these engines, have also resulted in the fact that today's engines perform under far more punishing conditions, examples of which include higher working temperature and higher mechanical stresses and speeds in the drive train. In conventional automobile engines for example the cam and lifter mechanisms commonly work at speed and undergo stresses as high as 1GPa or 1×10^9 Pascal [2]. The severity of the conditions under which engines operate had led to renewed interest in improving the performance and properties of the lubricants in engines since engine oils play the most important role in preventing engine parts from wearing and their performance is directly linked to the durability of automobile engines. Engine oils are made of carrier base oil (either mineral or synthetic or a blend of the two) and the additive package, which is present at typical 10wt% of the final blend. Additives are important to enhance different aspects of the performance of oils [3]. Engine oil additives are a relatively broad group of chemicals each designed to perform a certain task in engine oils. The most important types of engine oil additives are listed in table 1.1 with common examples of each of these additives.

One of the most important groups of additives present in engine oils are Zinc Dialkyl Dithiophosphates (ZDDPs) which primarily serve as antiwear additives as well as anti-oxidants [3, 8-11], detergents [6, 12] and extreme pressure agents [13]. ZDDPs have been continuously

used as anti wear additives in engine oils for over sixty years and are arguably the most successful engine oils additives ever invented [14].

Table 1.1: Common engine oil additives [3-7]

Engine Oil Additive	Primary Purpose	Common Example(s)
Antiwear Additives	Wear prevention	Zinc Dialkyl Dithiophosphats (ZDDPs)
Anti-oxidants	Enhancing oxidation stability of oil	Alkylated Diphenol Amines
Detergents	Protecting the oil against sludge formation	Calcium Sulfonate
Dispersants	Dispersing particles	Polyisobutylene (PIB) succinimide
Viscosity Index Improvers	Reducing difference in viscosities at different temperatures	Olefin Co-Polymers
Friction Modifiers	Improve its surface film forming characteristics	Organo-molybdenum compounds e.g. Molybdenum Dithiocarbamate
Rust/corrosion inhibitors	Preventing corrosion of engine surfaces and bearings	Barium Sulfonates Calcium Phenates
Foam Depressants	Retard the formation of foam and frothing in oil	hydrogen and silicon compounds

The mechanism by which ZDDP performs as an antiwear additive, involves break down of ZDDP and its reaction with the steel surface by Zn → Fe ion exchange and subsequent formation of an amorphous chemisorbed film containing zinc, phosphorus, oxygen and sulfur and also iron in the form of polyphosphates and sulfates of zinc and iron at temperatures above 80°C [3, 8, 10, 15-18]. Other studies using X-ray Absorption Near Edge Structure (XANES) spectroscopy have indicated that the film is made up two layers, with the outer layer consisting of long chain polyphosphates and the inner layers composed of shorter chain polyphosphates [19]. At lower temperatures the main antiwear mechanism of ZDDP is based on the formation of

a physisorbed film on the surface of the rubbing surfaces [15]. A recent review highlights many of the different theories on the formation of tribofilms generated by ZDDP [10] however none of these theories are conclusive on the matter and further studies will still be necessary to achieve a more accurate and comprehensive understanding of mechanisms of the anti wear action of ZDDP.

1.1 Drive for this research

Today, ZDDPs are the sole source of phosphorus in engines oils. Phosphorus that finds its way in the exhaust gases has been found to poison the catalytic converters in the exhausts system [20, 21]. These catalysts are connected to the exhaust pipe in automobiles. They are designed to convert harmful exhaust emissions (e.g. CO, NO_x, hydrocarbons) into harmless gaseous compounds (e.g. CO₂, NO₂, H₂O) before releasing them into the atmosphere thus reducing the detrimental effects of car emissions to the environment. Phosphorus (and sulfur) containing exhaust products (e.g. Phosphorus Oxides) have been shown to reduce the efficiency and the effective life of the catalyst in the catalytic converters by poisoning the catalytic sites in converter. This has been a major driving force behind progressive introduction of limits aimed first at reducing the amount of phosphorus and recently the amount of sulfur as well in engine oils. In the US, the current regulations for the latest generation of engines oils (GF4) restrict the phosphorus level in engine oils to a range of 0.06 to 0.08 weight percent while in 1980, engine oils could contain up to 1.2 weight percent phosphorus [14]. Similarly, the Sulfur and ash content in engine oils have also been subject to environmental regulations, further reducing the limit on the amount of ZDDP that can be added to engine oils. Table 1.2 shows the Phosphorus and Sulfur limits in engine oil specifications since these regulations have been put in place [14]. Reduction in the amount of ZDDP in engine oils compromises the anti wear properties and oxidation resistance of engine oils and significantly reduces engine life due to wear and oxide formation which can also lead to loss of energy efficiency as well as increased emissions. Addressing the environmental concerns associated with the presence of ZDDP in

engine oils while maintaining (and improving) antiwear properties of engine oils and thus not compromising engine durability and efficiency, poses significant challenges to oil and auto industry researchers as well as academic researchers working in the area of Tribology and lubrication.

Table 1.2: Timeline of phosphorus (P) and sulfur (S) limits in engine oil specifications [14]

1989	SG	No P, S limits
1994	SH, GF-1	≤ 0.12 % wt P
1997	SJ, GF-2	≤ 0.1 % wt P
2000	SL, GF-3	≤ 0.1 % wt P
2004	GF-4	$0.06 \text{ wt}\% \leq P \leq 0.08 \text{ wt}\%$ $\leq 0.5\% \text{wt S}$

These challenges cannot be tackled without a comprehensive understanding of the mechanisms that dominate the antiwear behaviors of engine oils containing ZDDPs. In spite of more than five decades of research work, the complexity of the antiwear mechanism by which ZDDP performs and the effect of other additive chemistries present in engine oils as well as difficulty in simulating different tribological systems and conditions present in engines has left us with very little understanding of the actual mechanisms involved. Achieving lower or zero phosphorus content in engine oils without losing antiwear benefits coming from ZDDP would require replacing ZDDP with phosphorus-free anti wear chemistries. Substantial research effort is has been done and is being done in this area by different research groups both in the industry and academia [14] but so far, there has been little success in finding a replacement compound for ZDDP that is both economically and environmentally a feasible choice [10]. Another approach is enhancing the anti wear action of ZDDP by modifying and fine tuning the molecular structure of ZDDP so that smaller amounts of the chemistry will be able to yield the same wear protection. In pursuit of the latter solution, the tribology research team at the University of Texas at Arlington has been able to fluorinate the ZDDP [22]. Fluorinated ZDDP with fluorine-phosphorus bond has been synthesized using Iron (III) Fluoride. Interactions between ZDDP

and FeF_3 and the synthesis process as well as the possible chemical structure of the fluorinated ZDDP have been studied by Mrs. Kajal Parekh and published in detail in her doctoral thesis [1] and will be reviewed briefly. Whilst preliminary data, had indicated the superiority of the anti wear action of fluorinated ZDDP over regular ZDDP, many questions remained unanswered on the mechanisms involved resulting in the observed improvement.

1.2 Objectives of research

This research work is aimed at establishing the superiority of fluorinated ZDDP over untreated ZDDP under tribological conditions similar to conditions in the internal combustion engines and to investigate the actual role of fluorine introduced in the molecular structure of ZDDP. An essential part of this study includes understanding the antiwear actions of fluorinated ZDDP as well as regular ZDDP by studying the formation mechanisms of anti wear films and characterizing these tribofilms from these two chemistries under different tribological conditions. The characterization methods employed will further deepen our understanding of the ZDDP and fluorinated ZDDP tribofilms from different properties standpoints. These characterization methods include several mechanical and chemical surface analysis methods that will look at the chemical compositions of the tribofilms through out the depth of the films as well as mechanical properties of these films, e.g. adhesion to substrate, modulus, scratch resistance, etc. Some of the techniques used in the process are unique to this research work and have not been used before for the purpose of characterizing tribofilms generated from ZDDP (and Fluorinated ZDDP). Many research groups have been actively involved in studying the anti wear action of ZDDP containing oils, trying to put together the pieces of the puzzle that has yet to be completed. Invaluable research work have been conducted by Zhang and Kasrai, *et al.* [23, 24], J.M. Martin, *et al.* [8, 25-29] and many others [30-33]. Müser, Nicholls, *et al.* have also predicted the anti wear mechanisms of pressure induced ZDDP tribofilms by using molecular scale simulation and modeling [34-37]. The methods used in this research work takes into account these recent works and their findings to further advance the current state of knowledge in this

field. Another aspect of the uniqueness of this study is the use of fluorinated ZDDP as an alternative to ZDDP. The fluorination of ZDDP has been attempted before, however, the existence of a phosphorus-fluorine bond was first observed as a result of the unique fluorination process developed at UTA [1] using iron (III) fluoride (FeF_3). The research work and characterization done on this fluorinated ZDDP will indeed be unique, as we will explore the benefits of replacing regular ZDDP with the fluorinated ZDDP. Preliminary studies had shown the fluorinated ZDDP to be superior to ZDDP as an anti wear additive. A more efficient chemistry will mean that smaller amounts of phosphorus, zinc and sulfur will need to be present in the engine oil to yield the same anti wear properties that would be needed if regular ZDDP is to be used.

1.3 Structure of this research

This dissertation is presented in seven chapters. Each chapter is included here with an outline and summary of contents detailed in the chapter later.

Chapter 1, introduction: This chapter introduces the reader to the drive and objectives behind the whole research work. It also includes a summary of what can be gained from such a study from research point of view.

Chapter 2, background: This chapter gives an overview tribology in internal combustion engines, engine oils, different types of wear phenomena, lubrication and wear in internal combustion engines, including different lubrication regimes. The structure, chemistry and antiwear mechanism of ZDDP and fluorinated ZDDP and ZDDP-additive interactions are also review in this chapter. The final section of this chapter reviews the nature and different types of tribological testing methods and their characteristics and reliability of their data.

Chapter 3, approach and experimental: Experimental methods and testing and characterization techniques used in this study are reviewed in the third chapter of this dissertation. This chapter includes an overview of the tribotesters used to produce wear data as well as the tribofilms samples. The type lubrication regime, dominant in these wear tests is also investigated.

Different characterization techniques reviewed in this chapter are SEM/EDS, FIB, TEM, AES, XANES, and nano-mechanical testing.

Chapter 4, lubrication with ZDDP under extreme pressure conditions: This chapter describes part of the study that was initially carried out on ZDDP to study the lubrication and antiwear properties and behavior of ZDDP under the conditions of the tribotests used for this study. ZDDP tribofilms generated by these tests are studied using some of the characterization techniques described in chapter 3.

Chapter 5, comparison of tribological behavior of fluorinated ZDDP and ZDDP: This chapter is the main part of dissertation and bulk of the data from both wear tests and characterization techniques on tribofilms formed by both chemistries (fluorinated ZDDP and ZDDP) are presented and discussed.

Chapter 6, load and duration effects studies: In this chapter, recent XANES and nano-indentation data from a test matrix designed to study the effect of scuffing load and test duration on tribofilms from ZDDP and fluorinated ZDDP are presented and discussed.

Chapter 7, ZDDP and fluorinated ZDDP; a phenomenological model: a comparative phenomenological model of the tribofilms generated from ZDDP and fluorinated ZDDP is developed. The model is hypothesized, based on the data acquired from different characterization techniques used in studying the tribofilms from both chemistries, i.e. SEM, EDS, TEM, AES, XANES spectroscopy and nanomechanical testing.

Chapter 8: conclusions: This chapter concludes on the dissertation and provides an overview of the scope of more research work that could supplement and/or complement this work.

CHAPTER 2

BACKGROUND

2.1 Tribology of engines: An Overview

Tribology is the study of the interactions between surfaces that are in contact and spans many disciplines including physics, chemistry as well as mechanical engineering and materials science [38, 39]. Contact between two surfaces that are in relative motion, is typically associated with a force resisting the sliding of the two surface against one another. This force is known as friction. In many cases, friction between moving parts in an engine is an undesired phenomenon that results in loss of energy as well as loss of material from the surfaces of these parts, i.e. wear. Almost all mechanisms lose their durability and reliability due to wear and internal combustion engines are not an exceptions. A significant portion of fuel energy losses in internal combustion engines occurs through overcoming friction forces in bearings, valve train, piston rings, and other moving parts of the engines and thus reducing friction in these locations, even in small scales can result in substantial improvements in fuel economy and thus reduction of emissions [1, 40]. Engine lubricants are designed to reduce friction as well as reduce and prevent wear in engines. Figure 2.1 shows in a general way the energy of the fuel is distributed in an automobile. About 60% of the energy generated by the fuel is dissipated and lost as heat through either cooling of the engine block or through exhaust gases. Mechanical losses (mainly from friction) account for 15% the total energy generated by the combustion process of the fuel. Only 25% of the energy generated ends up providing the power responsible for the motion of the vehicle [41]. About 80% of the mechanical losses are due to friction losses and they mainly occur in the piston assembly (about half) as well as bearings and the valve train (25 and 10% respectively, see figure 2.1).

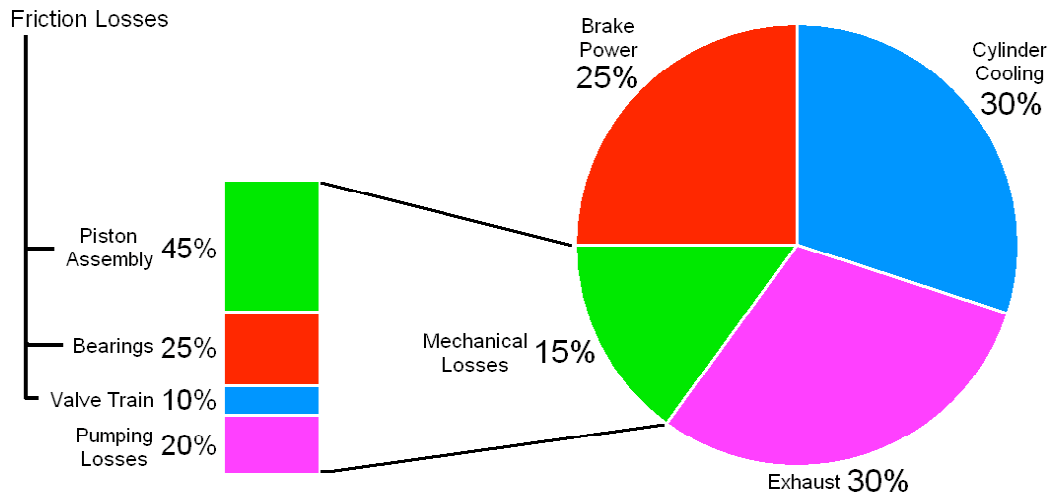


Figure 2.1: Typical fuel energy and mechanical loss distributions in an internal combustion engine [41].

Although much research has been directed towards improving engine efficiency by reducing the thermal losses (i.e. cooling and exhaust losses), the significance of mechanical losses should not be overlooked. It is estimated that a reduction of about 10% in the mechanical losses could lead to 1.5% (or more) reduction in fuel consumption through out the average life-span of automobile [41]. Although this may seem like a modest improvement it is significant in scope as millions of vehicle travel our roads and any such improvement could translate to significant savings in fuel costs as well as measurable reduction in emissions. In order to address the durability issues due to wear as well as friction mechanical losses, it is important to understand the lubrication and wear phenomena in internal combustion engines.

2.2 Wear in engines

2.2.1 Definition and mechanisms

Wear is generally defined as the phenomenon of material removal from a surface due to interaction from a mating surface. Wear is normally measured by measuring either the mass or the volume of the material removed due to contact between two surfaces [38, 42]. Wear is the result of material removal by physical separation due to microfracture, by chemical

dissolution, or by melting at the contact interface. From the viewpoint of contact configuration, i.e. motion of contacting surfaces, their geometry and the presence of third body particles interacting with the two surfaces, wear can be classified in different regimes that include (but are not limited to) normal or inclined compression and detachment, unidirectional sliding, unidirectional rolling, reciprocal sliding, reciprocal rolling, slipping, etc. Based on the mechanism by which wear occurs, wear can be classified into four major modes. The four fundamental wear modes are abrasive, adhesive, fatigue, and corrosive wear. In most cases, wear takes place through several modes of wear that may become the dominant mode of wear at different stages in tribological systems [43]. Figure 2.2 shows a schematic presentation of four representative modes of wear [38].

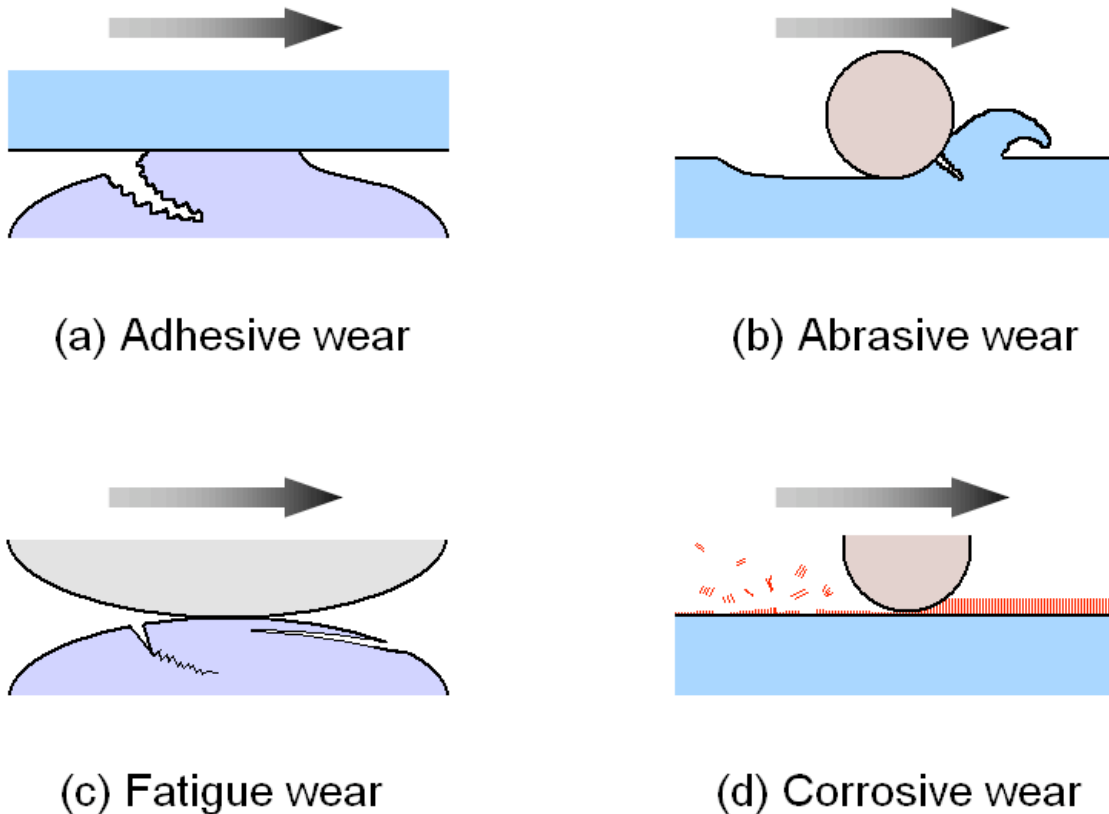


Figure 2.2: Schematic images of four representative wear modes.

2.2.1.1 Adhesive wear

Adhesive wear occurs when adhesive bonding between the contacting surfaces is strong enough to resist their relative motion resulting in large plastic deformations in the contact area due to compression and shearing. Plastic deformations lead to crack initiation; propagation and separation of material in the form of wear debris (figure 2.2 a). In most tribological systems experiencing adhesive wear, the process of adhesion, deformation (compression and shear) and wear debris formation is repeated over and over again resulting in the formation of relatively abundant and large wear particles contributing to further wear of the abrasive mode since the generated wear debris are generally abrasive due to high hardness (as a result of plastic deformations) and oxidation [38, 44].

2.2.1.2. Abrasive wear

Abrasive wear occurs when a relatively harder surface with a curved geometry slides on a relatively softer surface and removes material from the softer surface by ploughing through it (figure 2.2 b). In many cases (where relatively ductile metallic surfaces are present) the abrasive component of the tribological system are asperities and wear debris generated by different wear processes. These asperities and wear particles, in the case of metallic surfaces, are generally heavily work hardened (due to plastic deformations) and often oxidize quickly, turning into hard and brittle oxides and thus are much harder than the metallic surfaces the originated from. Depending on whether the nature and origin of the abrasive component, two types of abrasive wear regimes are generally recognized: (a) two body abrasion and (b) three body abrasion. In the latter mode, the abrasion is done by third body particles, e.g. wear debris [38, 45, 46].

2.2.1.3 Fatigue wear

There are other cases of wear where a certain number of repeated contacts are essential for the generation of wear particles by initiation and propagation of fatigue cracks. Wear generated after such contact cycles is called fatigue wear (figure 2.2 c). When the number

of contact cycles is high, the high-cycle fatigue mechanism is expected to be the wear mechanism. When it is low, the low-cycle fatigue mechanism is expected [38, 47].

2.2.1.4 Corrosion wear

Chemical reactions can occur on the contact surfaces in a tribological system due to presence of oxygen, corrosive liquids (third body), lubricants and other materials that can react with the surface materials. These tribochemical reactions can produce reaction films on the sliding surfaces. Shearing forces due to friction can remove this layer in the form of wear debris, thus resulting in overall removal of material from the surfaces. This process is known as corrosion wear (figure 2.2 d). The most common example of corrosion wear is oxidative wear observed on many metallic surfaces, including steels. In the case of steel, reaction with oxygen (from atmosphere or lubricant) results in forming of iron oxides. The oxide layer in this case is usually a mechanically weak and non-adherent layer is scraped off easily due to sliding friction and contact with asperities of the opposite sliding surface. Iron oxides particles generated during this wear process are by themselves, abrasive by nature and their entrapment between the two sliding surfaces leads to abrasive wear. This is another example of two wear modes simultaneously in action.

2.2.2 Stages of wear in tribosystems

Often, the wear process will undergo several stages as sliding of two surface against each other proceeds; at least three stages are normally identified during any wear process: At start-up the wear process begins with what could be called a break-in stage, during which steady-state conditions are building up (figure 2.3). The break-in may be very important for some sliding systems, as for many types of bearings and gears. During this stage the mating surfaces conform to each other in such a way that the load is more favorably distributed over the surfaces. During the early break-in stages, the wear rates may be relatively high since asperities on both mating surfaces abrade the opposing surface, leading to generation of conforming surfaces, larger contact area and smaller contact loads as a result of loads being

distributed over larger areas. In lubricated contacts, the break-in period is sometimes associated with the stage when protective, low friction tribofilms have not been formed yet. In these systems, high friction and relatively higher wear rates during the break in, provide the necessary conditions for tribochemical reactions necessary for the formation of anti—wear tribofilms that protect the surface during later stages of the wear process. Break-in is normally short compared to the whole lifetime of the component.

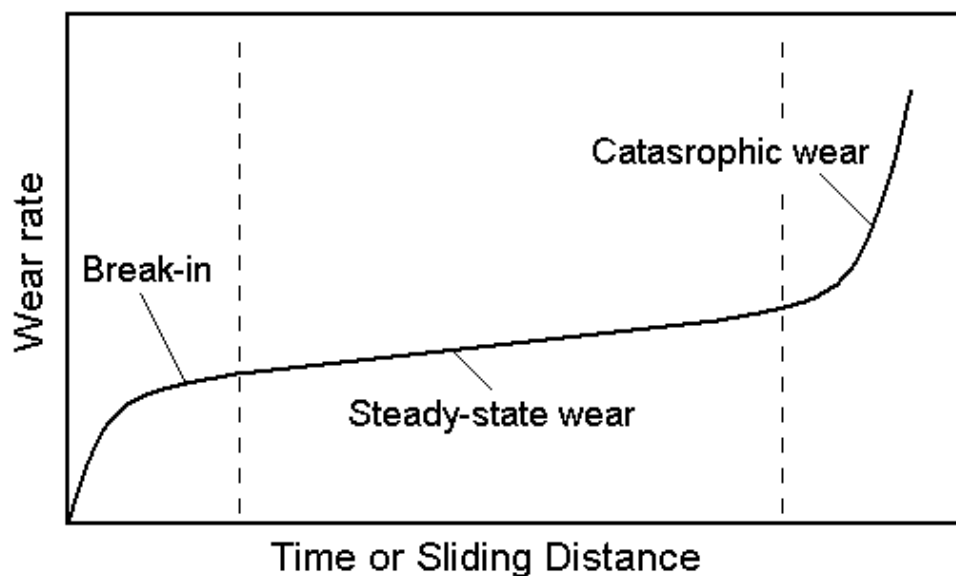


Figure 2.3: Typical wear stages appearing over longer service times in sliding contacts

Steady-state conditions with low wear rates and stable friction values should prevail for most of the lifetime of the system. In lubricated systems such as automobile engines, during the steady state conditions, a protective tribofilm is present that continuously undergoes wear and replenishment. The presence of the tribofilm in such lubricated systems minimizes wear of the components as the tribofilm itself works as a sacrificial layer against wear and compression and shearing forces. The steady state in these lubricated films will continue as long as the lubricant-surface tribological interactions favor new film formation and replenishment. Steady-state wear rates will eventually alter clearances or surface properties to the extent that components fail. In

lubricated systems this occurs when the lubricant is no longer able to participate in the tribochemical reactions that lead to formation and replenishment of a protective tribofilm. This failure results in a brief, final, catastrophic stage during which wear rates are high and severe surface damage occurs.

Only wear rates or friction forces measured during the relatively stable, steady-state conditions are useful in characterizing the long-term properties of the system. Damages to a failed component, which occurred just shortly before the failure, are not characteristic of the continuous wear of the materials, or the antiwear properties of the lubricant used in the system, and thus cannot explain the series of events leading to failure. Identifying the stage during which a component's surface damages (or their precursors) did appear, and what their importance is to overall performance of the component, is one of the more critical and challenging parts of analyzing the failure of tribological components and antiwear properties of lubricants used in them. To predict the onset of severe wear regimes is a challenge. In engine components, this corresponds to the onset of tribofilm failure as well as failure to replenish the film and it may occur due to a variety of reasons including degradation of the lubricant. Lubricant failure can occur as a result of oxidation, contamination (by wear debris, soot, carbon black, etc.) [48] or simply consumption of the antiwear chemistries, which makes replenishment of protective surface films impossible. Other reasons may include changing of working conditions such as speed of the components and the loads involved [38, 42, 43, 49].

2.3 Lubrication in internal combustion engines

Lubrication involves the process of introducing a layer of material (liquid, solid or a mix of both) in between two surface with relative motion and contact in order to reduce or prevent wear as well as to reduce friction. A lubrication system consists of moving surfaces under load with a lubricant in between [50]. The material introduced to perform this task is known as the lubricant. The type of lubricant employed for lubricating internal combustion engines is of liquid type and is primarily made of either mineral or base carrier oil together with the additive

package as discussed in chapter 1. In most cars, oil is pumped out of the oil pan and through the oil filter by the oil pump and then squirted under high pressure into bearings and cylinder walls before it tickles down into the sump where it is collected and pumped through the cycles again. Pistons and bearings (in camshafts and crankshaft) make up the two most critical lubrication systems in engines and need continuous lubrication. Apart from anti wear action and friction reduction, engine oils are also intended to dissipate the heat generated in engines (i.e. act as coolants) and to keep in suspension the contaminants and to remain effective in the presence of these contaminants which normally include water, acidic combustion products, and particulate matter (e.g. carbon black).

2.3.1 Lubrication regimes

Where liquid lubricants are employed to provide lubrication in components of a mechanism such as an automobile engine, three types of lubrication regimes may occur depending on different variables (e.g. load, surface roughness, amount of lubricant, etc.) that define the tribology of different components. These lubrication regimes have been identified as fluid film lubrication, *mixed* lubrication and *boundary* lubrication regimes.

2.3.1.1 Fluid film lubrication

In fluid film lubrication regimes, a thin film of liquid separates the solid components of a tribological system (i.e. the interacting surfaces) and the fluid film supports the load. In fluid film lubrication, the physical properties of the lubricant (e.g. viscosity, traction, load bearing capability, etc.) determine the performance capability. Fluid film lubrication can be divided into two different types; (a) *hydrodynamic* lubrication and (b) *elastohydrodynamic* lubrication. Hydrodynamic lubrication occurs where non-parallel interacting surfaces are present, providing for convergent fluid lubricant films which force the two surface apart and thus no contact is made possible between the two surfaces in relative motion. Journal bearings and thrust bearings are prototypes of hydrodynamic bearings [38, 39]. Under high contact loads, where deformable solid components are present, substantial local elastic deformations occur in fluid

film lubrication regime and the viscosity of the fluid film becomes a function of load while its effective thickness becomes insensitive to contact load. This form of fluid film lubrication is known as elastohydrodynamic (EHD) lubrication. [38, 51-54]. The effective thickness of the fluid film in EHD lubrication has been predicted by many equations, including those of Grubin [55], Dowson and Higginson [52], Archard and Cowking [56] and Hamrock and Dowson [53]. All these EHD theories have been shown to be in fair agreement with experimentally measured values [57]. Under more severe lubrication conditions, e.g. under extreme contact loads, the fluid film is no longer able to fully support the load and the surface asperities come into contact. Under these conditions, the lubrication regime becomes a mixed regime of boundary and EHD fluid film lubrication regimes.

2.3.1.2 Boundary lubrication

Boundary lubrication regime occurs at very high contact loads and low sliding speeds, as a result, considerable asperities interactions occur and asperities on the two rubbing surfaces collide and as result undergo deformations both elastic and plastic in nature as well as fracture [38, 51]. Even in fluid film lubrication, boundary lubrication occurs during start up and stopping, and during occasional asperity interaction that may occur during operation. Metal to metal contact between two surfaces in a lubricated contact results in shearing the surface asperities coming into contact, thus exposing fresh metal surface. The antiwear chemistries present in the lubricant (e.g. ZDDP in the case of engine oils), aided by frictional heating, react with the freshly exposed active surfaces and form protective surface thin films also known as tribofilms. Thus in boundary lubrication, both the chemistry of the lubricant and the material properties of the interacting surfaces, dictate the performance of the lubricant [38]. Tribofilms separate the two rubbing surfaces and are usually low-friction and wear resistant and protect the surfaces from further wear. During operation, these tribofilms can wear and regenerate.

Real surfaces in practical tribological systems consist of asperities of different sizes and thus when in contact, a wide range of stresses are produced within the contact zone. Therefore,

a mixed regime of boundary and EHL lubrication modes exists in such systems. An illustrated summary of different lubrication regimes is schematically shown in figure 2.4.

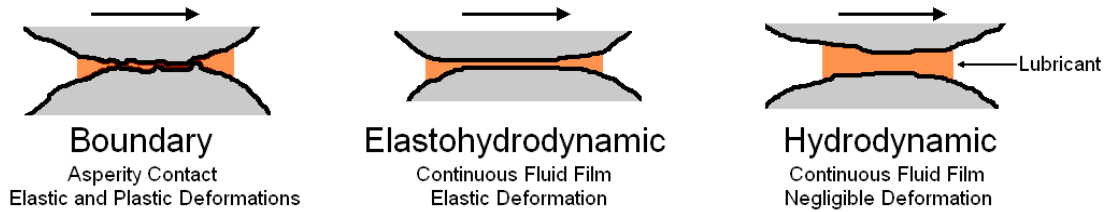


Figure 2.4: Schematic comparison of different lubrication regimes

2.3.1.3 Friction coefficient in lubricated contacts

Surface conditions and lubrication regime control tribological effects such as lubricant film thickness and coefficient of friction. Lubricated components of mechanical systems are normally designed to work under hydrodynamic lubrication regimes. Under these conditions, coefficient of friction is related to operating conditions, (i.e. absolute viscosity of oil, relative speed, component geometry, and load) by Petroff's formula. For journal bearings the Petroff's formula is stated by the following equation:

$$f = 2\pi^2 (r/c)(\mu N/P)$$

Equation 2.1

Where f is the coefficient of friction, μ is the absolute viscosity of the fluid lubricant, N is the shaft rotation speed, P is the load per unit of projected bearing area, r is the journal radius and c is the radial clearance. It has been observed that hydrodynamic lubrication regime which according to Petroff's formula translates to a linear relationship between coefficient of friction and the dimensionless bearing characteristic parameter $\mu N/P$ is only valid when $\mu N/P$ is greater than a certain value. This is intuitively obvious since lower viscosity oils (lower μ) are less likely to provide an adequate film thickness between the sliding surfaces to support contact loads and prevent asperity contact and/or interactions between the two surfaces. Also higher contact loads (higher P) will also result in squeezing out of the lubricant from the contact point as well as

making asperity contact more likely, which will result in the hydrodynamic lubrication to be lost and replaced by mixed mode and boundary lubrication regimes. This effect is shown in a graph known as Stribeck curve shown in figure 2.5 [38]. The Stribeck curve plays an important role in identifying boundary, mixed, elastohydrodynamic, and hydrodynamic lubrication regimes[58].

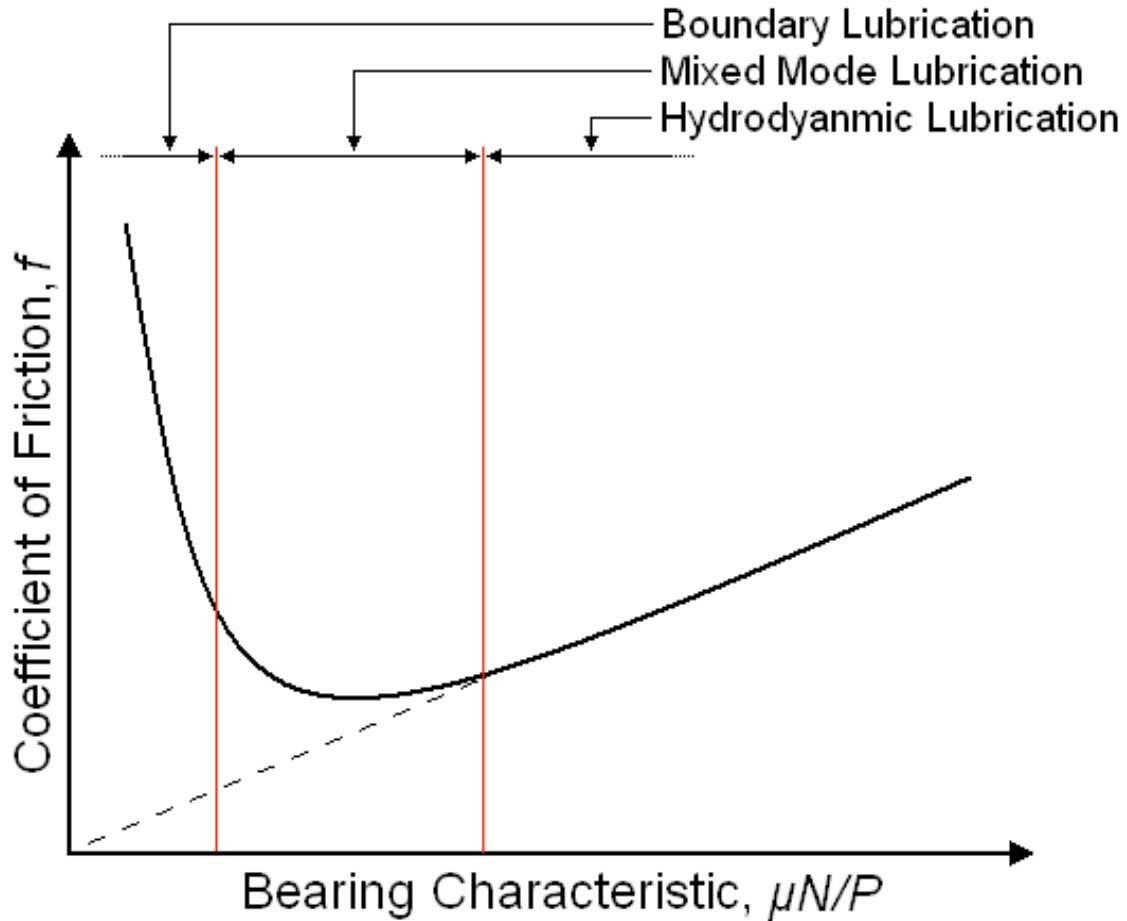


Figure 2.5: Stribeck curve

It is observed from the Stribeck curve that under boundary lubrication regime, friction follows a totally different trend with changing bearing characteristics. For example, increasing contact pressure actually increases coefficient of friction under boundary lubrication regime since it increases contact stresses between the asperities and thus increases chances of their

adhesion, which results in higher resistance against relative movement of the two surfaces and the coefficient of friction increases. Also low speeds under boundary lubrication will increase the number of asperities in contact with one another and will therefore have the same effect as increasing the contact load.

2.3.1.4 Lubricant film thickness in lubricated contacts

In fluid film lubrication regime, wear and friction both depend on the thickness of the lubricant film. The minimum film thickness in a lubricated contact, h_{\min} , is normally described by the dimensionless value, λ , which is also known as *dimensionless bearing stiffness* [1, 38, 51, 52], where $\lambda = h_{\min} / \Sigma R_a$ where ΣR_a is the sum of the average roughness (R_a) of the two surfaces, i.e. $\Sigma R_a = R_{a1} + R_{a2}$ where R_{a1} , R_{a2} are the roughness values for each surface. The value of λ is measure of the extent of asperity interactions during lubricated sliding and thus determines the type of lubrication regime present in a tribological system. For different lubrication regimes, the value of λ will fall in different ranges of values. In hydrodynamic fluid film lubrication regime where asperity contact is negligible and both friction and wear are very low, λ is larger than 5 ($\lambda > 5$). In elastohydrodynamic lubrication mode, the value of λ is smaller than 5, but normally larger than unity ($1 < \lambda < 5$). In boundary lubrication, where a thinner film compared to fluid film lubrication mode is present, the value of λ is generally smaller than unity ($\lambda < 1$) [1, 11, 38, 51, 52].

2.3.2 Antiwear additives and boundary lubrication

A significant portion of wear (nearly 70%) in engines occurs during the brief start up and acceleration periods. The amount of oil present in bearings and on cylinder surfaces is not enough to provide effective fluid film lubrication when engine is started. Lack of sufficient amount of lubricant results in asperity-asperity contact in these locations and thus the dominant lubrication regime during this short period is boundary lubrication regime. Reducing the amount of wear occurring at this time is determined by the presence of pre-formed solid tribofilms on these surfaces that are generated by the break down and antiwear action of antiwear additives

in oil. Antiwear additives are added to the base oil in order to form protective tribofilms during boundary lubrication [59]. When such protective films are formed, wear of mating materials is prevented and replaced by consumption of antiwear additive in the oil. Depending on the chemical nature of the antiwear additives, two types of antiwear effects have been identified by Martin, *et al.* [1, 59]:

1. Tribochemical reaction leading to formation of tribofilms by chemical reaction processes involving an active participation of both the contact surface material(s) and environmental factors (atmosphere, water etc) and their chemical interaction with the antiwear additive. In this case depending on the type of the additives, two types of mechanisms are observed:
 - a. Additives chemically react with the surface directly, e.g. sulfur and chlorine chemical compounds, fatty acids, fluorinated compounds.
 - b. Antiwear action by the additives occurs through thermal and/or oxidative degradation process of the additive e.g. metal dithiophosphates and phosphorus containing organic compounds.
2. Polymeric and non-sacrificial films. In this case, contact surfaces do not chemically partake in the formation of the antiwear film, although they may catalyze the process. This process also involves formation of high molecular weight compounds through polymerization process e.g. complex esters, solid lubricant additive like oil soluble molybdenum compounds, borate additives, double bond containing molecules etc.

Some antiwear additives used in engine oils include phosphate esters, sulfurized olefins, sulfurized sperm oil, metal dithiophosphates (e.g. zinc or molybdenum Dithiophosphates), borates and phosphites [1]. Of all antiwear additives, zinc dialkyl dithiophosphate has been the most cost effective antiwear additive and thus by far the most commonly used antiwear additives in conventional engine oil. The antiwear performance of ZDDP added to engine oils under boundary lubrication conditions depends on whether an effective antiwear tribofilm can be formed and be replenished continuously when worn.

A variety of film formation mechanisms have been proposed involving oxidation [17], hydrolysis [2] and thermal decomposition of ZDDP [60, 61]. A new theory based on computer simulations of zinc phosphates under extreme conditions, suggests that pressure-induced cross-linking is a key mechanism in the formation and functionality of antiwear tribofilms [34, 37, 62]. The properties of the boundary tribofilm formed under these conditions depend on the tribological decomposition products from ZDDP and other antiwear film-forming components and the interaction between these products and the surface(s). This is dictated by factors that include ZDDP concentration, the type of ZDDP used (basic or neutral, secondary or primary alcohol), contact pressure, temperature and surface chemistry, roughness and hardness [3, 15, 18, 63-65]. For example the presence of other components including detergents (e.g. calcium sulfonate) has been shown to generally have an antagonistic effect on the quality and effectiveness of the boundary lubrication film [9, 64, 66, 67]. Boundary lubrication conditions in engine parts have a significant contribution to the amount of wear observed in such components.

2.4 Zinc dialkyl dithiophosphates

2.4.1 Chemical structure and properties of ZDDP

The structural formula of ZDDP is shown in figure 2.6. *R* represents alkyl and/or aryl groups in the structure. When *R* represents alkyl groups (alkyl ZDDPs), it can either be primary, secondary or tertiary alkyl chain [11]. ZDDP is usually manufactured with dialkyldithiophosphates as intermediates, by a reaction of phosphorus pentasulfide with suitable alcohols. These intermediates (thiophosphates) are then neutralized by adding zinc oxide, yielding ZDDP. Whether the alkyl type *R* groups are of secondary or primary type as well as their chain length depends on the type of alcohols used in the manufacturing process of ZDDP. It has been observed that ZDDP derivatives containing alkyl type *R* groups generally have lower thermal stability but are better antiwear additives and have better hydrolytic stability than ZDDP derivatives with aryl *R* groups. Aryl type ZDDPs have a relatively higher manufacturing cost

than alkyl type ZDDPs. Aryl ZDDP films have different polyphosphate structure compared to the alkyl ZDDP films [68]. Among alkyl type ZDDPs, secondary alcohol ZDDP derivatives have been shown to be more effective antiwear additives than primary alcohol ZDDPs derivatives as they have lower thermal stability than primary alcohol ZDDPs [15, 69].



Figure 2.6 Structural formula of (neutral) ZDDP

Lower thermal stability normally translates to faster tribofilm formation during contact by the antiwear additive, thus ZDDP derivatives with lower thermal stability tend to have better antiwear performance in tribology bench tests that are usually run for much shorter periods of time in comparison to real life application of the lubricant. Since most engine oils are expected to perform for much longer time periods than bench tests, usually a blend of different ZDDPs is used in the additive package (usually a mixture of primary and secondary alcohol ZDDPs both in basic and neutral form). This helps in extending the antiwear performance of oil over the extended service cycle since the consumption of less thermally stable derivatives of ZDDP at the early stages of the service cycles ensures quick formation of an effective antiwear tribofilm while the presence of more thermally stable species of ZDDP that don't break down as early ensures a constant supply of antiwear chemistry towards the end of the service cycles of the engine oil.

2.4.2 Neutral and basic ZDDP

Commercially manufactured ZDDP is usually a mixture of two types of ZDDPs, i.e. neutral and basic. The structure shown in figure 2.6 is of the neutral ZDDP (monomer) with the

formula $[(RO)_2PS_2]_2Zn$. Depending on the nature of the alkyl group, the neutral ZDDP can exist as a dimer, or an infinite linear polymer in the solid state [70]. Both NMR [71, 72] and vibrational spectroscopy have shown that ZDDP exists as equilibrium between monomer and dimer in solution, as illustrated in figure 2.7 [1, 14].

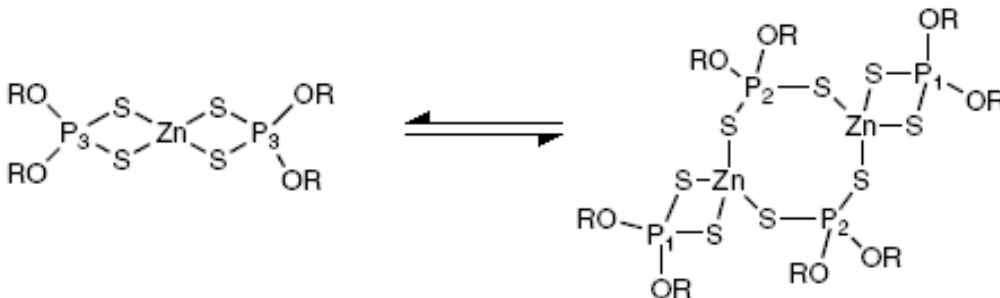
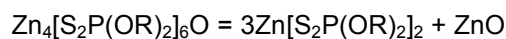


Figure 2.7: Monomer – dimer equilibrium of neutral ZDDP [72]

This equilibrium moves to favor the monomer as temperature is increased and, in both structures, four sulfur atoms are arranged equivalently in a tetrahedron around the zinc. The above findings were, however, carried out in relatively more polar solvents, and more recent, dynamic light scattering (DLS) work has suggested that there may also be tetrameric and even higher degrees of polymerization of ZDDP structures present in low polarity mineral oil solution [14, 73].

Basic ZDDP has the linear formula $[(RO)_2PS_2]_6Zn_4O$ with the molecular structure in solution shown in figure 2.8 [1, 14]. A Zn_4O core with four Zinc atoms in an almost perfect tetrahedral arrangement about a central oxygen atom has been observed in this structure. Basic ZDDP converts to ZnO and neutral ZDDP at elevated temperatures [74]. There has been little evidence of superiority of antiwear performance of either basic or neutral forms ZDDP and they have been found to be quite similar in that regard [68, 75, 76]. NMR studies by Harrison, *et al.* have shown that an equilibrium exists between basic and neutral ZDDP in solution with the following reaction [71]:



Equation 2.2

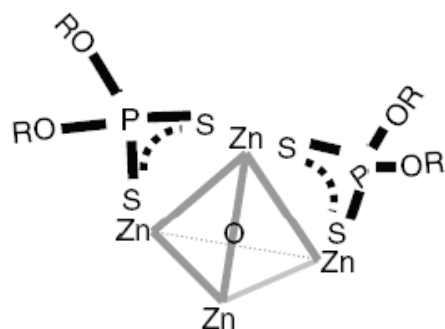


Figure 2.8: The structure of basic ZDDP [14]

2.4.3 Antiwear mechanisms of ZDDP

For the last sixty years, ZDDP has been added to engine oils to improve their antiwear and antioxidant properties. From the literature, three main ways that ZDDP acts as an antiwear agent have been proposed; (i) by forming a mechanically protective film; (ii) by removing corrosive peroxides or peroxy-radicals; (iii) by “digesting” hard and thus abrasive iron oxide particles [14]. As mentioned in section 2.3.2, in boundary lubrication, ZDDP reacts with the surfaces to form a protective film, referred to as a tribofilm. It is generally accepted that the tribofilm acts as a mechanical barrier preventing direct contact and adhesion between metal or metal oxide surfaces. The tribofilm is mainly an amorphous polyphosphate glass with a layered structure and can also digest oxides, which generally cause abrasive wear [26, 28]. In spite of large amount of research effort, the complete reaction mechanism by which ZDDP forms antiwear tribofilms on the tribosurfaces is not totally understood. The complexity of the mechanism arises from the fact that the antiwear process itself is multidisciplinary and requires knowledge of metallurgy, chemistry, metrology and mechanical design while the reactions, which ZDDP undergoes, are also complex in nature and dependant on many variables of the

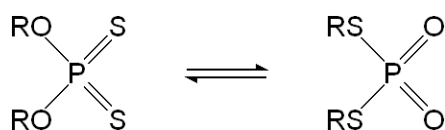
tribological system. It is strongly believed that the antiwear action in presence of ZDDP is due to products of the reaction between ZDDP and the tribosurfaces and not necessarily the precipitation of ZDDP from solution (oil) ZDDP in its intact form [17, 19, 75, 77]. Surface film formation due to reaction of ZDDP (dissolved in oil) and the surfaces of tribosystem occurs by the diffusion and absorption of ZDDP molecules on metal surfaces. Studies by Yamaguchi *et al.* [78, 79] have shown that the sulfur atom of the P=S bond in ZDDP molecules is adsorbed by iron atoms on the surface. This adsorption becomes irreversible [80] at temperatures above 60 °C due to observed ion exchange between zinc (from ZDDP) and iron. Depending on the mechanism of their formation, films formed by the reaction products between ZDDP and surfaces, two types of surface films have been studied: Thermal films and tribofilms.

2.4.3.1 ZDDP thermal films

Thermal films are generated by ZDDP on some metallic surfaces (e.g. steel and copper) when these surfaces are immersed in solutions (oil in most cases) containing ZDDP at temperatures above around 100 °C. These films are transparent, and solid and have been shown to poses antiwear properties [81]. The morphology of thermal films have been found to be quite different from tribofilms.

Studies by Aktary *et al.* and Fuller *et al.* have shown that the chemical mechanism of thermal film at relatively high temperatures (200 °C), close to the thermal degradation temperature of ZDDP involves deposition of break down products of ZDDP on metal surface [77, 82], however, thermal film formation is also observable in much lower temperatures (<100°C), which are considerably below the thermal break down temperature of ZDDP (i.e. 160-180 °C). Under these conditions, while no significant degradation of ZDDP is observed in the oil, thermal films form on certain metallic surfaces (e.g. steel), indicating a specific chemical reaction by the species that are adsorbed on to metal surfaces. The metallic surfaces where thermal film formation in lower temperatures has been found to be favorable (e.g. iron) are Lewis acids and hence they catalyze the thermal breakdown of ZDDP on the surface. The ion

exchange between zinc in ZDDP and surface metal ions including iron, results in the formation of dithiophosphates that are generally less thermally stable than ZDDP and thus are more likely to form thermally deposited films in lower temperatures [14, 77, 83]. XANES studies by Fuller *et al.* [68, 77] have partly confirmed the existence of dithionyl species formed by the following isomerization reaction of ZDDP through S/O exchange that can be facilitated at relatively low temperatures by the presence of some Lewis acids (e.g. iron surface):



Equation 2.3

2.4.3.2 ZDDP Tribofilms

The nature of antiwear tribofilms generated from ZDDPs in oils has been studied extensively using different characterization techniques that include surface technique such as X-ray photoelectron spectroscopy (XPS) [26, 84-86], Auger electron spectroscopy (AES)[8, 26, 87, 88], energy dispersive spectroscopy (EDS) [40, 87], XANES (X-ray absorption near edge structure) [66, 69, 75, 75, 89-93], scanning electron microscopy (SEM) coupled with focused ion beam (FIB) [8, 87, 90]. Morphology and mechanical properties of these films have also been studied by nano-scale mechanical testing (e.g. nano indentation)[29, 33, 87, 94-97] as well as atomic force microscopy (AFM)[69, 85, 98, 99]. According to a recent review by H. Spikes [14] some of our definite knowledge on the nature of ZDDP tribofilms as a result of the amount of research work done in this area can be summarized in the following points:

1. ZDDP tribofilms form at much lower temperatures than thermal films, even, although slowly, at room temperature. The rate of film formation increases with increasing temperature [83].

2. Tribofilms form only at the contact area when sliding contact occurs. ZDDP tribofilms do not normally form under rolling contact or in cases where the hydrodynamic fluid film of lubricant is sufficiently thick to prevent all asperity contact between the two surfaces.
3. Tribofilms are chemically similar to thermal films to a great extent with slight differences, for example using grazing-incidence X-ray fluorescence experiments, Hershberger *et al.* have found that thermally generated films from ZDDP have a higher concentration of zinc compared to mechanically formed tribofilms [31]. Tribofilms have been found to be mechanically much stronger than thermally formed films [29, 81, 83].
4. They usually rich thickness of about 50 to 150 nm before stabilizing at these thicknesses [83, 87, 100].

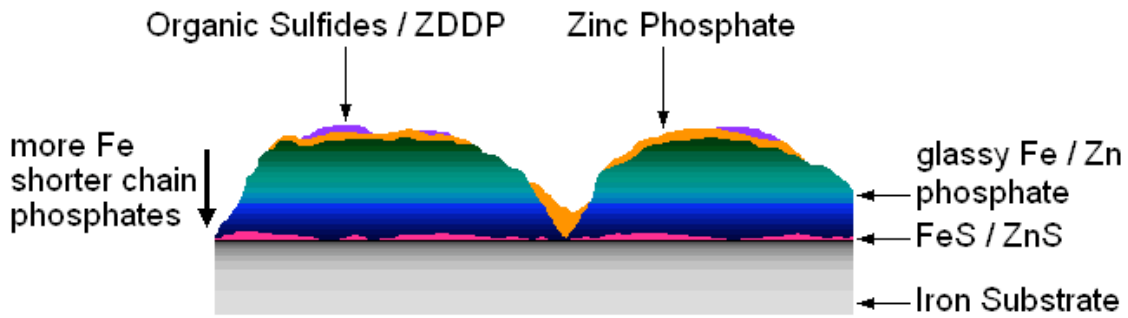


Figure 2.9 Schematic diagram of tribofilm chemical structure

5. They initially form as separate patches on steel surfaces and these gradually develop to form an almost continuous, but pad-like, structure separated by deep valleys [99]. The structure of these pads is schematically shown in figure 2.9. The pads consist mainly of amorphous and glassy polyphosphates, with a thin, outer layer of zinc polyphosphate (≈ 10 nm thick) grading to pyro- or orthophosphate in the bulk [26, 101]. The outer parts of the pad have mainly zinc cations, however the amount of iron cations increase deeper in the film and closer to the metal substrate surface [26]. Within the pads there is negligible thiophosphate [68] but sulfur is present as zinc and iron sulfide [86, 102]. On the metal surface below these pads there may be

a sulfur-rich layer of zinc or iron sulfide [103] although this has recently been disputed by Martin *et al.* [26].

6. Basic ZDDPs form very similar tribofilms to neutral salts but with shorter polyphosphate chains in the tribofilm [75].

2.4.4 ZDDP-additive interactions

As shown in table 1.1, ZDDPs are present in engine oils along with several other additives each added with a certain purpose most important of which include detergents, dispersants, antioxidants, viscosity index improvers, rust and corrosion inhibitors, anti foaming additives, pour point depressants, extreme pressure additives (in some cases, e.g. heavy duty oils) and friction modifiers. In general, engine oil additives can affect the antiwear properties of ZDDPs in three different ways:

1. By changing the nature of tribofilms,
2. By competing with ZDDP for the metallic tribosurfaces and thus reducing the sites available to ZDDP for tribofilm formation.
3. By thermally stabilizing the ZDDP and thus delaying the formation of antiwear tribofilms.

Few studies have looked at the interaction between these additives and the ZDDP in engines oils and their possible effect on ZDDP's antiwear performance [5, 6, 19, 66, 67, 89, 91, 104-110]. Some engine oil additives have been shown to be synergistic to the antiwear performance of ZDDP, while others tend to suppress and hinder the wear inhibiting properties of ZDDP. Yin and Kasrai *et al.* [19] have studied the effect of detergents and dispersants on the characteristics of the tribofilms generated from ZDDP using soft X-ray absorption spectroscopy and concluded that different detergents have different effects on the chemistry of the antiwear tribofilms formed, i.e. while calcium sulfonates (a common type of engine oil detergent) only affected the nature of the tribofilm at relatively high concentrations (> 2 wt%) by depleting the sulfur in the film without causing any change in the polyphosphates chain length, another type of detergents, namely calcium phenates, affect the film formation even when present at low

concentrations reducing the chain length of polyphosphates in the film and depleting the film from unchanged ZDDP. They also observed a strong interaction in the presence of polyisobutylene succinic anhydride polyamide dispersant which had a similar effect as the calcium phenate detergent. This observation was later confirmed by XANES studies carried out by Kasrai *et al.* [66, 67] who confirmed the existence of shorter chain polyphosphates and calcium phosphates in the presence of calcium sulfonate detergents instead of longer chain polyphosphates normally observe in tribofilms generated when ZDDP is present as the sole additive in base oil. Barcroft and Park [110] used a “hot-wire” technique, whereby a stainless steel wire was heated by passing electrical current through it, to evaluate ZDDPs alone and in the presence of other additives; a polymethacrylate viscosity improver, a succinimide dispersant, an over-based calcium sulfonate and an over-based calcium alkylsalicylate. SEM was used to study film formation on the wire. Whilst the methacrylate did not appear to affect the film which was formed by the ZDDP alone, the metal-containing additives and the succinimide did affect the films, either the rate of reaction, film thickness, morphology or film composition [3]. Antioxidants have also been found to interact with ZDDPs, although their interactions with has not been studied as extensively as detergents and dispersants. Recent studies by Somayaji and Aswath have shown that different antioxidants interact differently with ZDDPs in engine oils affecting both antiwear properties as well as oxidation stability of engines oils [104].

Apart from their effect on the nature of the tribofilms (chemical and mechanical) formed by ZDDP another aspect of ZDDP interactions with other engine oil additives is their effect on thermal stability of ZDDP. In a related study carried out at UTA by Huq and Aswath [111], Differential scanning calorimetry (DSC) was used to investigate the decomposition temperature of ZDDP in presence of common engine oil detergents and anti-oxidants. ZDDP and ZDDP mixture with each of the additives (detergents and anti-oxidants) was heated in hermetically sealed pans using a TA Instruments model 2010 DSC with a heating rate of 5°C/minute for a

temperature range running from room temperature (27°C) to 250°C. Tests were conducted in nitrogen environment with approximately 5 mg of sample in each case, maintaining a 1:1 ratio between ZDDP and the additive. Table 2.1 details the decomposition temperature of ZDDP and mixture of ZDDP with each additive. The ZDDP product used was a mixture with a 68 to 32 ratio of pure ZDDP and mineral oil. The ratio of ZDDP to additive was kept at 1:1 by weight. The results clearly indicate that the oil additives tested, i.e. the detergents and the anti-oxidants, suppress the decomposition of ZDDP resulting in higher decomposition temperatures. The detergents have a greater impact on the decomposition compared to the anti-oxidants tested. The stabilization of ZDDP in the presence of these additives reduces its efficiency as an antiwear agent [111].

Table 2.1: DSC measurements of decomposition temperature of ZDDP in the presence of some of the additives used in commercial engine oils [111].

Composition	Decomposition temperature of ZDDP (°C)
ZDDP	199.59
ZDDP + Mg-Sulfonate (Detergent)	226.16
ZDDP + Ca-Sulfonate (Detergent)	217.97
ZDDP + Ca-Phenate (Detergent)	221.95
ZDDP + Antioxidant (Moly DTC type)	215.55
ZDDP + Antioxidant (Diphenyl Amine type)	204.65
ZDDP + Antioxidant (Phenolic type)	203.15

2.5 Fluorinated zinc dialkyl dithiophosphate

2.5.1 Iron (III) fluoride and ZDDP interactions

The origin of this research work goes back to early years of this decade where the possibility of enhancing engine oils performance by the addition of polytetrafluoroethylene (PTFE) was explored by the research work carried out by the tribology research group at The University of Texas at Arlington and sponsored by the Platinum Research Organization of

Dallas, Texas. A process patented by the Platinum Research Organization (U.S. Patent No. 5,877,128) was studied where iron (III) fluoride (FeF_3) is introduced into engine oils containing dispersed PTFE to catalyze the absorption of PTFE onto the metal surfaces at normal engine operating temperatures (i.e. $\approx 100\text{ }^\circ\text{C}$) [1]. These studies however, revealed that FeF_3 worked in synergy with ZDDP and improved the antiwear characteristics of the oil, even in the absence of PTFE. DSC studies by Huq and Aswath [111] showed a reduction in the decomposition temperature of ZDDP in presence of ZDDP which implies that ZDDP antiwear films could form at lower temperatures and thus at earlier stages of the wear process in the presence of FeF_3 which results in better protection of the surfaces against wear. Further studies by K. Patel and Aswath showed marked improvement in the antiwear performance of ZDDP in the presence of dispersed FeF_3 even at very low levels of phosphorus [112].

2.5.2 Fluorinating the ZDDP

The observed synergy between ZDDP and FeF_3 led to further investigating this phenomenon, by Parekh and Aswath [1, 105] who studied the interactions between ZDDP and FeF_3 using a variety of techniques including nuclear magnetic resonance (NMR) and Fourier transform infra red (FT-IR) spectroscopy techniques as well as elemental analysis and tribological wear testing. Intermediate compounds as well as the final products of the decomposition reactions of ZDDP in presence and absence of FeF_3 were investigated using the abovementioned methods. Using ^{31}P NMR (decoupled with ^1H) and ^{19}F NMR, fluorinated phosphorus compounds were identified to have formed during the early stages of thermal reaction between ZDDP and FeF_3 . The end products of this reaction (i.e. the thermal decomposition of ZDDP in presence of FeF_3) were found to be protective fluorocarbon compounds. Through tribological wear tests, it was observed that the antiwear performance of oil samples containing the decanted early intermediate products of the baking of ZDDP- FeF_3 samples (with the same phosphorus content) at $150\text{ }^\circ\text{C}$ and nitrogen environment, i.e. the fluorinated phosphorous compounds, was consistently better than similar oils containing ZDDP

baked under identical conditions, but in the absence of FeF_3 as well as oils containing unbaked ZDDP. The fluorination process of ZDDP and the formation of fluorinated phosphorus compounds from ZDDP/ FeF_3 is observed to be a two step reaction; the first and the governing step being the complexing of FeF_3 with ZDDP followed by a fluorination step which forms the fluorinated ZDDP containing fluorinated phosphorus compounds. It was found that fluorinated phosphorus compounds could be formed under a wide range of reactions conditions. For example, it was observed that the same fluorinated reactions products formed at 150 °C could also be formed at 80 °C provided that a stable mixture of FeF_3 and ZDDP is blended by means of milling before the baking process. Naturally the baking process needs to be run for longer periods of time to achieve the same fluorination level of ZDDP (6 hours in nitrogen at 80 °C as opposed to 20 minutes at 150 °C) when lower temperatures are adapted for the reaction. The fact that the same fluorinated compounds are formed at temperatures well below the decomposition temperature of most ZDDPs (e.g. 80 °C), was helpful in optimizing the fluorination process at 80 °C (6 hours baking of ZDDP and FeF_3 in nitrogen) to ensure that ZDDP does not undergo thermal degradation during the fluorination process. In order to suppress the antioxidant behavior of ZDDP, the reaction is carried out in nitrogen environment [1, 22, 105, 113].

2.5.3 Fluorinated phosphorus compounds: Chemical structure

NMR studies and elemental analyses done by Parekh and Aswath [1, 105, 113] to determine the possible chemical structure of the fluorinated compounds of the fluorination process of ZDDP have shown the existence of a P-F bond in the structure as well as retention of the alkyl groups, phosphorus, sulfur and zinc in the structure. Figure 2.10 shows one of the possible structures that result from the fluorination process of ZDDP [113]. The common observation in all proposed structures for the chemical structure of the ZDDP fluorination products (including the structure shown in figure 2.10) is the existence of phosphorus-fluorine bond.

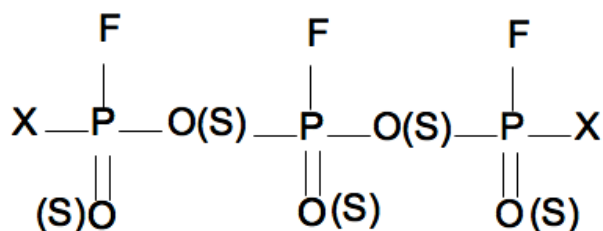


Figure 2.10: A possible chemical structure of a fluorinated phosphorus compound; X = R, OR, SR, R (may be same or different); $X \geq 1$, $n \approx 1$ or 2

2.6 Tribological testing

There are numerous ways that tribological tests can be designed and performed. The outcome(s) of a tribotest is a function of many factors, of which the first and most important are the characteristics of the materials couple and the type of lubricant, however equally important factors include contact geometry, surface roughness, environment of the test, mechanical system variables (load, speed, etc.). In order to produce relevant results from a tribological test that can be interpreted in a meaningful fashion, it is crucial to design and plan tribological tests in detail. Tribology testing methods can be classified according to realism, i.e. how closely they reproduce the conditions of the real application and how representative they are of the machine component and the conditions they are designed to simulate. Although it is always desired to have tribological tests that are as closely representative of the real equipment as possible, there are also many reasons (e.g. cost, control and measurement accuracy and time) to evaluate materials in tests that can hardly represent the real applications. Figure 2.11 shows the five levels of tribological tests (in addition to the field test of the entire system) identified in DIN 50 322 German industrial standards or Zum Gahr (1987). If for example the wear characteristics of the cylinder–piston system in a car engine are to be investigated, a field test would include the car, driven under realistic service conditions in the service environment. The whole vehicle could also be evaluated in a bench test with a better degree of test condition control, performed in a laboratory. To further reduce the cost of testing, only the important part of the system

(which is still a real system and not a model), the engine in this case, can be tested under controlled conditions in a laboratory. To simplify even further, only the important machine components can be evaluated in a component test. In the case of an automobile engine this can be a single piston and cylinder. Although component tests are normally similar to any bench or field test, the alterations in the system's environment are likely to affect the test conditions significantly; heat dissipation, vibrations, conditions of lubrication, etc., will not be entirely identical to the real life conditions. In order to increase efficiency and further improve the degree of control over the test conditions, a simplified component test is used. In the For an automobile engine test, an example of a simplified component test can be a tribometer with a reciprocating piece of the actual piston ring sliding on a surface of a small portion of the cylinder sleeve cut from the actual cylinder of the engine [114]. Another step towards simplifying the test and increasing control would be using a model test. With a simple model test a large range of materials can be easily, quickly, and cheaply evaluated, under well-controlled test conditions. For example, in order to evaluate different engine lubricants (oil) setups such as pin on disk or ball on cylinder lubricity evaluators can be used. These tests are hardly realistic and representative of the real components and condition, but are still found to be predictive of the performance of different lubricants in actual engines to a great extent. In general the degree of realism, in the data, wear and the surface damage features, and also the possibility of making reliable conclusions about performance or usability in an application, decreases when we go from the field test to the simpler model test [38, 115, 116]. Depending on the type of components used, simple model tests can be classified into the following three types:

1. Full tribocouple test: where both sliding surfaces are made of real components
2. Semi-tribocouple test: where only one of the sliding surface is made of real component and the other surface is a simulated component
3. Pure model test: where both surfaces are simulated components

Examples of standard model tribology tests used to evaluate lubricity of engine oils include ball on cylinder lubricity evaluator (BOCLE), high frequency reciprocating rig (HFRR), SRV, 4-ball wear (ASTM D-2266), and many other tests with a variety of contact geometry and configurations. Friction data (e.g. values of coefficient of friction) and the amount of wear are the outcomes derived from these tests to evaluate lubricity and different aspects of antiwear properties of engine oils. As mentioned above, these tests, being model tests, are not representative of real engine conditions, however they have undergone extensive optimization, and have been observed to reliably predict the behavior of engine oils in real engines to an acceptable extent.

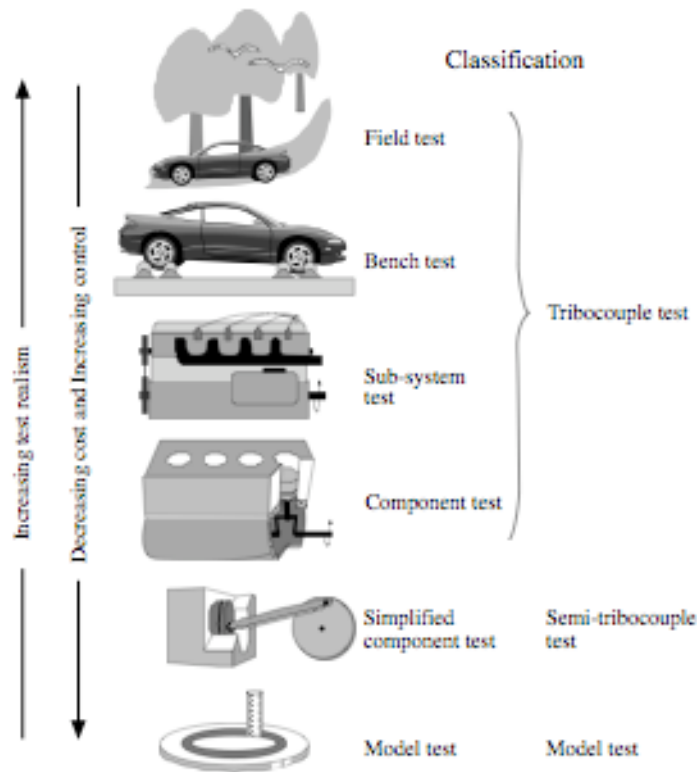


Figure 2.11: Classification of tribology testing methods based on degree of realism [38]

CHAPTER 3

APPROACH AND EXPERIMENTAL

3.1 Methods and techniques: An overview

The testing methods and experimental techniques will be explained in relative detail in this chapter while providing an outline for the approach used in this research. The study of antiwear performance of oils requires the study of antiwear tribofilms that are formed under different tribological conditions. Apart from providing a means for differentiating between the antiwear performances of different oils, tribological wear tests are essential to produce the tribofilm samples that undergo different characterization techniques used in this study. Characterization techniques used to study the structure and properties of tribofilms formed from ZDDP and fluorinated ZDDP include scanning electron microscopy (SEM) coupled with energy dispersive spectroscopy (EDS) and focused ion beam (FIB), transmission electron microscopy, auger electron spectroscopy, X-ray absorption near edge structure (XANES) spectroscopy. Mechanical properties of the tribofilms are investigated using a nano-indenter.

3.2 Tribological wear tests

The type of model wear test used in this study is a ball on cylinder lubricity evaluation (BOCLE) test based on ASTM method D5001 (ASTM Standards, Section 5, Vol. 3, 1993) which is the standard test method for measurement of lubricity of aviation turbine fuels. Two ball on cylinder testing equipment have been used for this study; a commercial Plint® BOCLE unit and an in-house designed and built unit (UTA built unit).

3.2.1 UTA-built BOCLE

In order to simulate boundary lubrication conditions and study the effects of the factors influencing the performance of the tribofilm generated under such conditions (e.g. contact

pressure, speed, chemistry and surface finish) a unique type of Ball-on-Cylinder tribological testing unit was designed and built. Contact stress is controlled by changing the applied load. The setup also allows for evaluating the performance of oil when it is present in nominal amounts ($< 100\mu\text{L}$) and in a closed system. The limited amount of oil used in the test system together with the relatively high scuffing loads used, yield tribofilm thicknesses that are in the mixed hydrodynamic to boundary lubrication regime at the early stages of the test and eventually end up in the boundary lubrication regime towards the end of the test. In addition to simulating extreme pressure lubrication regimes, as the oil is not changed during the test, it is possible to analyze the changes that the lubricant undergoes during the test. The BOCLE unit is designed to capture real time data like scuffing load, frictional force (and hence coefficient of friction) and contact point temperature.

3.2.1.1 Contact load

The load is applied pneumatically from the top as illustrated in figure 3.1(a) which is a schematic of the side view of the BOCLE unit. The vertical load can be controlled manually by opening/closing the air valve connected to an air pump. The setup also allows for changing the applied load during the test. The maximum designed load for the unit is 36 Kg. High contact loads can be used to simulate boundary condition lubrication and also extreme pressure conditions.

3.2.1.2 Friction force

The friction load is the load that resists the rotation of the ring while a vertical load is applied through the scuffing ball on the surface of the ring. The position of the friction load cell in the setup is shown in figure 3.1 (b). The ball holder can slide freely in the horizontal direction. When the vertical load is applied, the ball holder will be pushed against the friction load cell due to friction force. The friction force is then dynamically measured by the load cell and the friction co-efficient calculated.

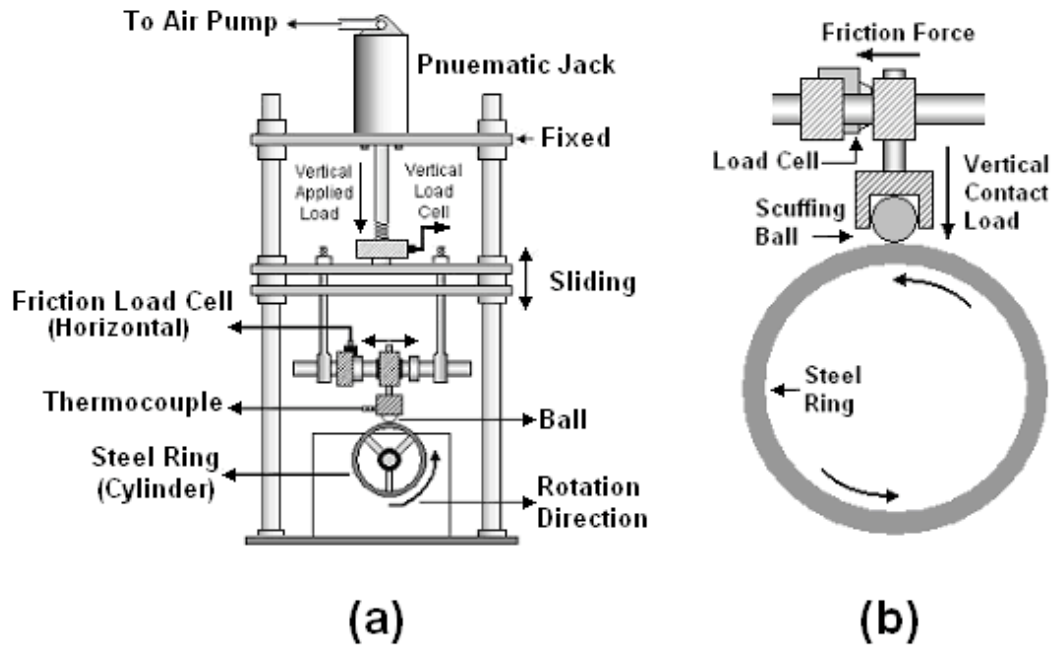


Figure 3.1 (a) Loading setup in the BOCLE: The load is applied pneumatically from the top of the setup. The vertical load cell directly measures the applied vertical load. The load is applied on the surface of the ring through a scuffing ball (steel or tungsten carbide) that is in contact with the surface of the steel ring. The friction load is measured by the friction load cell. (b) Friction force measurement: This load cell measures the horizontal force resisting the rotation of the ring, which is applied in the horizontal direction on the scuffing ball.

3.2.1.3 Temperature measurement

The BOCLE unit has the capability of measuring the temperature close to the contact point. A thermocouple is in contact with the scuff ball and is used to dynamically acquire temperature data (figure 3.2 (a)). The contact temperature is a useful measure of the events that are occurring at the boundary layer. The temperature data correlates well with friction events throughout the test as shown in figure 3.2 (b).

3.2.1.4 Data acquisition

A data acquisition software was developed using Agilent Technologies VEE Pro software. The data is displayed and recorded dynamically during the test. The data collected are time, number of cycles, friction force, contact load, temperature and the coefficient of friction

(calculated using the friction force and the contact load). The friction and temperature vs. number of cycles data were plotted for every test. In order to measure the amount of wear on the surface of the rings, the surface profile of the surface of the rings after each test is plotted using a stylus profilometer. The wear volume is then calculated.

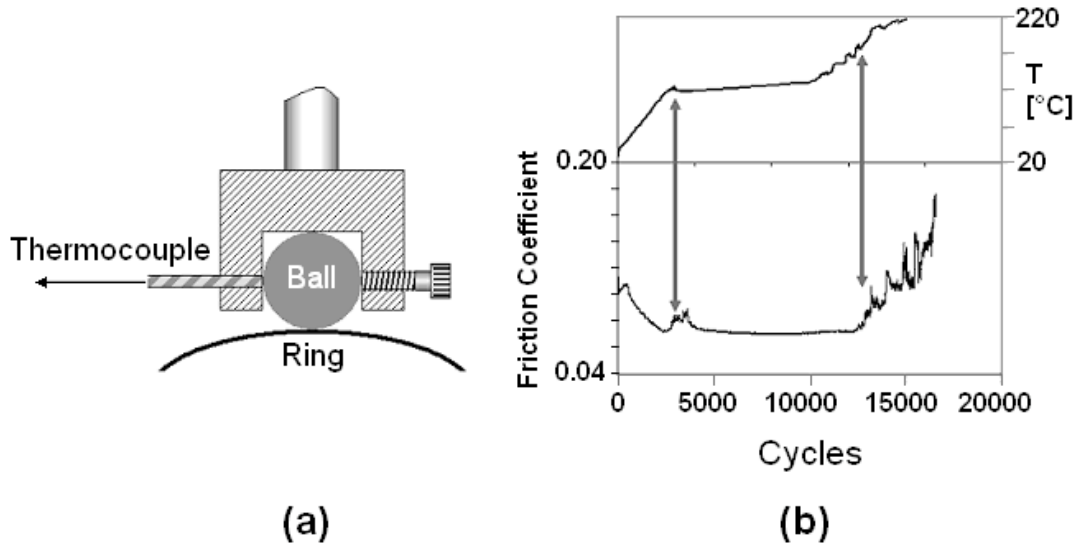


Figure 3.2: (a) The thermocouple is connected to the ball close to the contact point. The temperature measured at this spot can be correlated with the actual contact temperature at the contact point. (b) Temperature vs. cycles and coefficient of friction vs. cycles graphs for a typical test. The arrows indicate points of major frictional events which can be closely correlated with changes that occurred in the temperature.

3.2.2 Plint[®] BOCLE

The Plint[®] commercial ball on cylinder lubricity evaluator is similar in many aspects to the UTA built BOCLE unit. The major difference between in the case of Plint[®] BOCLE unit is in the way vertical load is applied. The load in the case of Plint[®] BOCLE is applied through a lever and dead weight mechanism. This method of loading does not allow for changing and adjusting the load once the test is underway. Here also coefficient of friction and temperature are measured in a manner similar to the UT built unit. Unlike the UTA built unit were both 12.7 and

6.35 mm (½ and ¼ inch) diameter scuffing balls can be used, the Plint® unit only allows for 12.7 mm (½ inch) diameter balls to be used in the tribology test. While the UTA built unit is better suited for all types of oils (due to flexibility in the loading regime and scuffing ball size), the Plint® BOCLE is also used to evaluate the lubricity of many fully formulated oils. Table 3.1 summarizes the specifications of the two ball on cylinder lubricity evaluators.

Table 3.1 Summarized specifications of the two BOCLE units used.

Parameter	Plint® BOCLE	UTA BOCLE
Ring type / diameter	Timken® bearing ring 58.2 mm	Timken® bearing ring 50 mm
Ball type / diameter	Tungsten carbide (grade 25 precision) 12.7 mm	Tungsten carbide (grade 25 precision) 6.35 and 12.7 mm
Rotation speed	700 rpm	700 rpm
Applied loads range / mechanism	297 – 420 N Dead weight	60 - 280 N Pneumatic
Measured variables	Coefficient of friction Temperature	Coefficient of friction Temperature

3.2.3 Fluid film thickness calculations and lubrication regime

In order to investigate the type of the lubrication regime present in wear tests carried out using the UTA built and the Plint® ball on cylinder lubricity evaluator, fluid film thickness during the wear tests is calculated using four of the most commonly used elastohydrodynamic (EHD) lubrication theories to estimate film thickness. To ensure accuracy and reliability of the calculation, four different equations commonly used for fluid film thickness calculations were used simultaneously to calculate the lubricant fluid film thickness in both BOCLE units. The four equations used are [57, 117]:

Grubin's equation [55] (Equation 3.1)

$$H = 1.95 G^{0.73} U^{0.73} W^{-0.091}$$

Dowson-Higginson [52] (Equation 3.2)

$$H = 1.6 G^{0.6} U^{0.7} W^{0.13}$$

Archard-Cowking [56] (Equation 3.3)

$$H = 2.04 (1 + (2R_x/3R_y))^{-0.74} G^{0.74} U^{0.74} W^{0.1}$$

Hamrock-Dowson [53] (Equation 3.4)

$$H = 3.63 (1 - e^{-0.68 k}) G^{0.5} U^{0.68} W^{0.1}$$

Where H is the ratio of film thickness to the equivalent radius in rolling direction. U , G and W are the speed, materials and load parameters respectively. R_x and R_y are equivalent radii in the sliding direction and transverse to it respectively. These values are calculated in table 3.2 for the case of the UTA built BOCLE unit, where a ¼ inch diameter ball is used and the applied load is 24 Kg. The effective film thicknesses (h) estimated by these different theories, range from 20 to 35 nm in this case. Boundary lubrication regime is in effect when the ratio of effective fluid film thickness to composite surface roughness ($h / \Sigma R_a$) also known as the lambda (Λ) ratio is smaller than unity [51]. Given the roughness (R_a) of the steel rings used being in the range of 0.2-0.3 μm and the roughness of the tungsten carbide ball being 0.05 μm , in comparison to the largest estimate of effective film thickness (h) of around 35 nm, the lambda ratio for this case falls well below the unity which confirms the dominance of boundary lubrication regimes in the wear tests that were carried out. The Plint[®] BOCLE unit also simulates boundary lubrication as it can be seen from the calculations done in table 3.3 which is similar to table 3.2 for the UTA built unit, the parameters in this table, however represent the values for the Plint[®] BOCLE when the applied load is 297 N under which most tests are run using this instrument. Again the maximum film thickness is calculated to be about 80 nm, which also yields a lambda ratio smaller than one.

Table 3.2: Lubricant and surface parameters and calculated effective film thicknesses for the UTA BOCLE unit operating under 24 Kg (235.2 N) applied load.

Parameter	Description	Formula	Value
E'	Reduced modulus of elasticity	$\frac{1}{E'} = \frac{1}{2} \left(\frac{1-\nu_1^2}{E_1} + \frac{1-\nu_2^2}{E_2} \right)$	339.2 GPa
G	Materials parameter	$\alpha \cdot E'$	3120.64
R_x	Equivalent radius in rolling direction	$\frac{1}{R_x} = \frac{1}{R_{x1}} + \frac{1}{R_{x2}}$	2.817 mm
R_y	Equivalent radius transverse to rolling direction	$\frac{1}{R_y} = \frac{1}{R_{y1}} + \frac{1}{R_{y2}}$	3.175 mm
U	Speed parameter	$\frac{u\eta_0}{E'R_x}$	7.73×10^{-12}
W	Load parameter	$\frac{F}{E'R_x^2}$	8.74×10^{-5}
E_1	Young's modulus for body 1 (steel ring)		200 GPa
E_2	Young's modulus for body 2 (tungsten carbide ball)		700 GPa
ν_1	Poisson's ratio for body 1 (steel ring)		0.3
ν_2	Poisson's ratio for body 2 (tungsten carbide ball)		0.24
F	Normal applied force		235.2 N
K	Ellipticity ratio ($k = 1$)		
A	Pressure-viscosity exponent (base oil)	$0.92 \times 10^{-8} \text{ m}^2/\text{N}$	
h	Atmospheric viscosity (base oil)	$0.004 \text{ N}\cdot\text{sec}/\text{m}^2$ (at 100°C)	
U	Average surface speed	$1832.6 \text{ mm}/\text{sec}$. (@700 rpm)	
R_{x1}	Radius of body 1 (steel ring) in sliding direction		25 mm
R_{x2}	Radius of body 2 (steel ring) in sliding direction		6.35 mm
H	Film thickness ratio $\frac{h}{R_x}$	Grubin's equation	1.255×10^{-5}
		Dowson – Higginson	1.122×10^{-5}
		Archard – Cowking	0.850×10^{-5}
		Hamrock – Dowson	0.710×10^{-5}
H	Effective film thickness	Grubin's equation	35 nm
		Dowson – Higginson	32 nm
		Archard – Cowking	24 nm
		Hamrock – Dowson	20 nm

Table 3.3: Lubricant and surface parameters and calculated effective film thicknesses for the Plint® BOCLE unit operating under 30 Kg (279 N) applied load.

Parameter	Description	Formula	Value
E'	Reduced modulus of elasticity	$\frac{1}{E'} = \frac{1}{2} \left(\frac{1-\nu_1^2}{E_1} + \frac{1-\nu_2^2}{E_2} \right)$	339.2 GPa
G	Materials parameter	$\alpha \cdot E'$	4070.4
R_x	Equivalent radius in rolling direction	$\frac{1}{R_x} = \frac{1}{R_{x1}} + \frac{1}{R_{x2}}$	5.224 mm
R_y	Equivalent radius transverse to rolling direction	$\frac{1}{R_y} = \frac{1}{R_{y1}} + \frac{1}{R_{y2}}$	6.35 mm
U	Speed parameter	$\frac{u\eta_0}{E'R_x}$	6.93×10^{-12}
W	Load parameter	$\frac{F}{E'R_x^2}$	3.21×10^{-5}
E_1	Young's modulus for body 1 (steel ring)		200 GPa
E_2	Young's modulus for body 2 (tungsten carbide ball)		700 GPa
ν_1	Poisson's ratio for body 1 (steel ring)		0.3
ν_2	Poisson's ratio for body 2 (tungsten carbide ball)		0.24
F	Normal applied force		297 N
k	Ellipticity ratio ($k = 1$)		
a	Pressure-viscosity exponent	$1.2 \times 10^{-8} \text{ m}^2/\text{N}$ (at 100°C)	
h	Atmospheric viscosity	$0.006 \text{ N}\cdot\text{sec}/\text{m}^2$ (at 100°C)	
u	Average surface speed	2047.4 mm/sec. (@700 rpm)	
R_{x1}	Radius of body 1 (steel ring) in sliding direction		58.9 mm
R_{x2}	Radius of body 2 (steel ring) in sliding direction		12.7 mm
H	film thickness ratio $\frac{h}{R_x}$	Grubin's equation	1.541×10^{-5}
		Dowson – Higginson	1.389×10^{-5}
		Archard – Cowking	1.076×10^{-5}
		Hamrock – Dowson	0.830×10^{-5}
h	effective film thickness	Grubin's equation	80.5 nm
		Dowson – Higginson	72.6 nm
		Archard – Cowking	56.2 nm
		Hamrock – Dowson	43.4 nm

3.3 Sample preparation and testing protocols

Tribofilms samples are generated by wear tests using the ball on cylinder lubricity evaluators described in the previous section. Both the balls and the rings used in the tests were ultrasonicated and cleaned by hexane and acetone and the surface of the ring was brushed in order to remove any pre-existing wear debris and machining oil. Once cleaned the ring and the ball are mounted on the BOCLE unit. In the case of the UTA BOCLE, in order to achieve consistent surface finish at the contact point for all tests, a break-in step is performed before every test in which 50 micro liters of base oil is applied on the surface of the ring, and the BOCLE unit is run for 500 cycles under the applied load of 6 Kg (1.46 GPa and 2.23 GPa for the $\frac{1}{2}$ and $\frac{1}{4}$ inch diameter balls respectively in terms of Hertzian contact load). The rotation speed is held constant at 700 cycles per minute through out the test. After 500 cycles, the BOCLE unit is stopped and the ring and the ball are cleaned *in-situ* with hexane and acetone to remove any debris present. This procedure smoothes the surface of the ring in contact with the ball without causing any detectable amount of wear on the surface of the ring, hence eliminating the effect of any inconsistency in surface finish that might exist from one surface to another. Following the break-in procedure, when $\frac{1}{4}$ inch scuffing balls are used, 30 micro liters of the oil being tested is applied on the surface of the ring in the form of a thin stripe (in the case of $\frac{1}{2}$ inch ball, 50 micro liters of oil is applied). The test is then started with an applied contact load of 6 Kg and after 500 rotations; it is ramped up to the final load (depending on the test) within 1500 rotations, after which the test is run under constant load for a desired number of cycles. In the case of the Plint[®] BOCLE, since load can not be controlled through out the test, the break-in step is skipped and the tests are run under the intended final applied load from the beginning. The amount of oil used in this case is 50 micro liters.

An important distinction between the approach used here and other methods in the literature [63, 118, 119] is the relatively small amount of oil that is applied is the only oil that is used to provide all the lubrication for the duration of the test. This approach allows for

examining the mechanism of formation, durability and eventual breakdown of the tribofilm without any replenishment of the boundary layer with fresh oil.

After the tests are run, the rings are used for both wear volume measurements and different surface characterization techniques used for determining the properties of the tribofilms generated during different tests. Due to the ball-on-cylinder configuration of the tribotests, the tribofilms are formed on a linear wear track on the outside surface along the circumference of the rings. For surface analysis techniques, a small portion of the rings, containing the wear track, is separated and prepared by cutting it with a low speed diamond blade in a mineral base lubricant to minimize contamination as well as to avoid heating up the samples which can change the nature and composition of the tribofilms.

3.4 Tribofilm characterization

3.4.1 SEM / EDS

In order to examine the chemical composition of the film, surface of the tribofilms generated from wear tests is analyzed using JEOL JSM 845 scanning electron microscope (SEM) coupled with energy dispersive X-ray spectroscopy (EDS). The acceleration voltage was set at 20KV and the working distance normally at 30 cm. For every sample, once an area of uniform film formation is located on the surface of the wear track, an EDS spectrum was obtained from that area of the tribofilm surface in order to identify some of the elements present in the film.

3.4.2 Focused ion beam (FIB)

A Zeiss Leo[®] Supra 55 scanning electron microscope and Zeiss Leo[®] focused ion beam (FIB) 1540XB microscope were used for film thickness analysis. For each sample, an area of uniform tribofilm on the surface of the wear track was located using the SEM, and then an area of 8 μm by 10 μm was selected and defined (through the software) and milled using a gallium ion beam. The ion beam sputters the surface material by raster scanning the selected area. The thickness of the material removed depends on the properties of the surface material as well as

the current intensity of the ion beam. The current and the number of scans in each case wear selected so that the depth of the sputtered area in each case was around 4 μm to ensure the full exposure of the tribofilm and the steel substrate profile through the thickness.. This process exposes the side profile of the tribofilm and the underlying substrate (steel). A secondary electron micrograph of the cross section of the film (and substrate) was generated using the secondary electron detector located at an angle of 54° from the direction vertical to the surface of the sample. Figure 3.3 schematically shows how the tribofilm thickness is measured using the FIB.

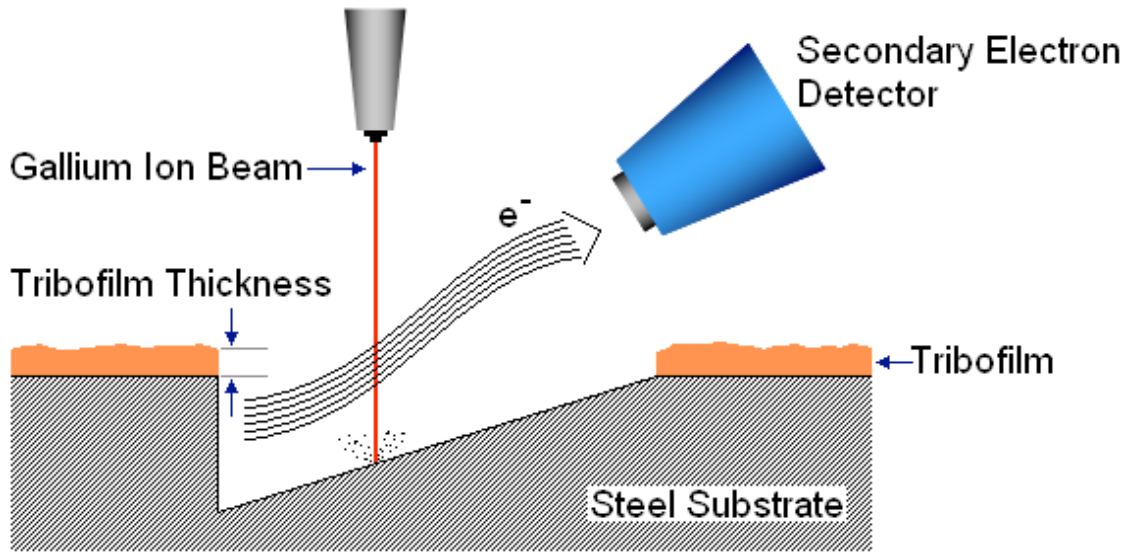


Figure 3.3: Schematics tribofilm thickness measurement using focused ion beam

3.4.3 Auger electron spectroscopy (AES)

3.4.3.1 Basics of AES

Auger electron spectroscopy has been used to probe the chemical and compositional surface environments of tribofilms [8, 26, 120, 121]. This spectroscopic technique is based on the Auger effect in which emission of an electron from an atom causes the emission of a second electron. The Auger effect was discovered first by Pierre Auger in 1952 while working with x-

rays using a Wilson cloud chamber. In Auger electron spectroscopy, surface atoms of the sample being studied are probed by an incident beam of electrons with energies in the range of 3 to 50 keV which results in some of the core level electrons being ejected and leaving behind a hole that is immediately filled by outer shell electrons. The energy lost by the outer shell electrons moving into lower energy core level holes is equal to the difference in orbital energies and can in turn, eject and emit another outer shell electron provided the transferred energy is greater than the orbital binding energy of that electron. This emitted electron is named Auger electron and its energy is characteristic of the emitting atoms and thus analyzed in the Auger electron spectroscopy (AES) technique. An Auger electron will have the following kinetic energy:

$$E_{Auger} = E_{core\ state} - E_{L1} - E_{L2} \quad (\text{Equation 3.5})$$

E_{Auger} is the kinetic energy of the emitted Auger electron and $E_{core\ state}$, E_{L1} and E_{L2} are respectively the core level, first outer shell, and second outer shell electron energies, measured from the vacuum level. The Auger electron energy emitted from the surface of a specimen (e.g. tribofilm) can be used to identify the elements in the surface layers of the specimen and their relative concentration.

3.4.3.2 Instrumentation

Auger electron spectroscopy is a very surface sensitive technique since the emitted Auger electrons have relatively small kinetic energies (0.05 keV to 3 keV) and at these energy ranges, electrons have a short mean free path within a solid and thus only Auger electrons emitted from the few nanometer depth of the surface of the specimen can escape and be detected. A typical AES setup is shown in figure 3.4. Focused electrons are incident on the specimen surface by an electron gun and emitted Auger electrons are detected and analyzed by the detection unit which consists of an an electron energy analyzer as well as an electron detector and the resulting signal is sent to the data acquisition unit which can plot the collected Auger electrons as a function of energy against the broad and varying secondary electron

background spectrum. The AES setup operates under ultra high vacuum (UHV) conditions (low $\approx 10^{-10}$ -torr range) to minimize the influence of the residual gases in the surface analysis measurements as well as to reduce electron scattering by the residual gases.

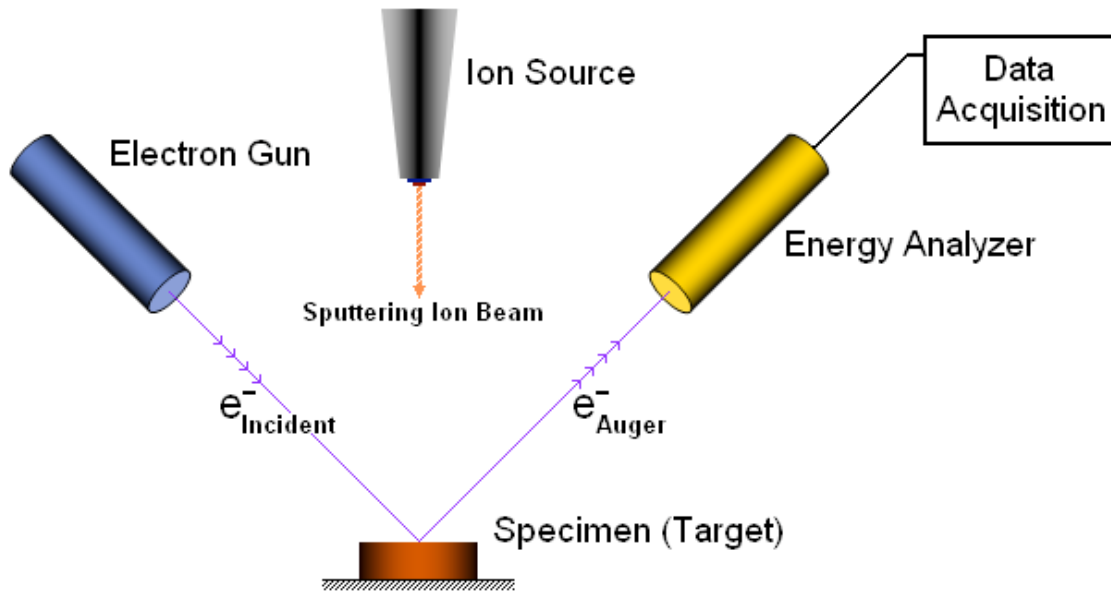


Figure 3.4: Schematic layout of AES experimental setup

Auger spectra can be obtained from areas of different sizes of the surface of the specimen depending on the spot size of the electron beam. Depending on how well the electron can be focused in a particular piece of equipment, some very small spot sizes of less than 500\AA can be achieved. This mode of operation where spectrum data is acquired from a small spot on the surface is usually referred to as point analysis. The electron beam can also be used to scan across a straight line or a given area which is known as scanning Auger microscopy (SAM). In this mode, the Auger spectrum data is acquired from a predefined area on the surface of the sample. Scanning electron microscopy is often coupled with AES to locate the area intended for surface analysis.

Many AES units, including the one used in this study, are equipped with an ion source that is used for depth profiling specimens. The ion source generates a beam of inert gas ions that are directed to sputter the surface layers, revealing underlying layers to generate Auger spectra from those layers and thus study the compositional changes through different layers of the specimen close to the surface. The intensity and scanning time of the ion beam dictates the thickness of the layer removed at each sputtering step.

Auger electron spectroscopy was used in this study to investigate the composition of the tribofilms on the surface of the wear tracks generated on ring specimens from ball on cylinder tribology tests. The AES unit used is a Perkin-Elmer[®] PHI 560 ESCA/SAM with a 2 μm spot size with the vacuum pressure maintained at or below 1.2×10^{-7} -torr. An 8 μm by 8 μm area of uniform tribofilm was selected to obtain Auger spectra. In order to obtain Auger electron spectra from different depths of the tribofilm, a selected area of 2 mm by 2 mm encompassing the track (and the selected area of the tribofilm) at its center was sputtered with Argon ion beam with an excitation voltage of 2KV for 12 seconds before each scan. Each scan was run for 5 minutes right at the center of the sputtered area to obtain an overall spectrum as well as the spectra for oxygen, sulfur, phosphorus, iron and carbon peaks. This step is repeated to obtain the same spectra at a deeper location in the film. The steps are repeated until no detectible amounts of phosphorus, oxygen and sulfur are observed. This correlates with reaching the steel substrate.

3.4.4 Transmission electron microscopy

Transmission electron microscopy (TEM) is a microscopy technique in which an electron beam is transmitted through an ultra thin specimen, interacting with the specimen as it passes through it producing an image that is formed from the electrons transmitted through the specimen, magnified and focused by an objective lens and projected on an imaging screen. For crystalline specimens in particular, TEM is a powerful characterization technique since such samples can diffract the incident electron beam and generate diffraction patterns that can be

used to identify the type of the material being studied. TEM has been used as characterization tool for studying tribofilms generated during different tribology tests [8, 49, 122, 123]. Wear debris generated during tribotests are well suited to be studied using transmission electron microscopy since they are normally very thin and need little preparation after being harvested from specimens that have undergone tribotesting.

The tribofilm formation during tribological tests is a dynamic phenomenon in which the antiwear films are formed by the break down of ZDDP (and fluorinated ZDDP) due to shearing pressure and high temperature, parts of the deposited film are then separated from the surface due to the same shearing forces. These particles either remain afloat inside the lubricant or are replenished back into the tribofilm through the duration of the tests [10, 10]. This means that wear debris present in tested oils are mainly made of tribofilm particles as well as the asperities generated at the early stages of each wear tests which usually consist of the substrate metal and its oxides [27].

To carry this part of the study, an available JEOL[®] 1200EX Transmission electron microscope (TEM) also coupled with EDS is used to examine the wear debris generated during wear tests. Since the wear debris are mainly parts of the tribofilm that have separated from the film, they can be examined to obtain their chemical composition and study properties of the tribofilm that would be otherwise difficult to examine such as the crystallinity of the tribofilm. The main advantage of chemical analysis of wear debris using the EDS coupled with TEM over EDS coupled with SEM is the fact that in the case of wear debris, unlike the tribofilm, there is no steel substrate present and thus any iron present in the wear particles can be detected without being concealed by the background iron peaks from the substrate. This is important as iron has been identified as one of the most important constituents of tribofilms. Samples for this study are prepared by collecting the tested oil after wear tests using a thin plastic film and placing a drop of that oil on a 3 mm copper grid with polymer transfer layer, the oil can then be washed off with hexanes while the debris are retained on the copper grid.

3.4.5 X-ray absorption near edge structure (XANES) spectroscopy

3.4.5.1 Overview and application in tribology

The characterization techniques previously mentioned, i.e. AES, SEM and TEM (both coupled with EDS) are all valuable techniques which provide insight into the chemical composition and morphology of tribofilms, however, these techniques fail to provide any information on the nature of the chemical bonds and the structural environment of the atoms in the compounds present through out the thickness of the film. X-ray absorption near edge structure (XANES) spectroscopy is an absorption spectroscopy technique that is capable of probing the local structural and bonding environment around selected atoms and can determine their formal valence (very difficult to experimentally determine in a nondestructive way); coordination environment (e.g., octahedral, tetrahedral coordination) and subtle geometrical distortions of it. XANES spectroscopy has become a common analytical tool in the study of surface films with the increasing availability of synchrotron radiation. Synchrotron radiation is electromagnetic radiation generated by the acceleration of ultra relativistic (i.e., moving near the speed of light) charged particles through magnetic fields in an electron or positron storage ring [124]. The broad spectral range of synchrotron radiation enables the wavelength to be varied making it ideal for element specific spectroscopic analyses, making the study of all but the lightest of elements possible. Since tribofilms are mainly amorphous in nature, another advantage of XANES is the fact that unlike diffraction-based techniques for studying atomic structure of matter, XANES does not require crystalline samples and thus has been used as a powerful analytical technique in the study of tribofilms generated from ZDDP by many research groups over the past decade [12, 26, 62, 66-69, 86, 89, 92, 125, 126], for instance, it has been used to characterize the polyphosphate chain lengths present in ZDDP tribofilms by Yin, Z. *et al.* [101].

The absorption spectrum displays an absorption edge associated with the excitation of a core shell electron (normally K-edge or L-edge). Right above the adsorption edge, a spectrum

taken of a condensed material exhibits an oscillatory structure which is the result of multiple scattering resonances of the photoelectron excited at the atomic absorption site (absorbing atom) and scattered by neighbor atoms. The peaks close to the absorption edge can be attributed to transitions to localized electronic states, with the edge position itself being related to the oxidation state of the absorbing atom. The strong oscillations just beyond the absorption edge, i.e. the X-ray absorption near edge structure (XANES), can be explained in terms of the multiple scattering of photoelectrons by the atoms in a local cluster around the absorbing atom.

3.4.5.2 XANES Experimental

Examination of XANES spectra with respect to model compound data can be used to provide information on the geometrical arrangement of the near neighboring atoms close to the absorbing site [124]. XANES spectroscopy can be performed in two different modes:

1. Total electron yield (TEY) mode that allows the examination of the surface layers (≈ 5 nm for L-edge and ≈ 50 nm for K-edge [63]).
2. Fluorescent yield (FLY) mode in which the data is acquired from the bulk of the matter beyond the outer surface layers (≈ 50 nm for L-edge and ≈ 300 nm for K-edge in the case of phosphorus and sulfur [63]).

The availability of these two modes of operation makes the study of chain length and chemical composition and structural environment variations through the depth of the tribofilm possible to some extent since the thickness of tribofilms generated by the tribotests used in this study were found to be between 80 to 150 nm [87]. The XANES experiments were run at two different synchrotron facilities.

The XANES experiments were run two different beamlines at two synchrotron facilities:

1. Variable line spacing plane grating monochromator (VLS-PGM) 11ID-2 at the Canadian Light Source (CLS) facility, Saskatoon, Saskatchewan, Canada.
2. The Canadian double crystal monochromator (DCM) at the Synchrotron Radiation Center (SRC) at the University of Wisconsin – Madison in Stoughton, Wisconsin.

The specifications of each beamline are shown in Table 3.4 [127, 128]. For both sulfur and phosphorus, X-ray absorption spectra were obtained near K- and L-absorption edges. This has been possible because each beamline offers a different range of energies. The VLS-PGM beamline is used to probe sulfur and phosphorus X-ray absorption spectra near their L-absorption edge since its energy range is 5.5 – 250 eV which encompasses the L-absorption edges for both sulfur and phosphorus (≈ 162 eV and ≈ 135 eV respectively). The DCM beamline with the energy range of 1500 to 4000 eV, is used to probe the X-ray absorption spectra of sulfur and phosphorus near their K-absorption edge (≈ 2470 eV and ≈ 2146 eV respectively).

Table 3.4: Specifications of the beamlines used in this study

Beamline	DCM	VLS-PGM
Energy Range	1500-4000 eV	5.5-250 eV
Spot Size horizontal x vertical	2 mm x 2 mm	500 μ m x 500 μ m
Resolution used	0.3 eV for P 0.5 eV for S	0.1 eV for P and S

3.5 Nano-mechanical testing

Mechanical properties of the tribofilms are studied using a Hysitron TriboIndenter[®], a high-resolution nano-mechanical test instrument capable of performing nano-scale indentation, scratch and other nano-mechanical tests as well as for imaging surfaces when used in scanning probe microscopy (SPM) mode. This instrument is the ideal tool in examining some of the mechanical properties of antiwear tribofilms that have remained mainly unknown to tribologists up until now. Three types of nano-mechanical tests, i.e. nano-indentation, nano-wear and scanning nano-wear tests will be run on tribofilm samples. While nano-indenters have recently been explored as a valuable tool in the study of mechanical characteristics of tribofilms [23, 29, 33, 94, 96, 99], most of these studies have remained limited to the nano-indentation. The scanning wear and nano scratch tests performed are unique to this study and have not been attempted before. Nano-mechanical testing will be carried on tribofilm samples generated from

wear tests that are run on oil samples containing ZDDP and Fluorinated ZDDP present in base oil. Nano-indentation, nano-scratch and nano-scale scanning wear tests are run on tribofilm samples generated from ZDDP and fluorinated ZDDP using the Hysitron[®] nano-mechanical test instrument. Nano-mechanical test were performed both at the University of Texas at Arlington on a Hysitron Ubi[®] 1 nano-mechanical testing system and also at Hysitron corporation's nano-mechanics research laboratory in Minneapolis, MN.

3.5.1 Nano-indentation tests

In quasi-static nano-indentation tests, normal force is applied to an indenter tip while measuring tip displacement into the sample. During indentation, the applied load force and tip displacement are continually measured, creating a load-displacement curve for each indent. In SPM mode, the TriboIndenter[®] can provide *in-situ* images of the sample before and after indentation. Such imaging is accomplished quickly and easily by utilizing the same tip for imaging as indentation. The surface of the tribofilms before indentation tests (and other nano-mechanical tests) is probed in the SPM mode to obtain topographic images of the surface as well as to ensure surface consistency, uniformity and smoothness that is associated with the presence of undamaged and well formed film, so that meaningful data can be obtained from each test. Nano-indentation tests are used to measure the reduced modulus as well as the hardness of tribofilms and provide opportunities to study the effect of the substrate, loading and formulation effects on these properties. Indents were run using two different types of quasi-static load functions; a trapezoidal and a cyclic loading load function. Both load functions were employed under the load control mode and the vertical displacement (penetration depth) of the indenter tip was continuously measured.

3.5.1.1 Trapezoidal single indents

Each indentation test with a trapezoidal load function is comprised of a 5-second loading segment, a 2-second holding segment (at the maximum load), and a 5-second unloading segment. The reduced modulus is measured during the unloading segment by

measuring the slope of the load-displacement curve at the early stages of unloading. The nano-indentation tests run at the Hysitron® nano-mechanics research laboratory were performed using a NorthStar® cube corner probe with < 40nm tip radius to determine hardness and reduced modulus values of the tribofilm located inside the wear track on cut portions of Timken steel ring samples generated by tribotests using the UTA built BOCLE unit. The nano indentation tests run sing the Hysitron Ubi 1 TriboIndenter® at UTA were performed using a Berkovich tip which is a three sided pyramid with a total included angle of 142.3 degrees and a half angle of 65.35 degrees.

The trapezoidal load function is shown in figure 3.5 (a), the response is the load-displacement curve from which the reduced elastic modulus is measured from the unloading segment (figure 3.5 b). Accurate measurement of the displacement of the tip during the indentation process allows for the calculation of the hardness and reduced elastic modulus of a film from a load–displacement curve (figure 3.5 b). The values are calculated from the initial slope of the withdrawal (unloading) in accordance with the Oliver and Pharr method [129]. For both indenter tips used, the TriboIndenter® was calibrated for compliance and tip abnormalities, using the manufacturer’s suggested method of measuring a succession of indents into a silica sample at different penetration depths to calculate the tip area function needed for calculating hardness. The reduced elastic modulus (E') is defined through the following equation (3.5);

$$\frac{1}{E'} = \frac{1}{2} \left(\frac{1-\nu_1^2}{E_1} + \frac{1-\nu_2^2}{E_2} \right) \quad \text{Equation 3.6}$$

where E_1 and ν_1 are the Young’s modulus and Poison’s ratio of the sample respectively and E_2 and ν_2 are the same values for the indenter tip [95].

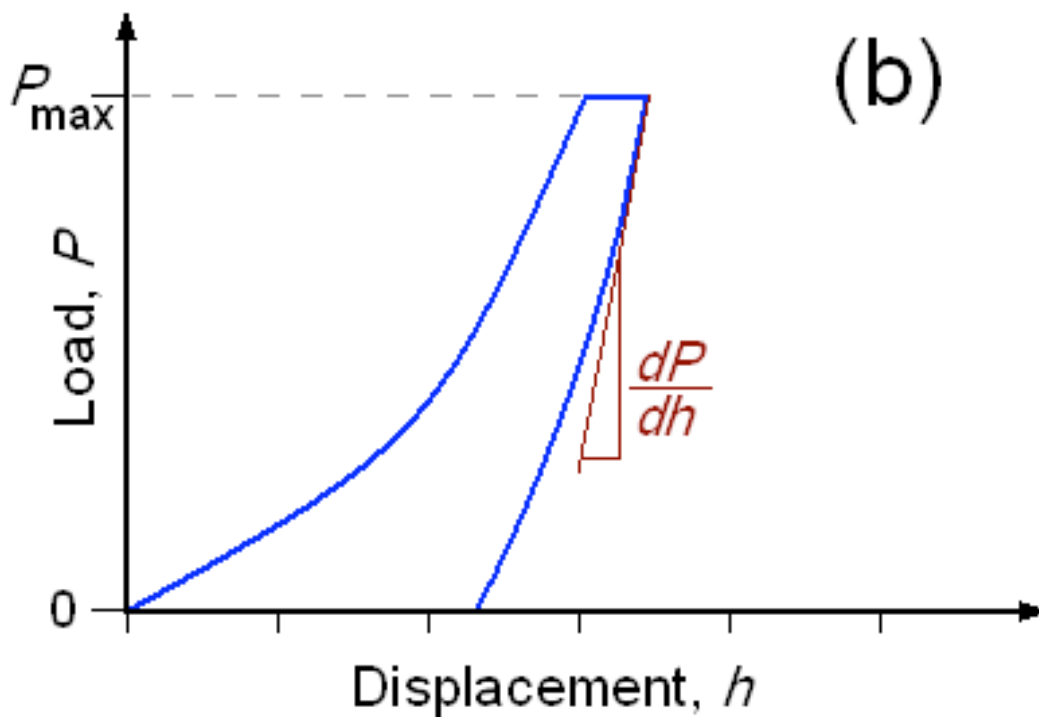
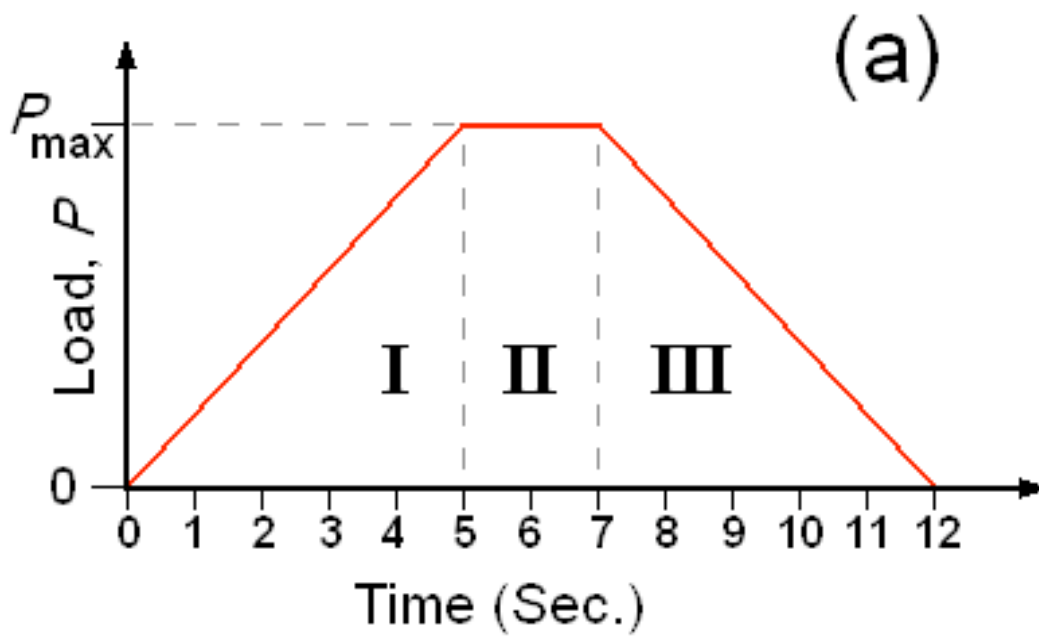


Figure 3.5: (a) Load function of trapezoidal single indentation test with; I: loading, II: holding and III: unloading segments, (b) Schematic of load-displacement curve

3.5.1.2 Cyclic loading indents

In cyclic loading indentation, the load function is series of trapezoidal loading cycles with a total of 25 cycles. Is made of a 1-second loading segment, a 1-second holding segment and a 1-second unloading segment. The maximum load for each holding segment is incrementally increased with each loading cycle with the first cycle having a maximum load of $0.15 \mu\text{N}$ and the final cycles having a maximum load of $500 \mu\text{N}$. The final load of unloading segment in each cycle is slightly higher than the starting load of the loading segment in that cycle. The load function of cyclic loading indents used in this study is shown in figure 3.6. All cyclic loading indentation tests were run at the University of Texas at Arlington using the Hysitron Ubi 1 TriboIndenter[®] with a Berkovich tip.

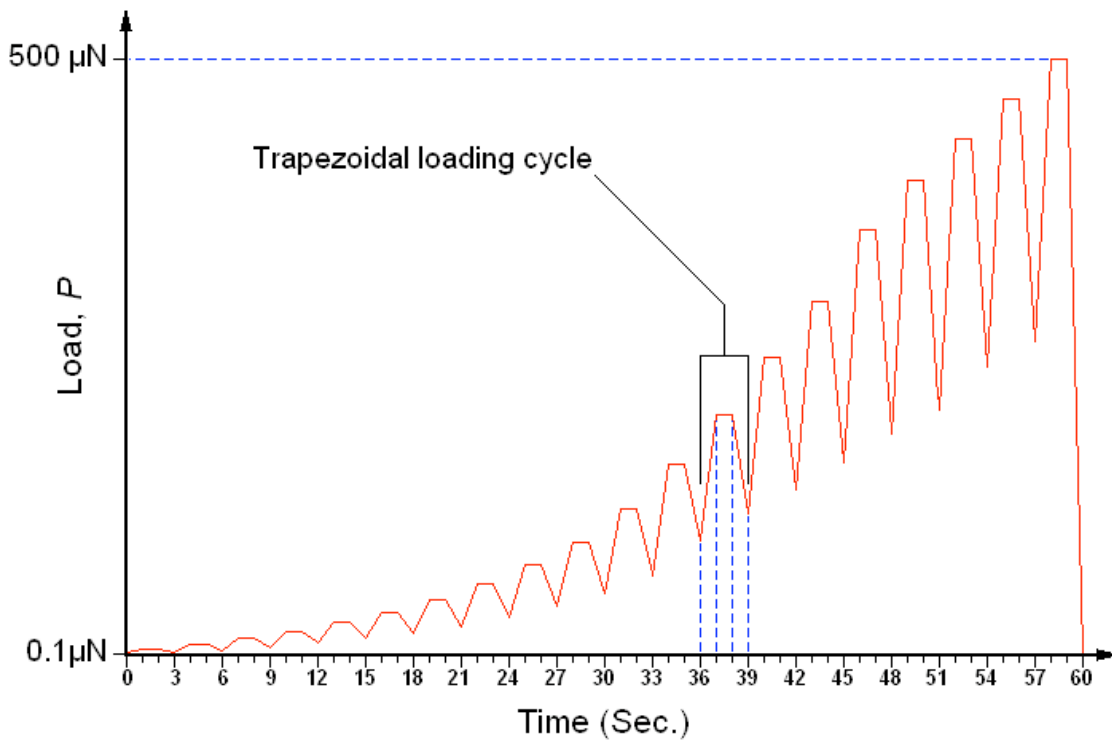


Figure 3.6: Load function of cyclic trapezoidal indentations

The main advantage of using cyclic indentation load functions in performing nano-indentation tests is the fact that many data points can be acquired within a fairly short period of time. The reduced elastic modulus can be measured during each unloading segment as described in the previous section using the Oliver-Pharr method. Hardness is also measured with each indentation cycle. Since the tip can penetrate further with each indentation cycle, the measured modulus and hardness values can be plotted against displacement of the tip in the vertical direction (i.e. penetration depth). The resulting modulus and hardness vs. depth data, will however be different from data collected from single indents run at different loads, since in the case of cyclic loading, all indentation cycles are performed on the same location on film and thus work hardening effects will inevitably skew the data to some extent while for single-indentation tests, each data point is collected from a different spot on the surface of the film.

3.5.2 Scanning wear tests

The wear tests were performed using the instrument's *in-situ* SPM mode. In this mode, the TriboIndenter[®] creates wear regions by raster scanning the indenter tip across the sample surface while maintaining a specified normal force or set point. Naturally, the depth of the wear region is dependent upon the set point, the number of scans, and the shape and composition of the tip but will provide a measure of the film resistance to shearing forces and the structural continuity of the tribofilm. Scanning wear tests were run at the Hysitron[®] nano-mechanics research laboratory using a 90° conical probe with 2µm tip radius.

3.5.3 Nano-scratch tests

In scratch mode, the TriboIndenter[®] is load-controlled and displacement sensing is in the normal direction (perpendicular) to the sample surface, while simultaneously displacement is controlled in the lateral direction parallel to the sample surface. During a scratch test, a normal force is applied to the indenter tip as a function of time in accordance with the scratch load function, while the tip is also driven towards the predetermined lateral position within a

specified amount of time. Normal force, normal displacement, lateral force, and lateral displacement are measured and recorded as a function of time. From these four parameters, some of the mechanical properties and tribofilm adhesion characteristics can be deduced. Scratch tests were run at the Hysitron[®] nano-mechanics research laboratory, using a 90° cube corner conical probe with 2 μ m tip radius and maximum normal force of 5000 μ N. The scratch load function consisted of a linearly ramped force scratch from zero to peak load in 30 seconds over a lateral displacement of 6 μ m.

CHAPTER 4

LUBRICATION WITH ZDDP UNDER BOUNDARY LUBRICATION CONDITIONS

This part of the study serves as a precursor to the study of the performance of fluorinated ZDDP in comparison to ZDDP since it establishes a baseline for the antiwear performance of ZDDP under the testing conditions of the tribological testing methods used in this study which were described in detail in the previous chapter. Characterization techniques described in the previous section were probed for the case of ZDDP, both alone and in the presence of two different additives (a detergent and an antioxidant). Part of the data obtained for this section from these characterization techniques as well as wear tests are later compared to the data obtained for fluorinated ZDDP.

4.1 Materials and procedures

A secondary ZDDP research sample (containing 7.2 wt% P) was obtained from Chevron Oronite[®], CA, USA. ZDDP was added to 100-neutral base mineral oil at two different loadings to achieve phosphorous concentrations of 0.05 and 0.10 wt%. Two additional samples, one containing ZDDP (0.10 wt% P) and 2 wt% calcium sulfonate (a commonly used detergent in engine oils) in base oil and the other containing ZDDP (0.10 wt% P) and diphenyl amine antioxidant (1 wt%) in base oil were also prepared for wear tests examining the effect of these two additives on the performance of ZDDP. Wear tests were run on the oil samples using the UTA BOCLE unit according to the testing protocol described in the previous chapter. Scanning electron microscope (SEM) coupled with Energy Dispersive X-ray Spectroscopy (EDS) was used to examine the chemical composition of the film and Focused Ion Beam (FIB) was used for film thickness analysis. Nanoscale mechanical properties of the tribofilms generated on the

surface of the rings were also examined using a TriboIndenter[®] at Hystron corporations' nano-mechanics research laboratory.

4.2 Results, observations and discussion

4.2.1 Friction, temperature and wear behavior

The different events that occur in a typical boundary lubrication test are examined in detail by conducting a series of tests that were stopped at different intervals and the surface profiles examined using a stylus profilometer.

The coefficient of friction vs. cycles data for a test carried out on the ¼ inch diameter tungsten carbide ball at an applied load of 24 Kg (3.56 GPa Hertzian load) are plotted in figure 4.1. It can be observed that there are fluctuations in the coefficient of friction initially (first 5000 cycles) followed by a plateau regime in which the coefficient of friction remains unchanged. This plateau regime is associated with the formation of a protective lubricating film on the surface of the ring and is followed by a surge in friction coefficient, which is coupled with the breakdown of the protective tribofilm. The duration of the test between the onset of breakdown of the tribofilm and final failure depends on a number of variables including the applied load and volume and chemistry of oil. The increase and fluctuation of the friction coefficient are associated with the failure of the protective lubricating film. The amount of wear occurring during the plateau regime of the test is nominal compared to the other stages of the test. This is verified by stopping similar tests at different stages of the test, i.e. beginning of the test (high friction), at the beginning, in the middle and at the end of the plateau regime and also at the final stages of the test. In addition to the coefficient of friction vs. number of rotations data the surface wear profiles at different stages of the test are also shown in figure 4.1.

At the beginning of the test, prior to the establishment of a stable tribofilm extensive wear occurs as shown in the profile (b) of figure 4.1. This amount of wear remains constant as long as the tribofilm remains intact (the plateau region in figure 4.1). On breakdown of the tribofilm there is a significant increase in the amount of measured wear as shown in profile (e).

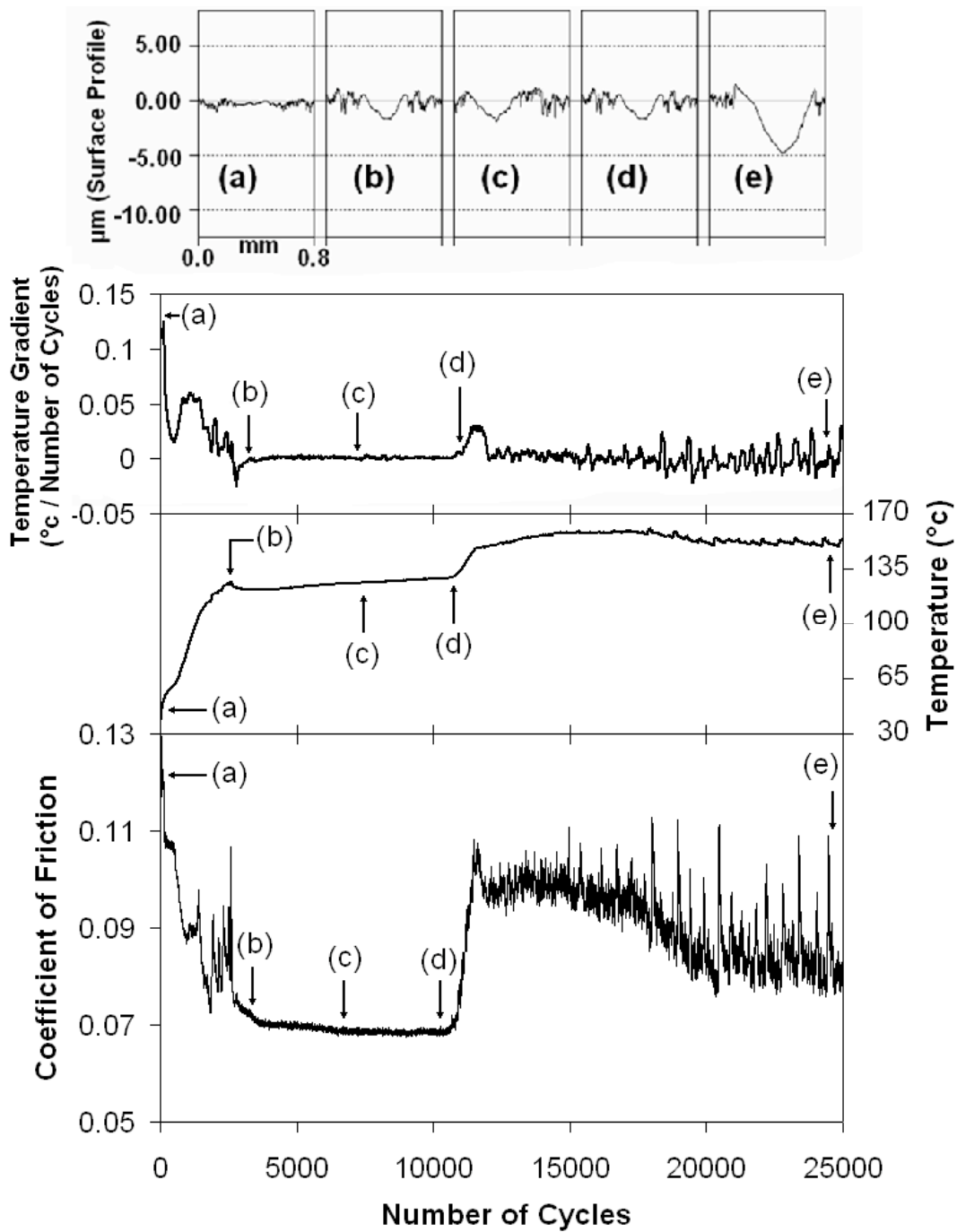


Figure 4.1: Friction, temperature and temperature gradient vs. number of cycles, data for a test run under 24 Kg applied load using a 1/4" diameter ball (3.56 GPa Hertzian load, on base oil + ZDDP with 0.10 wt% P) and the resulted wear profiles of the wear track generated on the surface of the ring at different stages; (a) At the start of the test, (b) the onset of the plateau region, (c) in the middle of the plateau region, (d) at the end of the plateau region and the start of the breakdown of the tribofilm, (e) at the end of the 25000 cycles.

The temperature close to the point of contact is measured with a thermocouple and is shown in the temperature vs. number of cycles part of figure 4.1. At the start of the test, there is a rapid increase in temperature associated with the lack of a stable tribofilm. Once a stable tribofilm is formed on the surface, the subsequent increase in temperature is much slower as reflected in the plateau region of the temperature vs. number of cycles plot. This is also reflected in the plot of the rate of change in temperature as a function of number of cycles where the smallest change in temperature is seen which is associated with the formation of a stable tribofilm. At the breakdown of the film i.e. point (d), there is a rapid increase in temperature as shown in the region between (d) and (e). The region between (d) and (e) corresponds to a situation where there is repeated formation and breakdown of a tribofilm. This is evident from the friction vs. number of cycles plot that shows sharp excursion in friction coefficient, the temperature plot shows undulations in this region. This behavior is represented by the plot of rate of change in temperature as a function of number of cycles that shows peaks associated with the excursions in friction coefficient. There is also a large increase in the amount of wear associated with this region. As shown by comparison between profiles (d) and (c).

Possible effects of the contact load on the duration and the onset temperature of the plateau regime are further explored in figure 4.2. Figure 4.2 shows that while the duration of the plateau region with the stable tribofilm is independent of the applied load, the temperature on the onset of the plateau region increases by 5-10 degrees Celsius as the Hertzian contact load increases by 0.10 GPa i.e. under higher contact loads, the break down of ZDDP and the formation of tribofilm results in higher temperatures. At the extreme load of 3.66 GPa there is no plateau region and no stable tribofilm is formed.

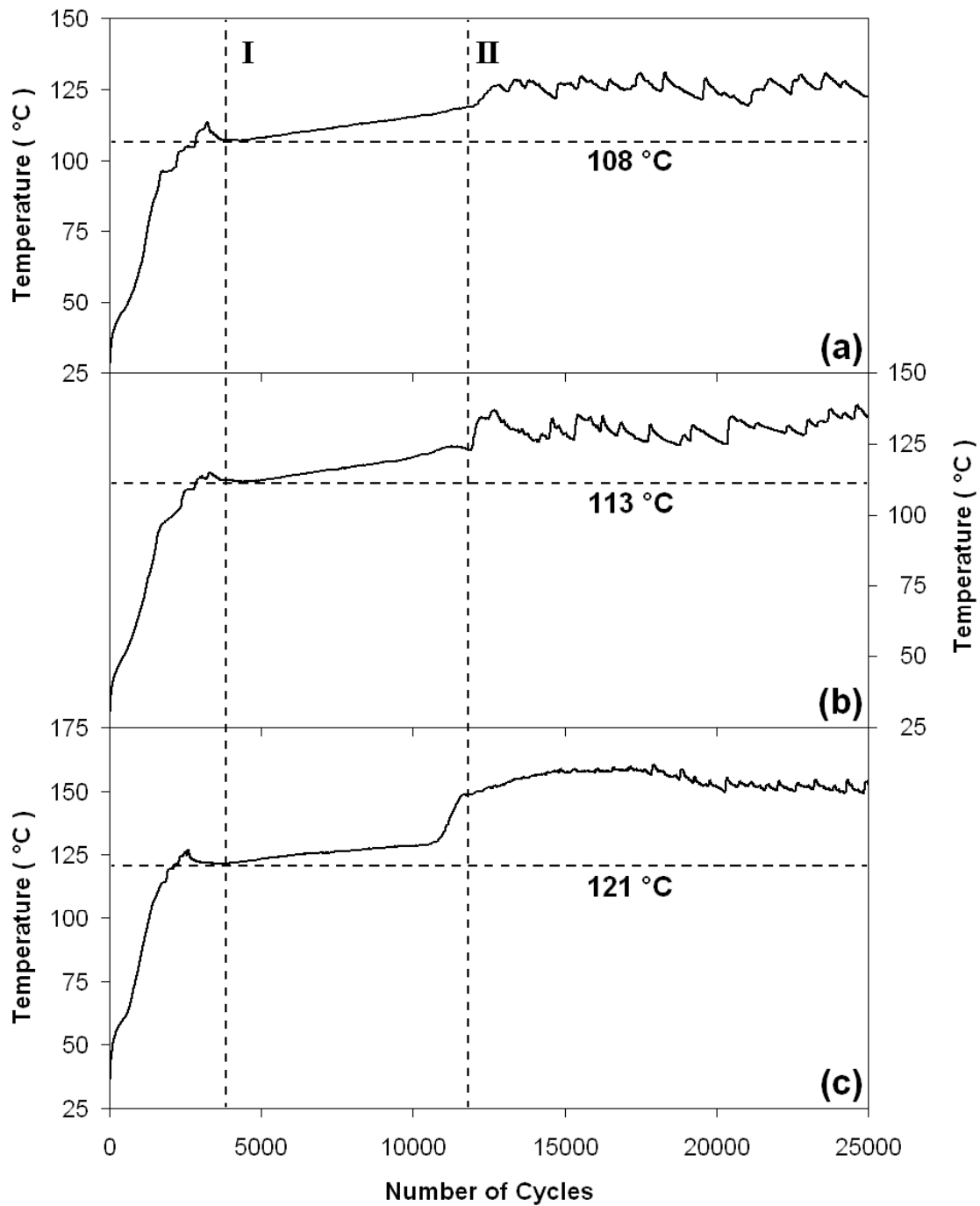


Figure 4.2: Temperature vs. number of cycles of three tests run using base oil + ZDDP (0.10 wt% P) using a ¼" diameter ball, with the applied loads of 3.35 GPa (a), 3.46 GPa (b) and 3.56 GPa (c), Lines I and II indicate the onset and the end of the plateau region associated with the formation and breakdown of the tribofilm respectively. The onset temperature for each load is also shown in each graph and indicates an increase of between 5-10 degrees Celsius with increasing applied load.

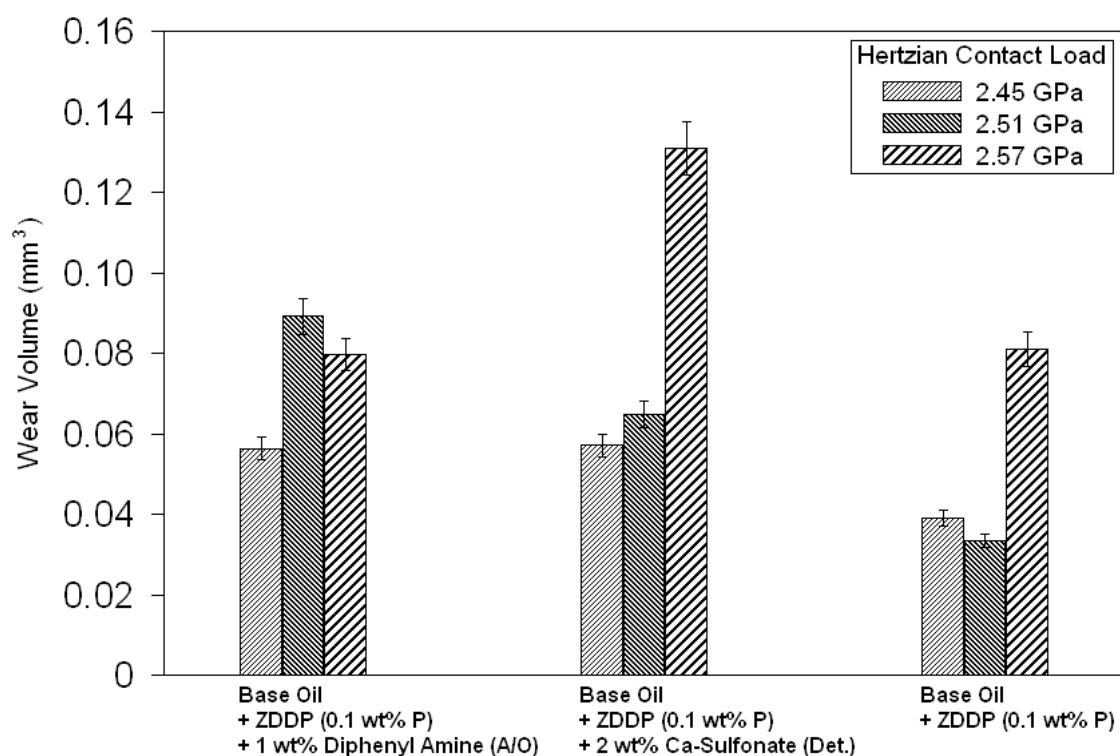


Figure 4.3: Wear volume data for tests run on three different formulations, containing ZDDP alone and with anti oxidant and detergent are shown. The tests were run using a ½ inch-diameter scuffing ball, for 25000 cycles.

4.2.2 The effect of additives

Influence of one additive at a time was evaluated on the antiwear performance of ZDDP under EP conditions. The test matrix of table 4.1 was run on the four oil samples. Three of the samples contain the same amount of ZDDP (0.10 wt% phosphorous). One sample contains 1 wt% anti oxidant (diphenyl amine) in addition to ZDDP and another contains 2 wt% detergent (calcium sulfonate) while the third sample does not contain any additional additives. All three samples were tested using a ½ inch diameter scuffing ball at the three different Hertzian contact loads of 2.41, 2.51 and 2.57 GPa to investigate the effect of these two additives. Figure 4.3 shows the wear volume data obtained for these three formulations at the three different loads. It can be observed that the antiwear performance of ZDDP was compromised when each of these

additives were present in comparison to with the case where only ZDDP is present in the mineral base oil as the sole additive.

Table 4.1: Test matrix of wear tests performed

Scuffing ball size	½ inch dia. ball			¼ inch dia. ball			
Hertzian Load (GPa)	2.45	2.51	2.57	3.35	3.46	3.56	3.66
Applied Load (Kg)	28	30	32	20	22	24	26
Oil Formulation Tested	Base Oil + ZDDP (0.10 wt% P)			Base Oil + ZDDP (0.10 wt% P)			
	Base Oil + ZDDP (0.10 wt% P) + 2 wt% Ca-Sulfonate						
	Base Oil + ZDDP (0.10 wt% P) + 1wt% Diphenyl Amine (A/O)			Base Oil + ZDDP (0.05 wt% P)			

4.2.3 Phosphorus concentration

Two formulation containing only base oil and ZDDP at two different loadings of phosphorous, i.e. 0.05 and 0.10 wt%, were tested using a ¼ inch diameter scuffing balls under four different Hertzian contact loads of 3.35, 3.46, 3.56 and 3.66 GPa (table 4.1). The wear volume results for these tests are shown in figure 4.4. While the overall performance is worsened for the formulation containing 0.05 wt% P for all loads compared to the case where 0.10 wt% P is present, yet it is observed that at the extremely high load of 3.66 GPa, this difference becomes more evident. At higher loads, the rise in contact temperature can be faster and the contact temperature is higher, resulting in burning off of the protective layer (the ZDDP break-down product). In addition, at higher loads the shearing effect of the scuffing ball may result in scraping off the layer from the surface; thus, more ZDDP would be needed to re-establish the antiwear transfer layer on the surface. At 0.05 wt% P, there is not enough ZDDP present in the oil to account for this loss and the surface is directly exposed to the scuffing ball surface for much longer time and the resulting wear is higher.

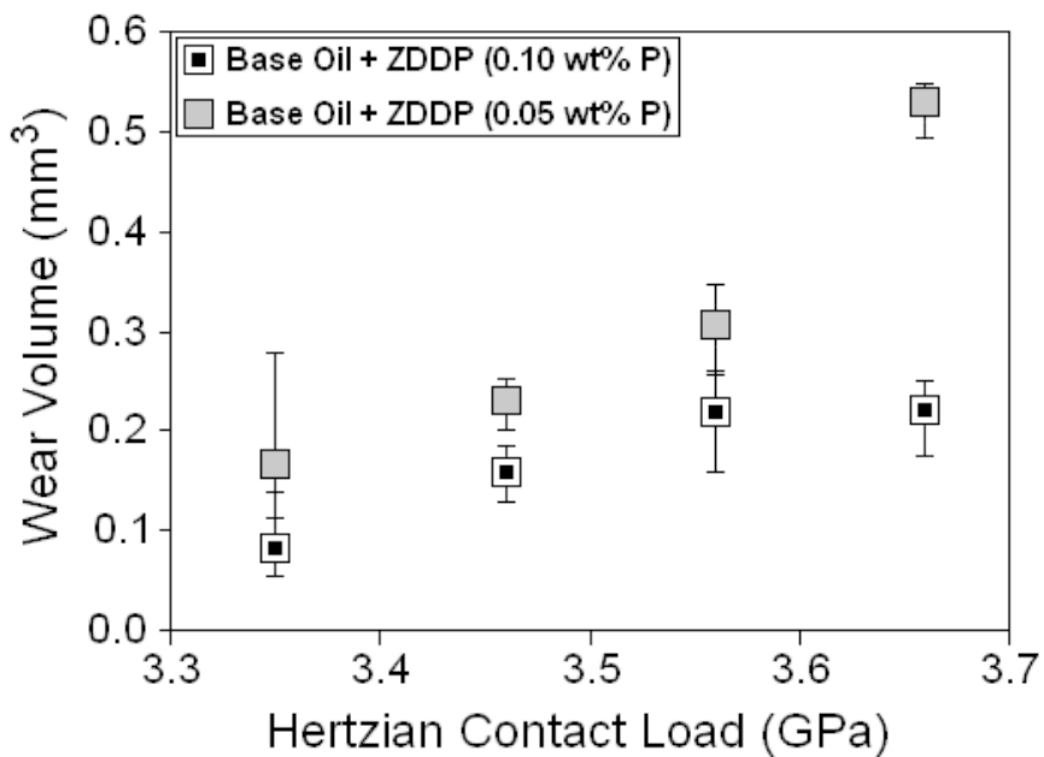


Figure 4.4: Wear volume vs. Hertzian contact load for the two different formulations: Base Oil + ZDDP with 0.10 and 0.05 wt% P. The tests were run using ¼ inch diameter tungsten carbide balls for 25000 cycles.

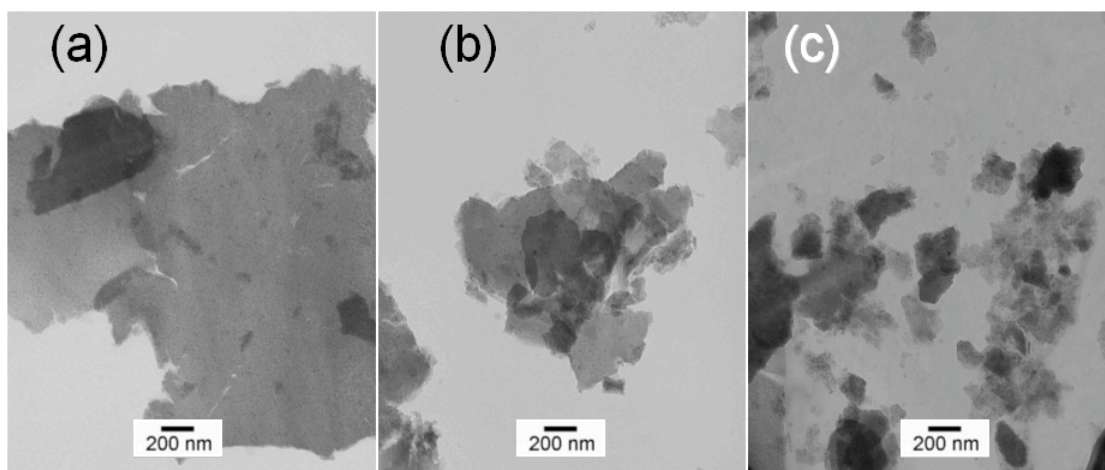


Figure 4.5: Bright field transmission electron micrograph (20K x magnification) of the wear debris harvested from wear tests run using oil containing base oil with 0.1 wt.% P at a Hertzian contact load of 3.56 GPa for (a) 5000, (b) 15000 and (c) 25000 cycles.

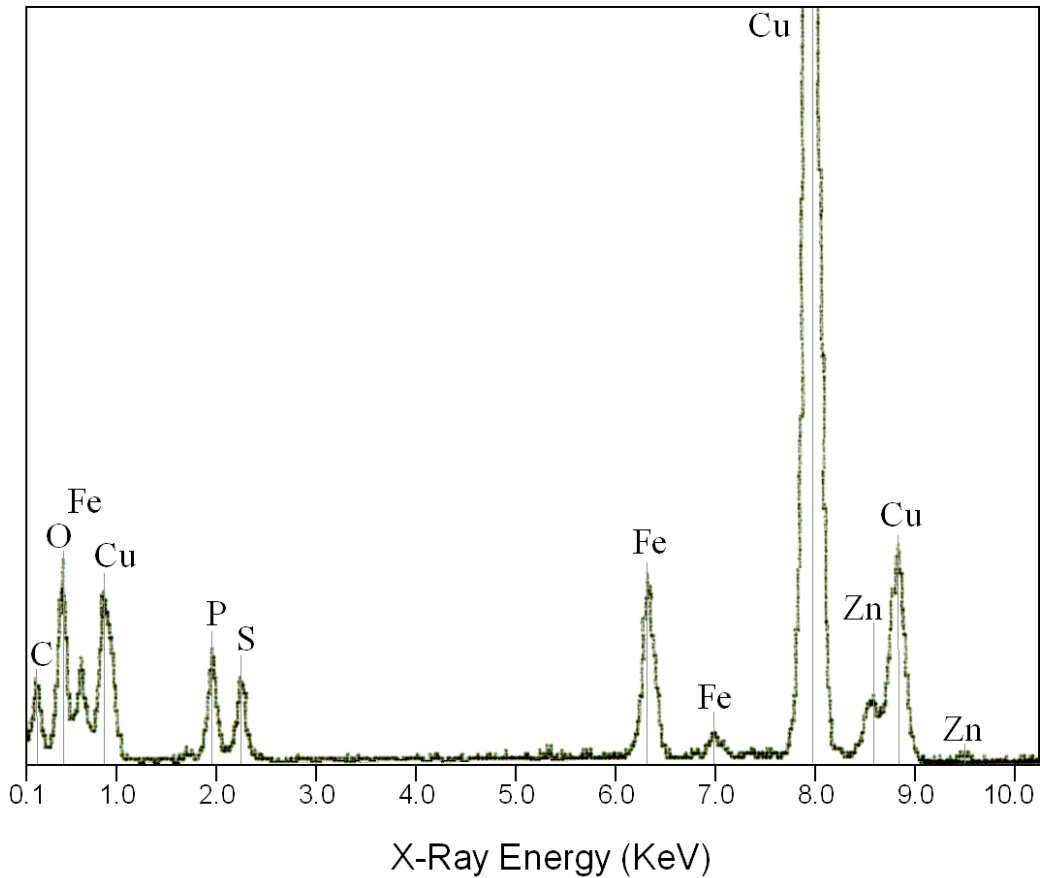


Figure 4.6: Energy dispersive X-ray (EDS) spectrum obtained from wear debris harvested from base oil sample containing ZDDP (0.10 wt% P) after 15000 cycles at the Hertzian contact load of 3.56 GPa.

4.2.4 TEM analysis of wear debris

In order to further study the nature of the tribofilm, the wear debris generated during a wear test were collected for observations using a 120 KeV analytical transmission electron microscope as described in the previous chapter. Figure 4.5 shows the transmission electron micrograph taken from wear debris of wear tests using the oil sample containing ZDDP and base oil with 0.10 wt% P tested under the Hertzian contact load of 3.56 GPa and for 5000 (a), 15000(b) and 25000(c) cycles. The images were taken at a magnification of 20000x and each show wear particles that are representative in size and shape of the majority of the particles seen for that particular sample. It is observed that the average size of the wear debris

decreases as the wear tests are run for longer periods of time. The size of the wear debris decreases throughout the test due to the milling of the particles under the extreme pressure conditions. The EDS spectrum of the wear debris shown in figure 4.6 for the test that was run on wear debris harvested after 15000 cycles is in agreement with findings of an earlier study by J.M. Martin *et al.* [27] showing the origin of the wear debris being the tribofilm. The spectrum confirms the presence of the main constituents of the tribofilm, i.e. phosphorus, sulfur, oxygen, carbon, iron and zinc and is similar to the EDS spectrum of the film obtained from the surface of the wear track that is shown in figure 4.9. Due to the presence of a steel substrate in the EDS spectrum obtained from the wear track (figure 4.8), iron peaks have a very high intensity the spectrum shown in figure 4.9 than in the spectrum obtained from the wear particles (figure 4.6) using TEM, hence the peaks arising from the presence of zinc in the tribofilm, are masked by the background generated from the steel substrate iron peaks in figure 4.8 while in the spectrum of figure 4.6, they are resolved and detected. The high intensity copper peaks observed in the spectrum of figure 4.6 are from the copper in the copper grid on which the wear particles are collected for TEM studies.

4.2.5 SEM and FIB analysis of tribofilm

An oil sample containing base oil with ZDDP (0.10 wt% P) was tested under the Hertzian contact load of 3.56 GPa (using ¼ inch diameter ball) for 15K cycles. The ring was then carefully cut and prepared for SEM and FIB analysis. The wear track area on the surface of each ring was observed under the SEM and an EDS map of phosphorous on the surface of the ring (in the vicinity of the contact area) was obtained. Figure 4.7 shows the scanning electron image of the surface of the ring where the wear track is located. The area in the immediate vicinity of the wear track is also visible in this image. The darker and smoother surface covering the wear scar in the middle area of figure 4.7 is the tribofilm generated by ZDDP. Figure 4.8 shows the EDS spectrum obtained from the tribofilm-covered region, which clearly confirms the presence of the film in this region as phosphorus, and sulfur peaks are quite visible.

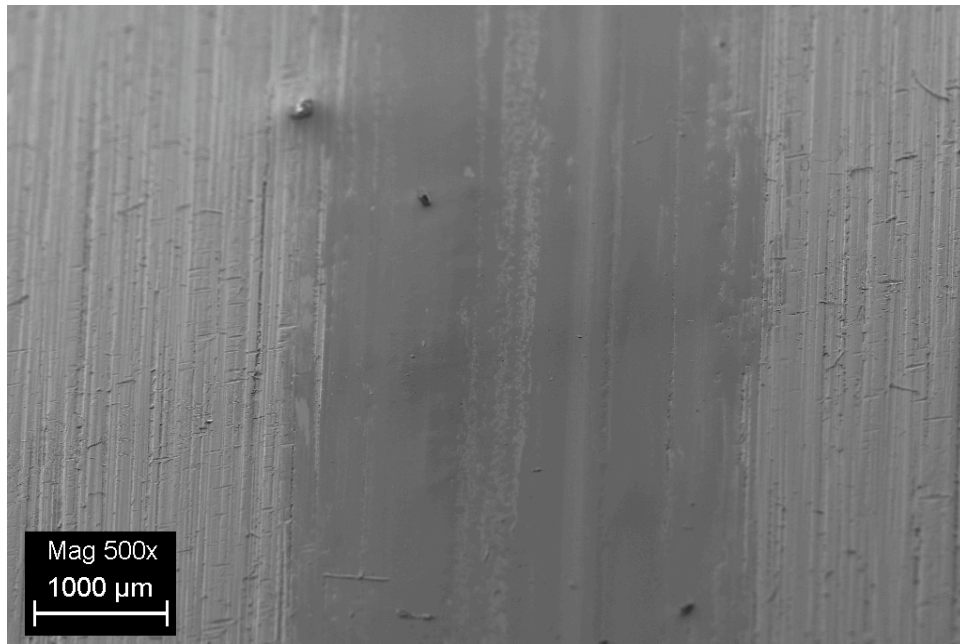


Figure 4.7: Secondary electron image of the wear track. The wear track shows a well-developed tribofilm over most of the surface, however, at certain locations the film has been ripped off from the surface.

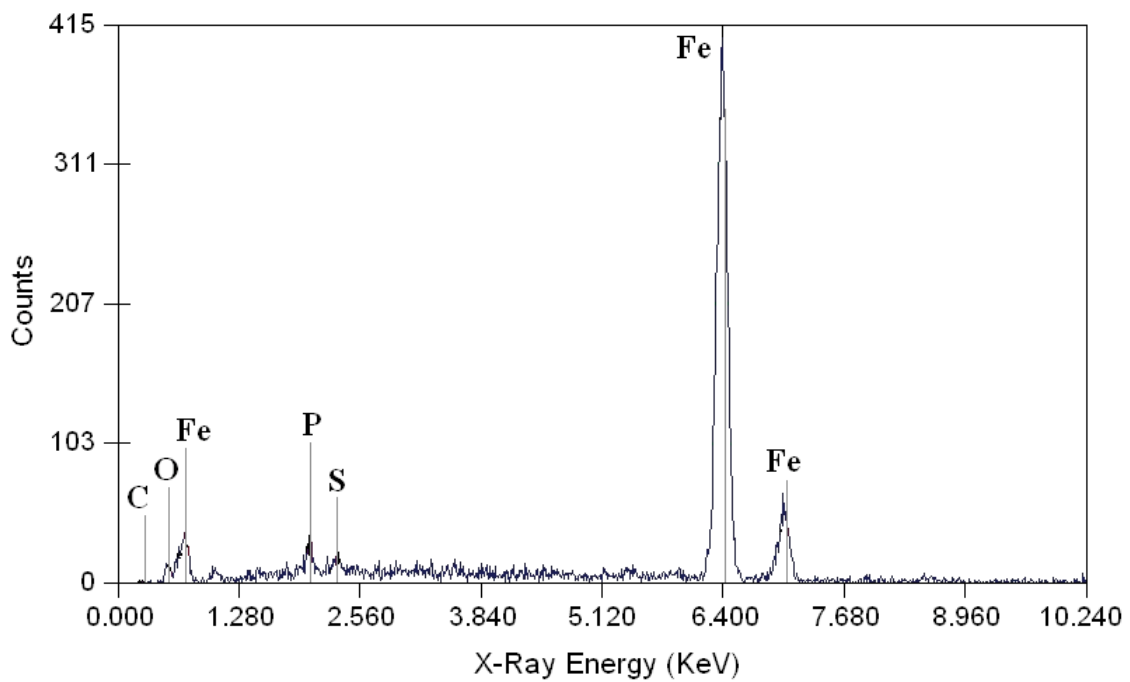


Figure 4.8: Energy dispersive X-ray (EDS) spectrum obtained from the tribofilm covering the wear track shown in figure 4.7.

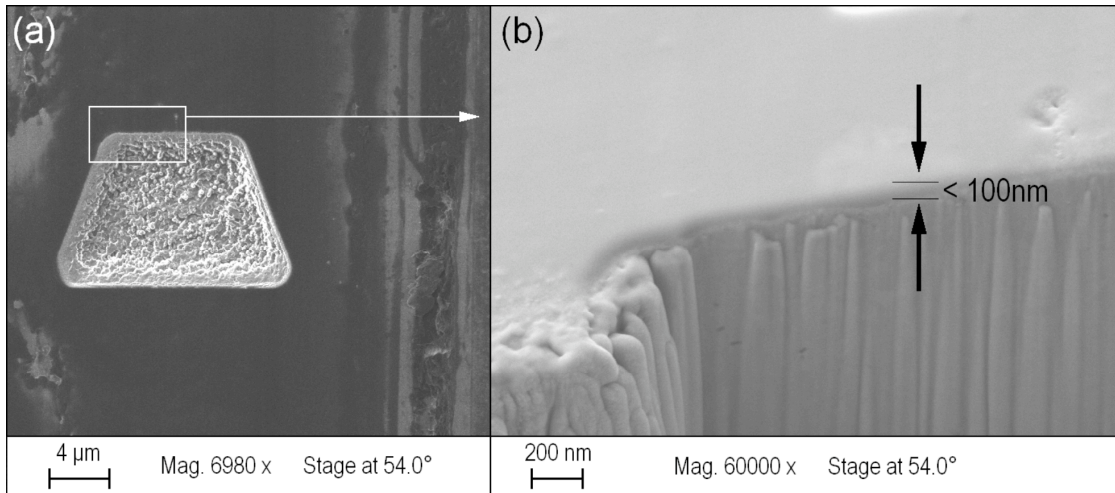


Figure 4.9: (a) A trench cut into the surface of a ring that was tested under boundary lubrication conditions. The smooth surface is a the tribofilm formed on the surface. The milling of the surface was conducted with gallium ion beam. (b) The image shows that the thickness of the tribofilm is approximately 100 nm thick and forms a very smooth surface conforming well to the substrate. The substrate is a 4140 steel with a fine pearlitic / bainitic microstructure. When ion milled, the softer Fe phase is preferentially removed revealing the underlying carbide structure.

In order to obtain a measure of the thickness of the film, focused ion beam was used to generate images of the cross section of the tribofilms for this sample. A trench of a depth of approximately 4 μm was created by ion milling of an area of 8 μm by 10 μm of the tribofilm. This trench is shown in figure 4.9 (a). Care was taken to select an area with continuous and uniform tribofilm. Figure 4.9 (b) is a scanning electron micrograph of the cross section of the tribofilm generated by the FIB. The thickness of the film is measured to be slightly less than 100 nm in the vicinity of the trenched area. Repeating the process at other locations on the tribofilm sample confirms this thickness to be consistent through out the tribofilm.

4.2.6 Nano-indentation and modulus mapping

The Hysitron TribolIndenter[®] was used to perform quasi-static indentation tests on the tribofilm generated on the same ring described in 4.2.6. The indenter tip used to measure the hardness and the reduced modulus of the tribofilm, is the NorthStar[®] cube corner probe as described in the previous chapter. Each indent consisted of a trapezoidal load function

comprised of a 5-second loading segment, a 2-second holding segment, and a 5-second unloading segment as shown schematically in figure 3.5 (a).

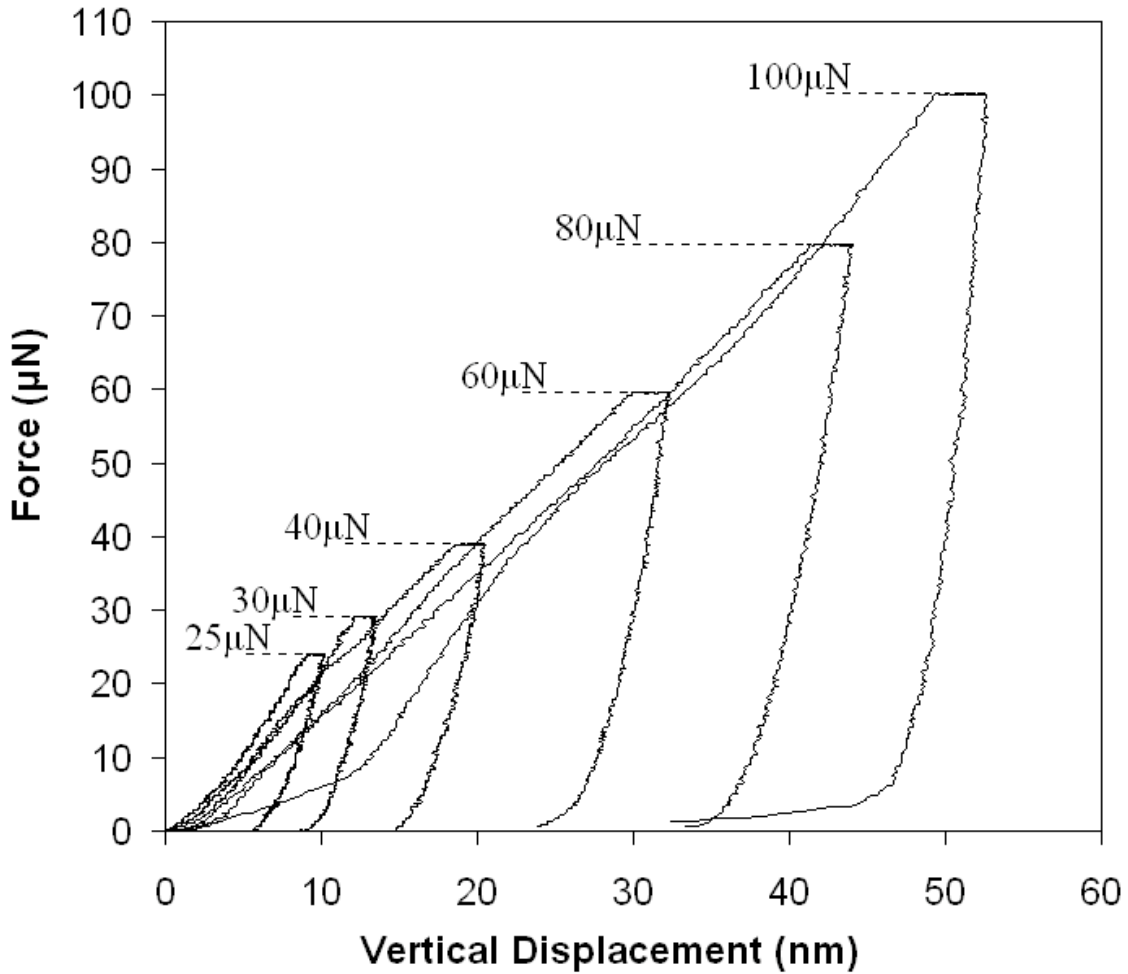


Figure 4.10: Force vs. displacement (penetration) graph for peak indentation loads ranging from 25 to 100 μN for the wear test run using oil containing base oil with 0.1 wt.% P at a Hertzian contact load of 3.56 GPa for 15000 cycles.

Once the uniformity of the film over the testing area was established, 10 load-controlled indents with peak loads ranging from 25 μN to 1500 μN were performed to measure tribofilm hardness and reduced modulus values as a function of contact depth, using the same load function described above. All indentations were performed in the same region on the tribofilm

within approximately 100 μ m of each other. To confirm accuracy of the data, for every maximum load, indents were repeated and were found to be very repeatable. Load vs. displacements graphs for indents with maximum loads ranging from 25 μ N to 100 μ N are presented in figure 4.10. Above 100 μ N, two indents with loads of 500 and 1500 μ N were performed. These two indents are not presented in figure 4.10 since the penetration depth is beyond the thickness of the tribofilm and well into the steel substrate and hence the data is not representative of the film properties.

The measured values of reduced modulus and hardness are shown in the plots of figure 4.11 for the peak loads ranging from 25 to 1500 μ N. It is observed that the measured values of hardness and reduced modulus for the two extreme loads of 500 and 1500 μ N are around 8 GPa and 200 GPa respectively which is consistent with such values for the steel substrate and remain constant from 500 μ N to 1500 μ N. For loads below 500 μ N on the other hand (25 – 100 μ N), the values of both hardness and reduced modulus decrease by increasing load and hence penetration. This observation suggests the presence of two layers in the tribofilm. A harder layer near the surface of the film and a softer layer closer to the substrate. The plots of figure 4.11 also confirm the observations made regarding the film thickness in the FIB image shown in figure 4.9. The measured values of hardness and reduced modulus range from 20.4 to 6.3 GPa and from 231 to 126 GPa. The thickness of the film can also be approximated using the data plotted in figure 4.11 which clearly indicate that the steel substrate properties are measured at contact depths of more than 100 nm which confirms the thickness of the tribofilm observed in the FIB Secondary electron image of the tribofilm and the steel substrate in figure 4.9.

In other studies of tribofilms, generated at constant loads, it was shown that the tribofilms are made up of two layers. The thicknesses of the films were also found to be around 100 nm, however, in a study, using MoDTP (Molybdenum Dithiophotes) and ZDDP mixture [8, 26, 101], it was shown that the hardness neat the surface of the tribofilm is lower than deeper in

the tribofilm. This difference in outcome may be attributed to the lighter contact loads used in their study. In a quantum chemical modeling study by Müser *et al.* [34-37] it was shown that pressure induced cross linking of the zinc polyphosphates near the surface result in tribofilms that are harder near the surface.

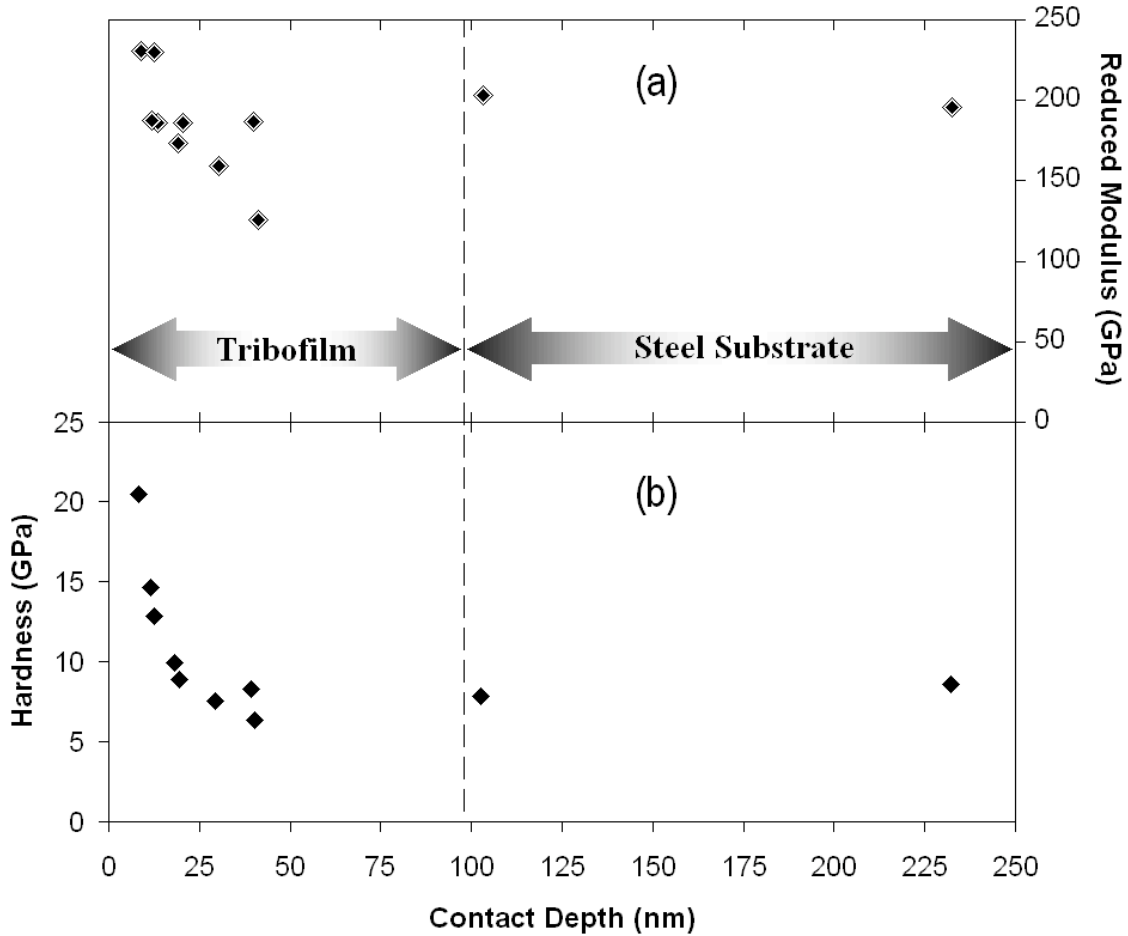


Figure 4.11: Plots of (a) reduced modulus and (b) hardness versus contact depth obtained from indents with peak loads ranging from 25 to 100 μN for the same sample as in figure 4.10.

This results is consistent with the findings of our experiments that indicate a near surface region with hardness as high as 20 GPa (Figure 4.11) compared to substrate hardness of 8 GPa (steel). In addition, the cross linked network of zinc polyphosphates results in moduli

of tribofilm (100-120 GPa) that are substantially lower than that of the steel substrate (200 GPa), thus the tribofilms behave as compliant surfaces, absorbing and dissipating energy when they go in and out of contact.

CHAPTER 5

COMPARISON OF TRIBOLOGICAL BEHAVIOR OF FLUORINATED ZDDP AND ZDDP

The purpose of this segment of the study is to establish the properties of tribofilms generated from fluorinated ZDDP in comparison to ZDDP. Tribological tests using oil samples containing both fluorinated ZDDP and untreated ZDDP were conducted to evaluate the wear performance of the two chemistries as well as to generate tribofilm samples for characterization of these films. The characterization techniques used have been discussed in detail in chapter 3 and are employed to examine the nature of the tribofilms.

5.1 Materials and procedures

Oil samples were prepared by adding the untreated secondary alcohol ZDDP research sample containing 7.2 wt.% phosphorus (see chapter 4) to 100 neutral mineral base oil at loadings of 0.10 and 0.01 wt.% phosphorus. Fluorinated ZDDP was also added to the same neutral base oil at loadings of 0.10 and 0.01 wt.% phosphorus.

The fluorinated ZDDP was produced by reacting the same ZDDP described above with FeF_3 [113]. The mixture was then centrifuged to separate fluorinated ZDDP as decant. The phosphorous, zinc and iron contents of the decanted material were measured according to ASTM D5185 analysis method using inductive coupled plasma atomic emission spectroscopy (ICP-AES) by Analytical Testing Services, (Franklin, PA, USA). Fluorine analysis was conducted separately by completely combusting to a fluoride and using iron chromatography by QTI laboratories (Whitehouse, NJ, USA) elemental analysis of the decanted material indicate the exact same zinc and phosphorus level as that of ZDDP (8.6 wt.% and 7.2 wt.% respectively), and also presence of fluorine in the fluorinated ZDDP at around 1.1 wt.%. The current knowledge on the chemical structure of the fluorinated ZDDP compounds is described in

chapter 2. Wear tests were carried out using the UTA BOCLE unit as well as the Plint[®] BOCLE unit which have according to the protocols described in chapter 3. Chemical analyses of tribofilms generated on the steel surfaces were carried out using Auger electron spectroscopy (AES) and scanning electron microscope (SEM) coupled with energy dispersive X-ray spectrometry (EDS). Wear debris were also examined using transmission electron microscopy (TEM) coupled with EDS. The crystallinity of the tribofilms and wear debris was examined by generating diffraction patterns using the TEM. Focused ion beam (FIB) was also used to image the substrate-tribofilm interface as well as to measure the thickness of the tribofilms. Nano-indentation was also used to examine the mechanical properties of the tribofilms by conducting nano indentation; nano-scratch and nano-wear tests on tribofilm specimens generated by fluorinated ZDDP and ZDDP. In addition to mechanical properties such as hardness and modulus profiles of tribofilms, the nano mechanical test data is also analyzed and utilized to identify the presence of different layers with different mechanical properties within the tribofilms generated with these two chemistries under different condition.

5.2 Results, observations and discussion

5.2.1 Friction, temperature and wear data

Wear tests were run on two oil samples each containing 0.10 wt % phosphorus with the source of phosphorus in one sample being untreated ZDDP and in the other fluorinated ZDDP. These wear tests are run under an applied Hertzian contact load of 3.56 GPa (i.e. 24 Kg applied load) for the duration of 15000 cycles.

In figure 5.1 the temperature (a) and the coefficient of friction (b) data are plotted against the number of cycles for wear tests run for 15000 cycles. Wear volume for these tests is also presented in figure 5.1 (c). The wear volume is an average of the amount of wear measured for each test and two additional repeats of each test (total of three runs). Three distinct regions can be observed in the friction vs. cycles data in each case. At early stages of each test, the coefficient of friction is observed to increase.

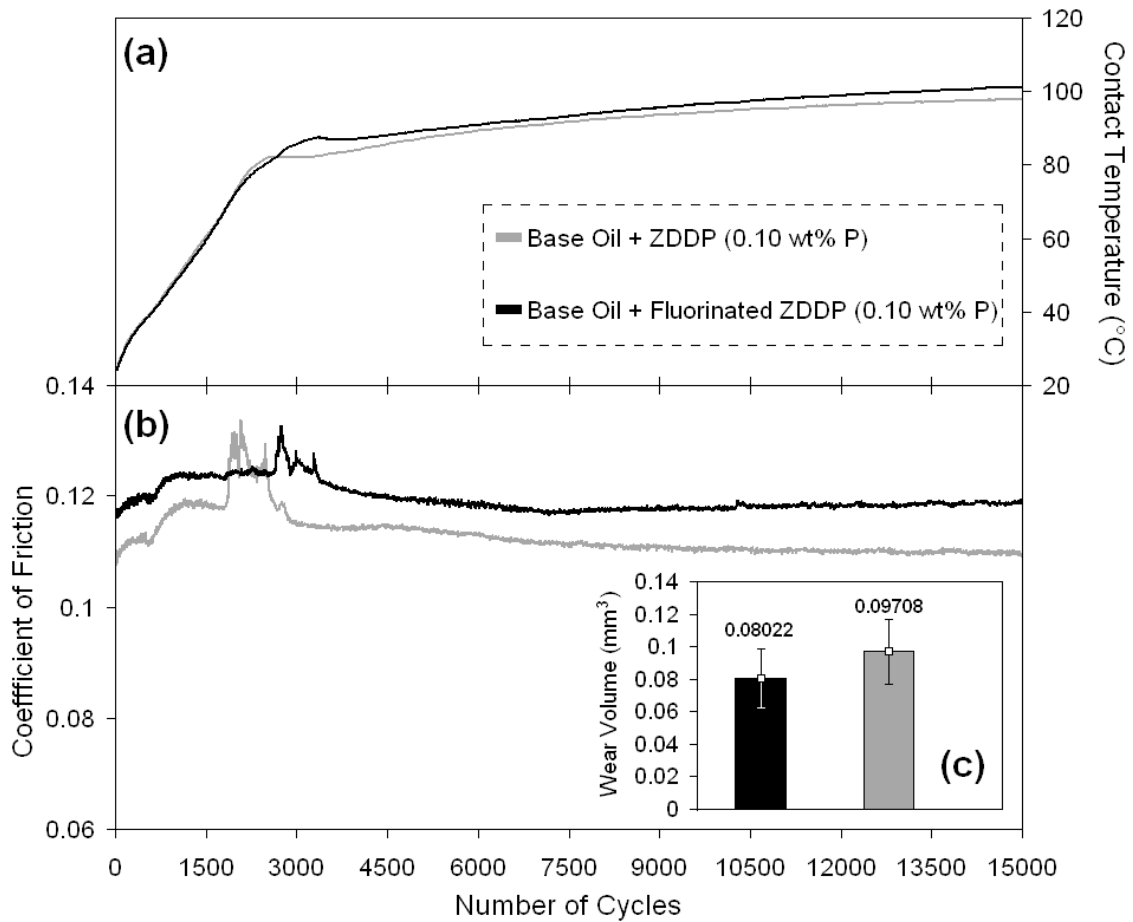


Figure 5.1: Tribological data for wear test run for 15000 cycles under 3.56 GPa Hertzian contact load on oils containing 0.10 wt% P: (a) temperature and (b) friction vs. number of cycles (c) wear volume data.

At around 2000 cycles, there is a sudden increase in the coefficient of friction followed by peaks and valleys. After this regime, the coefficient of friction stabilizes to a constant value at around 4000 cycles until the maximum number of cycles is reached. This plateau regime is associated with the formation of a stable tribofilm on the contact surface. Wear tests were also run on oil samples containing 0.01 wt% phosphorus under 3.05 GPa contact load (14 Kg applied vertical load). The tests were run for 15000 and 50000 cycles to examine the effect of test duration on the durability and antiwear performance of the tribofilms formed in each case. This level of phosphorus is well below the phosphorus level in GF4 engine oils. The tribological

data for 15000-cycle tests are presented in figure 5.2. The same set of data is shown in figure 5.3 for the tests run for longer periods of time, i.e. 50000 cycles.

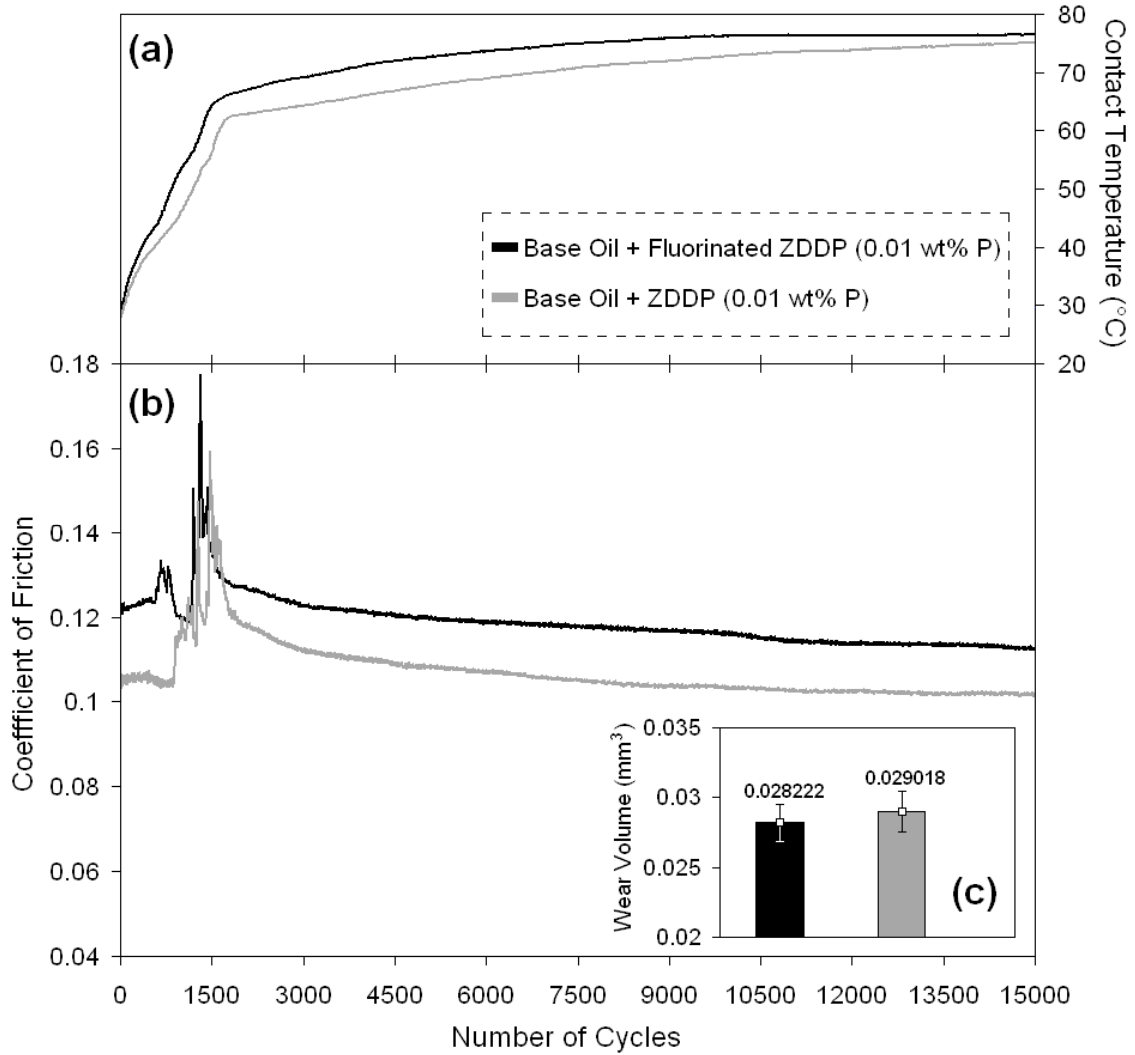


Figure 5.2: Tribological data for wear test run for 15000 cycles under 3.05 GPa Hertzian contact load on oils containing 0.01 wt% P: (a) temperature and (b) friction vs. number of cycles (c) wear volume data.

In all three cases it is observed that the wear volume is higher in the case of base oil mixed with untreated ZDDP than in the case where the phosphorus content comes from fluorinated ZDDP. This indicates the presence of a wear resistant tribofilm and hence better anti

wear performance by the fluorinated ZDDP as opposed to untreated ZDDP. While the numbers for wear volume are close for the case of oils containing 0.01 wt.% phosphorus, it is observed that this difference becomes greater when the tests are run for 50000 cycles and the improvement from fluorinated ZDDP over untreated ZDDP is significant.

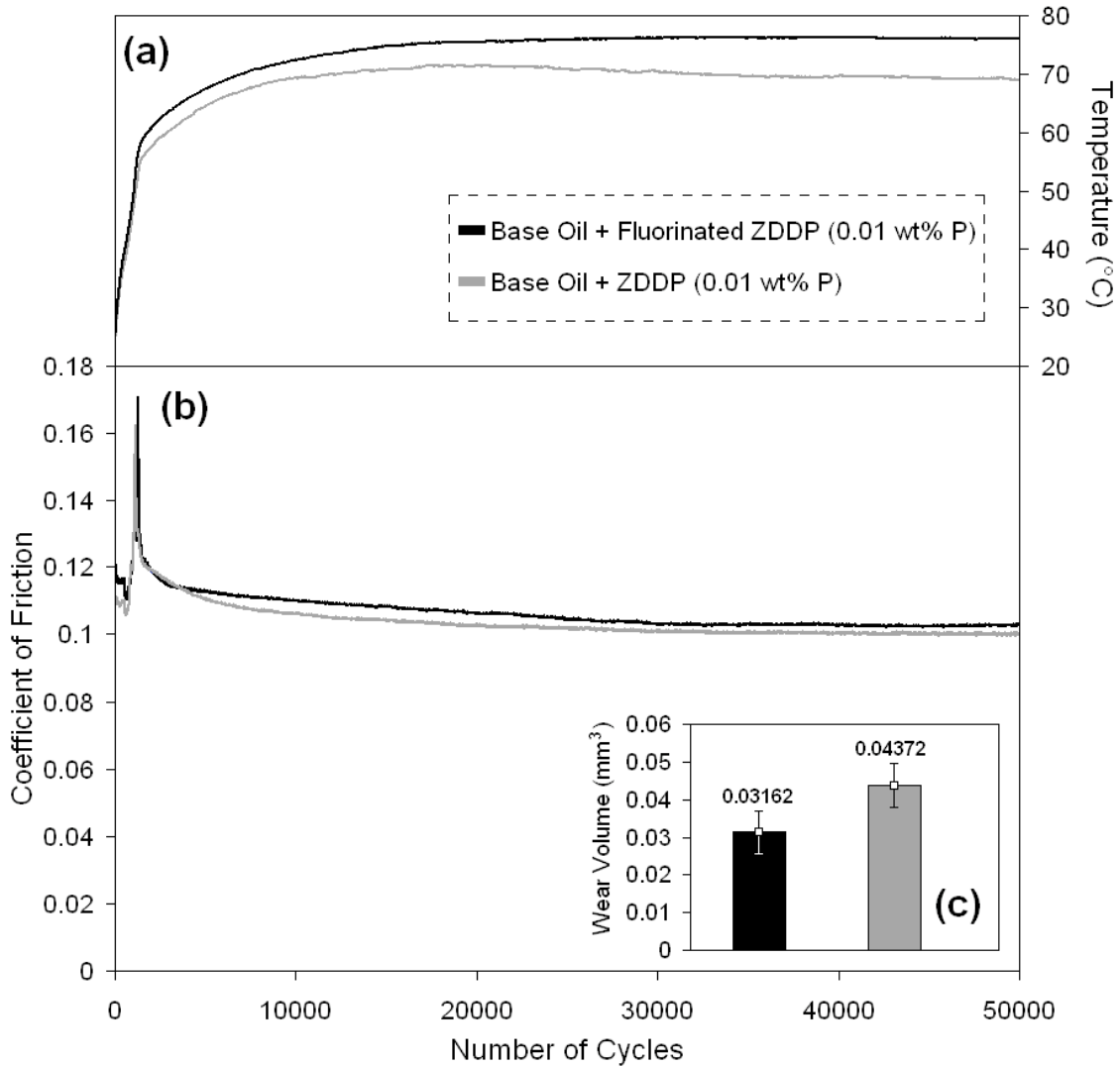


Figure 5.3: Tribological data for wear test run for 50000 cycles under 3.05 GPa Hertzian contact load on oils containing 0.01 wt% P: (a) temperature and (b) friction vs. number of cycles (c) wear volume data.

The wear data referred to in figures 5.1, 5.2 and 5.3 (c) are in line with observations made by Parekh and Aswath [130] for which the fluorinated ZDDP was produced by baking ZDDP and iron (III) fluoride at a higher temperature (150 °C) for shorter period of time (20 minutes). That data is shown in figure 5.4 for comparison.

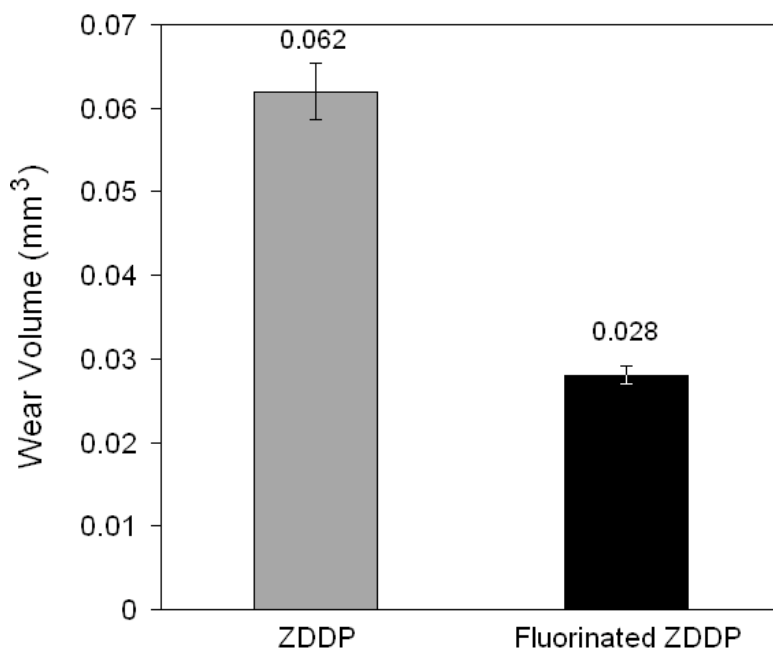


Figure 5.4: Wear data show for wear tests run on samples containing ZDDP and fluorinated ZDDP in base oil (0.10 wt% P) run under 3.56 GPa Hertzian contact load for 25K cycles [130].

Wear tests were also run on fully formulated oil samples using the Plint[®] BOCLE unit. Wear tests were run on two fully formulated oils. An oil samples were provided by Infineum corporation where formulated with all commonly used additives according to GF4 specification except for ZDDP (or any other antiwear additive). ZDDP and fluorinated ZDDP were added at low phosphorus loading of 100 ppm (0.01 wt%) to make two oil samples. Tests were carried out using the Plint[®] BOCLE unit under an applied load of 287 N and for 100K cycles. Details of the Plint[®] BOCLE operation specifications are described in chapter 3. Running the wear tests for

100K cycles in this series of tests allows for evaluating the durability of tribofilms generated as well as the antiwear performance of the two chemistries. Figure 5.5 shows wear volume data for the two oil samples in these tests.

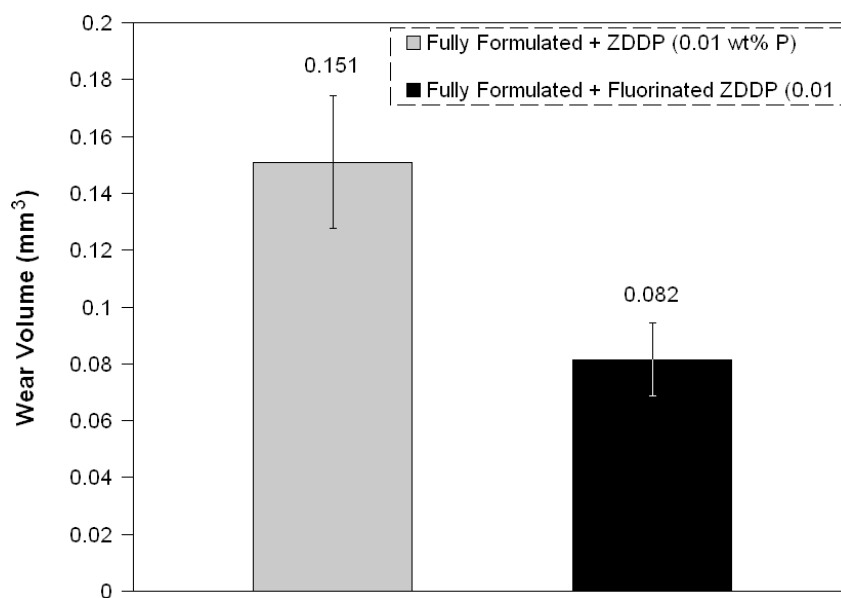


Figure 5.5: Wear data show for wear tests run on samples containing ZDDP and fluorinated ZDDP in fully formulated oil (0.01 wt% P) using the Plint[®] BOCLE.

5.2.2 SEM / EDS and FIB analysis of tribofilms

Scanning electron micrographs of two wear tracks (covered with tribofilm) formed by ZDDP and fluorinated ZDDP are shown in figures 5.6 (a) and 5.7 (a) respectively. To generate the SEM samples, wear tests were run under 3.56 GPa contact load for 15000 cycles on two oils samples containing 0.10 wt% phosphorus using the UTA BOCLE unit. For the sample shown in figure 5.6, the source of phosphorus in tested oil was untreated ZDDP and for the sample of figure 5.7, the source of phosphorus was fluorinated ZDDP. The EDS spectra for each case are shown figures 5.6 (b) and 5.7 (b). While there is almost no zinc present in either case, phosphorus and sulfur are both present in both cases. The high intensity of Iron peaks is from the Iron present in the steel substrate.

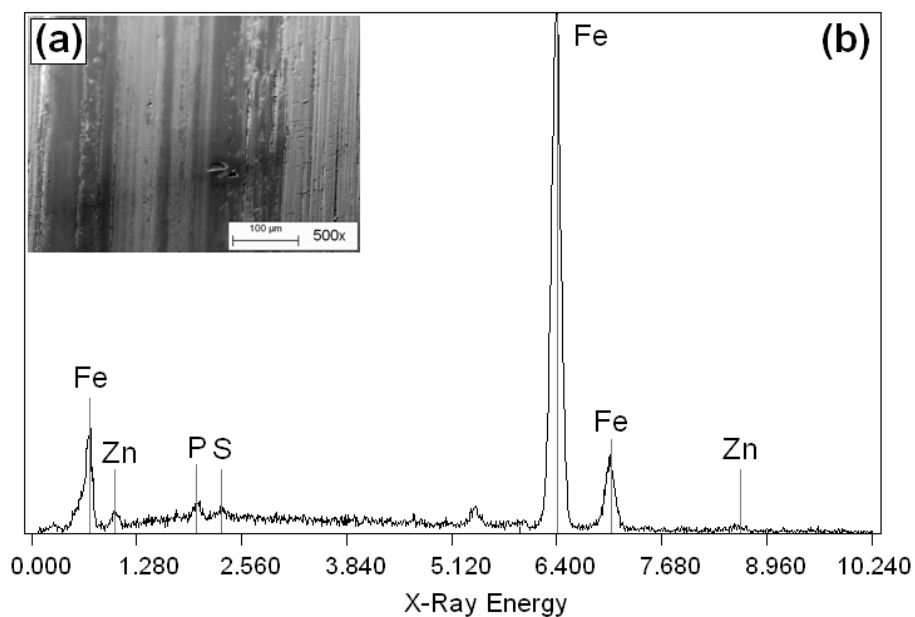


Figure 5.6: (a) Scanning electron micrograph of wear track from wear test run under 3.56 GPa Hertzian contact load for 15000 cycles on oil sample containing base oil and ZDDP (0.10 wt% P) and (b) EDS spectrum from the tribofilm.

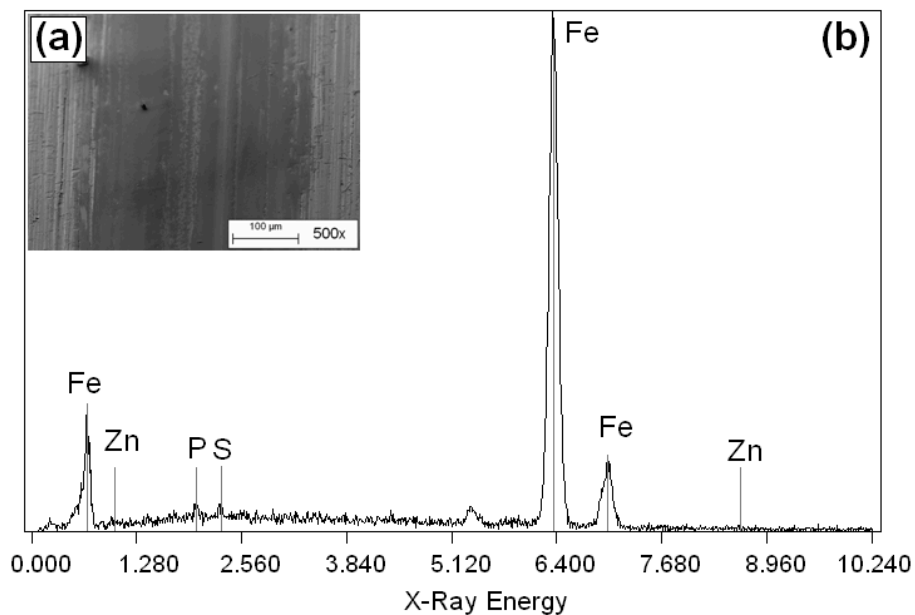


Figure 5.7: (a) Scanning electron micrograph of wear track from wear test run under 3.56 GPa Hertzian contact load for 15000 cycles on oil sample containing base oil and fluorinated ZDDP (0.10 wt% P) and (b) EDS spectrum from the tribofilm.

Scanning electron microscopy was also carried out on the wear scar created on tungsten-carbide balls during the tribotesting of the samples shown in figures 5.6 and 5.7. In both samples, the wear scar surface consist mainly of exposed tungsten-carbide phase, few separate patches of tribofilm are however observed on the surface of each wear scar as scattered dark patches shown in figures 5.8 (a, b) and 5.9 (a, b). EDS spectra acquired from these dark patches on wear surfaces shown in figures 5.8 (c) and 5.9 (c) show relatively strong sulfur and phosphorus peaks which were not observed from spectra obtained from areas of the wear scars not covered by these patches, which confirms that these patches are ZDDP and fluorinated ZDDP tribofilms. Due to the inert and passive nature of tungsten carbide phase, it is more likely that these separate patches of have actually been formed on the wear track surface on steel rings and then transferred to the opposite tribosurface, i.e. the tungsten carbide surface of the wear scar on the scuffing balls. This is in part, confirmed by the iron peaks observed in the EDS spectra of both samples, since the only source of iron in this tribosystem is the steel ring. Another observation in both EDS spectra of figures 5.8 and 5.9 is the presence of zinc peaks. Although both phosphorus and sulfur peaks have been observed in the EDS spectra obtained from both the tribofilms formed inside the wear track on the steel rings (figures 5.6 and 5.7) as well as the EDS spectra obtained from wear debris (using TEM) which are shown in figures 5.15 and 5.16 later in this chapter, no zinc peaks have been observed in either of these spectra. The presence of zinc in the spectra obtained from tribofilm patches on wear scars on tungsten carbide balls, can be interpreted as follows: the tribofilm patches transferred on the wear scar surface on the tungsten balls, have been removed from the outer layers (away from the steel substrate) of the tribofilms generated inside the wear track on the steel rings, they are richer in zinc in comparison to the inner layers of tribofilm as well as the bulk of tribofilm.

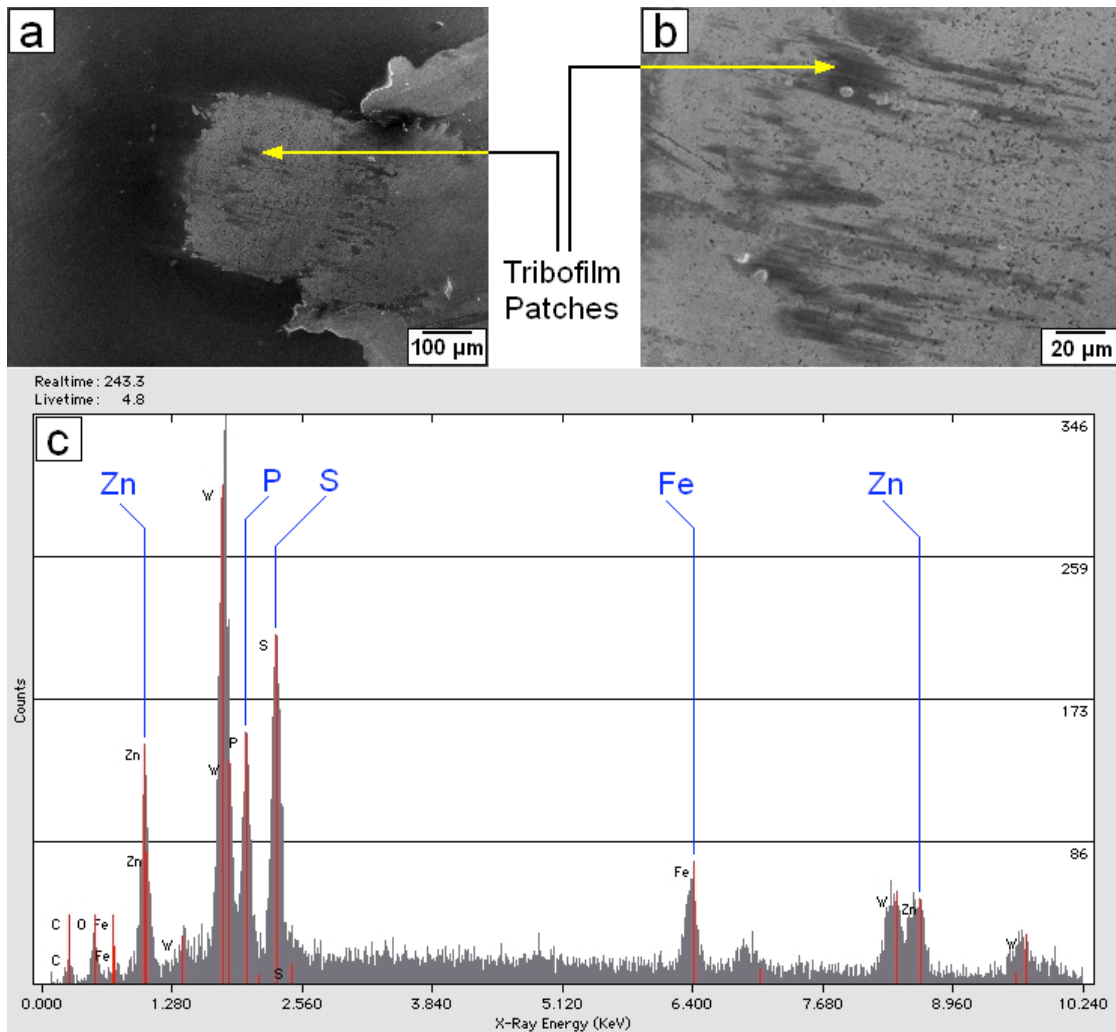


Figure 5.8: Scanning electron micrographs of post test wear scar on the scuffing ball at (a) 100x and (b) 500x magnification for the wear test run under 3.56 GPa Hertzian contact load for 15000 cycles on oil sample containing base oil and ZDDP (0.10 wt% P). Several patches of tribofilm are observed as dark spots inside the wear scar, and (c) the EDS spectrum obtained from a patch of tribofilm.

Scanning electron micrographs of the wear scar are shown in figures 5.8 and 5.9. At the lower magnification (100x) micrographs, the wear scar is visible as a circular bright area with small separate dark patches of tribofilm scattered on it. An area of dark, smooth surface is observable covering the area in the vicinity of the wear scars observed in each figure. This

smooth surface is thermally deposited tribofilm from ZDDP (figure 5.8) and fluorinated ZDDP (figure 5.9).

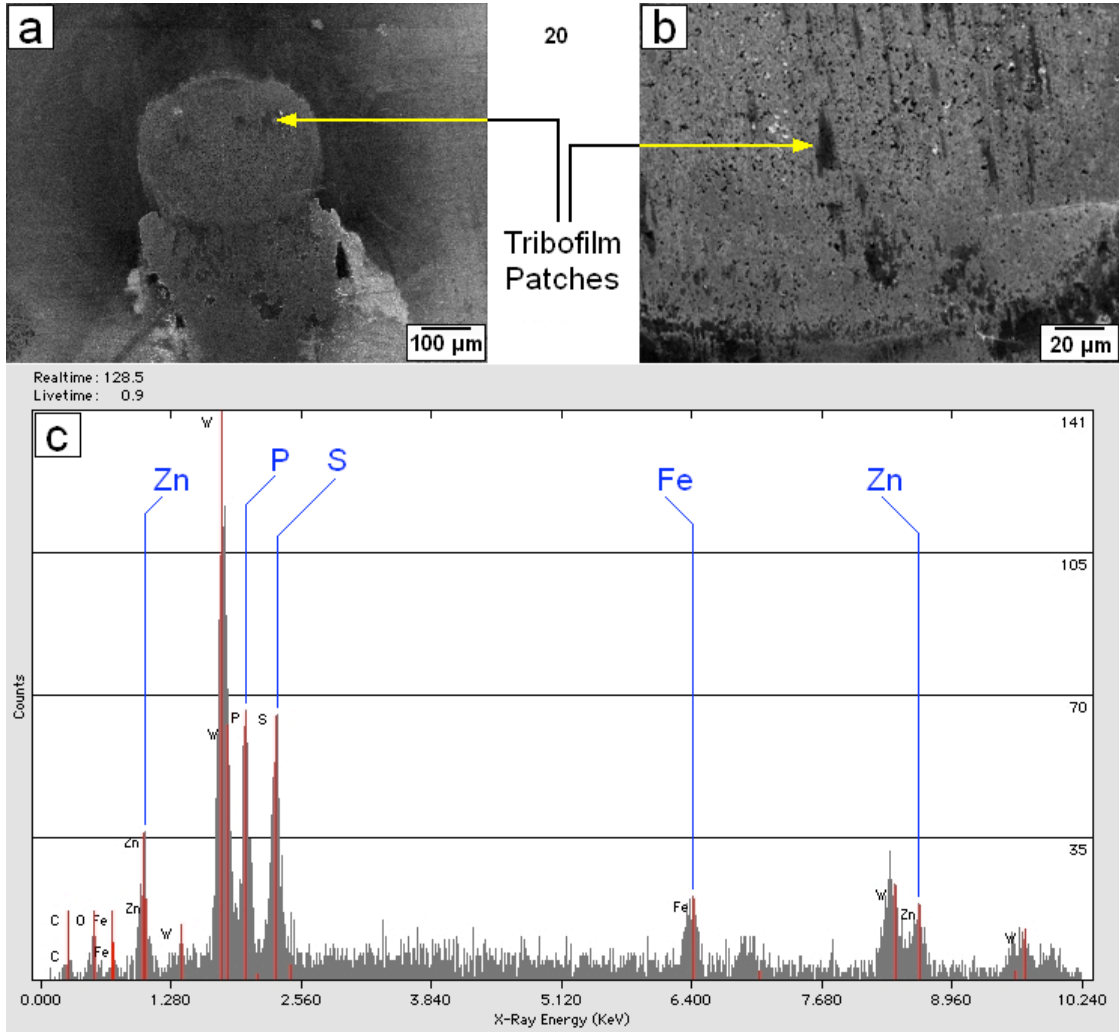


Figure 5.9: Scanning electron micrographs of post test wear scar on the scuffing ball at (a) 100x and (b) 500x magnification for the wear test run under 3.56 GPa Hertzian contact load for 15000 cycles on oil sample containing base oil and fluorinated ZDDP (0.10 wt% P). Several patches of tribofilm are observed as dark spots inside the wear scar, and (c) the EDS spectrum obtained from a patch of tribofilm.

The temperature vs. cycles curve for these two tests, shown in figure 5.1 (a) indicate that contact temperature during both tests has remained above 100 °C for most of the duration

of the test, as a result, ZDDP and fluorinated thermal films have been deposited in the vicinity of the contact point (i.e. wear scar) where temperatures have remained above the thermal decomposition temperature of both ZDDP and fluorinated ZDDP. EDS spectra obtained from this region (not shown) showed strong P, S and Zn peaks confirm this observation.

EDS spectra obtained from the surface of the wear scar generated on the tungsten-carbide scuffing balls, for both ZDDP and fluorinated ZDDP are quite identical. The only noticeable difference between the two spectra is the relative intensity of phosphorus and sulfur peaks; whilst in the case of fluorinated ZDDP, these peaks are of comparable intensity, in the case of ZDDP, the sulfur peak has a relatively higher intensity in comparison to the phosphorus peak. This trend is also observed in the relative intensity of the phosphorus and sulfur peaks in the EDS spectra acquired from the wear debris using the TEM which are shown in figures 5.15 (d) and 5.16 (d). Here also, phosphorus peak is relatively more pronounced in the case of fluorinated ZDDP than in the case of ZDDP. Since EDS data can vary from one location to another location on the surface of the tribofilms and from one run of the same test to another, the trend observed may be an artifact of the natural fluctuations in data and is not conclusive.

Focused ion beam was used to generate images of the cross section of the tribofilms formed on the wear track for both samples described above. A 4 μm -deep trench was created by ion milling of a uniform area of 8 μm by 10 μm of the tribofilm on each tribofilm sample described in 4.2.5. Figure 5.10 (a) is the same as figure 4.10 (b) and shows the SEM micrograph of the cross section of the tribofilm generated from ZDDP present in base oil (0.10 wt.% P) with an observed thickness of just below 100 nm. Figure 5.10 (b) shows a scanning electron micrograph of the cross section of the tribofilm generated from fluorinated ZDDP in base oil (0.10 wt.% P). It is observed that tribofilm in this case is almost twice as thick as in figure 5.10 (a). Also observable in the cross section view of the tribofilm in figure 5.10 (b) is the presence of two distinct layers of tribofilm. For the tribofilm generated from untreated ZDDP in

base oil (figure 5.10 b) on the other hand, no distinct layers are observable in cross sectional profile of the tribofilm.

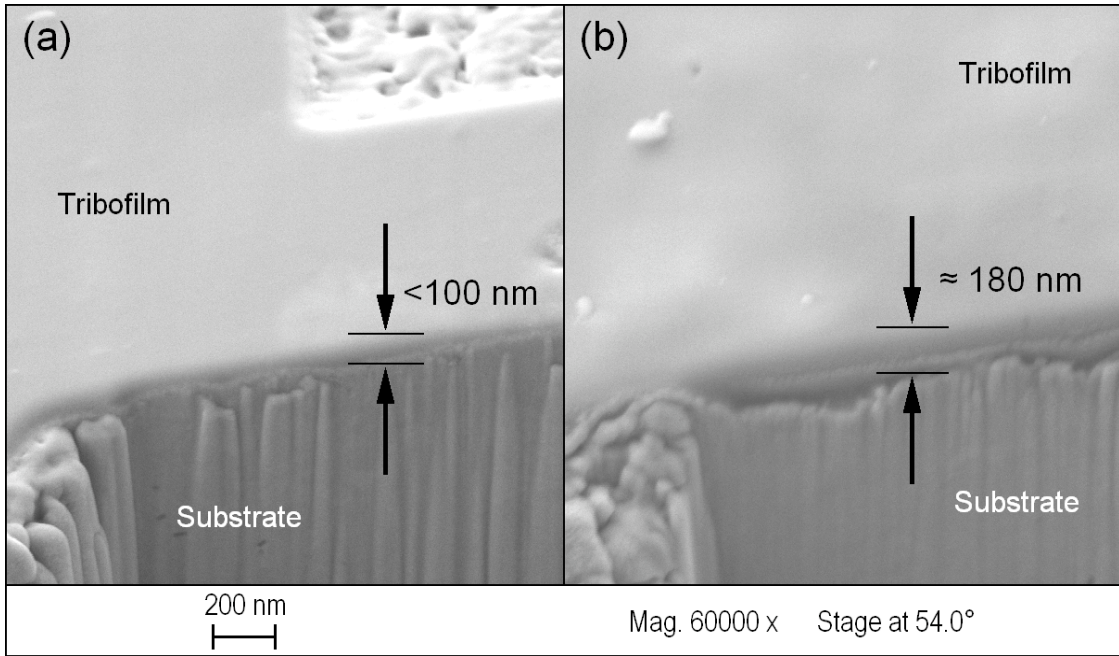


Figure 5.10: SEM micrographs of cross section of tribofilm and substrate on the edge of a trench ion milled by FIB for oils containing base oil and (a) ZDDP and (b) fluorinated ZDDP (both with 0.10 wt% P).

The SEM micrographs shown in figure 5.10 are representative of several similar observations that were made in this way using the FIB to measure the tribofilm thickness formed on the wear track on steel rings, and the measured tribofilm thickness was seen to be consistent with the values shown in figure 5.10 in different locations on the tribofilm. The thickness observed for the tribofilm generated from untreated ZDDP is found to be less than 100 nm, which is in agreement with several observations made by other investigators [10, 32, 131]. The thickness of the tribofilm generated from fluorinated ZDDP is around 180 nm. Improvements seen in the wear performance in the form of lower wear volume for fluorinated ZDDP can be attributed to the thicker tribofilm seen in figure 5.10.

5.2.3 Nano-mechanical tests

5.2.3.1 Nano-indentation tests

Nano-mechanical tests, i.e. nano-indentation, scratch and scanning wear tests were run on tribofilms generated from two different oil formulations, containing base oil and ZDDP in untreated and fluorinated form (0.10 wt.% phosphorus for both samples). This series of nano-mechanical tests were run at Hysitron corporation's nano-mechanics research laboratory in Minneapolis, MN. Tribofilms were generated by running wear tests for 15000 cycles under 3.56 GPa Hertzian contact load. Single indent nano-indentation tests were run in order to measure the values of reduced modulus as well as the hardness of the tribofilm for different penetrations depths. Each indent was done following a trapezoidal load function shown in figure 3.5 (a) using a NorthStar[®] cube corner probe with a tip radius of <40 nm. A series of nano-indentations with peak loads ranging from 25 μN to 1500 μN were run on each sample in a region of the surface of the wear track where a uniform tribofilm was formed. The uniformity and smoothness of the tribofilms was assessed using the TriboIndenter[®] in SPM mode to obtain *in-situ* topographic images of the surfaces being probed by raster scanning the tip on the surface. Figure 5.11 (a) shows the indentation force vs. vertical displacement of the indenter tip (penetration) plots for peak loads of 25, 30, 40, 60, 80 and 100 μN for the tribofilm generated for ZDDP. Figure 5.11 (b) shows the same plot for tribofilm generated from fluorinated ZDDP. Indentations with peak loads of 500 and 1500 μN were also performed, but were not included in the plots of figure 5.11 for simplicity. Each of the force vs. vertical displacement plots shown in figure 5.11 (b) show conformity (overlap) during the loading segment of each indentation and are observed to have two distinct regions of different slopes, i.e. at penetration depths below 15 nm (region I), the slope of each curve is steeper than the slope of the same curves than at penetration depths beyond 15 nm (region II). The difference in the slopes, although also present, is not as clear for the plots of figure 5.11 (a) and these plots do not have the conformity observed in the plots of figure 5.11 (b).

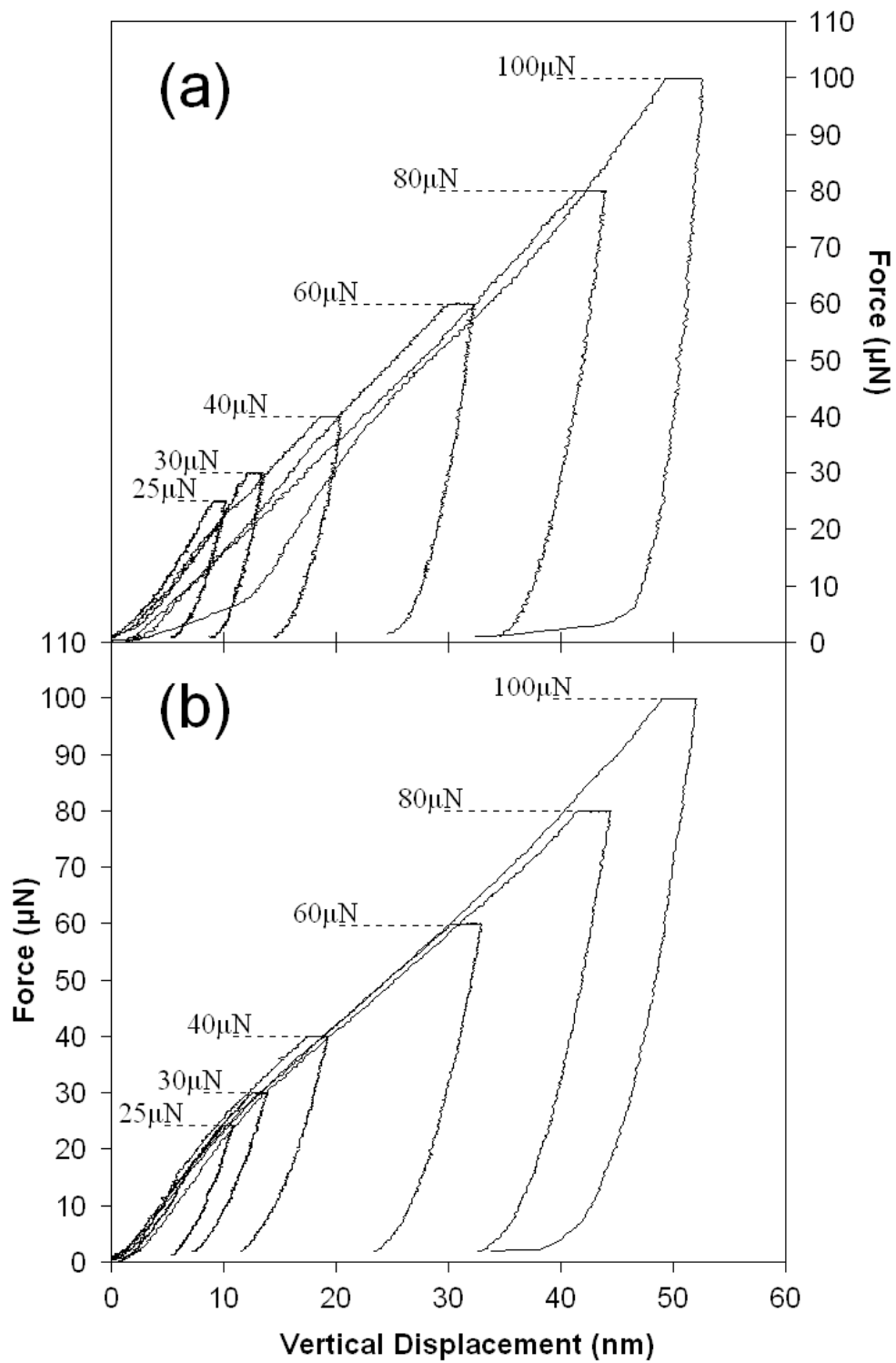


Figure 5.11: Load vs. vertical displacement graphs for peak indentation loads from 25 TO 100 μN for tribofilms generated from (a) base oil + ZDDP and (b) base oil + fluorinated ZDDP

This observation correlates with the observations made in the FIB/SEM images of figure 5.10 for which the tribofilm generated from fluorinated ZDDP (figure 5.10 b) has two visually distinctive layers while this is not the case for the film generated from untreated ZDDP. It also indicates that tribofilms generated from fluorinated ZDDP are more consistent across the surface in comparison to those formed by ZDDP.

The data from nano indentation tests can also be presented in terms of calculated reduced modulus as well as hardness of the tribofilm. In figure 5.12 (a), hardness data of the two tribofilms for different indentation peak loads are plotted against penetration depths. The hardness data follows the same decreasing trend for both the samples up until penetration depth of 50 nm; beyond this the value of hardness stays more or less constant for each sample. Observation of higher hardness values at lower penetration depths is in relative agreement with steeper slope of the force vs. penetration depth curves of figure 5.11 at penetrations below 15 nm. For both samples the hardness of the tribofilm at the surface of the film (depth >10 nm) is around 20 GPa, which decreases rapidly with increasing applied peak force and increasing penetration depths.

In figure 5.12 (b), the calculated reduced moduli of the two tribofilm samples are plotted against penetrations depths for different peak loads. The case can be made for the existence of a thinner film when untreated ZDDP is used as opposed to the case where fluorinated film is used. The values of reduced modulus decrease rapidly for both samples from maximum values at the surface region of both tribofilm samples, however, for the case where the tribofilm is generated by ZDDP (untreated) the decreasing trend of value of the modulus with higher penetration depths is abruptly reversed at a penetration depths less than around 60 nm where it increases to a constant value of approximately 200 GPa which is consistent with modulus of the substrate steel and indicates that the penetration is occurring in the steel substrate and not inside the tribofilm beyond the depth of 60 nm. For the tribofilm generated by fluorinated ZDDP, the decreasing trend (see trend line) does not start to reverse until penetration depth of around

150 nm where it slowly starts to increase to values close to that of substrate steel modulus. Thus while the thickness of the tribofilm is well below 100 nm for the tribofilm generated from untreated ZDDP, the film thickness is approximated to be around >150 nm for the film generated from fluorinated ZDDP. This also is in agreement with the values approximated for the thickness of the two tribofilms from the FIB/SEM images of figure 5.10.

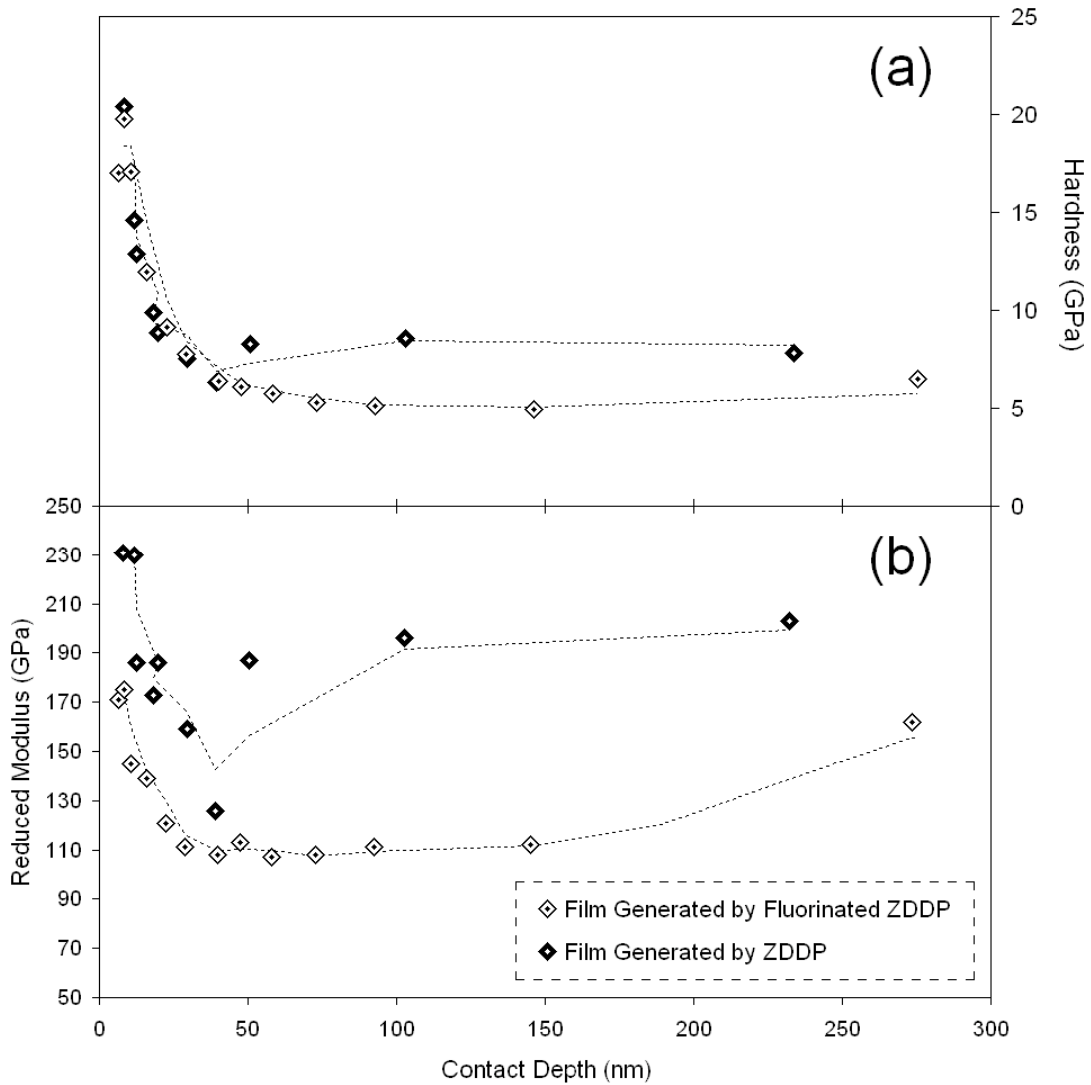


Figure 5.12: Plots of (a) hardness and (b) reduced elastic modulus vs. contact depth (vertical displacement of the tip) obtained from indents with peak loads ranging from 25 μN to 1500 μN for both tribofilm samples.

5.2.3.2 Nano-scratch tests

Scratch tests were also performed on the same samples of the tribofilm in order to investigate the scratch resistance of the film. Scratch tests were performed using a 90° cube corner conical probe with 2 μm tip radius and maximum normal forces of 5000 μN . The scratch load function consisted of a linearly ramped scratch force to a peak load of 5000 μN in 30 seconds while the tip is moved laterally over a distance of 6 μm during the application of the load. Figure 5.13 (a) shows the plot of the vertical applied force versus the vertical displacement (penetration into the tribofilm) of the tip of the probe through out the scratch, here the control variable is the load that is increased continuously from 0 to 5000 μN over 30 seconds and the depth of penetration is a response. Shown here is a comparison between films formed with fluorinated ZDDP and untreated ZDDP.

In figure 5.13 (b) the lateral force through out the scratch is plotted against lateral displacement (displacement along the length of the scratch). In this case the lateral displacement is increased from 0 to 6 μm continuously over the same period of 30 seconds when the vertical load is increased from 0 to 5000 μN . From figure 5.13 (b) it is evident that the lateral force required to continue through the scratch increases as the probe moves laterally and deeper to create the scratch. As the probe digs deeper into the scratch the contact area increases resulting in a increased resistance to further lateral motion. In addition the pileup of material ahead of the scratch increases the resistance to lateral motion. In this case the control variable is lateral motion that is increased from 0 to 6 μm and the lateral force, the resistance to the scratch is the response.

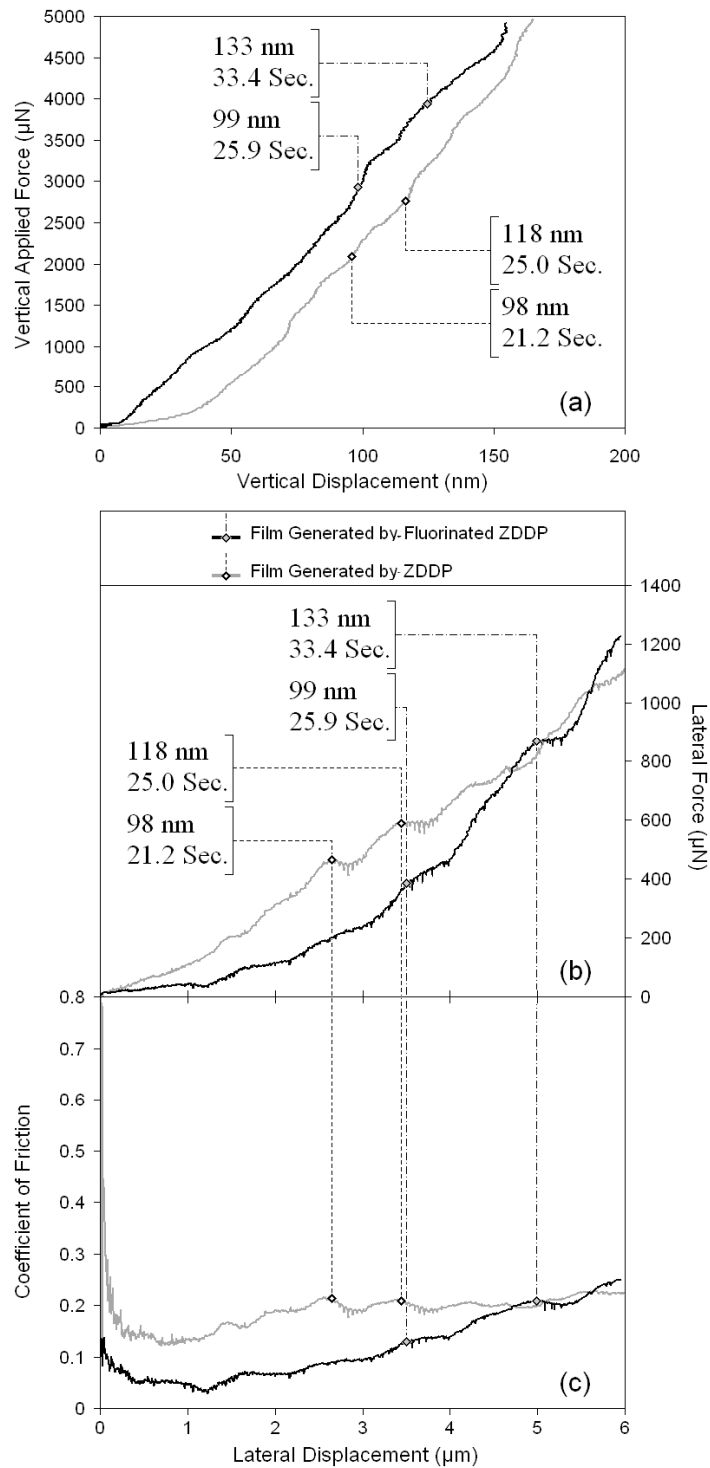


Figure 5.13: Data from a 5000 μN ramped force scratch test on the two tribofilm samples: (a) normal load (controlled) vs. vertical displacement and (b) lateral measured force and (c) coefficient of friction vs. lateral displacement (controlled).

The scratch test for the film formed by untreated ZDDP shows several points of interest at approximately 2.5 μm and 3.4 μm (that correspond to a penetration depth of ≈ 100 and ≈ 120 nm) where parts of the tribofilm comes free as evidenced by the constant to small drop in lateral force. In the scratch test conducted on the tribofilm formed by fluorinated ZDDP small drops in load are seen at a scratch position of 3.5 μm and more significant drops in lateral force at 5 μm . These locations correspond to a penetration depth of ≈ 100 and ≈ 130 nm. These depths at which decohesion occurs is consistent with the FIB studies that indicated a tribofilm of thickness around 100 nm for films formed by untreated ZDDP and around 130 nm for films formed from fluorinated ZDDP.

The ratio of the lateral resistance to scratch to the applied vertical load is the coefficient of friction. The coefficient of friction is plotted as a function of the lateral scratch position in figure 5.13(c). The coefficient is much higher at the very beginning of the scratch test for tribofilms formed from both ZDDP and fluorinated ZDDP as the lateral force needed to break into the film (which is much harder near the surface) is much higher than the lateral force needed to continue though the length of the scratch. Once the scratch is initiated, the coefficient of friction stabilizes to a value of around 0.2 for films from untreated ZDDP and 0.1 for fluorinated ZDDP. The differences in coefficient of friction between the two cases can be attributed to the fact that the untreated ZDDP offers less resistance to abrasion and consequently in a scratch test, as the test proceeds there is a larger amount of debris that the indenter has to plough through as the scratch proceeds. Towards the end of the scratch both the scratches have large pileups ahead of the indenter and have coefficients of friction that are comparable at 0.2. The undulations in the friction with local peaks and valleys relate to points where the tribofilm cracks and separates and corresponds to locations where lateral forces is constant or shows some drops in figure 5.13 (b).

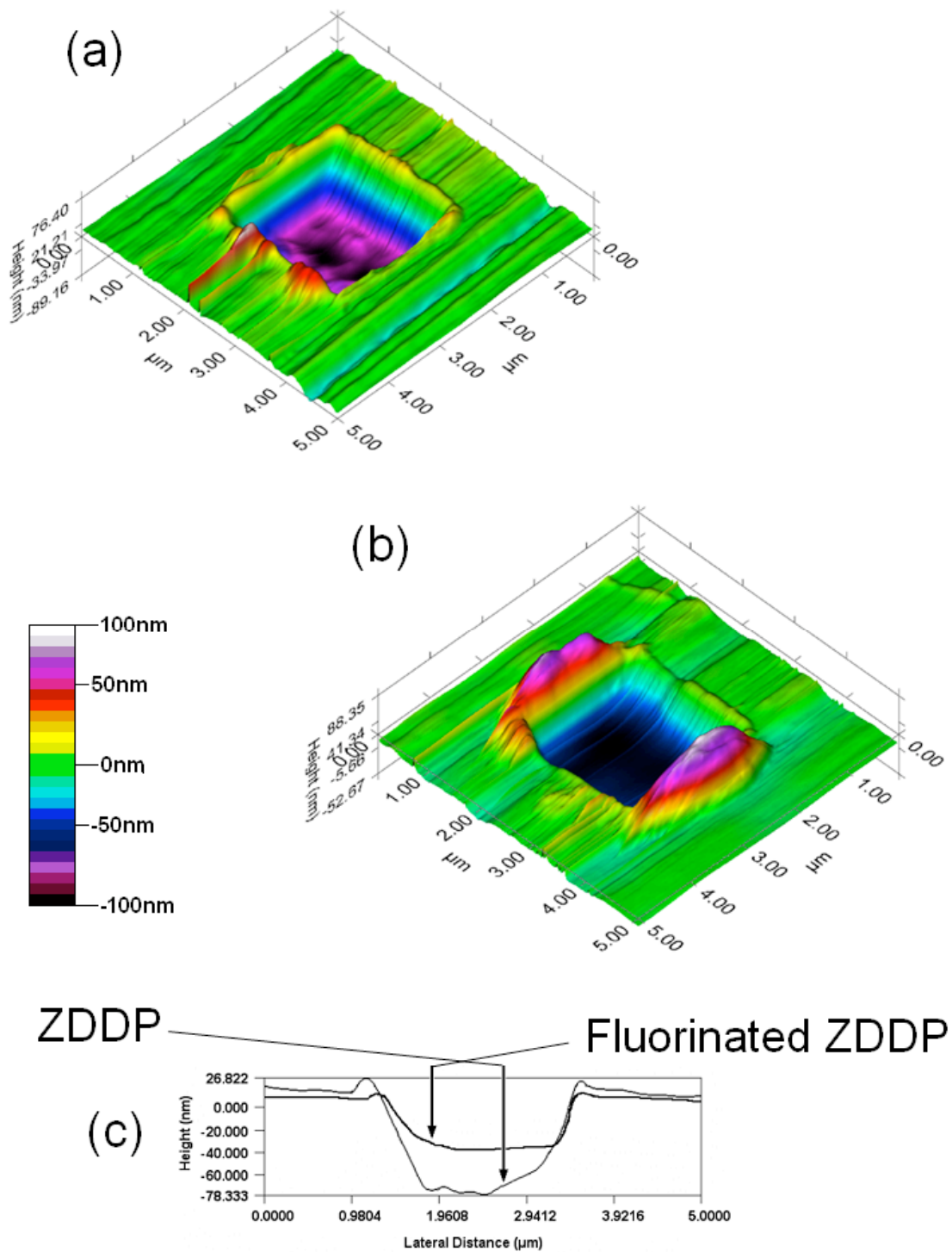


Figure 5.14: Three dimensional graphical SPM images of the tribofilm surfaces after scanning wear tests for (a) ZDDP and (b) fluorinated ZDDP tribofilms and (c) the cross sectional profile of worn surfaces.

5.2.3.3 Scanning wear tests

Scanning wear tests were run to investigate the wear resistance of the same tribofilm samples on which nano indentation tests were performed. Scanning wear tests were performed using the *in-situ* scanning probe microscopy (SPM) mode of the TriboIndenter[®]. In this mode, the instrument can create wear regions by raster scanning the indenter tip across the surface of the tribofilm samples while maintaining a specified normal force. The wear tests were run with a 75 μN normal force and four passes were performed on each sample. Three-dimensional representations of a 5 μm by 5 μm topographical *in-situ* SPM image of the tested area of each tribofilm are shown in figures 12 (a) and (b) for tribofilms generated from untreated ZDDP and fluorinated ZDDP respectively. The cross sectional profiles of the tested area for each sample are also shown in figure 5.14 (c).

It is observed in figure 5.14 that the tribofilm generated using the oil sample containing base oil with fluorinated ZDDP (0.10 wt.% P) is more resistant towards wear since the depth of the post-wear test surface profile in figure 5.14 (c) is almost half the depth of the worn area for the tribofilm sample generated by the oil sample containing base oil with untreated ZDDP (0.10 wt.% P). This observation is in correlation with scratch test data shown in figure 5.13 (a) which also indicates deeper probe penetrations for tribofilms generated from untreated ZDDP compared to the case of the fluorinated ZDDP under identical normal applied loads.

5.2.4 Transmission electron microscopy

The wear debris generated during wear tests can provide clues to the nature and chemical composition of the tribofilm from which the debris has been scraped off. Transmission Electron Microscopy was used to look at wear debris generated during wear tests run on two oil samples, one sample containing base oil and Fluorinated ZDDP and the other sample containing base oil and untreated ZDDP. As described in 1.3, the wear tests were performed under the applied Hertzian contact load of 3.56 GPa. The tests were run for full 25000 cycles to ensure generation of enough debris to be harvested for TEM analysis.

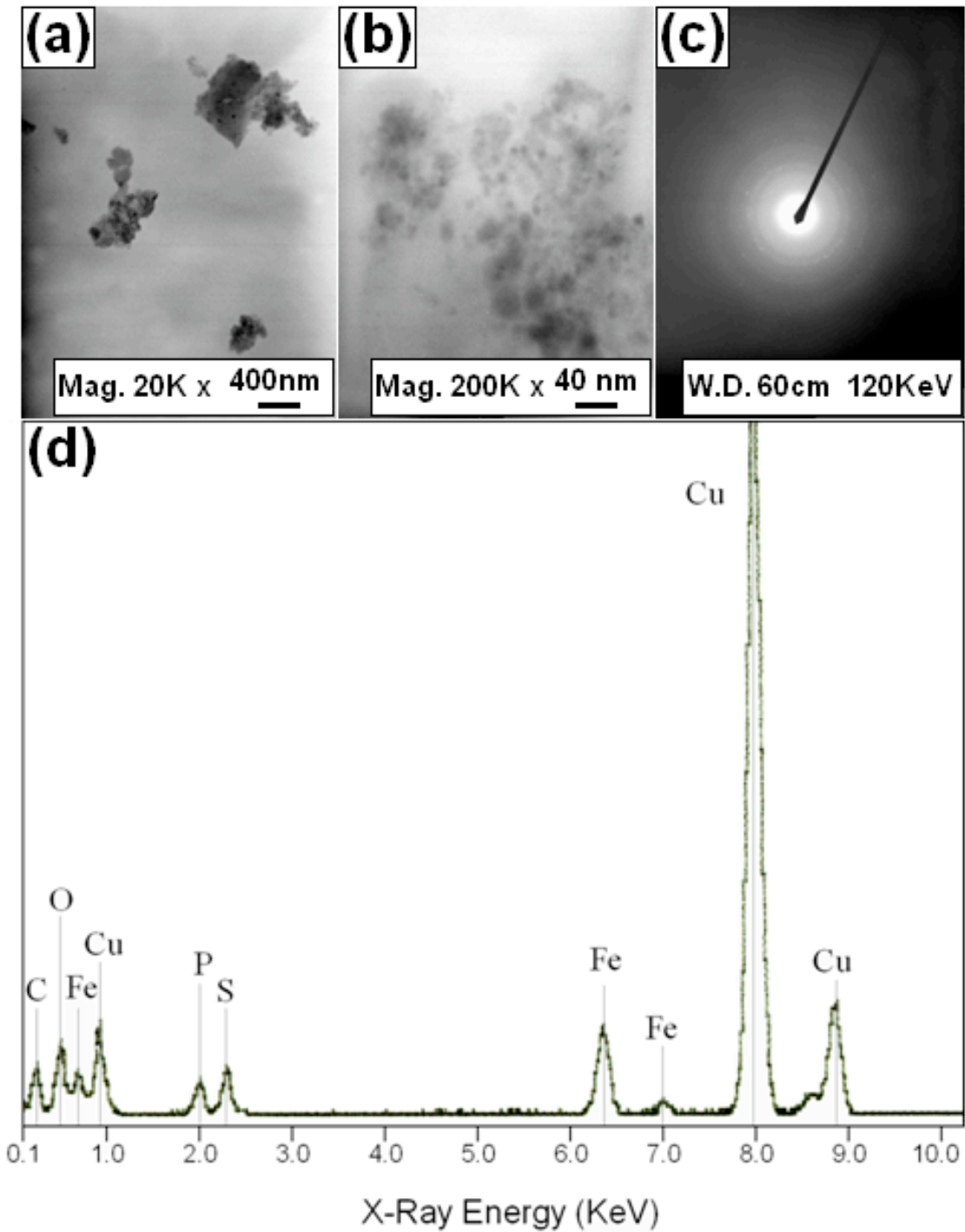


Figure 5.15: Transmission electron micrographs of wear debris flakes from ZDDP observed at (a) 20Kx and (b) 200Kx magnification, (c) diffraction pattern generated by the embedded particles and (d) the EDS spectrum obtained from the wear debris flakes.

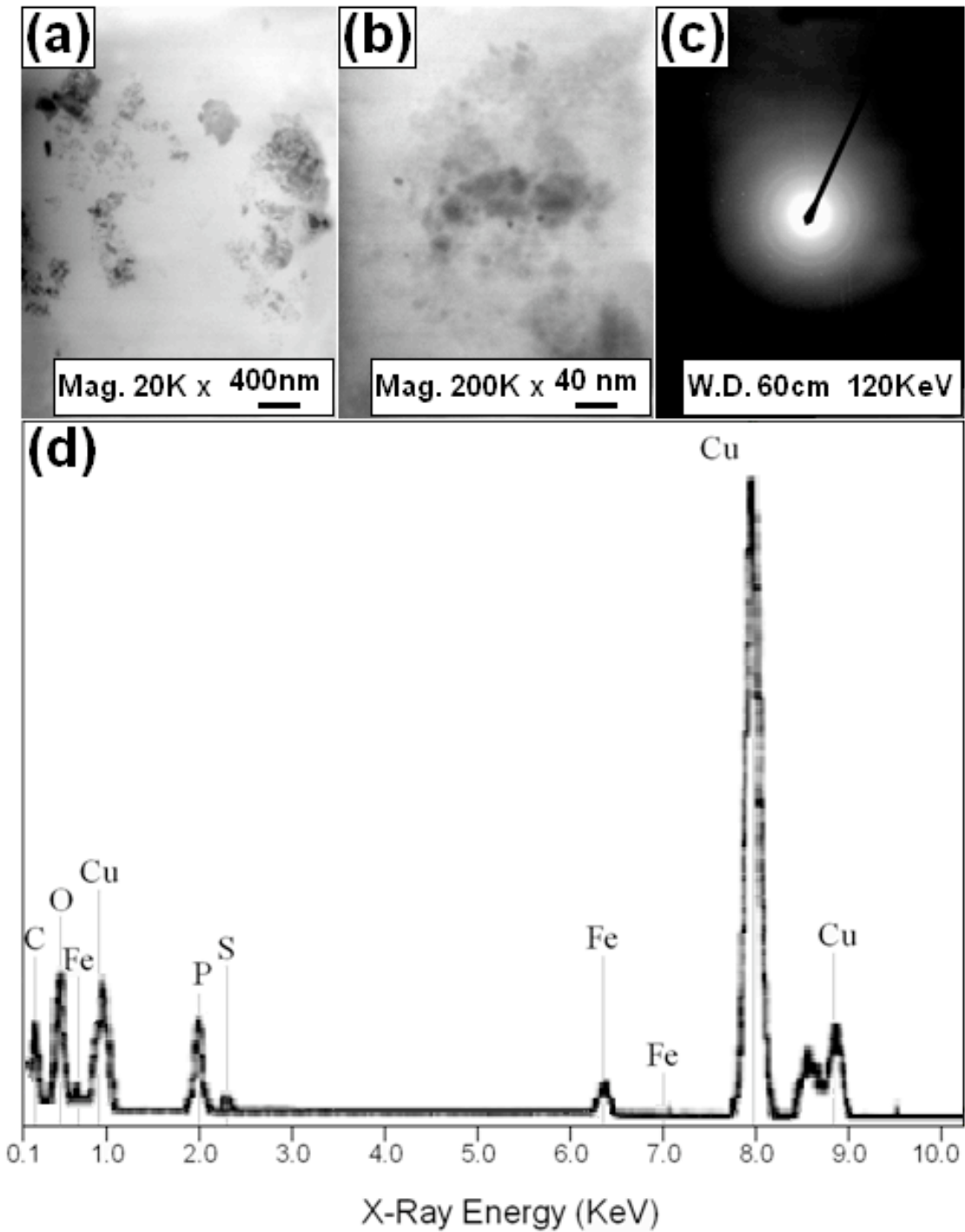


Figure 5.16: Transmission electron micrographs of wear debris flakes from fluorinated ZDDP observed at (a) 20Kx and (b) 200Kx magnification, (c) diffraction pattern generated by the embedded particles and (d) the EDS spectrum obtained from the wear debris flakes.

Figure 5.15 shows the TEM data for the wear debris from the oil sample containing untreated ZDDP. Figure 5.15 (a) is a low magnification (20000x) TEM image of a few wear debris flakes, which is representative in size of all the wear debris observed for this sample. The same particle is shown in figure 5.15 (b) at one order of magnitude higher magnification (200000x). Figure 5.15 (b) reveals the presence of small particles embedded within the wear debris flakes. The crystallinity of these embedded particles was examined by obtaining the diffraction pattern from the flake shown in figure 5.15 (b). The diffraction pattern is shown in figure 5.15 (c) clearly indicates some crystallinity of the particles since diffraction rings are relatively visible. Figure 5.16 shows the TEM data for the wear debris generated from wear tests using the oil sample containing fluorinated ZDDP. Similar to the case of untreated ZDDP (figure 5.15), the embedded particles are also visible here (figure 5.16 a) and are also found to be crystalline.

The EDS spectra for the two samples are shown in figures 5.15 (d) and 5.16 (d). Strong copper peaks are from the copper grid used to trap the wear debris. The major difference between the two spectra is the intensity ratio of sulfur to phosphorus. In the case of untreated ZDDP (figure 5.15 d), it is observed that both sulfur and phosphorus peaks are similar with the sulfur peak being of a slightly higher intensity. In the case of the fluorinated ZDDP however, while the sulfur peak intensity is minimal, the intensity of the phosphorus peak is relatively high.

Figure 5.17 shows a the TEM image of a wear debris at 200K magnification for tribofilm debris generated by fluorinated ZDDP (a) and ZDDP (b). Small particles appear as dark spots embedded inside the debris. While the tribofilm is believed to be amorphous, the selected area diffraction patterns obtained from these wear particles at very high magnifications reveal the crystalline nature of the particles embedded inside the wear debris in both cases. The electron diffraction ring pattern generated by this wear debris is shown next to the corresponding TEM micrograph in figure 5.17. The values of interplanar spacing, d_{hkl} are calculated for both cases

and are compared to the same values for pure iron [27], $\alpha\text{-Fe}_2\text{O}_3$ [132] and Fe_3O_4 [133] in table 5.1.

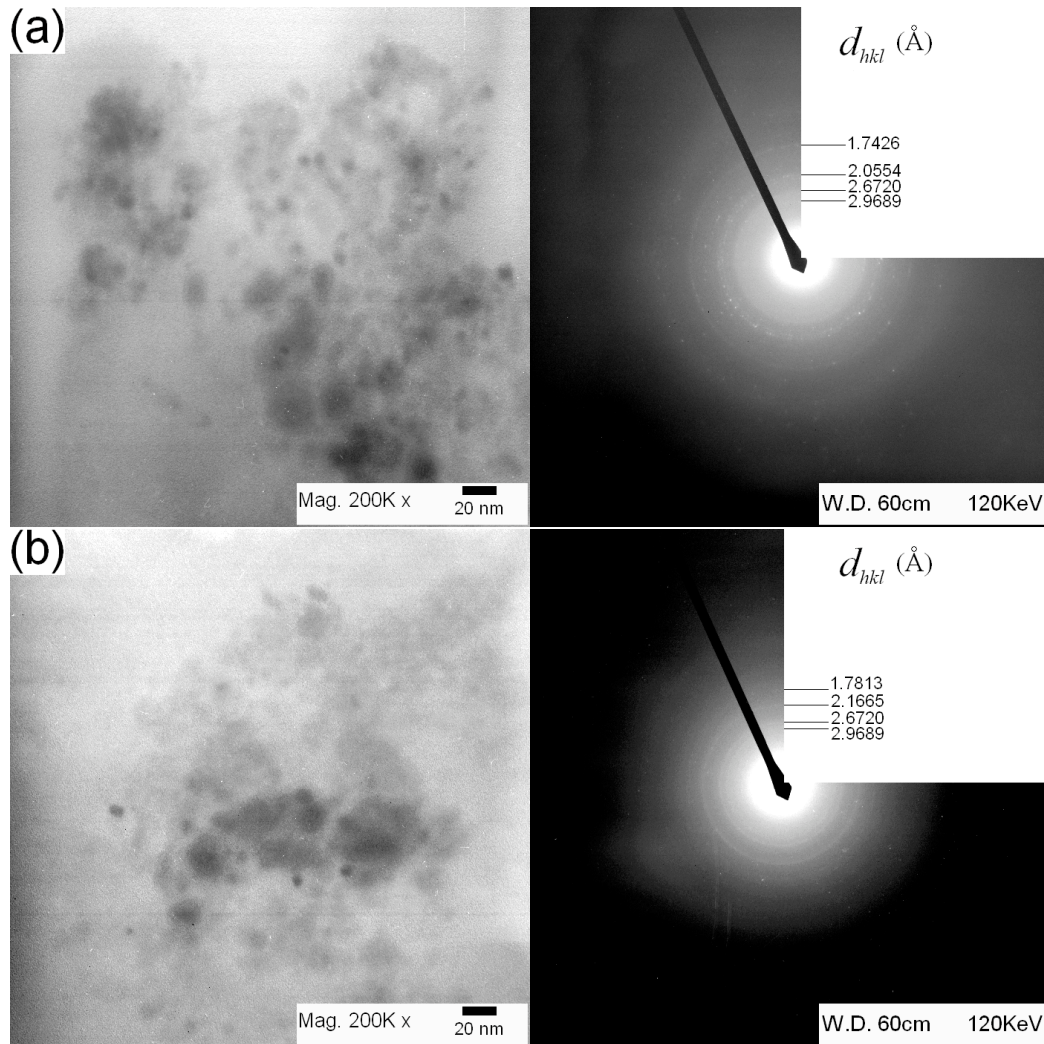


Figure 5.17: (a) Bright field transmission electron micrograph (200Kx magnification) of the wear debris harvested from wear tests run using oil containing base oil with 0.1 wt.% P at a Hertzian contact load of 3.56 GPa for 15000 cycles and (b) the corresponding electron diffraction ring patterns and calculated d_{hkl} values.

The values of interplanar spacing observed here for the embedded particles in wear debris samples from both fluorinated ZDDP and ZDDP closely match those for Fe_3O_4 . This

confirms that the smaller particles embedded within the wear debris flakes are predominantly Fe_3O_4 . In a related study [122], using ZDDP and iron (III) fluoride, the onset of film breakdown was related to formation of oxide particles in the tribofilm, the same samples were run for a larger number of cycles (100000 cycles) and there, it was observed that the embedded particles were made of Fe_2O_3 which indicates further oxidation of the oxide particles to higher oxidation states of iron. Since the only additive present in the oil sample which also acts as an anti-oxidant is ZDDP, further oxidation of the Fe_3O_4 particles into Fe_2O_3 through out the wear test occurs due to consumption of ZDDP which result in the loss of anti-oxidant properties. Other factors that are believed to contribute to oxidation process of these particles include the increase in the oxygen concentration in the oil due to the oxidation of oil.

Table 5.1: The calculated d_{hkl} spacing for the ring patterns observed in figure 5.17 compared to observed values for iron and two types of iron oxide [27, 132, 133].

d Spacing (Å)				
Reported Values			Observed Values	
Fe_3O_4	Fe_2O_3	Fe	Wear debris from F- ZDDP	Wear Debris from ZDDP
2.96	1.69	2.03	2.9689	2.9689
2.53	1.452	1.43	2.6720	2.6720
2.096	1.055	1.17	2.1665	2.0554
1.712	0.931		1.7813	1.7426
1.614				
1.483				

5.2.5 Auger electron spectroscopy

Auger electron spectroscopy (AES) was performed on the same tribofilm samples used for FIB and SEM studies. The sputtering parameters are described in section 3.4.3. After each sputtering cycle of 12 seconds, the data was collected by five minute scans. The AES data for phosphorus and sulfur are shown in figures 5.18 and 5.19 respectively. The data is plotted for

sputtering intervals of 24 seconds from no sputtering to a maximum of 240 seconds of sputtering. It is estimated that a total of 20-25 nm thickness of each tribofilm is removed and probed after the total 240 seconds of sputtering.

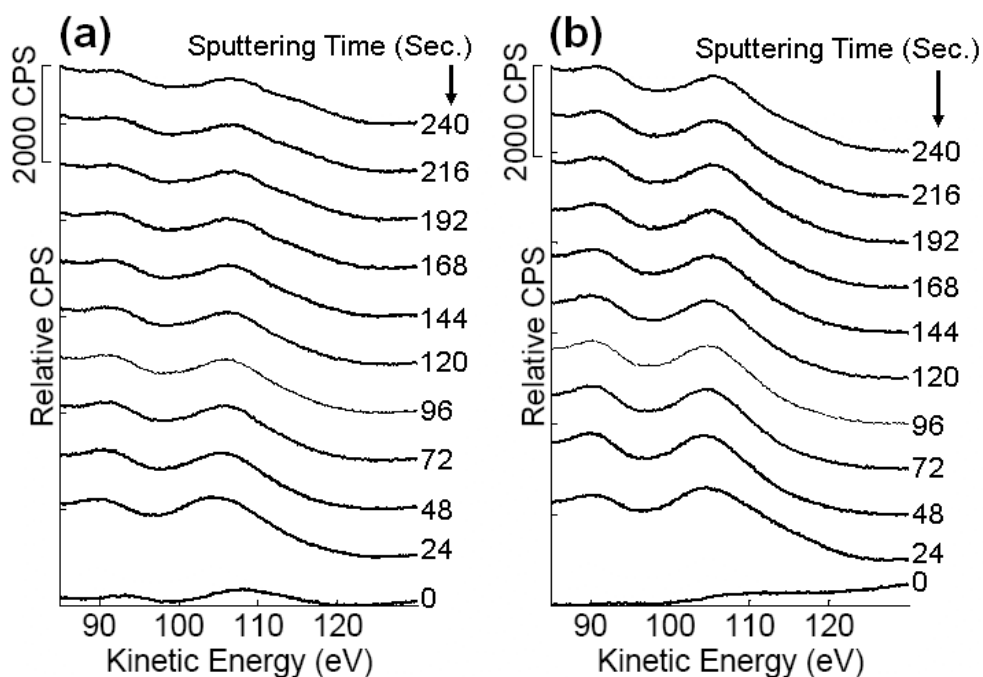


Figure 5.18: Auger phosphorus peaks for tribofilms generated using base oil and (a) ZDDP and (b) fluorinated ZDDP

Figure 5.18 (a) and 5.18 (b) show Auger spectrum in the vicinity of the phosphorus peaks for the tribofilm sample generated using ZDDP and fluorinated ZDDP respectively. It is observed that while there is a decrease in the phosphorus peak intensity in the case of ZDDP with increasing sputtering time, no significant change is observable in the intensity of these peaks in the case of fluorinated ZDDP.

Auger sulfur peaks after different sputtering times are shown for the oil sample containing untreated ZDDP in figure 5.19 (a). The same peaks for the case where fluorinated ZDDP was used are also shown in figure 5.19 (b). While there is a relatively observable

increase in the intensity of sulfur peaks with increasing sputtering time in the case of fluorinated ZDDP, little or no change is observed in the case of ZDDP. In order to better compare the relative intensities of the elemental peaks observed within the each sample, the area under the Auger spectrum peaks is calculated for phosphorus, sulfur, oxygen and iron for every minute of sputtering. When compared for the same sample, the area under the peak for each element is a measure of its relative concentration in the material. These results are shown in figure 5.20.

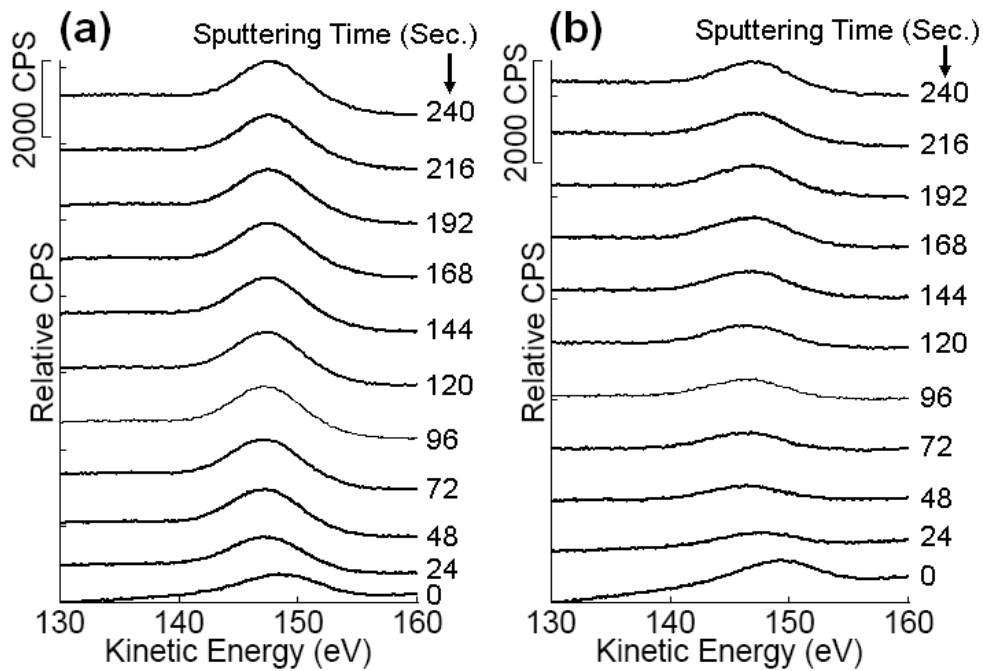


Figure 5.19: Auger sulfur peaks for tribofilms formed by (a) ZDDP and (b) fluorinated ZDDP

Since the total sputtering time is only 4 minutes, the total depth through which material is removed is estimated to be around 10 nm. The intensity of oxygen (figure 5.20) is relatively very high in comparison to sulfur, iron and phosphorus indicating the presence of an organic film on the surface of the tribofilm. This organic film is rich in oxygen in comparison to the tribofilm over which it rests.

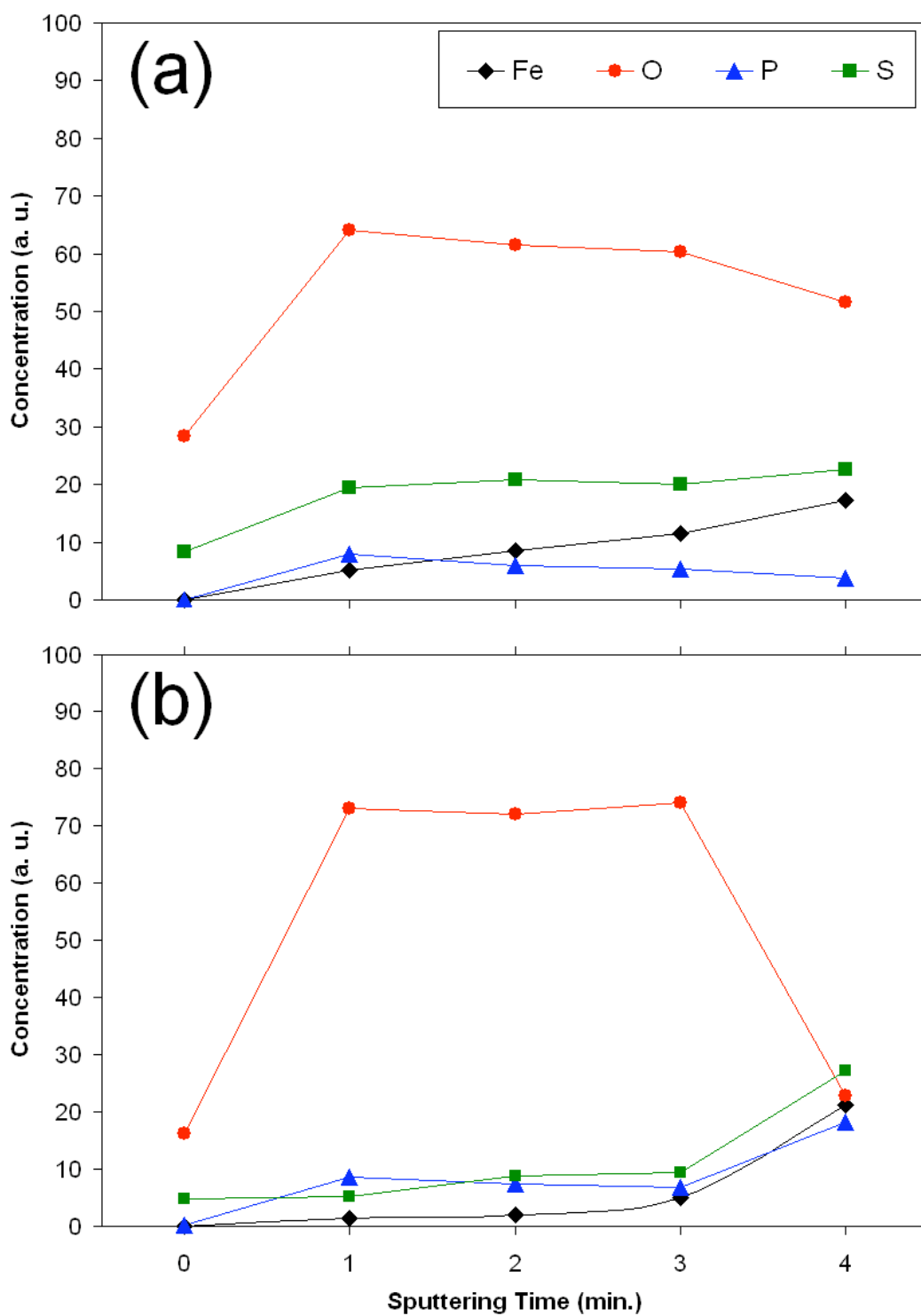


Figure 5.20: A graph of concentration (arbit. units) vs. sputtering time (min) of phosphorus, sulfur and iron for (a) ZDDP (0.1 wt. % P) and (b) fluorinated ZDDP (0.1 wt. % P) in mineral oil.

CHAPTER 6

LOAD AND DURATION EFFECTS ON TRIBOFILMS GENERATED BY FLUORINATED ZDDP AND ZDDP

In this chapter, tribofilms generated from both ZDDP and fluorinated ZDDP under different loading conditions and test durations are studied using nano-indentation and XANES spectroscopy.

6.1 Materials and procedures

Secondary ZDDP research sample and fluorinated ZDDP (from the same sample) were added to 100 neutral base oil at 800 ppm (0.08 wt%) of phosphorus. The 800 ppm phosphorus level was chosen to better simulated the current phosphorus levels in commercially available engine oils (GF4). Tribofilm samples were generated using the UTA BOCLE unit (see chapter 3). Wear tests were run under different applied loads and for different test durations using the same testing protocol described in chapter 3. Tribofilm samples were also prepared with the same procedure explained in chapter 3. Table 6.1 shows the test matrix run on these oils and the type of analysis carried out on the tribofilm samples generated from these tests. Due to limited available synchrotron beam time, XANES spectroscopy was not carried out on all tribofilm samples as shown in table 6.1.

6.2 Results, observations and discussion

6.2.1 XANES spectroscopy

XANES spectroscopy was run on the samples described in table 6.1 at two different beamlines at two synchrotron facilities; the collimated plane grating monochromator (VLS-PGM) 11ID-2 at the Canadian light source (CLS) facility in Saskatoon, Saskatchewan, Canada and the Canadian double crystal monochromator (DCM) at the synchrotron radiation center (SRC) at the university of Wisconsin – Madison in Stoughton, Wisconsin (described in detail 3.4.5). The

energy range as well as beam properties of each beamline are shown in table 3.4 in chapter 3. The main challenge in running XANES spectroscopy on tribofilm samples arises from the difficulties in aligning the beam on the tribofilm covered wear track due the small beam size in both beamlines (table 3.4) as well as the size and varying position of the wear track on cut samples of the steel rings (≈ 0.5 mm width).

Table 6.1: Wear test matrix run for XANES and nano-indentation studies

Formulation	Applied Load	Duration (Cycles)	Analyses
Base Oil + Fluorinated ZDDP (800 ppm P)	16 Kg	15000	XANES and Nano-indentation
	20 Kg	15000	
	24 Kg	15000	
	24 Kg	5000	Nano-indentation
	24 Kg	25000	
Base Oil + ZDDP (800 ppm P)	16 Kg	15000	XANES and Nano-indentation
	20 Kg	15000	
	24 Kg	15000	
	24 Kg	5000	Nano-indentation
	24 Kg	25000	

XANES spectroscopy was performed for energy ranges covering sulfur and phosphorus K-absorption edges (DCM beamline) and L-absorption edges (VLS-PGM beamline). In both cases XANES spectra were recorded in fluorescence yield (FLY) and total electron yield (TEY) modes. It is necessary to compare the acquired XANES spectra from tribofilm samples to those of model compounds in order to understand the chemical nature of the tribofilms by identifying the structural environment of sulfur and phosphorus atoms in the tribofilm. FePO_4 , $\text{Zn}_3(\text{PO}_4)_2$ are used as representative model compounds for phosphorus spectra and ZnS , ZnSO_4 and FeS are used as the model compounds for sulfur spectra in order to partly represent the possible phosphate, sulfates and sulfides present in tribofilms generated from ZDDP and fluorinated ZDDP.

6.2.1.1 Phosphorus K-edge XANES

Figures 6.1 and 6.2 show phosphorus K-edge spectra recorded in TEY (surface sensitive) and FLY (bulk sensitive) modes respectively. The single relatively intense peak is characteristic of phosphorus K-edge which is attributed to the transition of a phosphorus 1s electron to an empty p-like anti-bonding state [62]. In figure 6.1 the XANES spectra in TEY mode are shown for samples containing base oil and ZDDP and fluorinated ZDDP alongside the same spectra for the model compounds; $Zn_3(PO_4)_2$ and $FePO_4$.

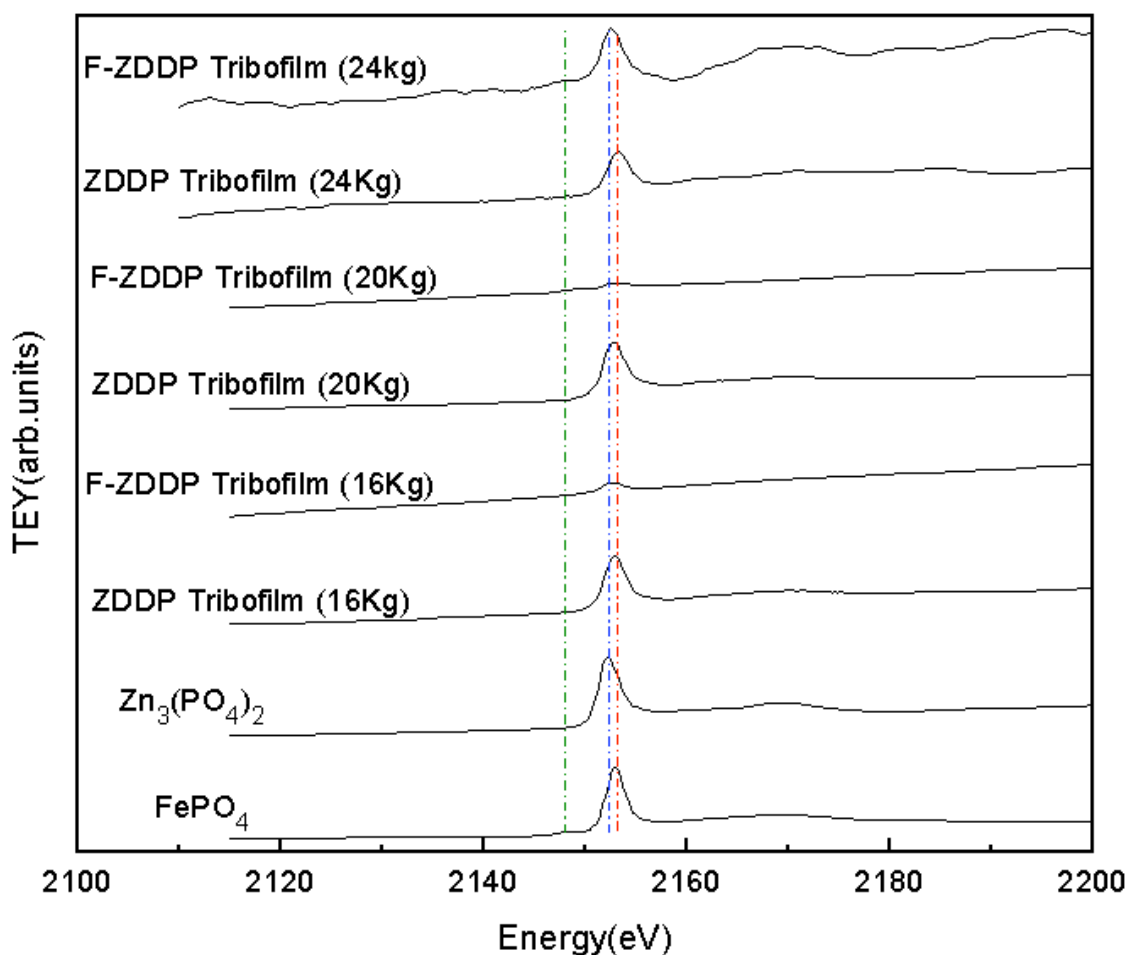


Figure 6.1: Phosphorus K-edge XANES spectra collected in TEY mode for tribofilms generated by samples containing base oil and ZDDP or fluorinated ZDDP under 16, 20 and 24 Kg applied scuffing loads and the same spectra recorded for model compounds, $Zn_3(PO_4)_2$ and $FePO_4$

The blue and red dashed lines are drawn along the peak positions for $Zn_3(PO_4)_2$ and $FePO_4$ respectively. While peaks for tests run under 16 and 20 Kg loads (wherever visible) lie in between the two dashed lines suggesting the presence of both model compounds, for tests run under 24 Kg applied scuffing load, a drift between the peaks for ZDDP and fluorinated ZDDP tribofilms is observed. In the case of ZDDP tribofilm the peak position matches with the peak position for $FePO_4$ and for fluorinated ZDDP the position of the dominant peak matches that of $Zn_3(PO_4)_2$. This is also the case for the FLY mode (figure 6.2).

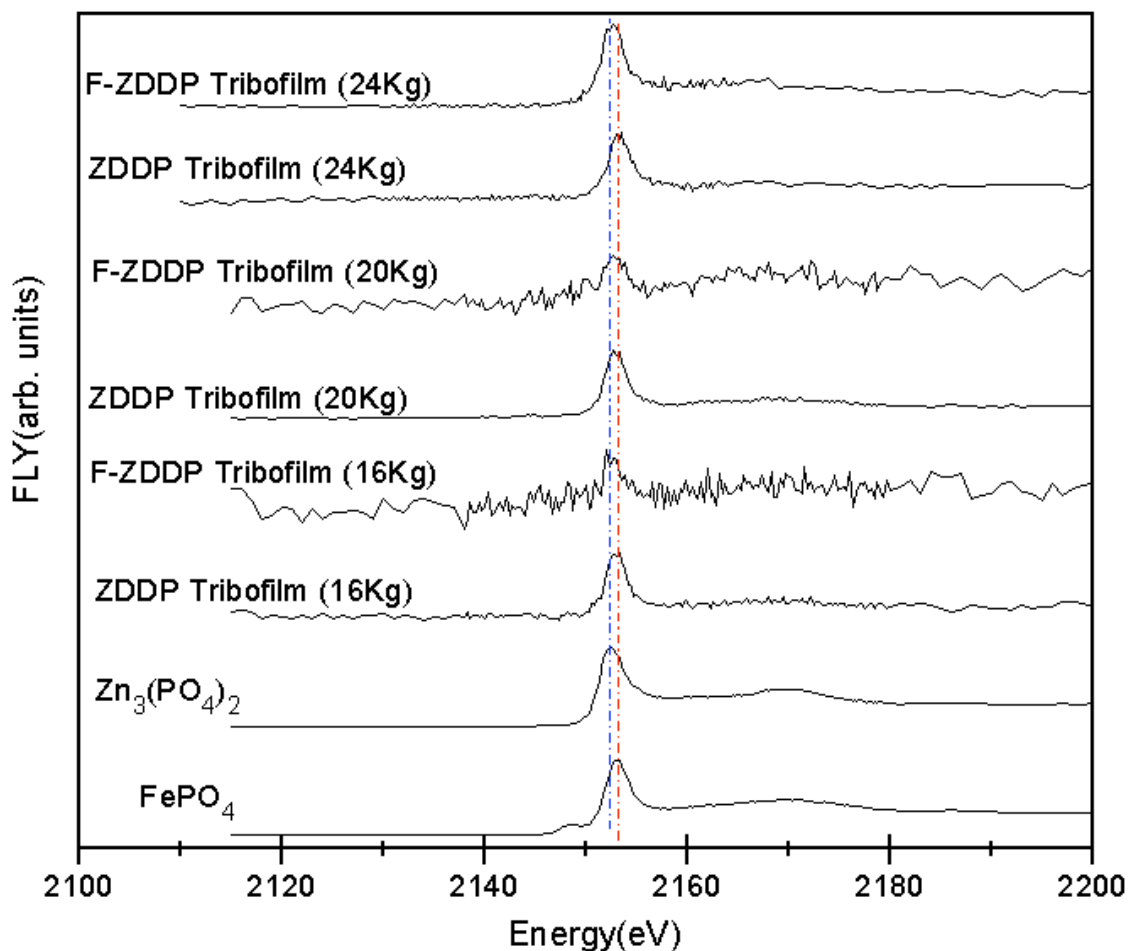


Figure 6.2: Phosphorus K-edge XANES spectra collected in FLY mode for tribofilms generated by samples containing base oil and ZDDP or fluorinated ZDDP under 16, 20 and 24 Kg applied scuffing loads and the same spectra recorded for model compounds, $Zn_3(PO_4)_2$ and $FePO_4$

However, since fluorinated ZDDP peaks for tests run under 16 and 20 Kg are relatively visible in the spectra recorded in the FLY mode (figure 6.2), in comparison to the TEY mode (figure 6.1) it is also observed that these peaks are located closer to the blue dashed line (peak position for $Zn_3(PO_4)_2$), in comparison to ZDDP peaks for the same loads which have fallen between the two lines. Thus it appears that the tribofilm generated from fluorinated ZDDP (under the testing conditions of this study) tend to contain more zinc phosphates than iron phosphates when compared to tribofilms generated under the same condition by ZDDP as the antiwear additive. In a similar study of ZDDP-generated tribofilms by Li and Kasrai *et al.* [62, 69] and using ZDDP (in pure powder form) and $Zn_4P_6O_{19}$ (a zinc poly phosphate) as model compounds, it has been shown that position of the phosphorus K-edge peak for pure ZDDP is ≈ 2148 eV and ≈ 2152 eV for $Zn_4P_6O_{19}$ (figure 6.3) which indicates that the tribofilm is mainly composed of polyphosphates formed from the decomposition of ZDDP.

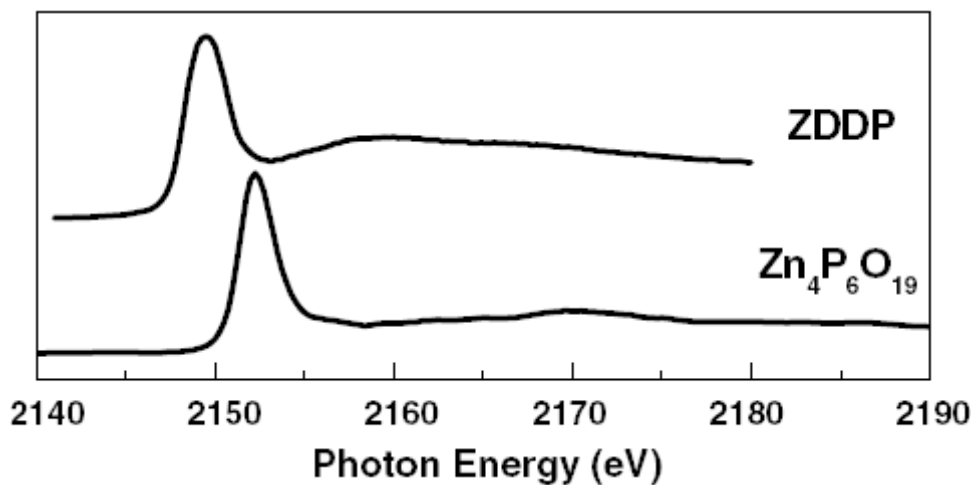


Figure 6.3: Phosphorus K-edge spectra (FLY mode) of untreated ZDDP powder and $Zn_4P_6O_{19}$ collected by Li and Kasrai *et al.* [69]

6.2.1.2 Phosphorus L-edge XANES

Phosphorus L-edge XANES spectra were collected in FLY mode on tribofilms generated by tests run under the applied scuffing load of 24 Kg on oils samples containing

ZDDP and fluorinated ZDDP in base oil (800 ppm P) and are shown in figure 6.4. The spectra collected in TEY mode did not yield conclusive data due to problems encountered with both the detector as well as aligning the samples. The model compounds used in this case are FePO_4 , $\text{Fe}_4(\text{P}_2\text{O}_7)_3$ and $\text{Zn}_3(\text{PO}_4)_2$.

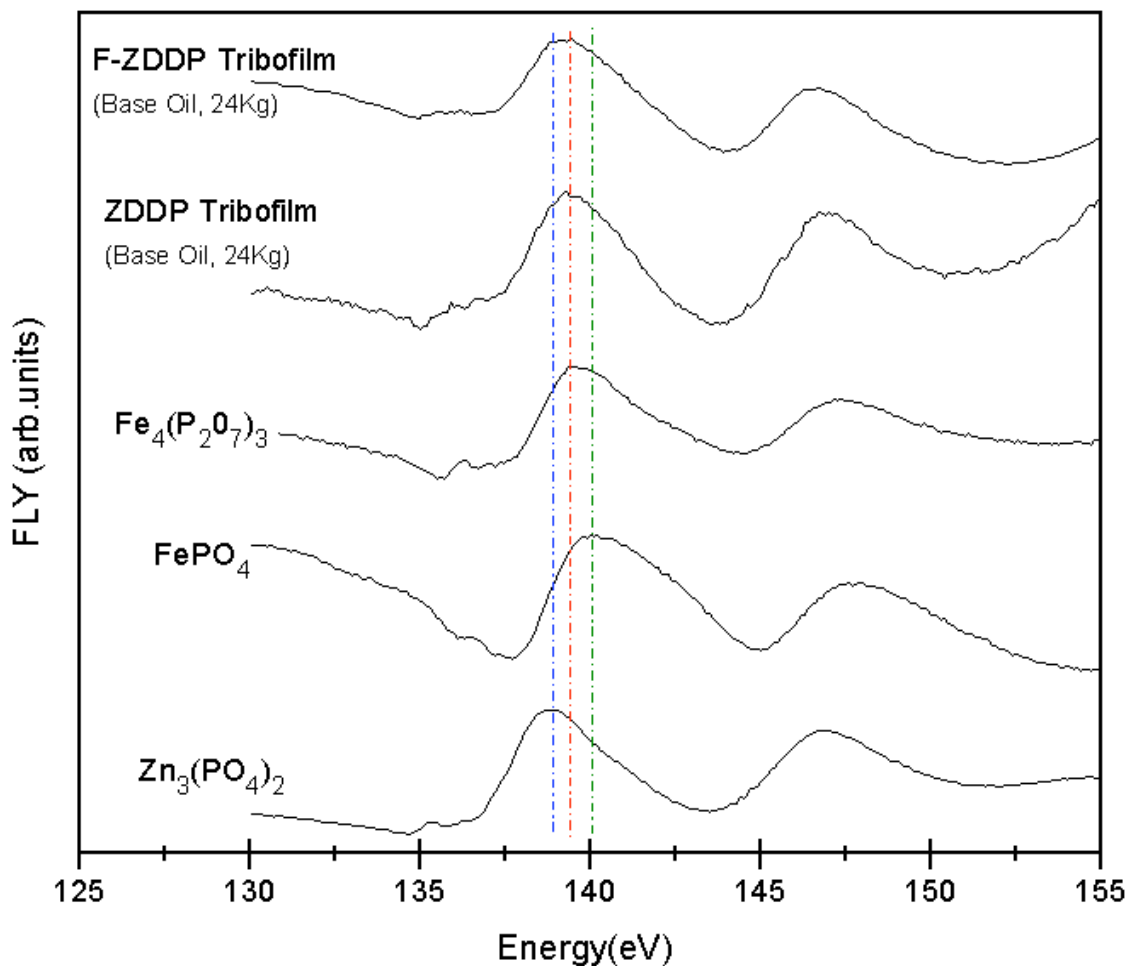


Figure 6.4: Phosphorus L-edge XANES spectra collected in FLY mode for tribofilms generated by samples containing base oil and ZDDP or fluorinated ZDDP under 24 Kg applied scuffing load and the same spectra recorded for model compounds FePO_4 , $\text{Fe}_4(\text{P}_2\text{O}_7)_3$ and $\text{Zn}_3(\text{PO}_4)_2$

The green, red and blue dashed lines in figure 6.4 indicate the positions of the peaks for FePO_4 , $\text{Fe}_4(\text{P}_2\text{O}_7)_3$ and $\text{Zn}_3(\text{PO}_4)_2$ respectively. The position of the P L-edge for fluorinated

ZDDP tribofilm is slightly different from that of the ZDDP tribofilm. While the position of the ZDDP tribofilm peak very closely matches that of the $\text{Fe}_4(\text{P}_2\text{O}_7)_3$ (red dashed line), the fluorinated ZDDP tribofilm peak has a wider crest that matches with both $\text{Fe}_4(\text{P}_2\text{O}_7)_3$ and $\text{Zn}_3(\text{PO}_4)_2$ (blue dashed line) peak positions indicating the presence of both compounds in the tribofilm. It is also observed that the position of the P L-edge peak for both ZDDP and fluorinated ZDDP tribofilms is shifted more towards the position of the same peaks for $\text{Fe}_4(\text{P}_2\text{O}_7)_3$ and $\text{Zn}_3(\text{PO}_4)_2$ compared to FePO_4 (green dashed line). This indicates that phosphorus is mostly present as polyphosphates rather than phosphates.

The phosphorus L-edge spectra (FLY mode) were collected for several other polyphosphates of zinc as model compounds by Dr. Kasrai and his research group at the university of Western Ontario (London, Ontario, Canada) were also collected using the same beamline used in this study and are in shown in figure 6.5 [62, 66, 69, 89, 90, 126]. These compounds include ZnPO_4 , $\text{Zn}_4\text{P}_6\text{O}_{19}$, $\text{Zn}_6\text{P}_{10}\text{O}_{31}$, $\text{Zn}_{10}\text{P}_{18}\text{O}_{55}$ and $\text{Zn}_{20}\text{P}_{38}\text{O}_{115}$. The phosphorus L-edge XANES spectra provide more information in comparison to the K-edge spectra. The L-edge is characterized by spin-orbit splitting of the phosphorus 2p electrons and their excitation to the anti-bonding orbitals. Peak c in figure 6.5 is attributed to the transition of the phosphorus 2p electrons to the t^*_2 molecular orbital [66, 134]. While the peaks labeled a and b in figure 6.5 are not present in the spectrum collected from ZnPO_4 , they are present in the spectra of longer chain polyphosphates and are located at ≈ 136 and ≈ 137 eV in the same figure. The peaks a and b (in figure 6.5) are assigned to the transitions from the $2p_{3/2}$ and $2p_{1/2}$ to anti-bonding orbital a^*_1 [62, 69] and are characteristic of the presence of the polyphosphate glass [26]. Peak d (also observed in the spectra of figure 6.4) is known as a shape resonance peak and is located at ≈ 146 eV in figure 6.5 and is only present when phosphorus is coordinated to three or more electronegative atoms such as oxygen and is characteristic of all phosphates regardless of structure (crystalline or amorphous) and the phosphate chain length. The chain length of the polyphosphate glass in antiwear tribofilms can be estimated from P L-edge XANES spectra. It

has been shown by Yin *et al.* [19, 101, 135] that the ratio of peaks a/c (in figure 6.5) is related to the polyphosphate chain length. Since peak a (as seen in figure 6.5) is almost invisible in the spectra obtained from ZDDP and fluorinated ZDDP tribofilms shown in figure 6.4, the collected spectra from both tribofilm samples indicates the dominant presence of short chain polyphosphates of zinc and iron over longer chain polyphosphates in both of these samples.

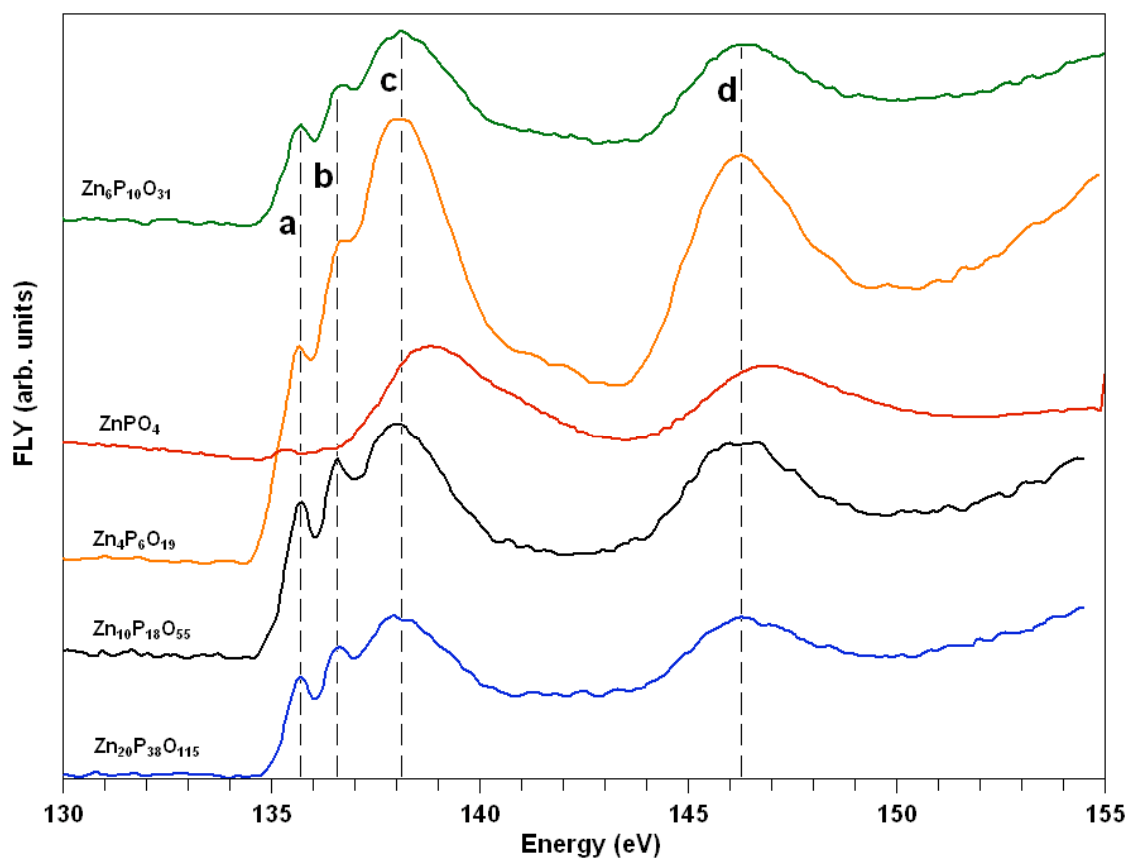


Figure 6.5: Phosphorus L-edge spectra obtained by Kasrai *et al.* for different zinc polyphosphates [62, 66, 69, 89, 90, 126].

6.2.1.3 Sulfur K-edge XANES

Sulfur K-edge spectra recorded in TEY and FLY modes are shown in figures 6.6 and 6.7 respectively and are compared to the same spectra for the model compounds ZnSO_4 and ZnS . Unlike phosphorus K-edge spectra shown in figures 6.1 and 6.2, the intensity of sulfur K-

edge peaks is not significant, however, the peaks observed in both modes (TEY and FLY) for all tribofilms samples are consistent with both model compounds and indicate the presence (although weak) of both chemistries ($ZnSO_4$ and ZnS) in the tribofilm.

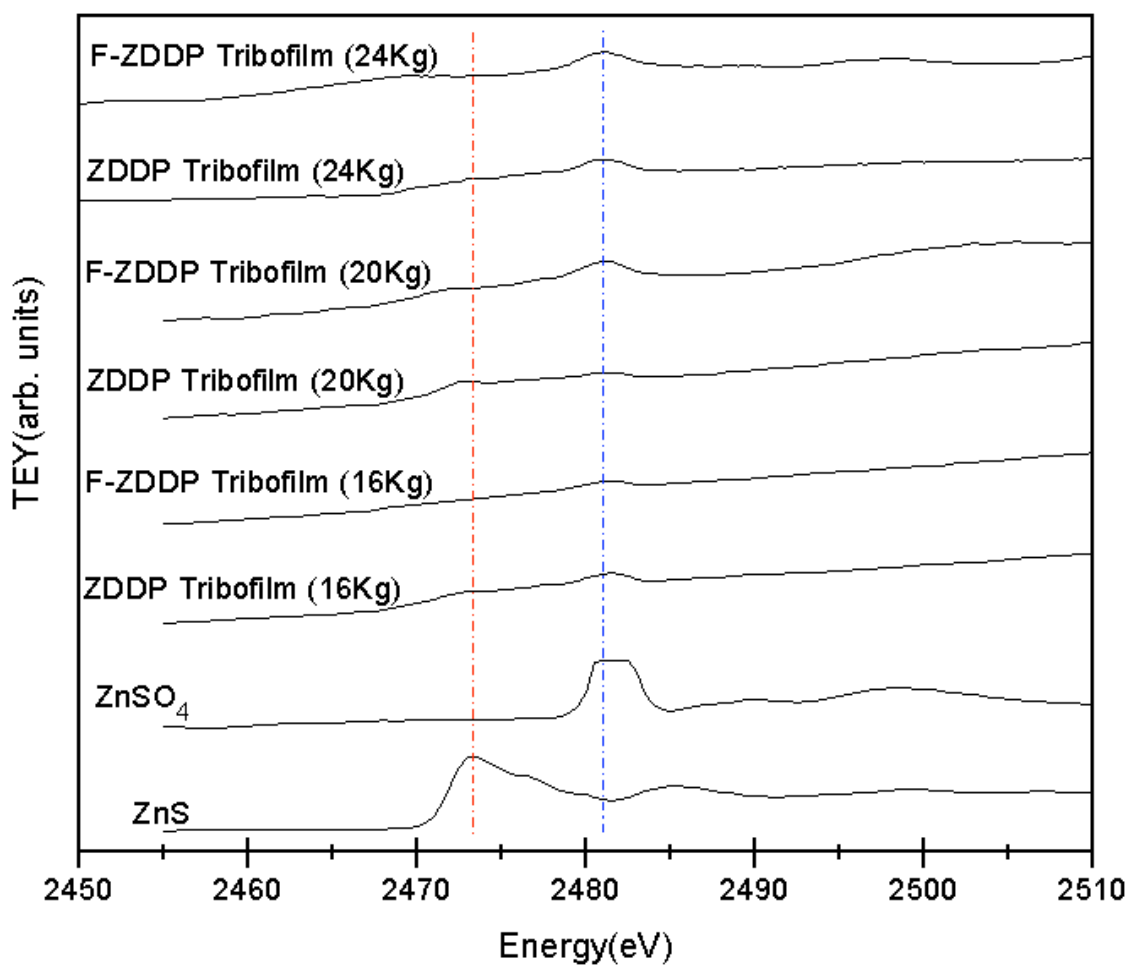


Figure 6.6: Sulfur K-edge XANES spectra collected in TEY mode for tribofilms generated by samples containing base oil and ZDDP or fluorinated ZDDP under 16, 20 and 24 Kg applied scuffing loads and the same spectra recorded for model compounds, $ZnSO_4$ and ZnS .

The sulfur signal is relatively strong in S K-edge spectra collected in the surface sensitive TEY mode (figure 6.6) while in the spectra collected in FLY mode (figure 6.7) reflecting the bulk chemistry for each sample, the signal to noise ratio of S K-edge peak(s) is quite small indicating visible difference between the bulk and the surface of the tribofilm in sulfur

concentration. While there is very little sulfur concentration through out the bulk of the film, sulfur concentration in the surface layers of the tribofilms is relatively higher.

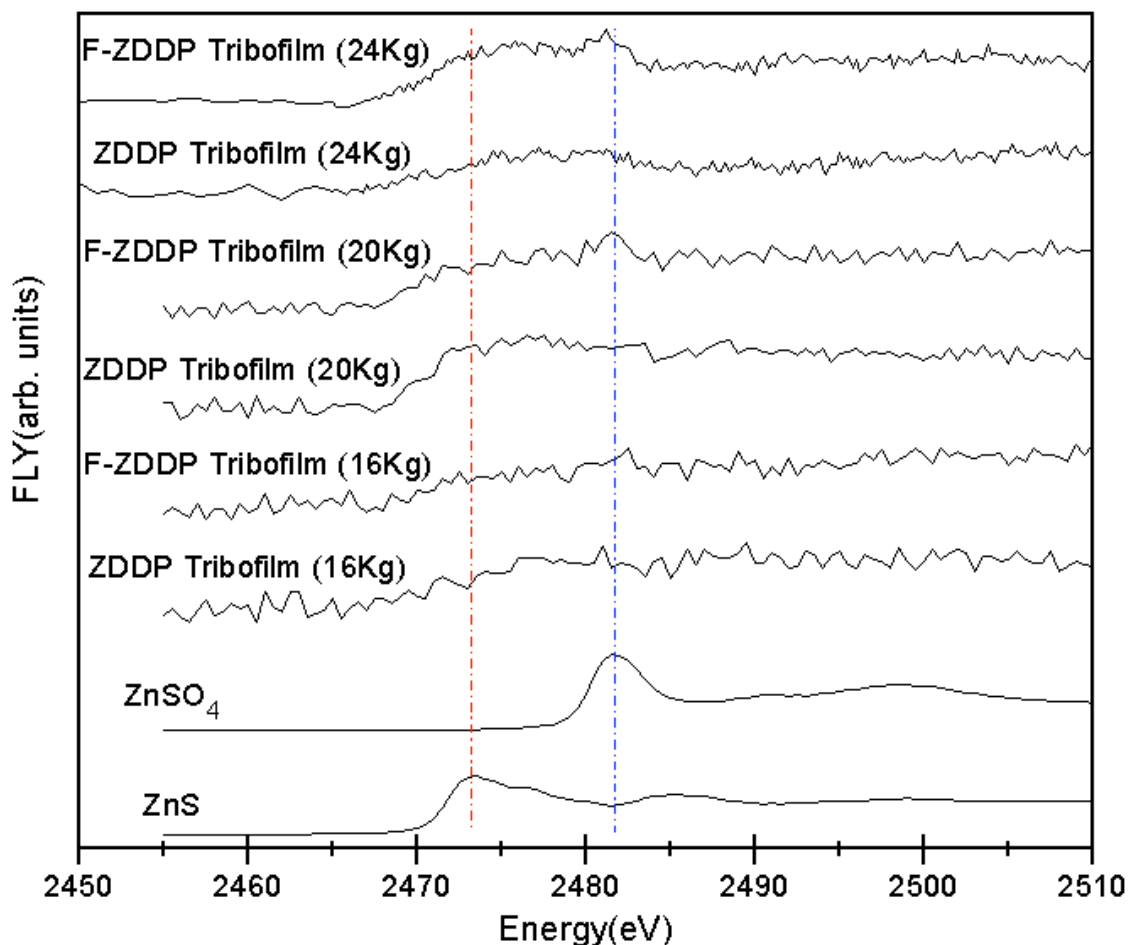


Figure 6.7: Sulfur K-edge XANES spectra collected in FLY mode for tribofilms generated by samples containing base oil and ZDDP or fluorinated ZDDP under 16, 20 and 24 Kg applied scuffing loads and the same spectra recorded for model compounds, ZnSO₄ and ZnS.

This observation is in agreement with the observations made by Varlot *et al.* [75] who also found that almost no sulfur was detected in the S K-edge spectra collected from the bulk of ZDDP tribofilms in the FLY mode. In the same study [75] the TEY S K-edge spectra were collected for FeSO₄, Fe₂(SO₄)₃, alkyl sulfide, FeS and basic ZDDP (pure powder) in addition to

the model compounds of this study (ZnS and ZnSO_4). The observed S K-edge peaks for all these compounds fall within the energy range observed in peaks collected from all tribofilm samples in figures 6.6 and 6.7, i.e. $\approx 2473\text{-}2482$ eV indicating that all these compounds may be present in the tribofilm.

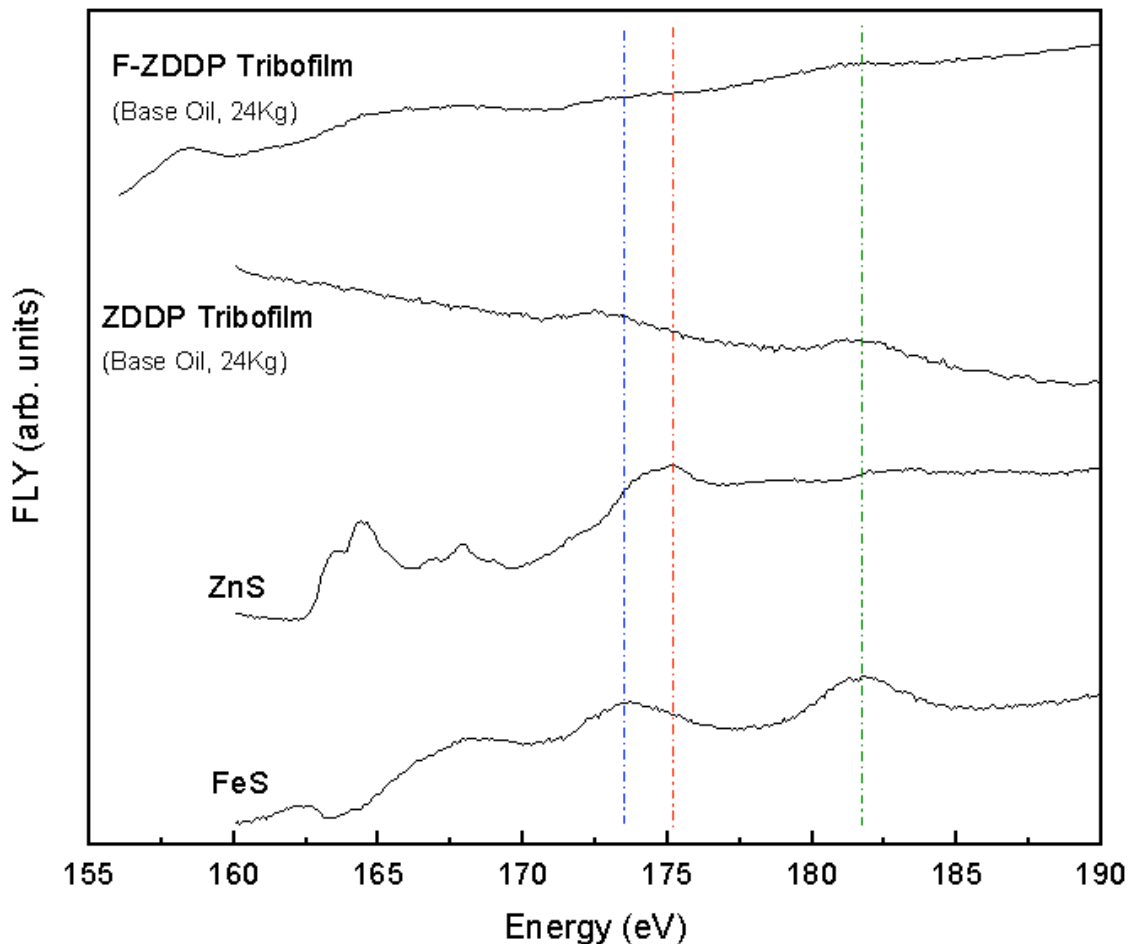


Figure 6.8: Sulfur L-edge XANES spectra collected in FLY mode for tribofilms generated by samples containing base oil and ZDDP or fluorinated ZDDP under 24 Kg applied scuffing load and the same spectra recorded for model compounds FeS and ZnS.

6.2.1.4 Sulfur L-edge XANES

Sulfur L-edge XANES spectra collected in FLY mode are shown in figure 6.8 for tribofilms generated by ZDDP and fluorinated ZDDP under 24 Kg scuffing load. The same

spectra is also collected for model compounds iron(II) sulfide (FeS) and zinc sulfide (ZnS). The collected S L-edge signal for both tribofilms is weak, thus the peaks observed in both cases are very small and only visible as bumps. However, in both cases, the location of these peaks is closely matched with the location of the peaks observed for FeS shown by blue and green dashed lines. Due to low signal intensities, it is not conclusive whether the location of ZnS peaks (red dashed line) can be matched with peaks collected from the two tribofilm samples.

6.2.2 Nano-indentation

Nano-indentation tests were performed on all tribofilm samples generated from the test matrix of table 6.1 in order to examine the effect of test duration and applied scuffing load on hardness and reduced elastic modulus of tribofilms generated by ZDDP and fluorinated ZDDP. Nano-indentation tests were run on each sample using the Hysitron Ubi[®] 1 Triboindenter. The indenter tip used in all these tests is a Berkovich tip, a three sided diamond pyramid with a total included angle of 142.3 degrees and a half angle of 65.35 degrees, an elastic modulus between 1,000 and 1,140 GPa and a Poisson ratio of 0.07. Two types of nano-indentation tests were run on each sample: trapezoidal single indents (described in 3.5.1.1) and cyclic trapezoidal indents (described in 3.5.1.2). A 60 μm x 60 μm area of the surface of the tribofilms inside the wear tracks was probed in the SPM mode to ensure presence of a smooth and consistent tribofilm within the testing area. Cyclic indentations were run with a maximum load of 500 μN and single indents were performed for 100, 500 and 1000 μN peak loads in order to probe film properties in different depths of the tribofilm. Each indentation was repeated over the probed area on several locations to assess the repeatability of observations. The minimum distance between indentation spots was kept at 5 μm to minimize the effect of the stress-strain fields generated in the immediate area of previous indentations.

6.2.2.1 Trapezoidal single indentation tests

The nano-indentation data for trapezoidal single indents is plotted in figures 6.9 through 6.13. The top graphs in each figure are the load vs. vertical displacement graphs for fluorinated

ZDDP (left) and ZDDP (right). Measured reduced elastic modulus (see 3.51) is also plotted against tip penetration depth (i.e. vertical displacement) in the middle section of each figure and hardness is plotted against the same in the bottom section of each figure. The scale on the vertical (y) axis for each pair of graphs plotted side by side in the same row of plots is exactly the same in each figure and the scale on the horizontal (x) axis of all the graphs in all these figure (6.9-13) is also identical (0 to 80 nm).

The nano-indentation data from fluorinated ZDDP and ZDDP tribofilm samples generated under 16 Kg applied scuffing loads (15K cycles) are shown in figure 6.9. The same data for tests run under 20 and 24 Kg loads (15K cycles) are shown in figures 6.10 and 6.11 respectively. In all cases, the 100 μN peak load indents have yielded a penetration depth of 10-15 nm while the average penetration of the tip for 500 μN peak load indentations is about 40-50 nm and 60-75 nm for indentations with the maximum load of 100 μN . The reduced elastic moduli measured for all tribofilms beyond the penetration depth of ≈ 65 nm approaches that of the steel substrate (≈ 200 GPa). A similar trend is observed for hardness values which also tend to settle at about 8 GPa (hardness of the steel substrate) with comparably little scatter, closer to the steel substrate. At lower depths however, some variations are observed in the measured reduced elastic moduli. For tribofilms generated by fluorinated ZDDP under 16 Kg scuffing loads for instance (figure 6.9), the value of reduced elastic moduli decreases from about 200 GPa at smaller depths of 10-13 nm to just below 150 GPa at depths of about 50 nm, however the moduli values obtained for the ZDDP tribofilm formed under the same scuffing load (16 Kg), follow an opposite trend in which the moduli values increase from about 130 GPa at 10-15 nm to about 200 GPa at 40-50 nm depths. The hardness values for same two samples (figure 6.9) follow a trend similar to the trend observed in the case elastic moduli values. The maximum vertical displacement observed in both samples of figure 6.9 is identical and about 65-68 nm.

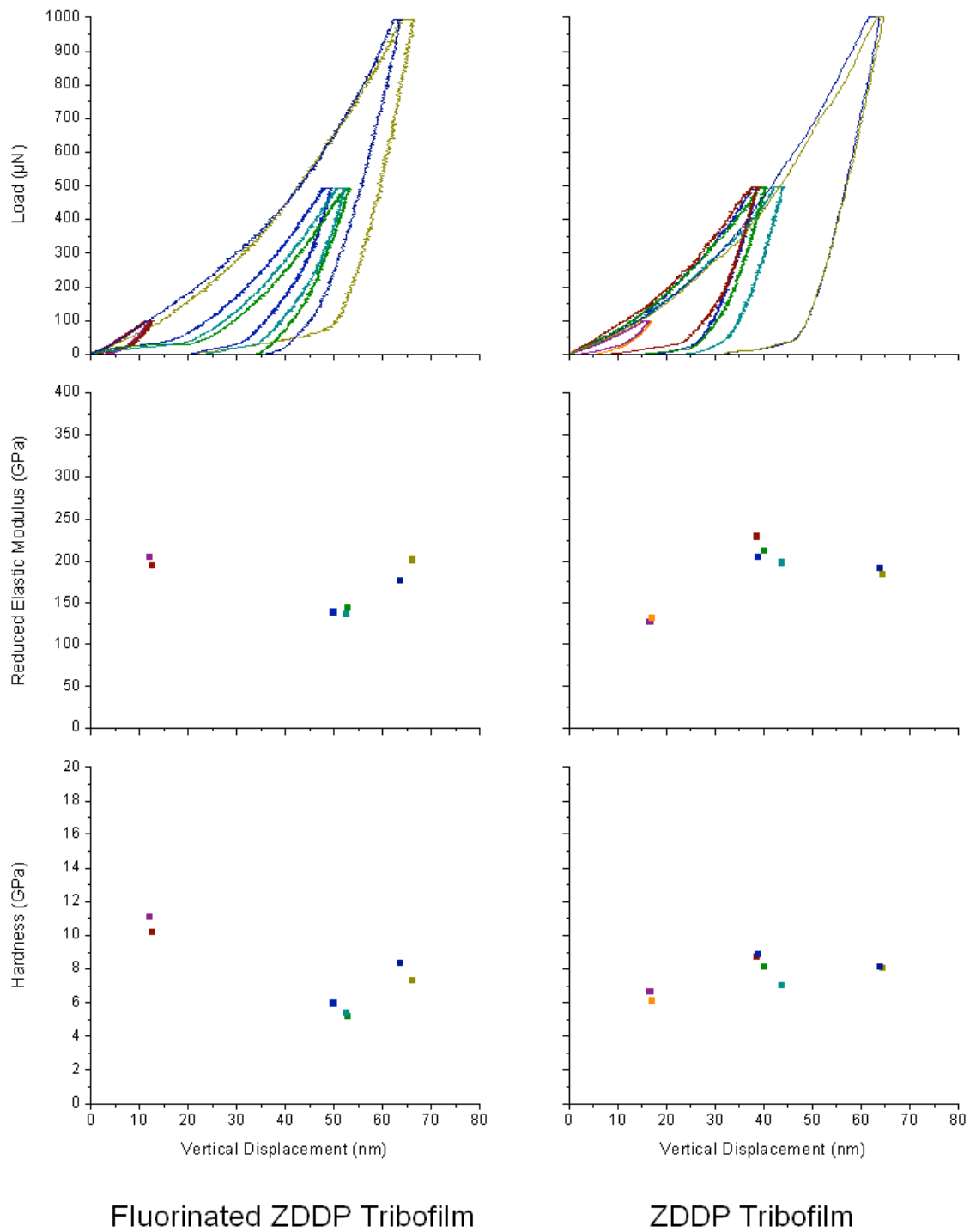


Figure 6.9: Representative load, modulus and hardness vs. penetration graphs for tribofilms generated by fluorinated ZDDP and ZDDP (800 ppm P in base oil) by tests run under 16 Kg scuffing load for 15K cycles.

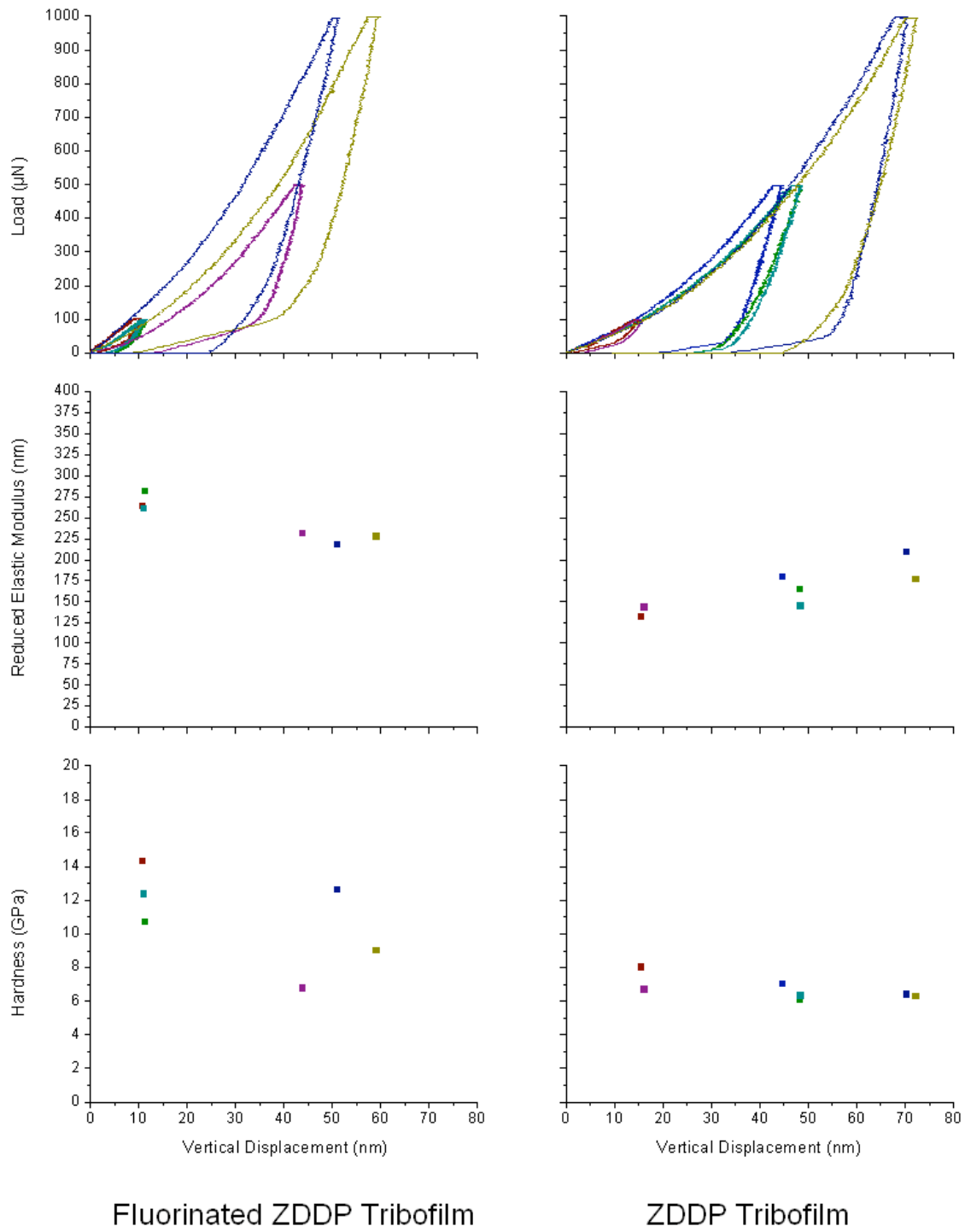


Figure 6.10: Representative load, modulus and hardness vs. penetration graphs for tribofilms generated by fluorinated ZDDP and ZDDP (800 ppm P in base oil) by tests run under 20 Kg scuffing load for 15K cycles.

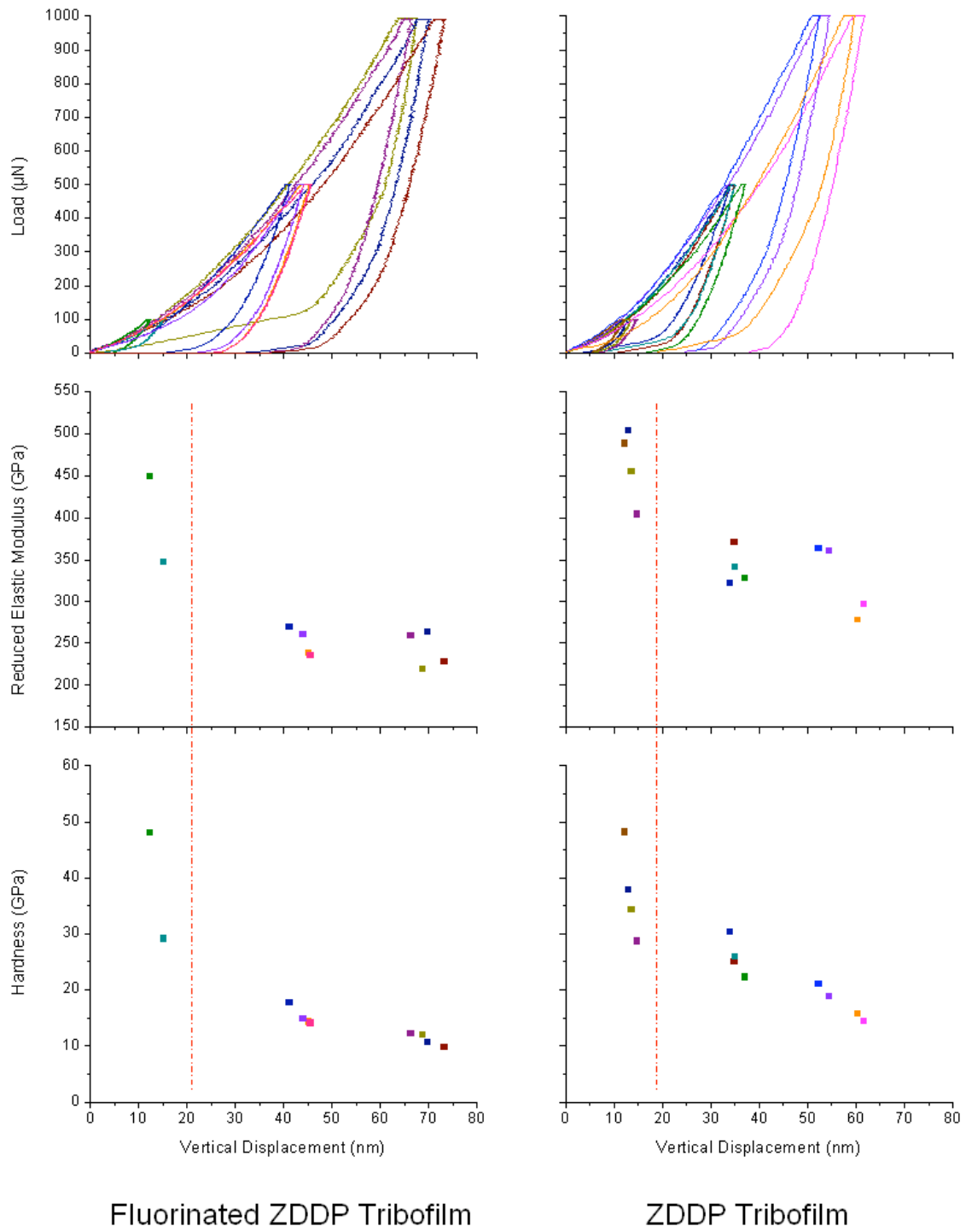


Figure 6.11: Representative load, modulus and hardness vs. penetration graphs for tribofilms generated by fluorinated ZDDP and ZDDP (800 ppm P in base oil) by tests run under 24 Kg scuffing load for 15K cycles.

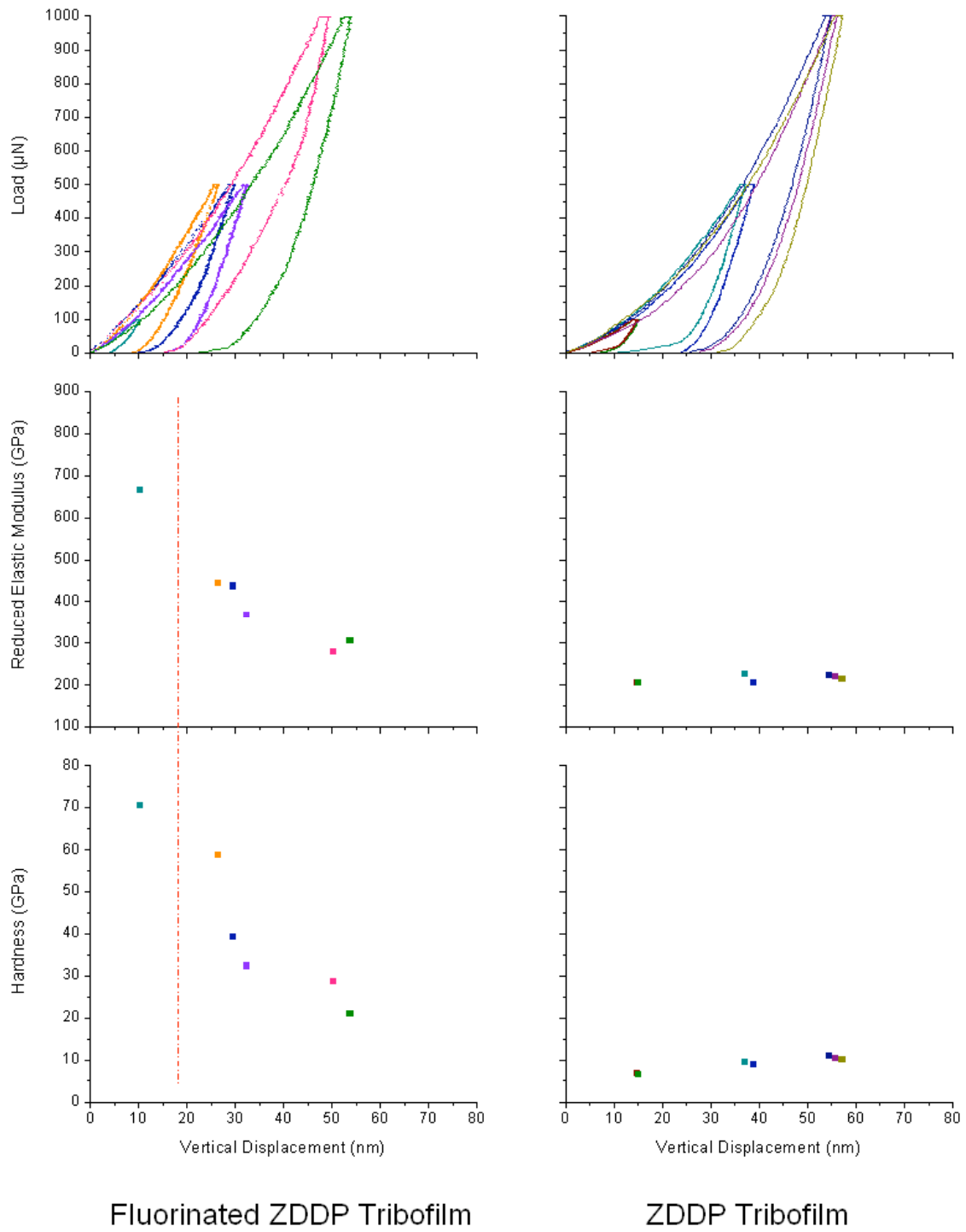


Figure 6.12: Representative load, modulus and hardness vs. penetration graphs for tribofilms generated by fluorinated ZDDP and ZDDP (800 ppm P in base oil) by tests run under 24 Kg scuffing load for 5K cycles.

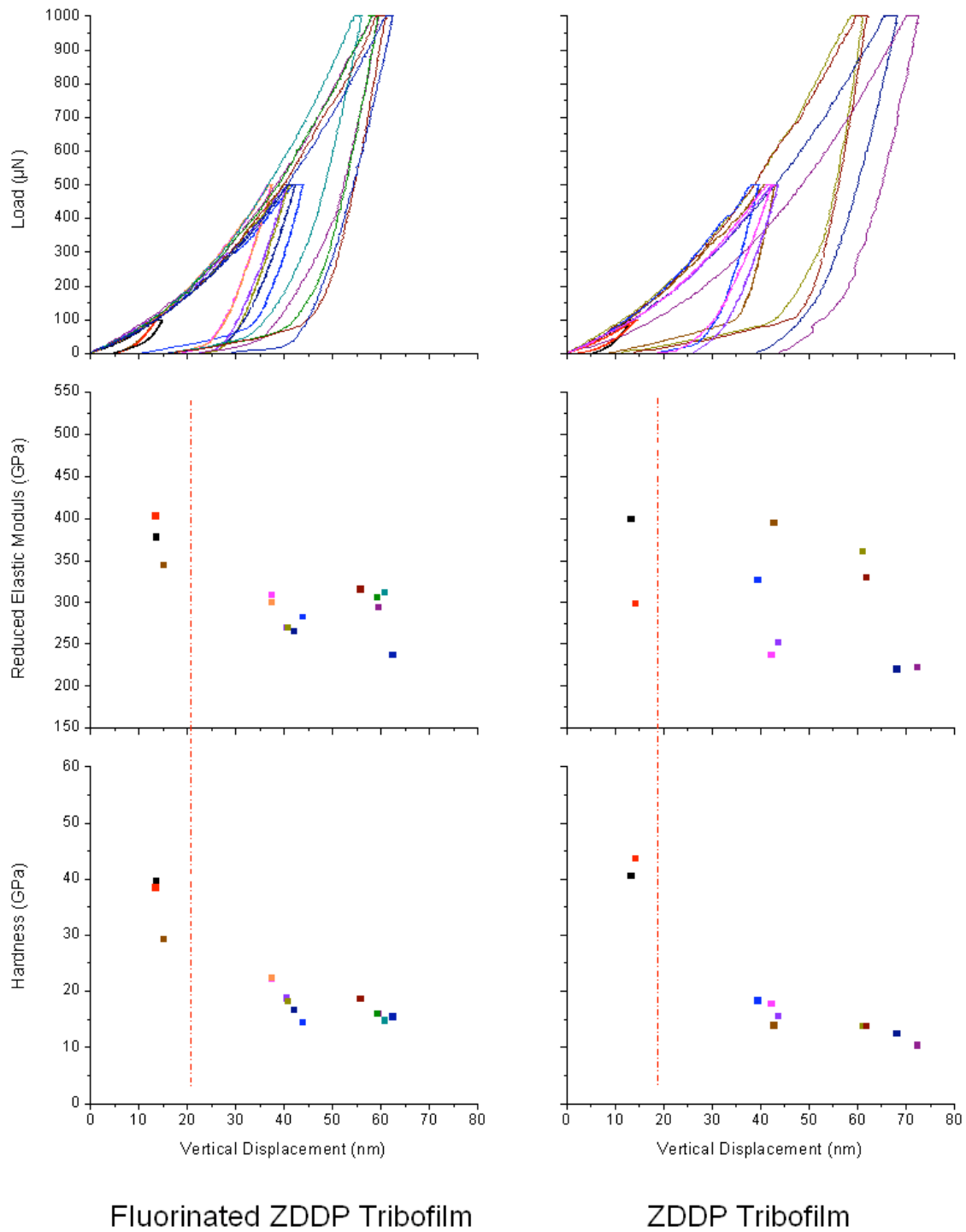


Figure 6.13: Representative load, modulus and hardness vs. penetration graphs for tribofilms generated by fluorinated ZDDP and ZDDP (800 ppm P in base oil) by tests run under 24 Kg scuffing load for 25K cycles.

For tribofilms formed under 20 Kg applied scuffing load (figure 6.10) the modulus values obtained for fluorinated ZDDP tribofilm have a range of ≈ 225 - 275 GPa which is relatively higher than the range of modulus values obtained for ZDDP tribofilm being between ≈ 125 to ≈ 200 GPa. Hardness values, although quite scattered, also point to a harder film in the case of fluorinated ZDDP. The maximum penetration of the indenter tip in case of fluorinated ZDDP tribofilm is about ≈ 60 nm and ≈ 75 nm for ZDDP tribofilm sample, generated under 20 Kg (figure 6.10), which is in agreement with the hardness data for this pair of tribofilm samples.

The nano-indentation data taken from fluorinated ZDDP and ZDDP tribofilms generated under 24 Kg loads (15K cycles) are shown in figure 6.11. In comparison to the data shown in figures 6.9 and 6.10, the modulus and hardness values obtained at displacements below 20 nm (corresponding to 100 μ N peak load indentations) are scattered and unrealistically high. This portion of data lies on the left side of the dashed red line for each sample in figure 6.11. The observed anomaly in this portion of data can be attributed to the fact that at such small penetration depths (< 15 nm) the tip area function is not accurately known resulting in difficulties in fitting the initial portion of the unloading segment of the load-displacement curve using the Oliver and Pharr method. Similar observations are made in data obtained from ZDDP and fluorinated ZDDP tribofilms run under 24 Kg for 5K and 25K cycles (figures 6.12 and 6.13 respectively). Unrealistic and highly scattered values of reduced elastic modulus and hardness in both cases (figures 6.12 and 6.13) may also be an artifact of several factors, including unknown tip area function for small penetrations, blunting, contamination and change of tip radius over time. The surface roughness and patchy nature and varying thickness of tribofilms tested is another reason for the scatter observed in collected data. Given the anomalies present in the data and the fact that measurements can vary depending on the location of the probed area on tribofilm samples, the data obtained from single trapezoidal indentation experiments is inconclusive in determining the effect of load and the number of cycles on the hardness and reduced elastic modulus of tribofilms since the observed data in all cases are within similar

values. It is observed, that, regardless of the scatter observed, the tribofilm samples investigated, in general have a reduced elastic modulus that is higher (≈ 250 GPa) or in the range of the steel substrate and are generally 3-4 GPa harder than the steel substrate which has a hardness value of about 8 GPa.

6.2.2.2 Cyclic trapezoidal indentation tests

Cyclic indentation tests with incremental loading were also carried out on the tribofilm samples from the test matrix shown in table 6.1 using the load function shown in figure 3.6. This data is presented in figure 6.14-18. The main advantage of cyclic indentation tests is the fact that unlike single indentation tests, here, the hardness and modulus vs. load data is collected from a single spot on the tribofilm. This allows to eliminate the scatter in data that arises from differences in film thickness and properties from one location to another on the same sample of tribofilm. However, since the data is collected by performing repeated incrementally loaded indents in the same spot, it is very likely that work hardening of the tribofilm over several indentations could skew the collected data. Each indentation was repeated several times over different locations on each tribofilm sample. For simplicity however, the data for one or two representative runs on each sample is shown figures 6.14-18.

The collected reduced elastic modulus and hardness data for depths below 10-15 nm show a great deal of scatter and point to unrealistically high values of hardness and modulus that are different from actual values in these penetration depths. This is again the result of the unknown tip area function at low penetration depths, and erroneous fitting of the unloading segment of the load-depth curve due to scattered values and small number of data points in the first few indentation cycles.

The data collected for tribofilms formed under different scuffing loads of 16, 20 and 24 Kg (all 15K cycles), are shown in figures 6.14, 6.15 and 6.16. If the data beyond the penetration depth of 20 nm is taken into consideration only, very little difference is found between the hardness and modulus values recorded. The reduced elastic modulus settles at ≈ 200 GPa

which identical to that of the steel substrate. The hardness values, with a few exceptions, also fall within 8-10 GPa, i.e. very close to the hardness of the steel substrate indicating the heavy influence of the steel substrate on the measured properties. In the case of the tribofilms generated under 24 Kg applied load (15K cycles) the tribofilm generated by ZDDP appears to be stiffer (and harder) than the fluorinated ZDDP film allowing for smaller overall tip penetration (35 nm) in comparison to fluorinated ZDDP film (47 nm). For the films generated under the same load (24 Kg) in 5K and 25K cycles tests (figure 6.17 and 6.18 respectively), the observed difference in hardness values (beyond the depth of 20 nm) is not as visible. The overall tip penetration on the other hand, is again smaller for ZDDP tribofilms than fluorinated ZDDP tribofilms by about 10 nm, a probable indication that the tribofilm formed by fluorinated ZDDP is thicker than the tribofilm formed by ZDDP under 24 Kg loads, regardless of the number of cycles for which the tribotests are run. This result is in agreement with the FIB and nano-mechanical observations made in the previous chapter with regards to tribofilms generated by these two chemistries.

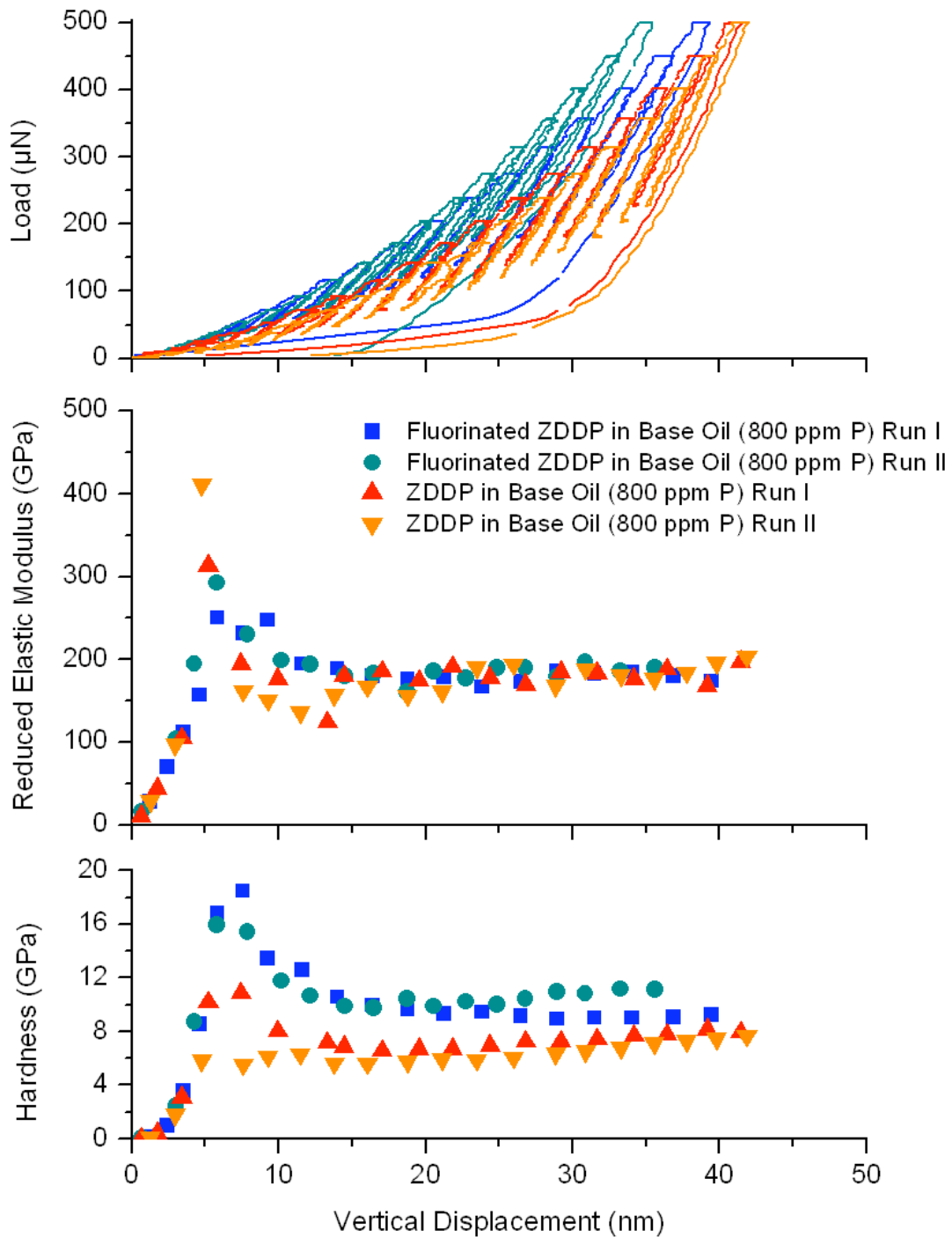


Figure 6.14: Representative load, modulus and hardness vs. penetration graphs from cyclic nano-indentation tests performed on tribofilms generated by fluorinated ZDDP and ZDDP (800 ppm P in base oil) by tests run under 16 Kg scuffing load for 15K cycles.

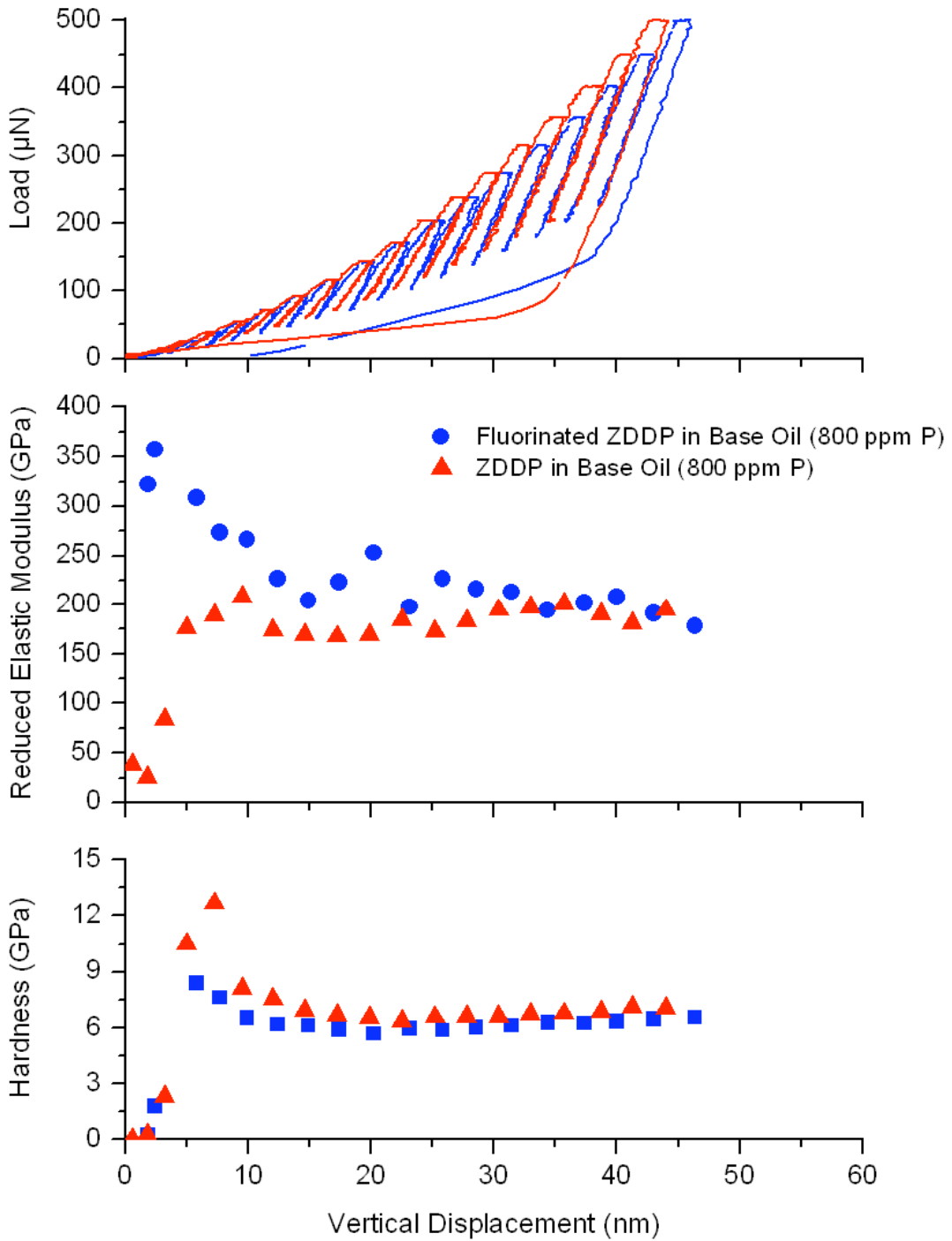


Figure 6.15: Representative load, modulus and hardness vs. penetration graphs from cyclic nano-indentation tests performed on tribofilms generated by fluorinated ZDDP and ZDDP (800 ppm P in base oil) by tests run under 20 Kg scuffing load for 15K cycles.

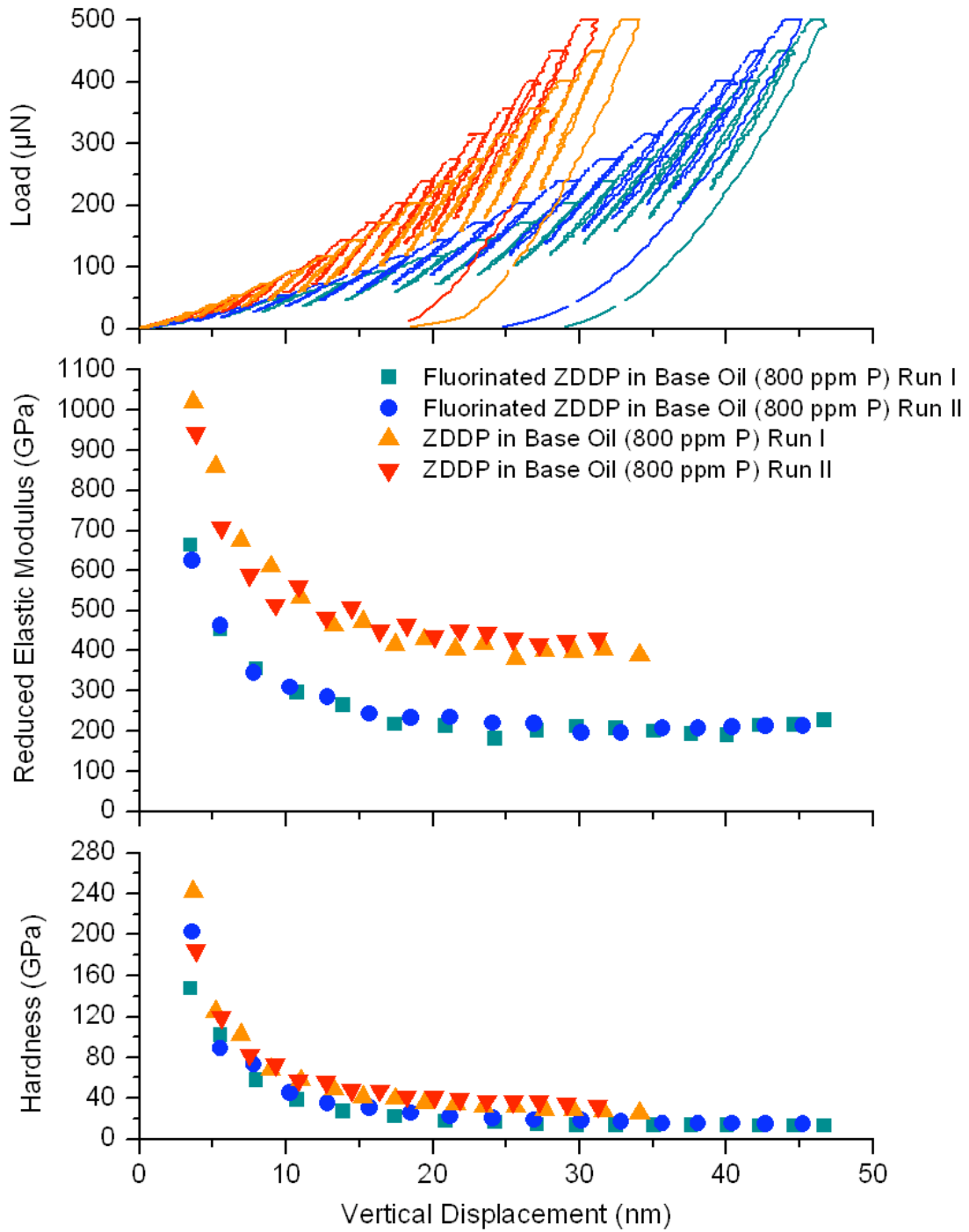


Figure 6.16: Representative load, modulus and hardness vs. penetration graphs from cyclic nano-indentation tests performed on tribofilms generated by fluorinated ZDDP and ZDDP (800 ppm P in base oil) by tests run under 24 Kg scuffing load for 15K cycles.

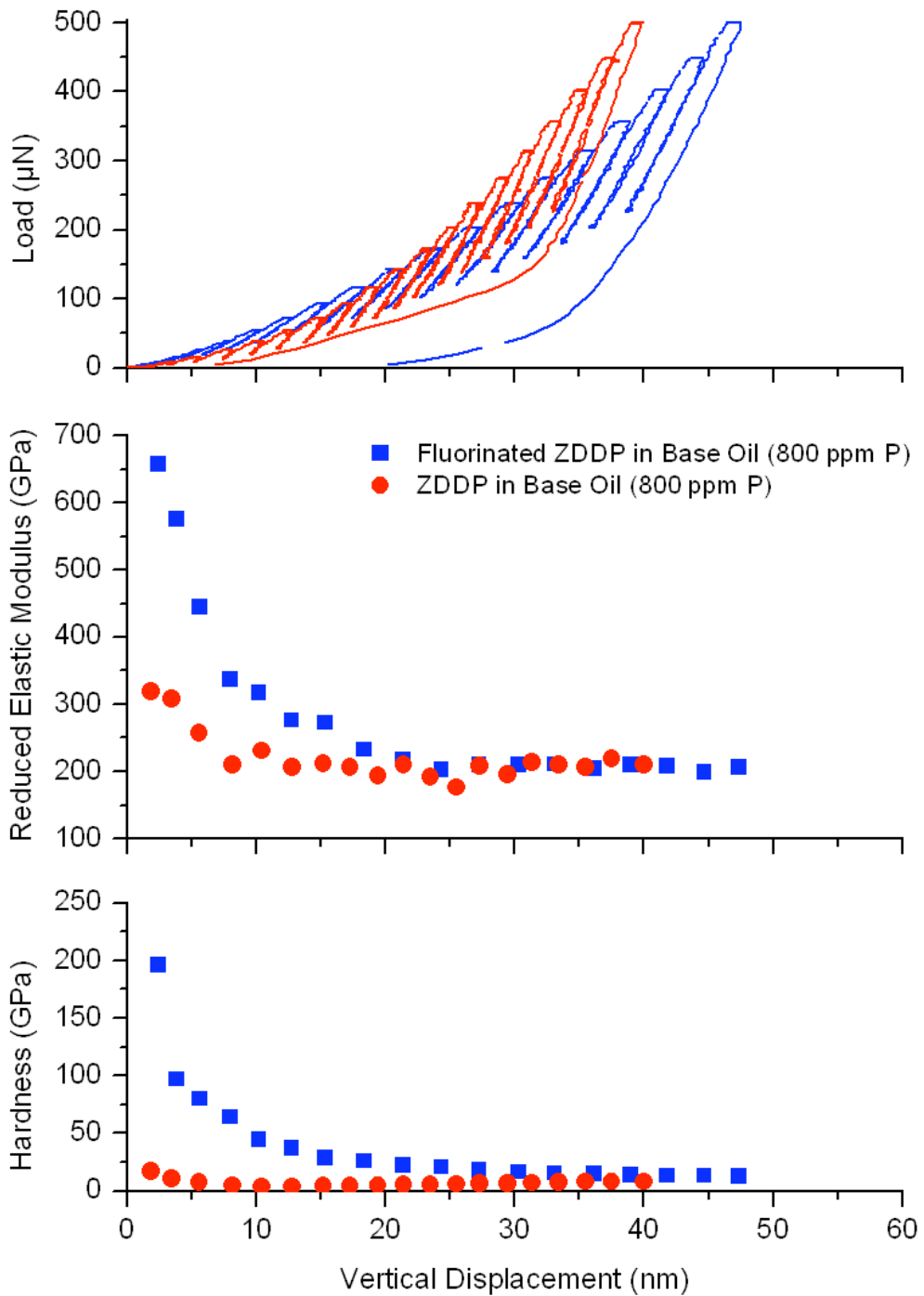


Figure 6.17: Representative load, modulus and hardness vs. penetration graphs from cyclic nano-indentation tests performed on tribofilms generated by fluorinated ZDDP and ZDDP (800 ppm P in base oil) by tests run under 24 Kg scuffing load for 5K cycles.

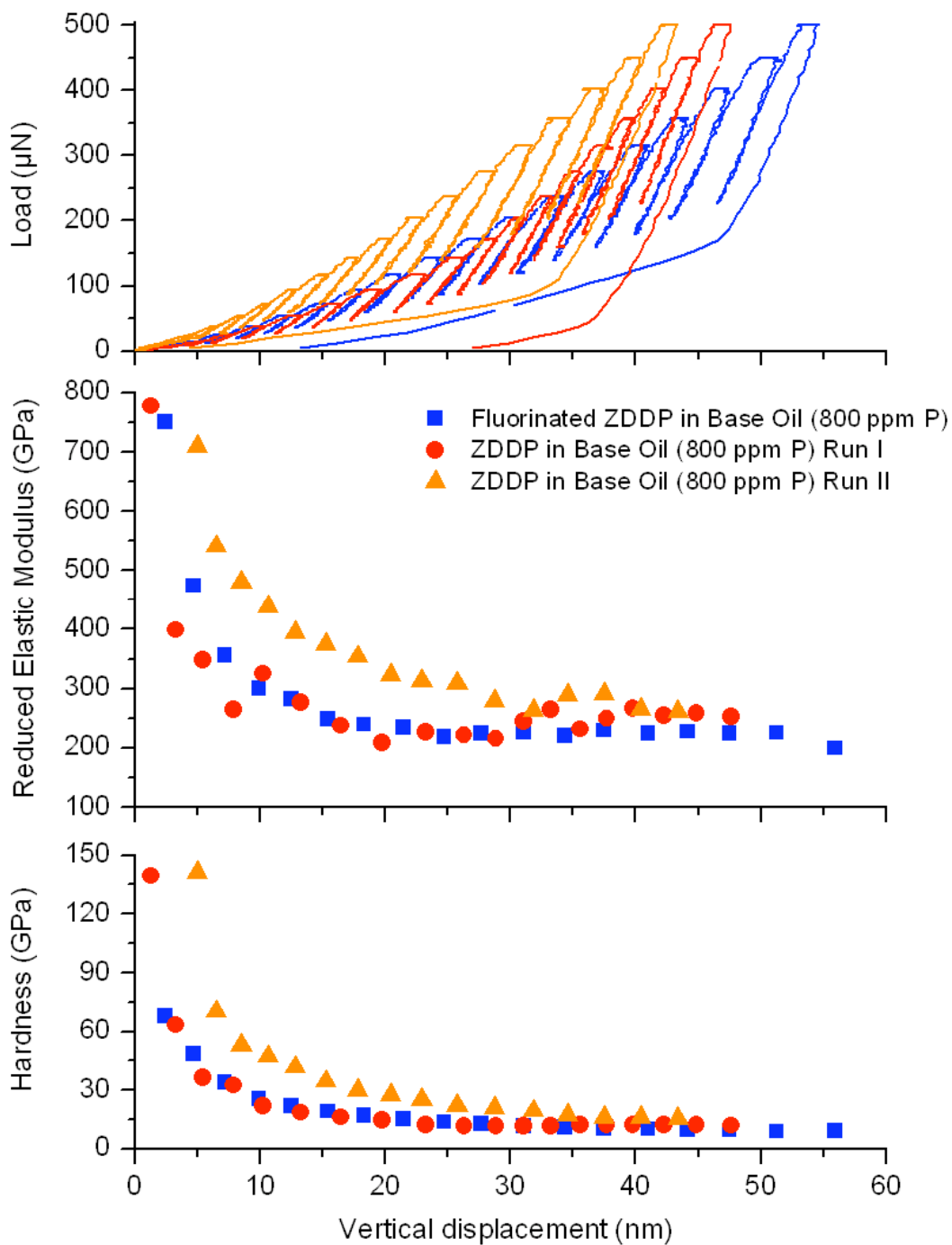


Figure 6.18: Representative load, modulus and hardness vs. penetration graphs from cyclic nano-indentation tests performed on tribofilms generated by fluorinated ZDDP and ZDDP (800 ppm P in base oil) by tests run under 24 Kg scuffing load for 25K cycles.

CHAPTER 7
FLUORINATED ZDDP AND ZDDP TRIBOFILMS:
A PHENOMENOLOGICAL MODEL

The characterization techniques used in this study have yielded several pieces of information that shed light on the chemical and physical structure, morphology and properties of tribofilms generated from fluorinated ZDDP and ZDDP under the testing conditions of this study. A phenomenological model is developed using the data acquired from each characterization technique in step-by-step fashion. In each step, the model is further developed in detail based on the information provided by each set of data and the observations made in other related research efforts in published literature.

The first set of data used in characterizing the two types of tribofilms is the scanning electron micrographs (SEM) and the EDS spectra obtained from tribofilms formed on the wear track of the steel rings (section 5.2.2). The obtained SEM micrographs point to a qualitatively rougher, less continuous tribofilm from ZDDP while the fluorinated ZDDP tribofilms appear to be smoother and more continuous. The EDS spectra from both tribofilms indicate a film containing zinc, phosphorus and sulfur in both cases. Since the substrate (steel ring) primarily consists of iron, the presence of iron peaks in the EDS spectra is not conclusive of the presence of iron in the tribofilms. Figure 7.1 is a schematic presentation of the structure of the two tribofilms based on the information derived from the SEM and EDS data (from ring samples). The presence of iron due to existence of iron in the substrate in the tribofilm is not yet established in this model. The presence of the strong phosphorus-fluorine bond in the structure of fluorinated ZDDP results in the presence of fluorine in the tribofilm generated by the fluorinated ZDDP, and thus it is predicted in the model shown in figure 7.1. The rougher ZDDP tribofilm is shown to have deeper grooves than the fluorinated ZDDP tribofilm.

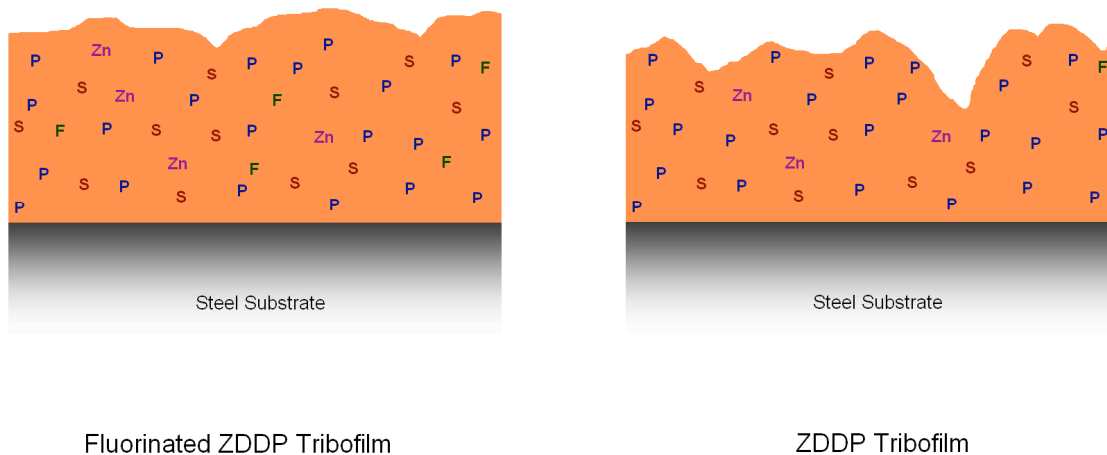


Figure 7.1: Tribofilm model constructed based on SEM and EDS data of tribofilms formed on the wear track of steel rings from ball on cylinder lubricity evaluation tests.

The film thickness measurements using the focused ion beam (shown in figure 5.10) indicated a tribofilm thickness of roughly 200 nm in the case of fluorinated ZDDP while the measured thickness of ZDDP tribofilm never exceeded 100 nm.

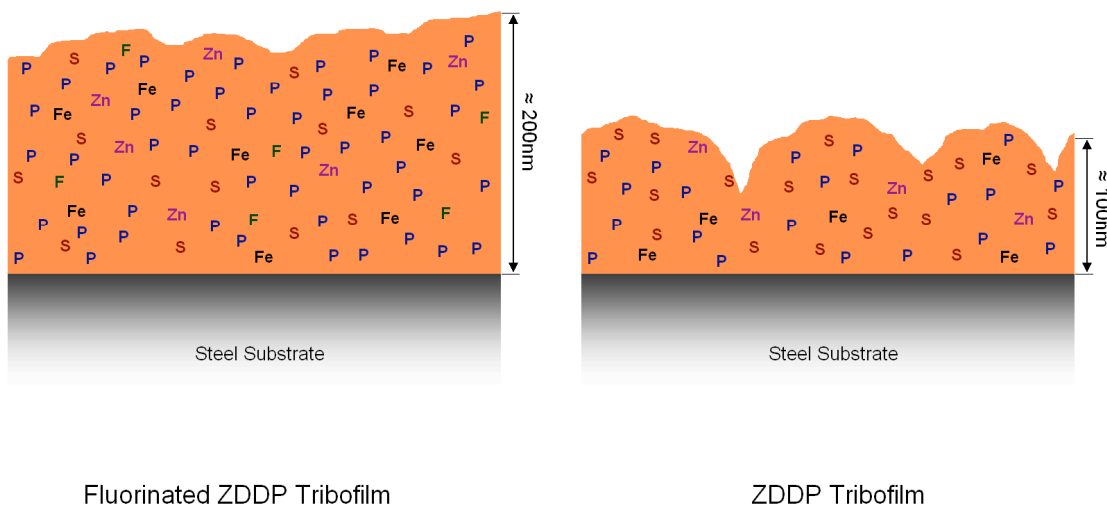


Figure 7.2: Tribofilm model further constructed based on film thickness measurements (using FIB) and EDS data of wear debris (TEM) and transfer films formed on the scuffing balls from BOCLE tests.

This difference in thickness is taken into account further developing the tribofilm model and is pointed out in figure 7.2. The tribofilm model shown in figure 7.2 is also further constructed by the EDS data from wear debris (TEM) and transfer films on the scuffing tungsten carbide balls (from BOCLE tests), which confirm the presence of iron in both types of tribofilms. This data also indicates higher relative sulfur to phosphorus concentration ratio (S/P) in ZDDP tribofilms. This difference in phosphorus and sulfur concentrations is also shown in the model presented in figure 7.2 where the fluorinated ZDDP model (left) is shown to contain more phosphorus and the ZDDP tribofilm model is shown to have more sulfur than phosphorus.

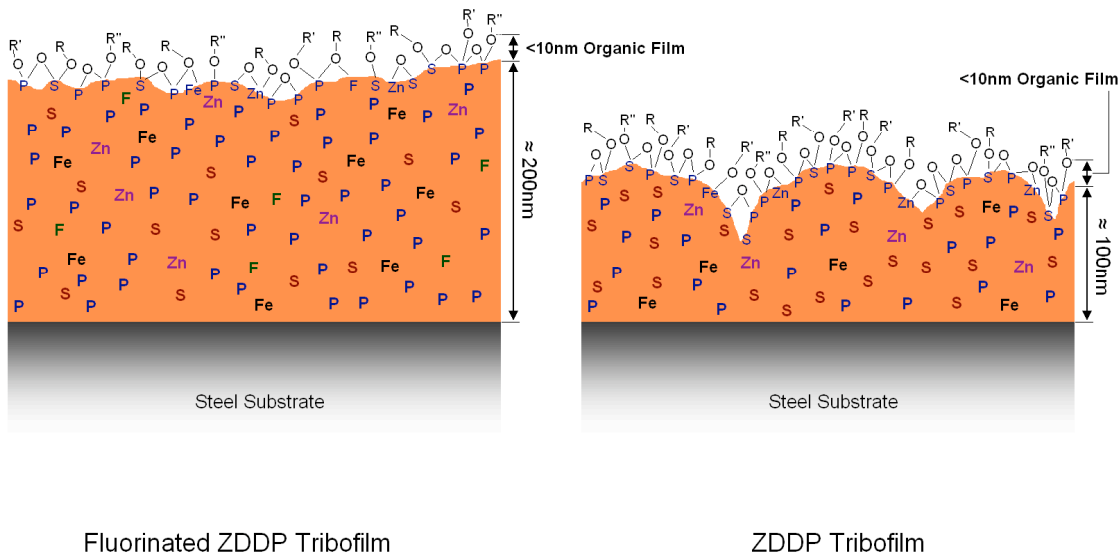
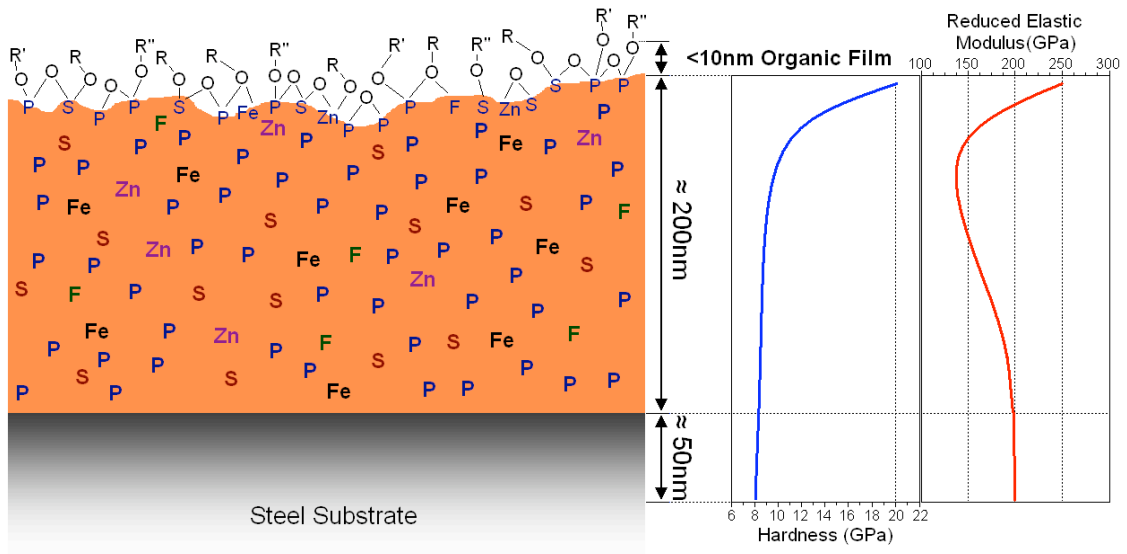
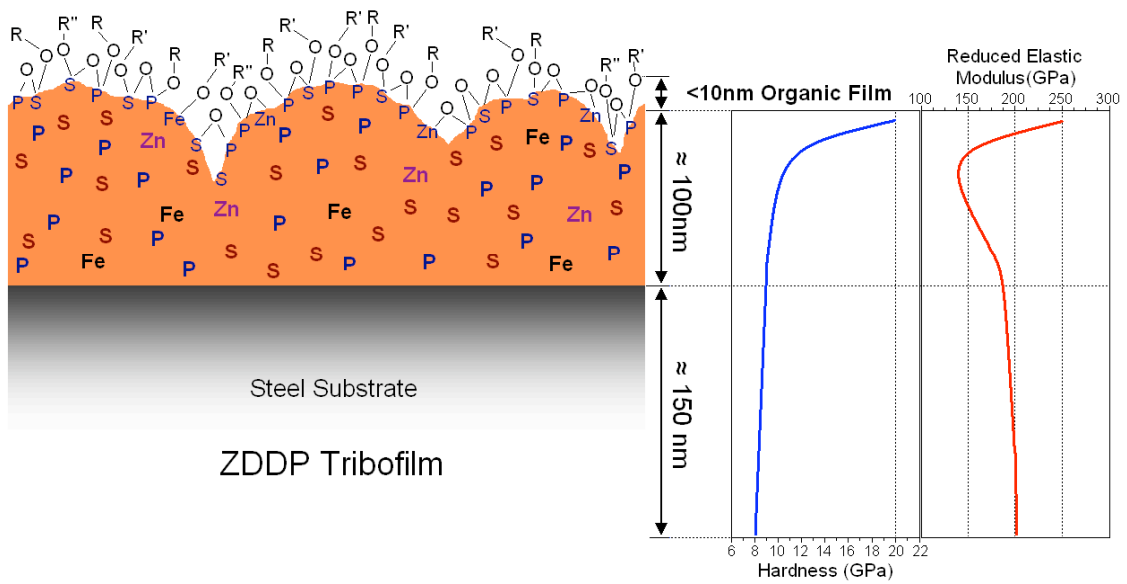


Figure 7.3: Tribofilm model further constructed based on Auger electron spectroscopy data.

Auger electron spectroscopy data (section 5.2.5) points to a relatively high concentration of oxygen on the surface layer of the tribofilm (< 10 nm) in the case of both antiwear chemistries. Since there is very little sulfur, iron and phosphorus present in the same depth, the observed oxygen is absorbed oxygen. This observation indicates that a thin organic chemisorbed film is present on the surface of the tribofilm. The oxygen-rich chemisorbed organic film is shown in the tribofilm model shown in figure 7.3 for both tribofilms. The oxygen atoms in this layer are bonded to phosphorus, sulfur and metal irons (Fe and Zn) in the tribofilm.



Fluorinated ZDDP Tribofilm



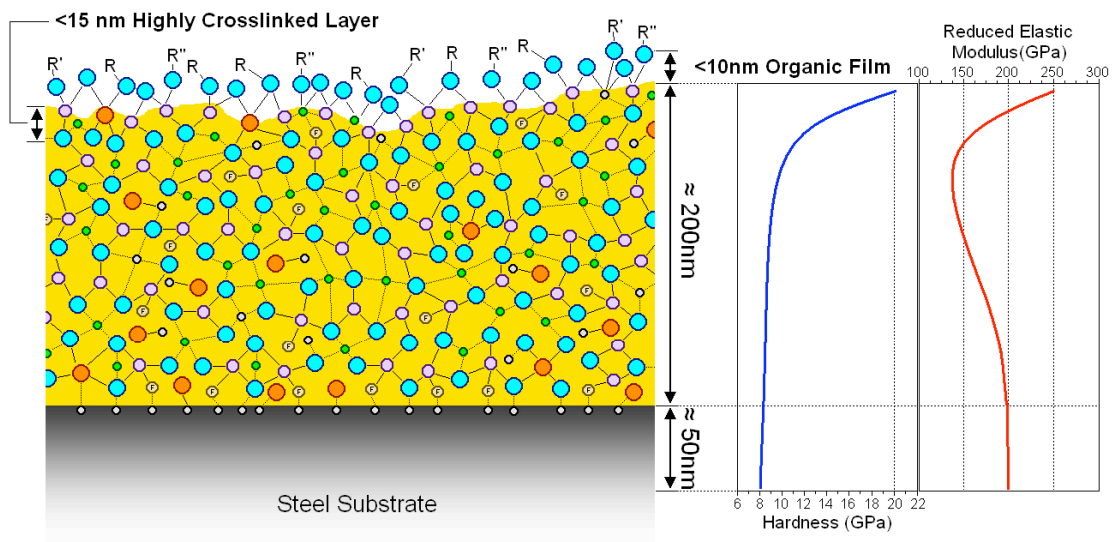
ZDDP Tribofilm

Figure 7.4: Tribofilm model further constructed based on nano-mechanical and nano-indentation testing data and observations.

Nano-indentation test data (section 5.2.3) follow similar trends for both tribofilms, however, due to smaller thickness of the ZDDP tribofilm, the values of hardness and reduced elastic modulus approach that of the substrate at smaller penetrations depths (≈ 100 nm). For both samples the hardness of the tribofilms is about 20 GPa near the surface (penetration depths of less than 15 nm) but rapidly decreases at larger tip penetration depths (vertical displacement) to 8 GPa, which is close to steel substrate hardness. A similar trend is observed for the values of reduced elastic modulus in these tribofilms. The measured value of reduced elastic modulus starts at about 250 GPa at the surface (< 15 nm depth) and sharply decreases to about 150 GPa through the middle part of the tribofilm only to creep up back to 200 GPa (i.e. the value of elastic modulus for the steel substrate) closer to the substrate. The average observed values of hardness and stiffness (reduced elastic modulus) are plotted for the profile of the tribofilm models for both chemistries in figure 7.4 for a total displacement (vertical) of 250 nm. Since the chemisorbed surface organic film is quite soft, in most cases, its effect is not picked up during nano-indentation testing.

XANES spectroscopy data obtained for the two tribofilms (chapter 6) provide the most valuable data needed for further developing this phenomenological model of the two types of tribofilms studied. The XANES spectroscopy observations are summarized as the following and the resulting model for the two tribofilms is shown in figure 7.5:

1. The tribofilms generated from fluorinated ZDDP mostly consist of short chain zinc polyphosphates while ZDDP tribofilms mostly contain short chain iron polyphosphates.
2. Sulfur is present as both sulfides and sulfates. A closer look at sulfur K-edge XANES spectra collected in TEY and FLY data (figures 6.6 and 6.7 respectively) shows that sulfide concentration is higher through out the thickness of the tribofilm while the sulfates are expected to be found more near the surface.
3. The sulfur L-edge XANES spectra show that the sulfides present in both tribofilms are iron sulfides rather than zinc sulfide.



Fluorinated ZDDP Tribofilm

- Sulfur
- Phosphorus
- Fluorine
- Zinc
- Iron
- Oxygen

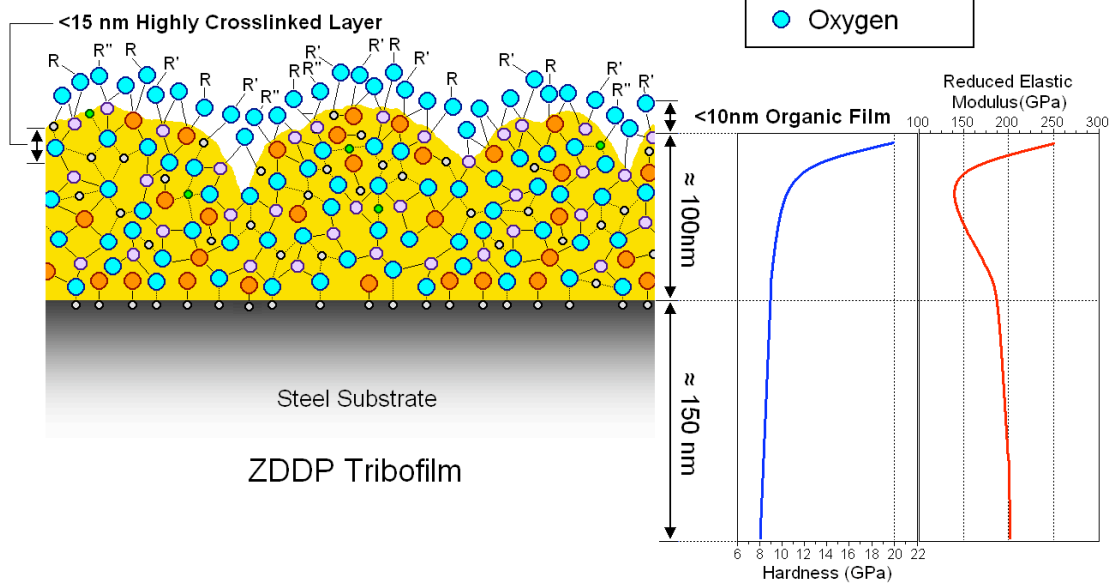


Figure 7.5: Tribofilm model further constructed based on XANES spectroscopy data.

The structure of the tribofilms is thus composed of phosphates and short chain polyphosphates as shown in the final presentation of tribofilm models in figure 7.5 for both

chemistries. The phosphates. Short chain polyphosphates as well as sulfide have been shown to be present as a chemically connected networked glass [14, 34-37]. The strong P-F bond in the fluorinated phosphorous compounds present in fluorinated ZDDP is highly unlikely to break during the tribofilm formation process, thus it is very likely that fluorine remains in the structure attached to phosphorus in the phosphate networked glass. The highly electronegative fluorine atoms in the P-F bond also enhance the affinity of the antiwear compound (fluorinated ZDDP) to the substrate iron surface during the early stages of tribofilm formation. While in the case of ZDDP tribofilms, the tribofilm is expected to contain more sulfides near the substrate by forming iron-sulfur bonds with the substrate iron atoms, the tendency of fluorine in the P-F bond (in the case of the fluorinated ZDDP) results in the attachment of the polyphosphate/phosphate glass to the iron in the substrate through F-Fe bonds. In the tribofilm models shown in figure 7.5, the ZDDP film is attached to the substrate mainly through S-Fe bonds while in the case of fluorinated ZDDP tribofilm model, both S-Fe and F-Fe bonds contribute to the adhesion of the tribofilm to the substrate. The presence of this bonding mechanism alongside the sulfides is believed to enhance the tribofilm adherence to the substrate, which explains the superior resistance to abrasion observed in the case of fluorinated ZDDP through nano-scratch and scanning nano-wear tests (section 5.2.3). The presence of zinc as the primary cation in the polyphosphate/phosphate glass in the case of fluorinated ZDDP as opposed to iron in the ZDDP tribofilms can also be explained when considering the role of fluorine in increasing the affinity of the antiwear compound (fluorinated ZDDP) to surface iron atoms in the substrate which results in enhancing the diffusion of more zinc thiophosphate compounds to the substrate surface before break down and Fe/Zn ion exchange could take place.

The observed hardness and stiffness trend observed for both tribofilms can also be explained through a hypothesis presented by Mosey *et al.* [34-37] suggesting that cross linking of the polyphosphate/phosphate networked glass is a pressure induced phenomenon. Given the severity of the tribological testing conditions, including the applied pressure, in this study, the

observed higher hardness and stiffness values observed at the top layers of the tribofilms (less than 15 nm) can be attributed to a higher level of cross linking between phosphates and polyphosphates in this layer. This high level of cross-linking occurs at the surface layers due to the fact that this layer is the primary load bearing part of the tribofilm through out each BOCLE test.

The above observations and hypotheses are schematically presented and summarized in figure 7.5 as the proposed models for tribofilms generated from fluorinated ZDDP and ZDDP under the testing conditions of this study.

CHAPTER 8

CONCLUSIONS

The different studies carried out in this research effort and data obtained from the wear tests as well as characterization techniques employed have yielded the following conclusions:

1. The UTA unit BOCLE unit was examined for its resolution by testing two different oil formulations (base oil + ZDDP containing 0.10 and 0.05 wt% phosphorous). These tests were also designed to provide an understanding of tribological characteristics of the setup used such as friction, temperature and wear data. Film thickness calculations carried out by plugging in the specifications of the UTA BOCLE unit showed the existence of boundary lubrication conditions during the tests run by this setup (this type of lubrication regime was also confirmed to exist in the tests run on the Plint® BOCLE unit as well). Test data such as friction/temperature vs. cycles as well as wear volume measurements and SEM/EDX maps of the surface of the tribofilms formed on the rings were analyzed. The testing method was proven to be very useful in comparing the effect of different variables on the efficiency of tribofilm formation and durability.
2. Wear volume results from the tests carried out on oils containing ZDDP as described in chapter 4 are indicative of the negative effect of the presence on the calcium sulfonate (detergent) and diphenyl amine (anti-oxidant) to the film forming efficiency of the ZDDP, in particular at higher contact loads. This observation is in agreement with DSC thermal analyses previously carried out on these samples.
3. Typical tribofilm thickness generated from oils containing ZDDP (with no additional additives) was found to be in the range of 100 nm and is confirmed by FIB and nanomechanical testing.

4. Nanomechanical testing of the tribofilm indicates that under extreme loads and boundary lubrication conditions, the films are made up of two distinctive layers, a surface layer with an approximate thickness of 15 nm that is significantly harder than the underlying film.

5. The wear performance of fluorinated ZDDP was found to be significantly better than the wear performance of untreated ZDDP under similar phosphorus levels. The improved wear performance was attributed to the improved, highly adherent tribofilm that was formed when fluorinated ZDDP was used. The thickness of the tribofilms was significantly higher when fluorinated ZDDP was used in comparison to untreated ZDDP. In addition the films formed when fluorinated ZDDP is used are much more resistant to abrasive wear under scanning wear conditions and nano-scratch conditions. The chemical makeup of the tribofilms formed using fluorinated ZDDP had significant amounts of phosphorous while tribofilms formed from untreated ZDDP had equal amounts of phosphorous and sulfur. Lastly the tribofilms formed using fluorinated ZDDP were largely amorphous and contained fewer number of crystalline oxide particles in comparison to tribofilms formed when untreated ZDDP was used. In conclusion, fluorinated ZDDP offers significant improvements in wear protection in comparison to traditional ZDDP.

6. XANES spectroscopy was run on tribofilm samples formed by ZDDP and fluorinated ZDDP under different loadings and durations. Comparing the phosphorus K-edge XANES spectra (collected in TEY and FLY mode) of tribofilms formed from ZDDP and fluorinated ZDDP under different scuffing loads with the P K-edge spectra for model compounds $Zn_3(PO_4)_2$ and $FePO_4$, indicated a stronger presence of zinc phosphates in fluorinated ZDDP films than iron phosphates when compared to tribofilms generated under the same testing conditions. The phosphorus L-edge data (obtained from tribofilms formed by both antiwear chemistries under 24 Kg scuffing load) reveal further information with regard to the chain length of the polyphosphates formed under the testing conditions of this study by both chemistries. Comparison of the P L-edge spectra (collected in FLY mode) of the tribofilms with several

polyphosphate compounds (of zinc and iron) revealed the dominant type of polyphosphates observed in the tribofilms formed in both case to be of shorter chain form. The sulfur K- and L-edge XANES spectra of the tribofilms collected in the surface sensitive TEY and bulk sensitive FLY modes indicated stronger presence of sulfur in the surface layers of the tribofilm than in the bulk. The model compounds for which the sulfur peaks of the tribofilm XANES spectra could be matched were $ZnSO_4$ and ZnS . No significant difference was observed in the K S-edge spectra of tribofilms generated by ZDDP and fluorinated ZDDP under scuffing loads of 16, 20 and 24 Kg. The sulfur L-edge XANES spectra (collected in the FLLY mode) obtained from both tribofilm samples (formed under 24 Kg scuffing load) also showed little difference between the two chemistries, however, confirmed the presence of both iron (II) and zinc sulfides in the tribofilm although the low peak intensities observed points to relatively low concentrations of sulfur in the tribofilm samples of this study.

7. Nano-indentation tests were performed on tribofilm samples generated by ZDDP and fluorinated ZDDP under different scuffing loads (16, 20 and 24 Kg) and different test durations (5K, 15K and 25K cycles) using two different load functions: single trapezoidal indents carried out under 100, 500 and 1000 μN and cyclic multiple trapezoidal indents (with peak load of 500 μN). The obtained modulus and hardness data from lower penetration depths (<20 nm) into the tribofilms were unrealistic and scattered mainly due to difficulties in fitting the unloading curve (using the Oliver and Pharr method) and unknown nature of the indenter tip's area function at low penetrations depths. Reduced elastic modulus and hardness data beyond the depth of 20 nm indicated little difference between tribofilms that were test. The little differences observed can be attributed to varying film properties within each sample rather than the difference in the antiwear action of the two chemistries. An observable trend within the data however is the smaller overall penetrations of the indenter tip in ZDDP tribofilms in comparison to fluorinated ZDDP tribofilms generated under 24 Kg loads with different durations which is in agreement

with the larger thickness of the fluorinated ZDDP tribofilms observed in the previous parts of this study.

8. A phenomenological model was developed using the data acquired from the different techniques used to characterize the tribofilms. The morphology, elemental composition and thickness of the tribofilm were determined using the SEM, TEM, EDS and FIB data respectively. Auger electron spectroscopy data indicate that both tribofilms are found to be covered by a soft oxygen rich organic film. The model was further constructed using nano-mechanical testing and XANES spectroscopy data. The XANES spectroscopy data indicated the presence of a phosphate/polyphosphate glass network also containing sulfides (ZnS) and sulfates. The fluorine present in the P-F in the case of fluorinated ZDDP enhances the adhesion to the substrate by bonding with iron in the substrate resulting in superior abrasion resistance properties. Hardness and stiffness depth profiles of the tribofilms indicated the presence of a harder and stiffer layer very near to the surface of the tribofilm (< 15 nm) which is attributed to higher levels of cross-linking in this part of the tribofilm.

REFERENCES

- [1] Parekh, K., 2006, "Interactions between Antiwear Agent and Novel Additive in Engine Oils"
- [2] Spedding, H., and Watkins, R. C., 1982, "Antiwear Mechanism of ZDDP's - 1," *Tribology International*, **15**(1) pp. 9-12.
- [3] Barnes, A. M., Bartle, K. D., and Thibon, V. R. A., 2001, "A Review of Zinc Dialkyldithiophosphates (ZDDPS): Characterisation and Role in the Lubricating Oil," *Tribology International*, **34**(6) pp. 389-395.
- [4] Hsu, S. M., Martin, J. M., and Nakayama, K., 2005, "Additives and Tribochemistry," *Proceedings of the World Tribology Congress III - 2005*, pp. 597.
- [5] Unnikrishnan, R., Jain, M. C., Harinarayan, A. K., 2002, "Additive-Additive Interaction: An XPS Study of the Effect of ZDDP on the AW/EP Characteristic of Molybdenum Based Additives," *Wear*, **252**(3-4) pp. 240-249.
- [6] Ramakumar, S. S. V., Aggarwal, N., Madhusudhana Rao, A., 1994, "Studies on Additive-Additive Interactions: Effects of Dispersant and Antioxidant Additives on the Synergistic Combination of Overbased Sulphonate and ZDDP," *Lubrication Science*, **7**(1) pp. 25-38.
- [7] Bartha, L., Deak, G., Hancsok, J., 2001, "Polyfunctional PIB Succinimide Type Engine Oil Additives," *Lubrication Science*, **13**(4) pp. 313-328.
- [8] Minfray, C., Martin, J. M., Esnouf, C., 2004, "A multi-technique approach of tribofilm characterisation," *Proceedings of the 30th International Conference on Metallurgie*, Apr 28-May 2 2002, Elsevier, San Diego, CA, United States, **447-448**, pp. 272-277.

- [9] Kapsa, P., Martin, J. M., Blanc, C., 1981, "Antiwear Mechanism of Zddp in the Presence of Calcium Sulfonate Detergent." *Journal of Lubrication Technology, Transactions ASME*, **103**(4) pp. 486-496.
- [10] Nicholls, M. A., Do, T., Norton, P. R., 2005, "Review of the Lubrication of Metallic Surfaces by Zinc Dialkyl-Dithiophosphates," *Tribology International*, **38**pp. 15-39.
- [11] Khorramian, B. A., Iyer, G. R., Kodali, S., 1993, "Review of Antiwear Additives for Crankcase Oils," *Wear*, **169**(1) pp. 87-95.
- [12] Ferrari, E. S., Roberts, K. J., Sansone, M., 1999, "A Multi-Edge X-Ray Absorption Spectroscopy Study of the Reactivity of Zinc Di-Alkyl-Di-Thiophosphates Anti-Wear Additives: 2. in Situ Studies of steel/oil Interfaces," *Wear*, **236**(1-2) pp. 259-275.
- [13] Barcroft, F. T., Bird, R. J., Hutton, J. F., 1982, "The Mechanism of Action of Zinc Thiophosphates as Extreme Pressure Agents," *Wear*, **77**(3) pp. 355-384.
- [14] Spikes, H. A., 2004, "The History and Mechanisms of ZDDP," *Tribology Letters*, **17**(3) pp. 469-489.
- [15] So, H., Lin, Y. C., Huang, G. G. S., 1993, "Antiwear Mechanism of Zinc Dialkyl Dithiophosphates Added to a Paraffinic Oil in the Boundary Lubrication Condition," *Wear*, **166**(1) pp. 17-26.
- [16] Sheasby, J. S., Caughlin, T. A., and Habeeb, J. J., 1991, "Observation of the Antiwear Activity of Zinc Dialkyldithiophosphate Additives," *Wear*, **150**(1-2) pp. 247-257.
- [17] Willermet, P. A., Dailey, D. P., Carter, R. O., III, 1995, "Mechanism of Formation of Antiwear Films from Zinc Dialkyldithiophosphates," *Tribology International*, **28**(3) pp. 177-187.

- [18] Neville, A., and Kollia-Rafailidi, V., 2002, "A Comparison of Boundary Wear Film Formation on Steel and a Thermal Sprayed Co/Cr/Mo Coating Under Sliding Conditions," *Wear*, **252**(3-4) pp. 227-239.
- [19] Yin, Z., Kasrai, M., Bancroft, G. M., 1997, "Application of Soft x-Ray Absorption Spectroscopy in Chemical Characterization of Antiwear Films Generated by ZDDP Part II: The Effect of Detergents and Dispersants," *Wear*, **202**(2) pp. 192-201.
- [20] Kroger, V., Lassi, U., Kynkaanniemi, K., 2006, "Methodology Development for Laboratory-Scale Exhaust Gas Catalyst Studies on Phosphorus Poisoning," *Chemical Engineering Journal*, **120**(1-2) pp. 113-113-118.
- [21] Rokosz, M. J., Chen, A. E., Lowe-Ma, C. K., 2001, "Characterization of Phosphorus-Poisoned Automotive Exhaust Catalysts," *Applied Catalysis B: Environmental*, **33**(3) pp. 205-205-215.
- [22] Parekh, K., and Aswath, P. B., 2006, "Synthesis of Fluorinated ZDDP," Anonymous American Society of Mechanical Engineers, pp. IJTC-12053.
- [23] Zhang, Z., Yamaguchi, E. S., Kasrai, M., 2005, "Tribofilms generated from ZDDP and DDP on steel surfaces: Part 1. Growth, wear and morphology," 2005 World Tribology Congress III, American Society of Mechanical Engineers, New York, NY 10016-5990, United States, Washington, D.C., United States, pp. 617-618.
- [24] Zhang, Z., Yamaguchi, E. S., Kasrai, M., 2005, "Tribofilms generated from ZDDP and DDP on steel surfaces: Part 2: Chemistry," 2005 World Tribology Congress III, American Society of Mechanical Engineers, New York, NY 10016-5990, United States, Washington, D.C., United States, pp. 619-620.

- [25] Martin, J. M., and Minfray, C., 2005, "Antiwear chemistry in presence of ZDDP," 2005 World Tribology Congress III, Sep 12-16 2005, American Society of Mechanical Engineers, New York, NY 10016-5990, United States, Washington, D.C., United States, pp. 599-600.
- [26] Martin, J. M., Grossiord, C., Le Mogne, T., 2001, "The Two-Layer Structure of ZnDTP Tribofilms: Part I: AES, XPS and XANES Analyses," *Tribology International*, **34**(8) pp. 523-530.
- [27] Martin, J. M., Mansot, J. L., Berbezier, I., 1984, "The Nature and Origin of Wear Particles from Boundary Lubrication with a Zinc Dialkyl Dithiophosphate," *Wear*, **93**(2) pp. 117-126.
- [28] Martin, J. M., 1999, "Antiwear Mechanisms of Zinc Dithiophosphate: A Chemical Hardness Approach," *Tribology Letters*, **6**(No. 1) pp. 1-1-8.
- [29] Bec, S., Demmou, K., Loubet, J., 2005, "Mechanical properties of ZnDTP tribofilms measured by nanoindentation at controlled temperature," 2005 World Tribology Congress III, Sep 12-16 2005, American Society of Mechanical Engineers, New York, NY 10016-5990, United States, Washington, D.C., United States, pp. 823-824.
- [30] Hsu, S. M., and Gates, R. S., 2005, "Boundary Lubricating Films: Formation and Lubrication Mechanism," *Tribology International*, **38**(3) pp. 305-312.
- [31] Hershberger, J., Ajayi, O. O., and Fenske, G. R., 2005, "Zinc Content of ZDDP Films Formed Thermally and Mechanically," *Tribology International*, **38**(3) pp. 299-303.
- [32] Ji, H., Nicholls, M. A., Norton, P. R., 2005, "Zinc-Dialkyl-Dithiophosphate Antiwear Films: Dependence on Contact Pressure and Sliding Speed," *Wear*, **258**(5-6) pp. 789-799.
- [33] Ye, J., Araki, S., Kano, M., 2005, "Nanometer-Scale Mechanical/Structure Properties of Molybdenum Dithiocarbamate and Zinc Dialkylsithiophosphate Tribofilms and Friction

Reduction Mechanism," Japanese Journal of Applied Physics, Part 1: Regular Papers and Short Notes and Review Papers, **44**(No. 7B) pp. 5358-5361.

[34] Mosey, N. J., Woo, T. K., and Müser, M. H., 2005, "Mechanism of Wear Inhibition by ZDDP Lubricant Additives - Insights from Molecular Scale Simulations," American Chemical Society, Division of Petroleum Chemistry, Preprints, **50**(3) pp. 332-335.

[35] Mosey, N. J., Woo, T. K., and Müser, M. H., 2005, "Rational Design of New Anti-Wear Additives for Engine Lubricants through Molecular Simulation," American Chemical Society, Division of Petroleum Chemistry, Preprints, **50**(3) pp. 291-294.

[36] Mosey, N. J., Müser, M. H., and Woo, T. K., 2005, "Molecular Mechanisms of Anti-Wear Pad Formation and Functionality of Lubricant Additives," Science, **307**(No. 5715) pp. 1612-1615.

[37] Mosey, N. J., Woo, T. K., Kasrai, M., 2006, "Interpretation of Experiments on ZDDP Anti-Wear Films through Pressure-Induced Cross-Linking," Tribology Letters, **24**(No. 2) pp. 105-105-114.

[38] Bhushan, B., 2000, "Modern Tribology Handbook, Volume 1," C R C Press LLC, United States of America, pp. 1760.

[39] Bhushan, B., 2000, "Modern Tribology Handbook, Volume 2," C R C Press LLC, United States of America, pp. 1760.

[40] Morina, A., and Neville, A., 2007, "Understanding the Composition and Low Friction Tribofilm formation/removal in Boundary Lubrication," Tribology International, **40**(10-12) pp. 1696-1704.

- [41] Taylor, C. M., 1998, "Automobile Engine tribology—design Considerations for Efficiency and Durability," *Wear*, **221**(1) pp. 1-8.
- [42] Hokkirigawa, K., 2001, "Introduction to Wear," *Toraibarojisuto/Journal of Japanese Society of Tribologists*, **46**(4) pp. 271.
- [43] Kato, K., 2002, "Classification of Wear mechanisms/models," *Proceedings of the Institution of Mechanical Engineers, Part J: Journal of Engineering Tribology*, **216**(6) pp. 349-356.
- [44] Mishina, H., Sasada, T., Norose, S., 1979, "FORMATION OF FLAKE-LIKE WEAR PARTICLES CAUSED BY PRESS-SLIDE FLATTENING OF ADHERED FRAGMENTS," *Journal of Japan Society of Lubrication Engineers*, **24**(9) pp. 585-591.
- [45] Trezona, R. I., Allsopp, D. N., and Hutchings, I. M., 1999, "Transitions between Two-Body and Three-Body Abrasive Wear: Influence of Test Conditions in the Microscale Abrasive Wear Test," *Wear*, **225-229** pp. 205-214.
- [46] Gates, J. D., 1998, "Two-Body and Three-Body Abrasion: A Critical Discussion," *Wear*, **214**(1) pp. 139-146.
- [47] Lee, Y., and Kim, B., 1999, "Influence of the Boundary Lubricating Conditions of Three Different Fluids on the Plastic Fatigue Related Mechanisms of Wear and Scuffing," *Wear*, **232**(1) pp. 116-121.
- [48] Berbezier, I., Martin, J. M., and Kapsa, P., 1986, "Role of Carbon in Lubricated Mild Wear," *Tribology International*, **19**(3) pp. 115-122.
- [49] Scherge, M., Martin, J. M., and Pohlmann, K., 2006, "Characterization of Wear Debris of Systems Operated Under Low Wear-Rate Conditions," *Wear*, **260**(4) pp. 458-461.

- [50] Hsu, S. M., 2004, "Molecular Basis of Lubrication," *Tribology International*, **37**(7) pp. 553-559.
- [51] Dowson, D., 1992, "Developments in Lubrication - the Thinning Film," *Journal of Physics D: Applied Physics*, **25**(1A) pp. 334-334-339.
- [52] Dowson, D., and Higginson, G.R., 1966, "Elastohydrodynamic Lubrication," Pergamon Press, London, UK, pp. 235.
- [53] Hamrock, B. J., and Dowson, D., 1977, "ISOTHERMAL ELASTOHYDRODYNAMIC LUBRICATION OF POINT CONTACTS," *Journal of Lubrication Technology, Transactions ASME*, **99** pp. 15-23.
- [54] Archard, J. F., 1985, "Friction between Metal Surfaces," *Wear*, **113**(1) pp. 3-16.
- [55] Grubin, A.N., 1949, "Fundamentals of the hydrodynamic theory of lubrication of heavily loaded cylindrical surfaces," Central Scientific Research Institute for Technology and Mechanical Engineering, Moscow,USSR, pp. 337.
- [56] Archard, J. F., and Cowking, E. W., 1965-1966, "Elastohydrodynamic lubrication at point contacts," **180**, pp. 47-47-56.
- [57] Coy, J. C., Gorla, R. S. R., and Townsend, D. P., 1979, "COMPARISON OF PREDICTED AND MEASURED ELASTOHYDRODYNAMIC FILM THICKNESS IN A 20-MILLIMETER-BORE BALL BEARING," NASA Technical Paper, (154) pp. 28.
- [58] Lu, X., Khonsari, M. M., and Gelinck, E. R. M., 2006, "the Stribeck Curve: Experimental Results and Theoretical Prediction," *Journal of Tribology*, **128**(4) pp. 789-789-794.

- [59] Tonck, A., Martin, J. M., Kapsa, P., 1979, "Boundary Lubrication with Anti-Wear Additives: Study of Interface Film Formation by Electrical Contact Resistance," *Tribology International*, **12**(5) pp. 209-213.
- [60] Coy, R. C., and Jones, R. B., 1981, "The Thermal Degradation and EP Performance of Zinc Dialkyldithiophosphate Additives in White Oil," *Tribology Transactions*, **24**(1) pp. 77-90.
- [61] Jones, R. B., and Coy, R. C., 1981, "The Chemistry of the Thermal Degradation of Zinc Dialkyldithiophosphate Additives," *Tribology Transactions*, **24**(1) pp. 91-97.
- [62] Li, Y., Pereira, G., Lachenwitzer, A., 2007, "X-Ray Absorption Spectroscopy and Morphology Study on Antiwear Films Derived from ZDDP Under Different Sliding Frequencies," *Tribology Letters*, **27**(3) pp. 245-253.
- [63] Varlot, K., Kasrai, M., Bancroft, G. M., 2001, "X-Ray Absorption Study of Antiwear Films Generated from ZDDP and Borate Micelles," *Wear*, **249**(12) pp. 1029-1035.
- [64] Lin, Y. C., and So, H., 2004, "Limitations on use of ZDDP as an Antiwear Additive in Boundary Lubrication," *Tribology International*, **37**(1) pp. 25-33.
- [65] Tse, J. S., Song, Y., and Liu, Z., 2007, "Effects of Temperature and Pressure on ZDDP," *Tribology Letters*, **28**(1) pp. 45-49.
- [66] Kasrai, M., Fuller, M. S., Bancroft, G. M., 2003, "X-Ray Absorption Study of the Effect of Calcium Sulfonate on Antiwear Film Formation Generated from Neutral and Basic ZDDPs: Part 1 - Phosphorus Species," *Tribology Transactions*, **46**(4) pp. 534-542.
- [67] Kasrai, M., Fuller, M. S., Bancroft, G. M., 2003, "X-Ray Absorption Study of the Effect of Calcium Sulfonate on Antiwear Film Formation Generated from Neutral and Basic ZDDPs: Part 2 - Sulfur Species," *Tribology Transactions*, **46**(4) pp. 543-549.

- [68] Fuller, M., Yin, Z., Kasrai, M., 1997, "Chemical Characterization of Tribochemical and Thermal Films Generated from Neutral and Basic ZDDPs using X-Ray Absorption Spectroscopy," *Tribology International*, **30**(4) pp. 305-315.
- [69] Li, Y., Pereira, G., Kasrai, M., 2007, "Studies on ZDDP Anti-Wear Films Formed Under Different Conditions by XANES Spectroscopy, Atomic Force Microscopy and ^{31}P NMR," *Tribology Letters*, **28**(3) pp. 319-328.
- [70] Kastelan-Macan, M., Petrovic, M., Haiduc, I., 1995, "Stereochemical Aspects of Phosphor-1,1-Dithiolato Metal Complexes (Dithiophosphates, Dithiophosphinates): Coordination Patterns, Molecular Structures and Supramolecular Associations," *Polyhedron*, **14**pp. 3389-3389-3472.
- [71] Harrison, P. G., and Kikabhai, T., 1987, "Proton and Phosphorous ^{31}P NMR Study of ZDDP in Solution," *Journal of the Chemical Society, Dalton Transactions: Inorganic Chemistry*, **16**(4) pp. 807-807-813.
- [72] Harrison, J. J., Chan, C. Y., Onopchenko, A., 2007, "Neutral Zinc(II) O,O-Di-Alkyldithiophosphates - Variable Temperature ^{31}P NMR and Quantum Chemical Study of the ZDDP Monomer-Dimer Equilibrium," *Magnetic Resonance in Chemistry*, **46**(2) pp. 115-115 - 124.
- [73] Yamaguchi, E. S., Primer, R. L., Aragón, S. R., 1997, "Dynamic Light Scattering Studies of Neutral Diisobutyl Zinc Dithiophosphate," *Tribology Transactions*, **40**pp. 330-330-338.
- [74] Yamaguchi, E. S., Primer, R. L., Aragón, S. R., 1998, "Dynamic Light Scattering Studies of Basic Diisobutyl Zinc Dithiophosphate," *Tribology Transactions*, **41**pp. 233-233-240.
- [75] Varlot, K., Kasrai, M., Martin, J. M., 2000, "Antiwear Film Formation of Neutral and Basic ZDDP: Influence of the Reaction Temperature and of the Concentration," *Tribology Letters*, **8**(1) pp. 9-16.

- [76] Yamaguchi, E. S., Ryason, P. R., Labrador, E. Q., 1996, "Comparison of the Relative Wear Performance of Neutral and Basic ZnDTP Salts," *Tribology Transactions*, **39**(1) pp. 220-224.
- [77] Suominen Fuller, M. L., Kasrai, M., Bancroft, G. M., 1998, "Solution Decomposition of Zinc Dialkyl Dithiophosphate and its Effect on Antiwear and Thermal Film Formation Studied by X-Ray Absorption Spectroscopy," *Tribology International*, **31**(10) pp. 627-644.
- [78] Yamaguchi, E., Ryason, P., and Labrador, E., 1995, "Inelastic Electron Tunneling Spectra of Neutral and Basic Zinc Dithiophosphate on Native Aluminum Oxide Surfaces," *S T L E Tribology Transactions*, **38**(2) pp. 243.
- [79] Yamaguchi, E. S., and Ryason, P. R., 1993, "Inelastic Electron Tunneling Spectra of Lubricant Oil Additives on Native Aluminum Oxide Surfaces," *Tribology Transactions*, **36**(3) pp. 367-374.
- [80] Dacre, B., and Bovington, C. H., 1982, "ADSORPTION AND DESORPTION OF ZINC DI-ISOPROPYLDITHIOPHOSPHATE ON STEEL," **25**(4) pp. 546-554.
- [81] Bancroft, G. M., Kasrai, M., Fuller, M., 1997, "Mechanisms of Tribochemical Film Formation: Stability of Tribo- and Thermally-Generated ZDDP Films," *Tribology Letters*, **3**(1) pp. 47-47-51.
- [82] Aktary, M., McDermott, M. T., and Torkelson, J., 2001, "Morphological Evolution of Films Formed from Thermooxidative Decomposition of ZDDP," *Wear*, **247**(2) pp. 172-179.
- [83] Fujita, H., and Spikes, H. A., 2004, "The Formation of Zinc Dithiophosphate Antiwear Films," *Proceedings of the Institution of Mechanical Engineers, Part J: Journal of Engineering Tribology*, **218**(4) pp. 265-277.

- [84] Costello, M. T., and Urrego, R. A., 2007, "Study of Surface Films of the ZDDP and the MoDTC with Crystalline and Amorphous Overbased Calcium Sulfonates by XPS," *Tribology Transactions*, **50**(2) pp. 217-226.
- [85] Hague, T., Morina, A., Neville, A., 2007, "Study of the ZDDP Antiwear Tribofilm Formed on the DLC Coating using AFM and XPS Techniques," *Journal of ASTM International*, **4**(7) .
- [86] De Barros, M. I., Bouchet, J., Raoult, I., 2003, "Friction Reduction by Metal Sulfides in Boundary Lubrication Studied by XPS and XANES Analyses," *Wear*, **254**(9) pp. 863-870.
- [87] Mourhatch, R., Parekh, K., and Aswath, P. B., 2006, "A multi technique study of the tribological behavior and the tribofilms generated from fluorinated thiophosphate compounds in comparison to normal ZDDP," *STLE/ASME International Joint Tribology Conference, IJTC 2006*, American Society of Mechanical Engineers, New York, NY 10016-5990, United States, San Antonio, TX, United States, pp. 12.
- [88] Georges, J. M., Martin, J. M., Mathia, T., 1979, "MECHANISM OF BOUNDARY LUBRICATION WITH ZINC DITHIOPHOSPHATE," *Wear*, **53**(1) pp. 9-34.
- [89] Yu, L. G., Yamaguchi, E. S., Kasrai, M., 2007, "The Chemical Characterization of Tribofilms using XANES - Interaction of Nanosize Calciumcontaining Detergents with Zinc Dialkyldithiophosphate," *Canadian Journal of Chemistry*, **85**(10) pp. 675-684.
- [90] Pereira, G., Lachenwitzer, A., Kasrai, M., 2007, "A Multi-Technique Characterization of ZDDP Antiwear Films Formed on Al (Si) Alloy (A383) Under various Conditions," *Tribology Letters*, **26**(2) pp. 103-117.
- [91] Kasrai, M., Vasiga, M., Fuller, M. S., 1999, "Study of the Effects of Ca Sulfonate on Antiwear Film Formation by X-Ray Absorption Spectroscopy using Synchrotron Radiation," *Journal of Synchrotron Radiation*, **6**(3) pp. 719-721.

- [92] Kasrai, M., Yin, Z., Fuller, M., 1997, "Application of XAFS in Tribology: P and S L-Edge XANES Spectroscopy of Antiwear Films," *Journal De Physique.IV : JP*, **7**(2) pp. 2-847.
- [93] Kasrai, M., Brown, J. R., Bancroft, G. M., 1996, "Sulphur Characterization in Coal from X-Ray Absorption Near Edge Spectroscopy," *International Journal of Coal Geology*, **32**(1) pp. 107-135.
- [94] Komvopoulos, K., Yamaguchi, E. S., Do, V., 2004, "Nanomechanical and nanotribological properties of an antiwear tribofilm produced from phosphorus-containing additives on boundary-lubricated steel surfaces," 2004 ASME/STLE International Joint Tribology Conference, American Society of Mechanical Engineers, New York, NY 10016-5990, United States, Long Beach, CA, United States, pp. 1631-1636.
- [95] Nicholls, M. A., Norton, P. R., Bancroft, G. M., 2004, "Nanometer Scale Chemomechanical Characterization of Antiwear Films," *Tribology Letters*, **17**(No. 2) pp. 205-205-216.
- [96] Ye, J., Kano, M., and Yasuda, Y., 2002, "Evaluation of Local Mechanical Properties in Depth in MoDTC/ZDDP and ZDDP Tribochemical Reacted Films using Nanoindentation," *Tribology Letters*, **13**(1) pp. 41-41-47.
- [97] Aktary, M., McDermott, M. T., and MacAlpine, G., 2002, "Morphology and Nanoindentation Profiles of Automotive Engine Components," *Surface Engineering*, **18** pp. 70-74.
- [98] Topolovec-Miklozic, K., Forbus, T. R., and Spikes, H. A., 2007, "Film Thickness and Roughness of ZDDP Antiwear Films," *Tribology Letters*, **26**(2) pp. 161-171.
- [99] Aktary, M., McDermott, M. T., and McAlpine, G. A., 2002, "Morphology and Nanomechanical Properties of ZDDP Antiwear Films as a Function of Tribological Contact," *Tribology Letters*, **12**(3) pp. 155-155-162.

- [100] Suominen Fuller, M. L., Rodriguez Fernandez, L., Massoumi, G. R., 2000, "The use of X - ray Absorption Spectroscopy for Monitoring the Thickness of Antiwear Films from ZDDP," Tribology Letters, **8**(4) pp. 187-187-192.
- [101] Yin, Z., Kasrai, M., Fuller, M., 1997, "Application of Soft x-Ray Absorption Spectroscopy in Chemical Characterization of Antiwear Films Generated by ZDDP Part I: The Effects of Physical Parameters," Wear, **202**(2) pp. 172-191.
- [102] Elgin, M., Rossi, A., and Spencer, N. D., 2003, "X-Ray Photoelectron Spectroscopy Analysis of Tribostressed Samples in the Presence of ZnDTP: A Combinatorial Approach," Tribology Letters, **15**(3) pp. 199-199-209.
- [103] Bec, S., Tonck, A., Georges, J. M., 1999, "Relationship between mechanical properties and structures of zinc dithiophosphate anti-wear films," London, UK, **455** pp. 4181-4181 - 4203.
- [104] Somayaji, A., and Aswath, P. B., Accepted (2008), "Antiwear Perforce of ZDDP and Fluorinated ZDDP in the Presence of Antioxidants," Tribology Transactions, .
- [105] Parekh, K., Mourhatch, R., and Aswath, P. B., 2005, "ZDDP-additive-catalyst interactions in engine oil," American Society of Mechanical Engineers, New York, NY 10016-5990, United States, pp. 661-662.
- [106] Varlot, K., Martin, J. M., Grossiord, C., 1999, "A Dual-Analysis Approach in Tribochemistry: Application to ZDDP/calcium Borate Additive Interactions," Tribology Letters, **6**(Nos. 3-4) pp. 181-181-189.
- [107] Kapur, G. S., Chopra, A., Sarpal, A. S., 1999, "Studies on Competitive Interactions and Blending Order of Engine Oil Additives by Variable Temperature ³¹P NMR and IR Spectroscopy." Trib.Trans., **42**(4) pp. 807-812.

- [108] Wu, Y. L., and Dacre, B., 1997, "Effects of Lubricant-Additives on the Kinetics and Mechanisms of ZDDP Adsorption on Steel Surfaces," *Tribology International*, **30**(6) pp. 445-453.
- [109] Misra, A. K., Mehrotra, A. K., and Srivastava, R. D., 1975, "Antiwear Characteristics of Additives: Synergistic and Adverse Effects," *Wear*, **31**(2) pp. 345-357.
- [110] Barcroft, F. T., and Park, D., 1986, "Interactions on Heated Metal Surfaces between Zinc Dialkyldithiophosphates and Other Lubricating Oil Additives." *Wear*, **108**(3) pp. 213-234.
- [111] Huq, M. Z., Chen, X., Aswath, P. B., 2005, "Thermal Degradation Behaviour of Zinc Dialkyl Dithiophosphate in Presence of Catalyst and Detergents in Neutral Oil," *Trib.Lett.*, **19**(2) pp. 127-134.
- [112] Patel, K., Aswath, P. B., and Elsenbaumer, R. L., 2005, "Development of Low Phosphorous Engine Oils," American Society of Mechanical Engineers, New York, NY 10016-5990, United States, pp. 557-558.
- [113] Parekh, K., Aswath, P. B., Shaub, H., 2006, "Low-Phosphorous Lubricant Additive," **11/182,023**(US 2006/0014652) .
- [114] Ye, Z., Zhang, C., Wang, Y., 2004, "An Experimental Investigation of Piston Skirt Scuffing: A Piston Scuffing Apparatus, Experiments, and Scuffing Mechanism Analyses," *Wear*, **257**(1-2) pp. 8-31.
- [115] Woydt, M., and Kelling, N., 2001, "Tribological testing of lubricants and materials for the system "piston ring/cylinder liner" outside of engines," *Bench Testing of Industrial Fluid Lubrication and Wear properties used in Machinery Applications*, American Society for Testing and Materials, Seattle, WA, United States, pp. 153-167.

- [116] Voitik, R. M., 1993, "Realizing bench test solutions to field tribology problems by utilizing tribological aspect numbers," Proceedings of the Symposium on Tribology: Wear Test Selection for Design and Application, Publ by ASTM, Philadelphia, PA, USA, Miami, FL, USA, pp. 45-59.
- [117] Hernandez Battez, A., Fernandez Rico, J. E., and Garcia Cuervo, D., 2003, "Rolling Contact Fatigue in Lubricated Contacts," Tribology International, **36**(1) pp. 35-40.
- [118] Martin, J., Grossiord, C., Le Mogne, T., 2000, "Transfer Films and Friction Under Boundary Lubrication," Wear, **245**(1) pp. 107-115.
- [119] Martin, J. M., Mansot, J. L., Berbezier, I., 1986, "Microstructural Aspects of Lubricated Mild Wear with Zinc Dialkyldithiophosphate," Wear, **107**(4) pp. 355-366.
- [120] Briggs, D., and Grant, J.T., 2003, "Surface Analysis by Auger and X-ray Photoelectron spectroscopy," IM Publications and Surface Spectra Limited, Manchester, UK, pp. 1-885.
- [121] Glaeser, W. A., Baer, D., and Engelhardt, M., 1993, "In Situ Wear Experiments in the Scanning Auger Spectrometer," Wear, **162-164**(Part 1) pp. 132-138.
- [122] Huq, M. Z., Aswath, P. B., and Elsenbaumer, R. L., 2007, "TEM Studies of Anti-Wear films/wear Particles Generated Under Boundary Conditions Lubrication," Tribology International, **39**(1) pp. 111-111-116.
- [123] Mourhatch, R., and Aswath, P. B., 2006, "Mechanism of Boundary Lubrication with Zinc Dialkyl Dithiophosphate," American Society of Mechanical Engineers, pp. IJTC-12054.
- [124] Ferrari, E. S., Roberts, K. J., and Adams, D., 1999, "A Multi-Edge X-Ray Absorption Spectroscopy Study of the Reactivity of Zinc Di-Alkyl-Di-Thiophosphates (ZDDPS) Anti-Wear Additives: 1. an Examination of Representative Model Compounds," Wear, **236**(1-2) pp. 246-258.

- [125] Ferrari, E. S., Roberts, K. J., and Adams, D., 2002, "An X-Ray Absorption Spectroscopy Examination of Structural Changes to Zinc Di-Alkyl-Di-Thiophosphate (ZDDP) Following Milling in the Presence of Iron Oxides and Subsequent Thermal Processing," *Wear*, **253**(7-8) pp. 759-767.
- [126] Bakunin, V. N., Kasrai, M., Kuzmina, G. N., 2007, "Influence of Temperature and ZDDP Concentration on Tribochemistry of Surface-Capped Molybdenum Sulfide Nanoparticles Studied by XANES Spectroscopy," *Tribology Letters*, **26**(1) pp. 33-43.
- [127] The Canadian Light Source; www.lightsource.ca.
- [128] The Synchrotron Radiation Center (SRC); www.src.wisc.edu.
- [129] Oliver, W. C., and Pharr, G. M., 1992, "Improved Technique for Determining Hardness and Elastic Modulus using Load and Displacement Sensing Indentation Experiments," *Journal of Materials Research*, **7**(6) pp. 1564-1580.
- [130] Parekh, K., and Aswath, P. B., 2006, "Synthesis of Fluorinated ZDDP Compounds," STLE/ASME International Joint Tribology Conference, IJTC 2006, .
- [131] Pidduck, A. J., and Smith, G. C., 1997, "Scanning Probe Microscopy of Automotive Anti-Wear Films," *Wear*, **212**(2) pp. 254-264.
- [132] Kundu, T. K., Mukherjee, M., Chakravorty, D., 1998, "Growth of Nano- α -Fe₂O₃ in a Titania Matrix by the sol-gel Route," *Journal of Materials Science*, **33**(No. 7) pp. 1759-1759-1763.
- [133] Li, J., Zeng, H., Sun, S., 2004, "Analyzing the Structure of CoFe-Fe₃O₄ Core-Shell Nanoparticles by Electron Imaging and Diffraction," *Journal of Physical Chemistry B*, **108**(37) pp. 14005-14005-14008.

[134] Nicholls, M. A., Norton, P. R., Bancroft, G. M., 2004, "X-Ray Absorption Spectroscopy of Tribofilms Produced from Zinc Dialkyl Dithiophosphates on Al-Si Alloys," *Wear*, **257**(3-4) pp. 311-328.

[135] Yin, Z., Kasrai, M., Bancroft, G. M., 1995, "X-Ray-Absorption Spectroscopic Studies of Sodium Polyphosphate Glasses," *Physical Review B: Condensed Matter*, **51**(23) pp. 742.

BIOGRAPHICAL INFORMATION

Ramoun Mourhatch received his B.Sc. in Materials Science and Engineering from the Sharif (Aryamehr) University of Technology in Tehran, Iran, in 2002. He started graduate studies at UT Arlington in fall 2002. He continued his research towards a Ph.D. degree under the supervision of professors Pranesh B. Aswath and Ronald L. Elsenbaumer. A member of the tribology Research group, his research focuses on the study and characterization of tribofilms generated as a result of the anti-wear mechanism and chemistry of engine oils and their components on lubricated surfaces in internal combustion engines.